Synthesis and Reactivities of Highly Oxidized [Fe_4S_4] Clusters
特異な高酸化状態を有する[Fe_4S_4]クラスターの合成と反応性に関する研究

Thesis by
Kazuki Tanifuji
谷藤　一樹

Department of Chemistry, Graduate School of Science, Nagoya University
Nagoya, Aichi, Japan
(Year)
2013

Table of Contents

Chapter 1: General Introduction

Chapter 2: Synthetic Analogues of [$Fe_4S_4(Cys)_3(His)$] in Hydrogenases and [$Fe_4S_4(Cys)_4$] in HiPIP Derived from All-Ferric $Fe_4S_4\{N(SiMe_3)_2\}_4$

Chapter 3: A Convenient Route to Synthetic Analogues of the Oxidized Form of High-Potential Iron-Sulfur Proteins

Chapter 4: Synthesis and Properties of a Thiolate-Bridged [Fe_4S_4]-[Fe] Cluster Relevant to the Active Site of Sulfite Reductase

Chapter 5: Formation of a Nitrogenase P-cluster [Fe_8S_7] Core via Reductive Fusion of Two All-Ferric [Fe_4S_4] Clusters

Chapter 6: Inter-Conversion Between [Fe_4S_4] and [Fe_2S_2] Clusters Bearing Amide Ligands

Chapter 1

General Introduction

1.1. Opening Remarks

Iron-Sulfur (Fe-S) clusters are one of the most ancient, ubiquitous and functionally versatile metallo-cofactors intervening in various cellular processes, and the significance of Fe-S biogenesis systems in Bacteria and Eukarya is beyond all doubt from the standpoint of current bioinorganic chemistry.[1] When the Fe-S clusters were discovered as acid-labile protein cofactors in the early 1960s,[2] the only known biological role of these clusters was agents of electron transfer.[3] However, the essential participation of Fe-S clusters was appreciated later in major biological processes like nitrogen fixation, photosynthesis, and respiration, demonstrating the long-lasting importance of Fe-S clusters in various ways.[3]

Toward a better understanding on biological Fe-S clusters, biologists and chemists have been taking two major strategies: detailed spectroscopic and experimental analyses of Fe-S proteins and chemically synthesized models. The results from these approaches partly complemented each other and have shed light on their biological behavior.

The inorganic cores of prevalent Fe-S clusters are described as [Fe_2S_2], [Fe_3S_4], and [Fe_4S_4], which are bound to protein backbones through the coordination of thiolate,

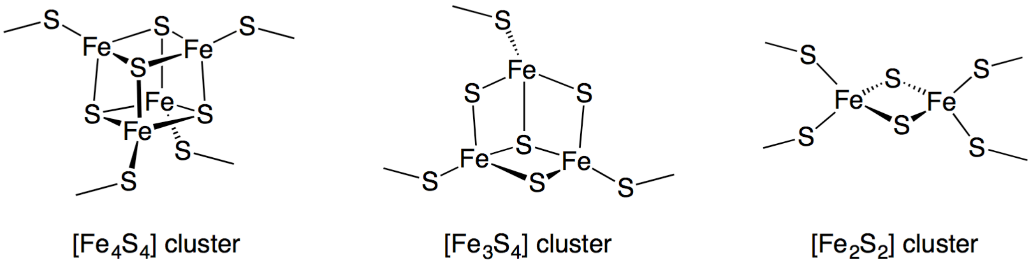

Figure 1.1. Schematic description of [Fe_4S_4], [Fe_3S_4], and [Fe_2S_2] clusters.

$^{-}$SR, arising from cysteine (Cys) residues (Figure 1.1).[4] With regard to this [Fe_4S_4], which are bound to protein backbones through the coordination of thiolate, dissertation dealing with synthetic [Fe_4S_4] clusters, the following two sections summarize the functions, structures, and properties of [Fe_4S_4] clusters in representative proteins, and the historical overview of synthetic [Fe_4S_4] clusters.

1.2. Biological [Fe_4S_4] Clusters

The distribution of [Fe_4S_4] clusters in metallo-proteins is widespread, and living organisms have made this type of clusters functionalize in various biological processes, such as respiration, central metabolism, substrate conversions, gene regulation, RNA modification, and DNA repair and replication.[5] This section describes an overview of how [Fe_4S_4] clusters work in living matters with respect to these functions.

1.2.1. [Fe_4S_4] clusters as Electron Carriers

One of the prominent features of [Fe_4S_4] clusters is their accessibility of multiple oxidation states. In other words, [Fe_4S_4] clusters are capable of accepting and releasing electron(s), and in fact, this property is applied in electron transfer sequences in many organisms.

1.2.1.1. Ferredoxin and High-potential Iron-sulfur Protein

Ferredoxin (Fd) and High-potential Iron-sulfur protein (HiPIP) represent the [$Fe_4S_4(Cys)_4$] clusters (Figure 1.1)[6, 7] with $[Fe_4S_4]^{2+}/[Fe_4S_4]^{+}$ redox couple for the former and $[Fe_4S_4]^{3+}/[Fe_4S_4]^{2+}$ for the latter. The contrast of redox couples is highlighted by their redox potentials, –250 to –650 mV vs NHE for Fd[4c] and +50 to +500 mV vs NHE for HiPIP.[8] Despite of the wide-ranging electrochemical potentials, the stable resting state of both Fd and HiPIP is $[Fe_4S_4]^{2+}$.

It is not surprising to find organisms which take the advantage of wide electrochemical potentials. HiPIP is found in oxidizing conditions, and serves as one of the soluble electron carriers in the electron transfer chain of purple photosynthetic bacteria. The electron transfer from the HiPIP of *Rhodoferax fermentans* to the photosynthetic reaction center (RC) has been demonstrated by kinetic experiments.[9] The interaction between RC and HiPIP has been also indicated by the crystal structure of *Thermochromatium tepidum.*[10] Fd is more abundant as an electron carrier, and is particularly common in electron transfer pathways of reducing activities, such as nitrogen fixation, nitrate reduction, sulfite reduction, CO_2 reduction, and radical S-adenosyl-methionine reduction.[11]

Since Fd is more prevalent than HiPIP, the oxidized form of HiPIP in the $[Fe_4S_4]^{3+}$ state is relatively exceptional. Thus there must be a strategy for HiPIP to stabilize this high oxidation state. For the origin of the stable oxidation states of Fd and HiPIP, the importance of the environment around $[Fe_4S_4]$ cluster has been pointed out. The amino acid sequence analysis around the $[Fe_4S_4]$ clusters of HiPIPs revealed the conserved hydrophobic alkyl or aromatic groups of glycine, phenylalanine, tryptophan, and tyrosine.[12] The role of these conserved residues are to form a hydrophobic cavity around the $[Fe_4S_4]$ cluster in HiPIP, and the stability of the $[Fe_4S_4]^{3+}$ state was found to be deteriorated when some of these residues were substituted into less bulky and polar ones.[13] The NMR studies on mutant HiPIP by Bertini and co-workers indicated that point mutation of a residue of the hydrophobic cavity enhances water accessibility to facilitate the hydrolysis of the $[Fe_4S_4]^{3+}$ cluster.[14] Furthermore, hydration of $[Fe_4S_4]$ cluster is suggested to account for most of the redox potential difference between Fd and HiPIP.[15] The hydrophobic cavity of HiPIP should contribute, therefore, to stabilize $[Fe_4S_4]^{3+}$ state not only kinetically but also thermodynamically.[8]

1.2.1.2. [$Fe_4S_4(Cys)_3(His)$] in Hydrogenases

The [Fe_4S_4] clusters are present not only as soluble electron carriers but also as Fe-S cluster relays mediating intra-protein electron transfer. Alignments of Fe-S clusters are found in enzymes with large proteins, in which active sites are deeply buried. Notable examples are the [NiFe] and [FeFe] hydrogenases, which catalyze the inter-conversion between hydrogen and proton plus electrons. While the enzymatic reactions take place at the [NiFe] or [FeFe] dinuclear active sites (Figure 1.2), the electrons are transferred between the protein surface and the active site through the relay of [Fe_4S_4] and [Fe_3S_4] (and [Fe_2S_2]) clusters.[16, 17]

Interestingly, the surface-located [$Fe_4S_4(Cys)_3(His)$] (His = histidine) cluster is common for [NiFe] and [FeFe] hydrogenases. While the His ligation is rare for [Fe_4S_4] clusters, its importance has been implicated for the [NiFe] hydrogenase of

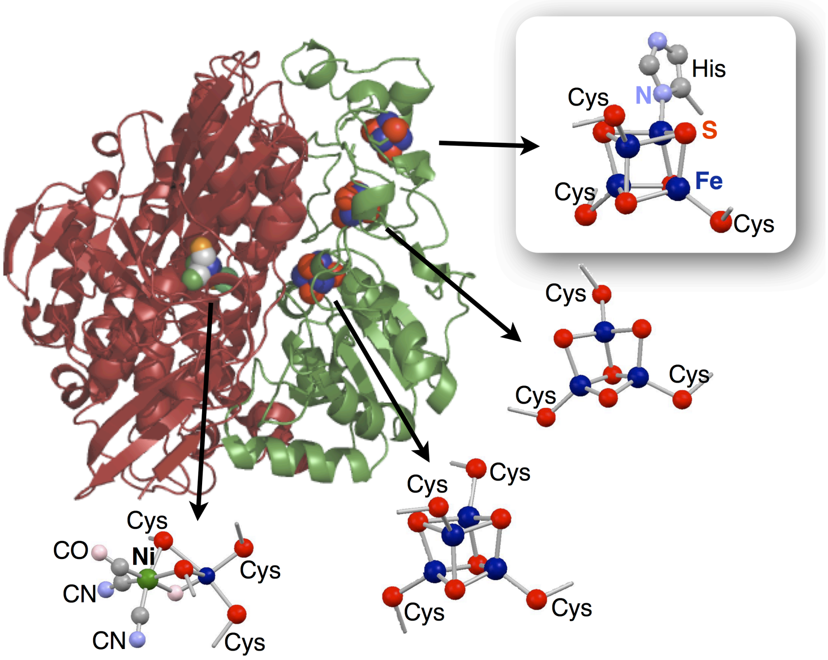

Figure 1.2. Crystal structure of [NiFe] hydrogenase from *Desulfovibrio gigas* (PDB ID: 2FRV).[16b] The [NiFe] active site and Fe-S clusters are shown in ball and stick model.

Desulfovibrio fructosovorans (*Df*). When the His residue attached to the [Fe_4S_4] cluster was mutated into Cys or glycine (Gly), the hydrogen oxidation activities decreased to 3 or 1.7% of that of wild-type protein.[18]

On the other hand, redox potentials of [$Fe_4S_4(Cys)_3(His)$] and [$Fe_4S_4(Cys)_4$] in the wild type and mutant of [NiFe] hydrogenase were suggested to be similar (<50 mV difference),[19] and the same trend was also observed in the [FeFe] hydrogenase.[20] It is certain that the His residue holds a key in the electron transfer pathway; however, the detailed function of His remains unclear.

1.2.2. [Fe_4S_4] Clusters in Catalysis

While the primary biological role of [Fe_4S_4] clusters is to transfer electrons, some are known to be involved in catalytic transformation reactions. The roles of [Fe_4S_4] cluster active sites in the reactions can be classified into the following three categories: (1) binding substrates at an iron atom for conversion, (2) supply of an electron to substrates to generate activated organic species, and (3) supply/accept of an electron to/from substrates through metallo-centers attached to the [Fe_4S_4] cluster.

1.2.2.1. Aconitase

Aconitase is the best characterized among the enzymes featuring an [Fe_4S_4] active site.[21] This enzyme catalyzes the stereospecific inter-conversion between citrate and isocitrate via *cis*-aconitate, constituting a part of TCA cycle (tricarboxylic acid cycle, also called as Krebs cycle) for the production of NADH. The [Fe_4S_4] active site of aconitase is supported by three Cys thiolates, leaving one of the iron atoms (the *unique* iron) as the substrate binding site. Based on the crystallographic studies using deactivated substrates and point mutations, the detailed catalytic mechanism has been proposed.[22] A simplified description of the reaction mechanism is shown in Scheme 1.1, where the Cys thiolates are omitted for clarity. The isomerization from citrate to isocitrate occurs at the *unique* iron. Citrate binds to the *unique* iron as a chelate ligand using the hydroxyl group and the alpha-carboxyl group, furnishing a hexa-coordinate iron atom having a water molecule. Dehydration of the citrate results in *cis*-aconitate as an stable intermediate. This step involves a sequential protonation/deprotonation process promoted by the His and Ser (Serine) residues around the [Fe_4S_4] active site. The *cis*-aconitate intermediate undergoes the reversible coordination/dissociation of *α*- and *β*-carboxylates, leading to the flipping with respect to the C*α*-C*β* double bond. Finally, *cis*-aconitate is hydrated to give (2*R*, 3*S*)-isocitrate. To note, Scheme 1.1 consists of a non-redox reaction sequence, where the *unique* iron serves as a Lewis acid site.

Aconitase is known to convert its Fe-S cluster core dependent on the oxidation

Scheme 1.1.

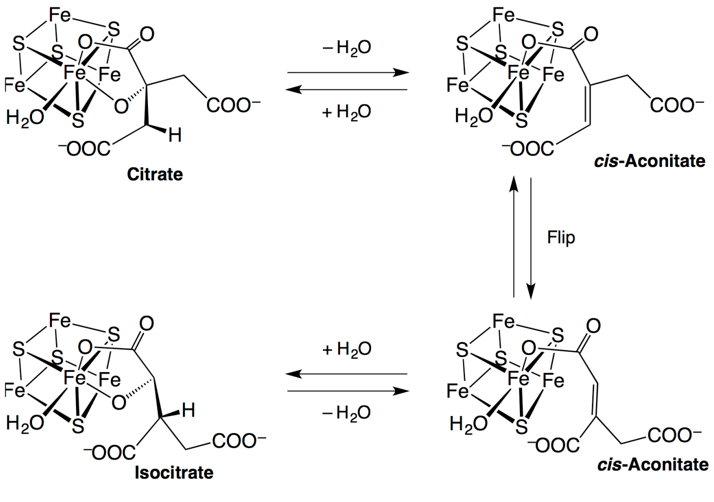

states.[21, 23] While the active form of aconitase contains an [Fe_4S_4] cluster, the aerobic oxidation or the chemical oxidation (with ferricyanide) lead to the inactive form with an [Fe_3S_4] cluster via loss of the *unique* iron atom.[24, 25] The addition of Fe^{2+} ion and a reducing agent to the inactive form results in the formation of the [Fe_4S_4] cluster and the recovery of the catalytic activity.[25, 26]

In mammalian cells, two aconitase isozymes are present: the mitochondrial aconitase and the cytosolic aconitase. The latter is a bifunctional enzyme called as iron regulatory protein 1 (IRP1), which also works in the regulation of iron metabolism.[27] The totally different two activities are controlled by assembly/disassembly of the [Fe_4S_4] cluster. The holo form of IRP1 having an [Fe_4S_4] cluster catalyzes the substrate conversion. When the protein is over-oxidized, the Fe-S cluster is removed from the binding site to give a colorless apo-protein. This apo form binds to some mRNAs to enhance iron uptake and inhibit iron storage.[28] In this process, the [Fe_4S_4] cluster works as a structural switch to change the protein conformation for sensing an environmental factor.

1.2.2.2. Radical S-adenosyl-methionine Reductase Familly

In the radical *S*-adenosyl-methionine (SAM) reductase superfamily of enzymes, the [Fe_4S_4] cluster active site provides an electron for the reduction of SAM, which undergoes homolytic cleavage of the C-S bond to produce methionine and 5′-deoxyadenosyl radical ($DOA^\bullet$).[29] The $DOA^\bullet$ radical is known as the initiator for diverse biological reactions, *i.e.* synthesis of bio-active compounds like biotin, benzylsuccinate, and lipoate, repair of DNA, reduction of ribonucleotides, and the biosynthesis of cofactors for metallo-proteins. Some of these functions are analogous to those of adenosyl-cobalamin which also generates the DOA$^\bullet$ radical, but the radical-SAM reductases mediate the wider range of reactions.

In the protein sequences of radical-SAM reductases, there is a highly conserved CxxxCxϕC (ϕ = tyrosine, phenylalanine, histidine or triptophan) peptide domain. This domain provides three Cys thiolate ligands for an [Fe_4S_4] cluster, which is about 7-10 Å away from the nearest protein surface. The fourth iron site of the [Fe_4S_4] cluster is occupied by the amino nitrogen (2.0-2.6 Å) and the carboxylate oxygen (2.0-2.5 Å) atoms of SAM (Figure 1.3).[29b] Interestingly, the crystal structures of pyruvate formate-lyase-activating enzyme (PFL-AE) reveal that the hepta-peptide substrate leads to a specific orientation of SAM moiety in which the sulfur atom has close proximity to the *unique* (fourth) iron (3.2 Å).[30] This observation indicates the importance of the binding of substrate for the generation of the DOA$^\bullet$ radical from SAM.[31]

The close contact of the [Fe_4S_4] cluster with SAM and the binding of substrate narrows the potential gap between SAM and the cluster. The redox potential of

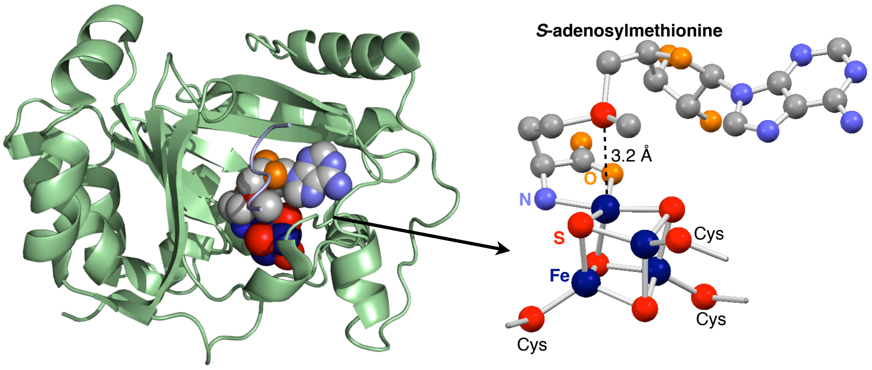

Figure 1.3. Crystal structure of pyruvate fumarate-lyase-activating enzyme (PFL-AE) (left) and an expanded view of the [Fe_4S_4] active site (right) (PDB ID: 3CB8).[30]

$[Fe_4S_4]^{2+}/[Fe_4S_4]^{+}$ process for SAM-bound Lysine 2,3-aminomutase (LAM) shifts from –430 mV to –600 mV vs NHE upon binding of substrate (lysine) and simultaneously the reduction potential for SAM in this Michaelis complex appears at –990 mV.[32] It is conceivable that the binding of SAM and lysine leads to less solvent exposure of the $[Fe_4S_4]$ cluster. Thus, one of the reasons for potential shift would be analogous to that discussed for Fd and HiPIP.[15] However, the detailed mechanism of how SAM ligation affects the redox potential of the cluster remains unclear.

1.2.2.3. Sulfite Reductase Family, [FeFe] Hydrogenase, and Acetyl CoA Synthase

The last group of metallo-proteins in which $[Fe_4S_4]$ clusters participate in redox of substrates through metallo-centers include (i) the sulfite reductase family, (ii) the [FeFe] hydrogenase, and (iii) the CO dehydrogenase/acetyl coenzyme A synthase (CODH/ACS). The active sites of these enzymes consist of mono- or di-nuclear reaction sites directly attached to $[Fe_4S_4]$ clusters through a Cys thiolate.[4c, 33] The structures and functions of their active sites are briefly summarized below.

Sulfite reductase of *Escherichia coli*, which catalyzes the six-electron reduction of SO_3^{2-} to S^{2-} (eq. 1.1), is the first structurally characterized among three enzymes.[34]

$$SO_3^{2-} + 6e^- + 8H^+ \rightarrow H_2S + 3H_2O \quad \textbf{(1.1)}$$

In the active site of sulfite reductase (Figure 1.4), one of the axial coordination sites of siroheme serves as the binding site of substrate, while the other site is capped by a Cys thiolate, which bridges to the $[Fe_4S_4]$ cluster.[35] The Mössbauer[36] and ESR[37] spectra of this enzyme in several oxidation states suggest that the $[Fe_4S_4]$ cluster would not only mediates electron transfer to the catalytically active iron but electronically couples with siroheme in the catalytic cycle.

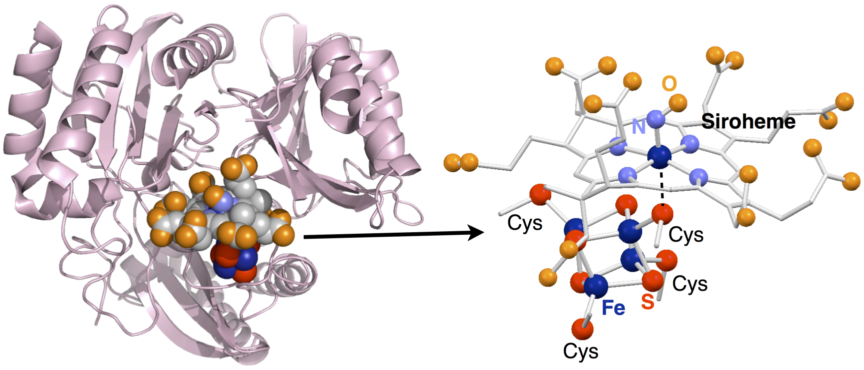

Figure 1.4. Crystal structure of sulfite reductase (left) and an expanded view of the active site (right) with NO occupying one of the axial sites of siroheme (PDB ID: 6GEP).[35b]

CO dehydrogenase/acetyl coenzyme A synthase (CODH/ACS) is a bifunctional metallo-protein which plays a key role in the initial few steps of the CO_2 fixation pathway called as Wood-Ljungdahl pathway. This enzyme consisting of a complex of multiple protein units mediates two independent but coupled reactions, the CO_2 reduction to CO at CODH (eq. 1.2) and the acetylation of coenzyme A (CoA) at ACS (eq. 1.3) where CFeSP denotes the corrinoid Fe-S protein.[38]

$$2e^- + 2H^+ + CO_2 \rightleftharpoons CO + H_2O \qquad \textbf{(1.2)}$$

$$CO + CH_3\text{—}CFeSP + CoA^- \rightleftharpoons \text{acetyl—CoA} + CFeSP \qquad \textbf{(1.3)}$$

The CO molecule produced at the active site of CODH is delivered to the active site of ACS through the substrate channel in the protein matrix. The active site of ACS is called as A-cluster, which is a dinuclear Ni-Ni complex connected to an $[Fe_4S_4]$ cluster through a Cys bridge (Figure 1.5). One of the nickel atoms *distal* to the $[Fe_4S_4]$ cluster (Ni_d) is supported by a Cys-Gly-Cys tripeptide moiety serving as a tetradentate diamide-dithiolate ligand, which bridges with Cys thiolates to the other nickel *proximal* to the $[Fe_4S_4]$ cluster (Ni_p). In the crystal structure, both Ni_p and Ni_d

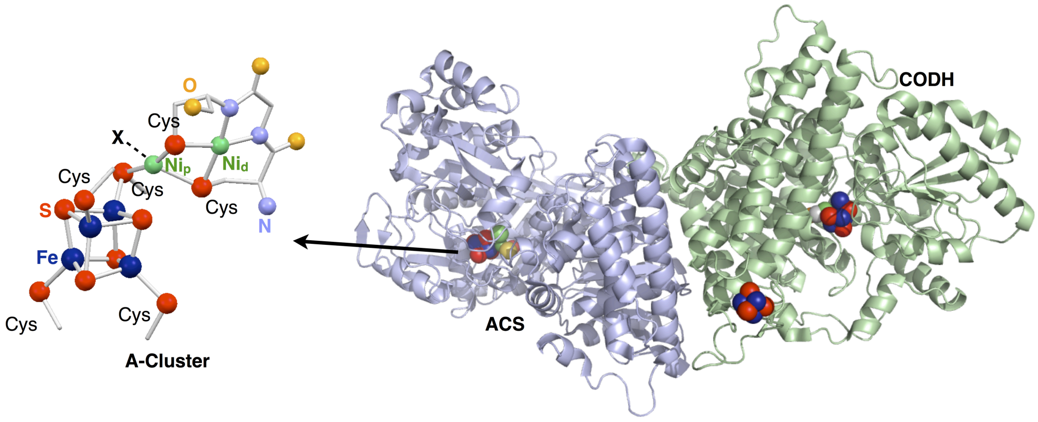

Figure 1.5. Crystal structure of CODH/ACS (right) and an expanded view of A-cluster (left) (PDB ID: 1OAO).[39c]

atoms are in a square-planar geometry, and Ni_p has an unidentified ligand X (possibly CH_3). While there is a Cys bridge between the *proximal* nickel (Ni_p) and the [Fe_4S_4] cluster, [39] this Cys thiolate on Ni_p has been suggested to be labile in the enzymatic cycle to accommodate substrates (CH_3 and/or coenzyme A (CoA)). Liberation of the bridging Cys from Ni_p generates two *cis*-oriented sites in a square-planar nickel center, which would bind both CH_3 and CoA to generate the CH_3-Ni-thiolate(CoA) moiety as an intermediate. The subsequent insertion of CO into Ni-CH_3 to generates the acetyl-Ni-CoA moiety, which undergoes the reductive elimination of acetyl-CoA to complete the enzymatic cycle.

In some microbes molecular hydrogen is utilized in energy-related reactions involving long-range electron transfer. The [FeFe] hydrogenase is one of the metallo-enzymes which catalyzes the reversible inter-conversion of H_2 into two protons and two electrons (eq. 1.4).[40]

$$H_2 \rightleftharpoons 2H^+ + 2e^- \qquad \textbf{(1.4)}$$

Because of the high catalytic activity (e.g. 9000 molecules H_2 per second), this enzyme

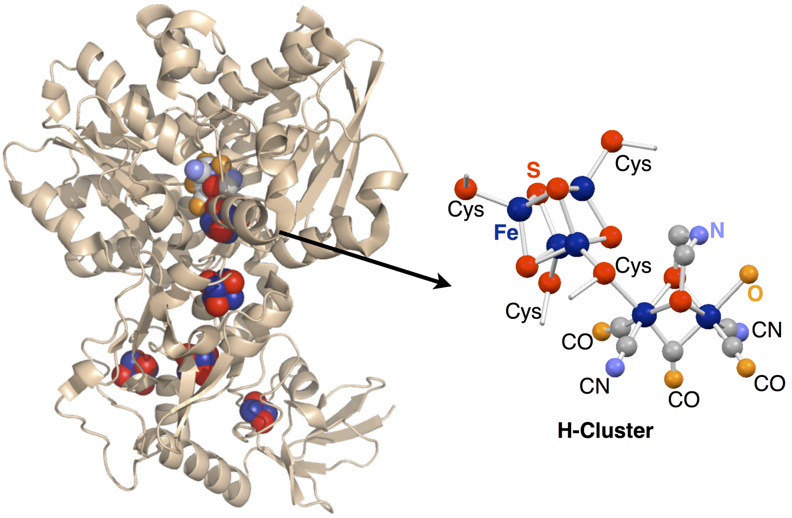

Figure 1.6. Crystal structure of the [FeFe] hydrogenase (left) and an expanded view of H-cluster (right) (PDB ID: 3C8Y).[17c]

draws much attention in relation to the technologies in fuel cells and industrial hydrogen production. The active site of the [FeFe] hydrogenase is called as H-cluster, and is composed of a dinuclear Fe-Fe unit and an [Fe_4S_4] cluster linked by a Cys thiolate (Figure 1.6).[17] There is a bridging dithiolate ligand in the Fe-Fe unit, and CO and CN ligands are bound to iron atoms. The central atom of the dithiolate ligand in the Fe-Fe has been unidentified for a decade, but was recently characterized as nitrogen based on the ^{14}N hyperfine sublevel correlation spectroscopy (HYSCORE) investigation[41] and the activation experiments of apo [FeFe] hydrogenase with synthetic analogues.[42]

1.2.3. Core Transformations of [Fe_4S_4] clusters in Fe-S Proteins

Dominant biological [Fe_4S_4] clusters are robust and thus function without significant structural changes. On the other hand, core transformations of [Fe_4S_4]

clusters in several proteins have been discovered recently. Two representative examples are noted below.

1.2.3.1. P-cluster Maturation

Molybdenum (Mo)-dependent nitrogenase is an enzyme, which catalyzes the reduction of atmospheric N_2 into NH_3 under ambient pressure and temperature. This enzyme consists of two component proteins: (1) MoFe protein, an $\alpha_2\beta_2$ tetramer catalyzing the substrate reduction, and (2) Fe protein, the ATP-dependent reductase for MoFe protein. The MoFe protein has two unique metal sulfur clusters in each $\alpha\beta$ subunit pair. One is the active site called FeMo-cofactor, which is a $[MoFe_7S_9C]$ cluster bound to homocitrate, His, and Cys. The other is P-cluster, which is an $[Fe_8S_7]$-type electron mediator (Figure 1.7).[43] The biological assembly processes for these two intricate clusters appeared to be extremely complicated requiring the gene products of *nifS*, *nifU*, *nifB*, *nifE*, *nifN*, and *nifH*.[44]

P-cluster is constructed at the place where it functions in MoFe protein, and hence the process is termed *in situ* assembly. A schematic description of this process based

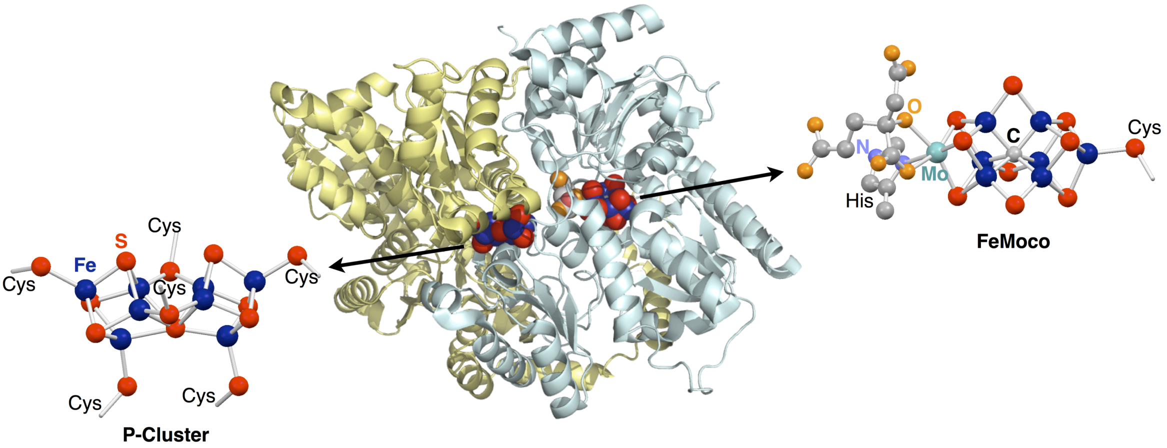

Figure 1.7. Crystal structure of nitrogenase, FeMoco and P-cluster (PDB ID: 3U7Q).[43b]

on the gene deletion experiments by Ribbe and co-workers is shown in Figure 1.8, in which a deletion target is described as Δ*nifX* (*X* = *H* or *B*).[45] It should be pointed out that Δ*nifH* stands for the lack of Fe protein. Prior to the reaction depicted in Figure 1.8, the precursor of P-cluster (P*-cluster) needs to be supplied to MoFe protein from NifS and NifU. Since Δ*nifH* MoFe protein shows the Fd^{red}-like $S = 1/2$ electron spin resonance (ESR) signal which is different from that of P-cluster, P*-cluster has been ascribed to $[Fe_4S_4]$-like cluster(s).[46] Fe K-edge X-ray absorption spectroscopy (XAS)/ extended X-ray absorption fine structure (EXAFS) and variable-temperature and variable-magnetic field magnetic circular dichroism (VTVH-MCD) studies, afterwards, indicate that P*-cluster consists of a pair of an $[Fe_4S_4]^+$ cluster and a diamagnetic and distorted $[Fe_4S_4]$-like cluster.[47] Treatment of Δ*nifH* MoFe protein with Fe protein, MgATP, and dithionite led to the disappearance of the $S = 1/2$ signal and the appearance of an EPR signal specific to the P-cluster in the IDS-oxidized state.[48] Whereas there has been no crystal structure of P*-cluster, the

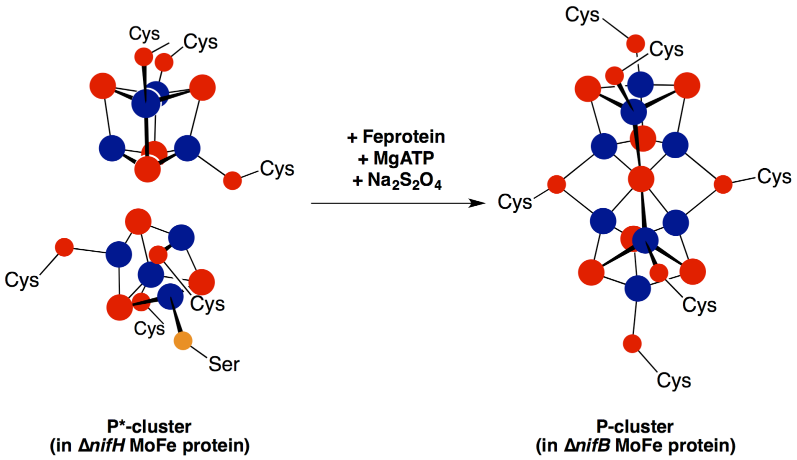

Figure 1.8. Schematic description of P-cluster maturation.[45b] Water molecules are proposed to fill the vacant sites of Fe atoms in P*-cluster. Fe = blue, S = red, and O = orange.

presence of a pair of [Fe_4S_4]-like clusters is unambiguously supported by the spectroscopic data.

P-cluster maturation from Δ*nifH* MoFe protein depends on the concentration of dithionite (reductant) and the presence of Fe protein (MoFe protein reductase), and thus suggests that the reduction of P*-cluster is a key for the formation of P-cluster.[48] It is interesting to find that the maturation process of the unique [Fe_8S_7] core of P-cluster, a fusion of two [Fe_4S_4] clusters, relate to the oxidation state of the P*-cluster.

1.2.3.2. Oxygen Sensor

When Fe-S clusters are in highly oxidized states, the stability of these clusters dramatically decreases. In other words, Fe-S clusters can be easily damaged by reactive oxygen and nitrogen species (ROS and RNS, respectively), which lead to the transformation or even the loss of Fe-S cluster. This intricate behavior of Fe-S clusters enables them to sense environmental stresses caused by ROS and RNS.[49] Fumarate and nitrate reduction (FNR) protein is a representative sensor protein having an [Fe_4S_4] cluster.

FNR protein is a global regulator, which controls transcription of genes in response to cellular O_2 level. The functional units in FNR protein are sensory domain and DNA-binding domain (Figure 1.9).[50] Under anaerobic conditions, this protein forms a homodimer complex and associates with specific DNA sequences as a result of the binding of O_2-labile [Fe_4S_4] cluster to four conserved Cys thiolates in the sensory domain. The Mössbauer spectroscopy revealed that the exposure of FNR protein to O_2 leads to the conversion of the [Fe_4S_4] cluster into the [Fe_2S_2] cluster.[51] The [Fe_2S_2] form of FNR protein exhibits decreased DNA-binding affinity

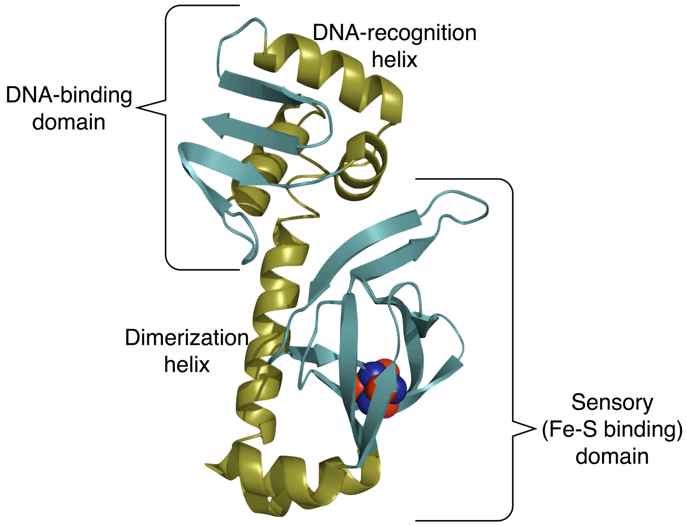

Figure 1.9. Predicted molecular structure of FNR protein.[50] [Fe_4S_4] cluster is shown as sphere model colored blue (Fe) and red (S).

because of the conformational change and the dissociation of FNR dimer to monomers caused by the conversion of the [Fe_4S_4] cluster.[52] The recovery of the [Fe_4S_4] cluster in FNR protein occurs upon treatment of the protein with dithiothreitol (DTT) and ferrous ion under an anaerobic condition.[53] Although over-exposure of FNR protein to O_2 results in the complete loss of the Fe-S cluster, it is still unclear whether [Fe_2S_2] or cluster-deficient FNR protein is the physiological aerobic form.

A two-step mechanism is proposed for the O_2-induced conversion of the [Fe_4S_4] cluster of FNR protein.[50,54] The first step is one-electron oxidation of the [Fe_4S_4] cluster and subsequent removal of Fe^{2+} ion to give an intermediary [Fe_3S_4] cluster. The second step is the spontaneous loss of an Fe^{3+} ion from the [Fe_3S_4] cluster to give an [Fe_2S_2] cluster. This step accompanies by the removal of two S atoms, and on the basis of the resonance raman spectrum of the resultant [Fe_2S_2] cluster, the two sulfur atoms have been suggested to insert into the Fe-Cys bonds to give persulfide ligands.[53] The mechanism of the conversion from [Fe_4S_4] to [Fe_2S_2] has been inferred on the basis of various kinetic experiments. On the other hand, identification methods for the Fe-S species of FNR protein have been limited to the Mössbauer and ESR spectra, and no crystallographic data is available for any state of FNR protein. Thus further structural characterization will be required to provide a better understanding on the mechanism of this cluster conversion at molecular level.

1.2.4. Section Conclusions

As reviewed in this section, biological [Fe_4S_4] clusters are essential cofactors working in various organisms. The specific functions and properties (e.g. reactivity and redox potential) of these [Fe_4S_4] clusters are controlled by custom-made *rational design* of environments. A protein-based approach has the advantage of directly giving us knowledge about how [Fe_4S_4] clusters behave. On the other hand, this approach gives us difficulty in the observation of only target cluster in case that there are multiple clusters in the protein. Difficulty also remains in distinguishing the effects of coordinating ligands and of other amino acid residues. In this regard, synthetic clusters have an advantage, as their environmental factors are simpler.

1.3. Synthetic [Fe_4S_4] Clusters

The chemistry of synthetic [Fe_4S_4] clusters emerged in early 1970s. The first paper in this field was the synthesis of [$Fe_4S_4(SCH_2Ph)_4]^{2-}$ by Holm and co-workers,[55] and thereafter, numerous clusters have been synthesized and characterized. This section summarizes representative examples of [Fe_4S_4] clusters modeling those in nature. Abiological [Fe_4S_4] clusters and [M_4S_4] (M = transition metals) clusters are reviewed in other publications.[56]

1.3.1. $[Fe_4S_4]^{3+}$ Clusters

The $[Fe_4S_4]^{3+}$ state is isoelectronic with the oxidized form of High-Potential Iron-sulfur Proteins (HiPIP^{ox}) and the highest oxidation level in three-state hypothesis.[7a] In common with the observation of HiPIP (described in 1.2.1.1), model clusters in this state are sensitive to environmental factors such as ligand substituents and solvent. The first example, $[Fe_4S_4(S^tBu)_4]^-$, was detected electrochemically from the dianion $[Fe_4S_4(S^tBu)_4]^{2-}$ in CH_2Cl_2.[57,58] Similarly, a series of $[Fe_4S_4(SR)_4]^-$ (e.g. R = Ph and ^{i}Pr) were observed in CH_2Cl_2 but not in MeCN or DMF.[59] As an exception, $[Fe_4S_4(SAd)_4]^{2-}$ exhibited a quasi-reversible $[Fe_4S_4]^{3+}$/ $[Fe_4S_4]^{2+}$ redox couple in DMF and aqueous micellar solutions.[60] Meanwhile, even less basic solvent (CH_2Cl_2 and $PhNO_2$) were found not to secure $[Fe_4S_4]^{3+}$ clusters having small thiolates such as $^-$SEt and $^-SCH_2CH_2OH$.[59d] These results suggest that both steric protection by substituents and low basicity (nucleophilicity) of solvents promote the stability of electrophilic $[Fe_4S_4]^{3+}$ core by inhibiting nucleophilic attack from solvent molecules and other species.

The isolated $[Fe_4S_4]^{3+}$ cluster has been limited to $[Fe_4S_4(STip)_4]^-$ (Tip = 2,4,6-triisopropylphenyl), which was prepared by chemical oxidation of $[Fe_4S_4(STip)_4]^{2-}$ (eq. 1.5).[61]

$$[Fe_4S_4(STip)_4]^{2-} + [Cp_2Fe]^+ \rightarrow [Fe_4S_4(STip)_4]^- + Cp_2Fe \quad \textbf{(1.5)}$$

The ESR spectrum of this cluster is similar to those of HiPIP^{ox}. The observed rhombic signal (g = 2.10, 2.05, 2.03) is consistent with an $S = 1/2$ ground state as a result of the antiferromagnetic coupling among iron centers.[62] The Mössbauer spectra gave a more detailed interpretation. That is, four irons are separated into two pairs, which consist of an $Fe^{2.5+}$-$Fe^{2.5+}$ dimer ($S = 9/2$) with a delocalized ferric center and an Fe^{3+}-Fe^{3+} dimer with localized ferric centers. On the other hand, electron-nuclear double resonance (ENDOR) and ESR spectra of $[Fe_4S_4(SCH_2Ph)_4]^-$ created by γ irradiation yielded a different description: $S = 7/2$ for the delocalized dimer and $S = 3$ for the localized dimer.[63] Since the spectroscopic studies on $[Fe_4S_3]^{3+}$ clusters are limited, the structures and physical properties of $[Fe_4S_3]^{3+}$ clusters still remain to be elucidated.

1.3.2. $[Fe_4S_4]^{2+}$ Clusters

As mentioned above, $[Fe_4S_4]^{2+}$ is isoelectronic with Fd^{ox} and HiPIP^{red}, and is the resting oxidation state of $[Fe_4S_4]$ clusters under physiological condition.[15] The same is true for the synthetic analogues. Since the first synthesis of $[Fe_4S_4(SCH_2Ph)_4]^{2-}$ in the early 1970s, more than 70 of $[Fe_4S_4]^{2+}$ clusters have been synthesized by virtue of their ease in handling compared with clusters in other oxidation states.[57]

Thiolate-bound $[Fe_4S_4]^{2+}$ clusters can be synthesized by self-assembly reactions of ferrous or ferric ion, thiolates (^-SR), and inorganic sulfur or hydrosulfide ion (^-SH) in adequate stoichiometric proportion (eq. 1.6, 1.7, and 1.8).

$$\begin{aligned}&4\mathrm{FeCl_3} + 6\,{}^{-}\mathrm{SR} + 4\,{}^{-}\mathrm{SH} + 4\,{}^{-}\mathrm{OMe}\\ &\qquad\rightarrow [\mathrm{Fe_4S_4(SR)_4}]^{2-} + \mathrm{RSSR} + + 12\mathrm{Cl}^{-} + 4\mathrm{MeOH}\end{aligned} \qquad \textbf{(1.6)}$$

$$4\mathrm{FeCl_2} + 10\,{}^{-}\mathrm{SR} + 4\mathrm{S} \rightarrow [\mathrm{Fe_4S_4(SR)_4}]^{2-} + 3\mathrm{RSSR} + 8\mathrm{Cl}^{-} \qquad \textbf{(1.7)}$$

$$4\mathrm{FeCl_3} + 14\,{}^{-}\mathrm{SR} + 4\mathrm{S} \rightarrow [\mathrm{Fe_4S_4(SR)_4}]^{2-} + 5\mathrm{RSSR} + 12\,\mathrm{Cl}^{-} \qquad \textbf{(1.8)}$$

These reactions consist of the following elementary steps; (1) coordination of thiolates to irons (formation of iron-thiolate complexes), (2a) oxidation of irons by inorganic sulfur or (2b) replacement of ${}^{-}$SR with ${}^{-}$SH followed by dissociation of HSR to leave S^{2-} on iron, (3) elimination of a thiolate ligand as a half of disulfide (RS-SR) to reduce irons, and (4) assembly of the resultant coordinatively unsaturated Fe-S species to satisfy the coordination number of irons. Steps (3) and (4) are repeated until the iron atoms satisfy the tetrahedral $Fe(S)_4$ geometry in the thermodynamically stable $[Fe_4S_4]^{2+}$ form. The repeated number of steps (2a) or (2b) (and the following steps (3) and (4)) is dependent on the stoichiometry of reagents. Several Fe-S and Fe-thiolate complexes have been isolated as relatively stable intermediates (Scheme 1.2).[64]

Two approaches are known to replace thiolates (${}^{-}$SR) in the $[Fe_4S_4]^{2+}$ clusters to different ones (${}^{-}$SR′) (eq. 1.9 and 1.10). These reactions are basically in equilibrium, and the difference of ligand basicities (nucleophilicities) controls the reactions.

$$[\mathrm{Fe_4S_4(SR)_4}]^{2-} + 4\mathrm{HSR'} \rightarrow [\mathrm{Fe_4S_4(SR')_4}]^{2-} + 4\mathrm{HSR} \qquad \textbf{(1.9)}$$

$$[\mathrm{Fe_4S_4(SR)_4}]^{2-} + 2\mathrm{R'SSR'} \rightarrow [\mathrm{Fe_4S_4(SR')_4}]^{2-} + 2\mathrm{RSSR} \qquad \textbf{(1.10)}$$

Ligands to be replaced with thiolate ligands in $[Fe_4S_4(SR)_4]^{2-}$ are not limited to thiolates with different substituents. For example, selenolates can be incorporated according to eq. 1.11.[65] Treatment of $[Fe_4S_4(SR)_4]^{2-}$ with PhCOX (X = Cl or Br) results

Scheme 1.2.

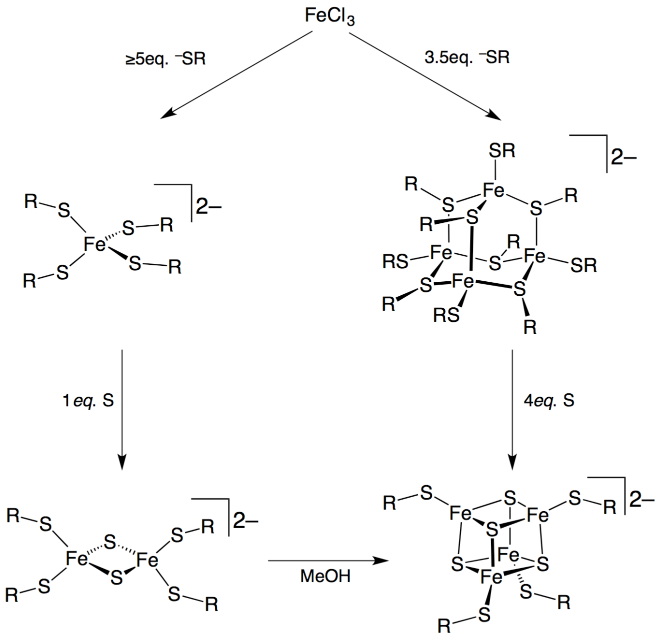

in the irreversible replacement of thiolates with halides, forming thioester (PhCOSR).[66]

As described in Section 1.2, [NiFe] hydrogenase, aconitase, and radical SAM family commonly have [3:1] site-differentiated [Fe_4S_4] clusters in the electron relay or the active sites. In general, ligand substitution reactions of synthetic [Fe_4S_4] clusters are reversible in polar solvent, and thereby it is problematic to replace only one ligand of homoleptic $[Fe_4S_4L_4]^{2-}$ clusters. The major approach to synthesize site-differentiated clusters utilizes a series of trithiolate ligands.[67] Because of the chelate effect, these ligands effectively cap the three of four coordination sites and restrict a reactive site on the *unique* iron of a [Fe_4S_4] cluster (an example is shown in Scheme 1.3). The incorporation of a wide variety of ligands (e.g. pyridines, alkoxides, phosphines, and hydroxide) was observed by ^{1}H NMR spectra,[68] and

Scheme 1.3.

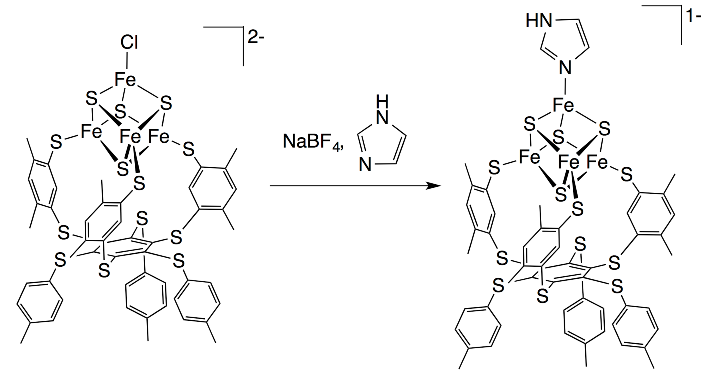

additionally some of crystal structures have been reported.[69] However, since the substitution at the unique iron is still reversible, the isolation of target compounds is inherently difficult in many situations.

1.3.3. $[Fe_4S_4]^+$ Clusters

This state is the same as Fd^{red} oxidation level. Seven examples of $[Fe_4S_4(SR)_4]^{3-}$ (R = Bz, Cy, Ph, *o*-$C_6H_4S^tBu$, *p*-C_6H_4Br, SH, ^tBu) were structurally characterized and isolated by three methods: (1) reduction of corresponding dianion by sodium acenaphthylenide (eq. 1.11), (2) self-assembly from $FeCl_2$, 2 equiv of a thiolate, and 1 equiv of NaSH, and (3) one-pot reaction of $Fe(PEt_3)_2Cl_2$ with 1.8 equiv of $(NEt_4)(SH)$ and 1 equiv of Na_2S.[70]

$$[Fe_4S_4(SR)_4]^{2-} + Na[C_{12}H_8] \rightarrow [Fe_4S_4(SR)_4]^{3-} + C_{12}H_8 + Na^+ \qquad \mathbf{(1.11)}$$

In the latter two reactions, some kind of oxidants must be included to generate Fe^{3+} center because $[Fe_4S_4]^+$ state can be formally interpreted as $Fe^{3+}3Fe^{2+}$ state. However, these oxidative species have remained unclear to date. In contrast to $[Fe_4S_4]^{3+}$ clusters, clusters in $[Fe_4S_4]^+$ state are relatively stable in basic solvents such as MeCN, DMF, and hexamethylphosphoramide (HMPA), corresponding to the solvent accessibility of $[Fe_4S_4]$ clusters in Fd. Perhaps it is because low electrophilicity of irons inhibit nucleophilic attack from solvents and reductive elimination of thiolates.

The frozen solution ESR spectra of this class of clusters showed signals in $g \approx 2$ and $g \approx$ 4-5 regions at low temperature (<20 K) condition.[70d] The signals in the former region are also characteristic in Fd^{red},[71] and additionally at least one Fd from *Bacillus polymyxa* exhibits a signal at $g \approx 4.3$ ascribed to higher spin state.[71a] These signals in two different regions are interpreted as a result of physical mixtures of S = 1/2 and 3/2 states. Mössbauer spectra of the clusters are nearly featureless but imply that inequivalence of Fe subsites is intrinsic property to $[Fe_4S_4]^+$ clusters.[70a]

1.3.4. $[Fe_4S_4]^0$ Clusters

The aforementioned MoFe protein reductase, NifH, is the only known $[Fe_4S_4]$ enzyme which can be reduced to $[Fe_4S_4]^0$ state by the strong reductants Ti^{3+}(citrate).[72] Likewise, this state was electrochemically detected as $[Fe_4S_4]^+/[Fe_4S_4]^0$ redox couple in the measurements of $[Fe_4S_4(SR)_4]^{2-}$.[73] Although $[Fe_4S_4(SR)_4]^{4-}$ has not been isolated, $[Fe_4S_4]^0$ clusters were synthesized by using an appropriate ligand, PR_3 (R = Cy, ^{i}Pr, and ^{t}Bu),[74] $^-$CN,[75] or a N-heterocyclic carbene (NHC).[76]

When phosphines were used, $[Fe_4S_4]^0$ core was afforded from the reduction of $[Fe_4S_4(PR_3)_4]^+$ by sodium acenaphthylenide or potassium benzophenone ketyl. Formally, this reaction gives the corresponding $[Fe_4S_4]^0$ cluster, but owing to spontaneous elimination of phosphines the isolated products were di- or tetracubane clusters (Scheme 1.4). These core structures depend on the phosphine substituents, as are $[Fe_4S_4(PCy_3)_3]_2$ and $[Fe_4S_4(PR_3)_2]_4$ (R = ^{i}Pr and ^{t}Bu) of which each cubane core is

Scheme 1.4.

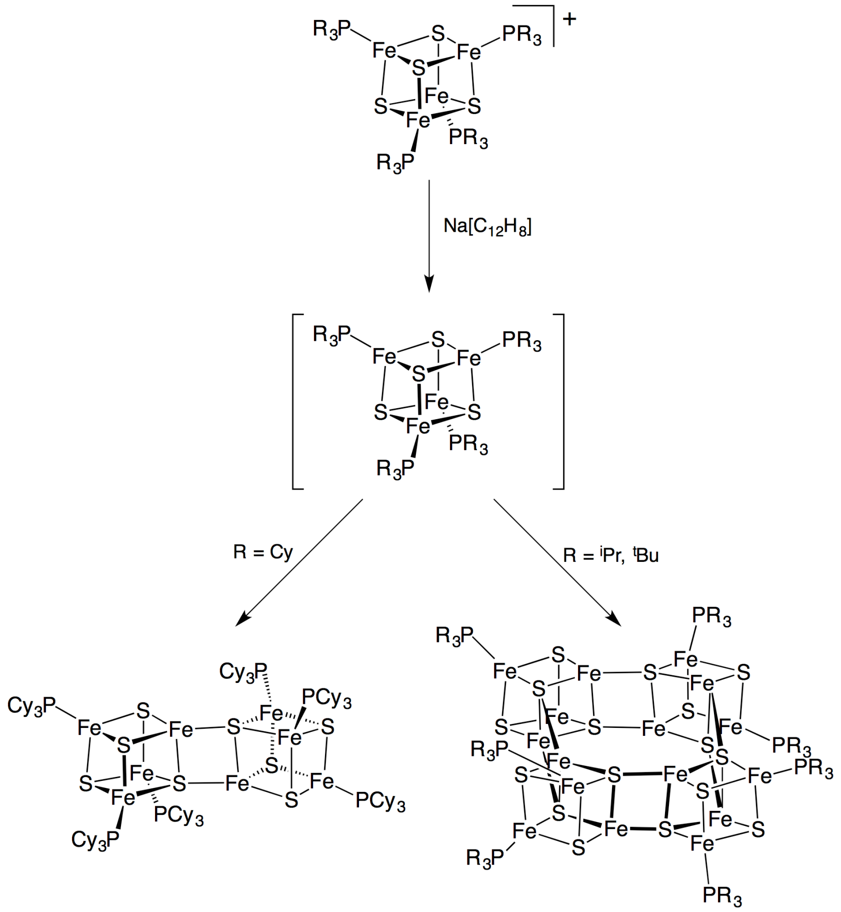

directly linked through Fe-S bonds.

The first monocubane $[Fe_4S_4]^0$ cluster $[Fe_4S_4(CN)_4]^{4-}$ was prepared by the ligand substitution and the reduction of $[Fe_4S_4(P^iPr_3)_4]^+$.[75] The key factor to inhibit spontaneous ligand elimination is π acidity of cyanide ligands. The back-donation from electron-rich iron centers strengthens the interaction between iron and cyanide.

On the other hand, strong electron donor can also stabilize $[Fe_4S_4]^0$ core. The NHC-bound cluster $[Fe_4S_4(^iPr_2NHCMe_2)_4]$ ($^iPr_2NHCMe_2$ = 1,3-diisopropyl-4,5-dimethylimidazol-2-ylidene) was synthesized by the cleavage of dicubane cluster

$[Fe_4S_4(^iPr_2NHCMe_2)_3]_2$ derived from polycubanes having P^iPr_3 (eq. 1.12), or self-assembly reaction with a sufficient amount of the carbene (eq. 1.13).

$$[Fe_4S_4(^iPr_2NHCMe_2)_3]_2 + 2\,^iPr_2NHCMe_2 \rightarrow 2\,[Fe_4S_4(^iPr_2NHCMe_2)_4] \quad \textbf{(1.12)}$$

$$4FeCl_2(P^iPr_3)_2 + 4\,(Me_3Si)_2S + 4\,^iPr_2NHCMe_2 \\ \rightarrow [Fe_4S_4(^iPr_2NHCMe_2)_4] + 8Me_3SiCl + 8P^iPr_3 \quad \textbf{(1.13)}$$

NHC is generally known as a ligand that is not only strong σ-donor but variable π-acceptor.[77] In this case, perhaps the latter property is suited for the isolation of monocubane cluster.

To assess the electronic structure, zero-field Mössbauer spectra of $[Fe_4S_4(CN)_4]^{4-}$ and $[Fe_4S_4(^iPr_2NHCMe_2)_4]$ were measured.[75, 76] The spectra fit to two quadrupole doublets in an intensity ratio of 3:1, though rational interpretation has not been presented.

As an unusual example, $[Fe_4S_4(NO)_4]$ has been synthesized by the self-assembly of $Hg[Fe(CO)_3(NO)]_2$ with elemental sulfur.[78] This cluster can be reduced to the mono- and dianion state electrochemically, and the monoanion $[Fe_4S_4(NO)_4]^-$ was also isolated.[79] It is quite difficult to estimate a precise oxidation state of $[Fe_4S_4]$ core because of the variability for the ionic description of NO ligand. However, since the ligands have linear configuration in the crystal structure, these were interpreted as three-electron donor.

1.3.5. [Fe$_4$S$_4$] Core Transformations

On one hand, the core transformations of $[Fe_4S_4]$ clusters have been found in nature as shown above. On the other hand, the corresponding reactions of synthetic $[Fe_4S_4]$ clusters are rare.

Scheme 1.5.

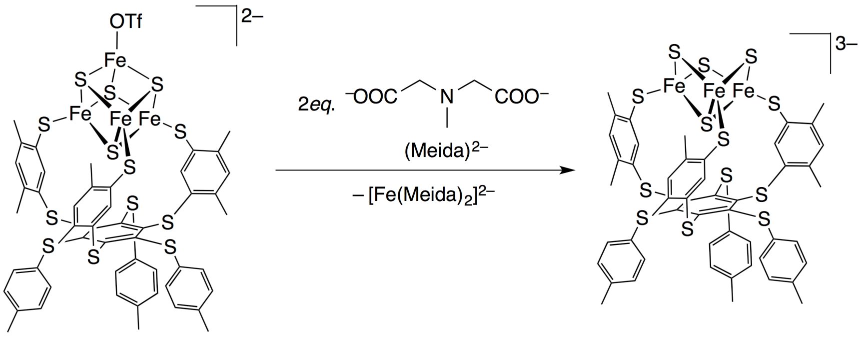

The aforestated trithiolate ligand was appeared to be a useful template to convert [Fe_4S_4] to cuboidal [Fe_3S_4] core. The site-differentiated [Fe_4S_4] cluster, [$Fe_4S_4(LS_3)(OTf)]^{2-}$ [LS_3 = 1,3,5-tris((4,6-dimethyl-3-mercaptophenyl)thio)-2,4,6-tris-(*p*-tolylthio)benzenate], reacted with 2 equiv of *N*-methylimidodiacetate (Meida) to form $[Fe_3S_4(LS_3)]^{3-}$ and $[Fe(Meida)_2]^{2-}$ (Scheme 1.5).[67a, 80] The afforded [Fe_3S_4] cluster not only reproduced [Fe_4S_4] core by the reaction with $[FeCl_4]^{2-}$, but formed a series of [MFe_3S_4] (M = Ti, Co, Ni, Cu, Mo, Pd, Ag, W, and Pt) clusters by the addition of suitable complexes.[81]

Also for $[Fe_4S_4X_4]^{2-}$ (X = halides), several core transformations have been reported. The oxidation of $[Fe_4S_4X_4]^{2-}$ (X = Cl, Br) with $[Cp_2Fe]^+$ afforded "prismane" cluster $[Fe_6S_6X_6]^{2-}$ quantitatively (Scheme 1.6, left).[82] The core recovery from [Fe_6S_6] cluster occurred by the treatment of $[Fe_6S_6Cl_6]^{2-}$ with excess X^- or heating the solution of $[Fe_6S_6Cl_6]^{3-}$ up to around 80°C.[83] Besides, the treatment of $[Fe_4S_4X_4]^{2-}$ (X = Cl, Br) with 2 equiv of $FeX_2(PEt_3)_2$ led to the formation of the other "basket" [Fe_6S_6] cluster [$Fe_6S_6X_2(PEt_3)_4$] (Scheme 1.6, right).[84] In contrast to these, FNR protein-like transformation of [Fe_4S_4] to [Fe_2S_2] cluster has not been well described in literature.

In a different way, desulfurization of an [Fe_4S_4] core has been reported by Holm et al.[85] The reaction of $[Fe_4S_4(NO)_4]$ with PPh_3 resulted in the formation of the cuboidal $[Fe_4S_3]$ cluster $[Fe_4S_3(NO)_4(PPh_3)_3]$ (Scheme 1.7). The removed sulfur was transformed into phosphine sulfide ($S{=}PPh_3$), and hence the reduction of Fe-S core simultaneously occurred.

Since $[Fe_4S_4]$ core is one of the most thermodynamically stable structures in Fe-S clusters, transformations of this core requires strategies to give meta-stable clusters, that is, the incorporation of ancillary ligand and the selection of the unstable oxidation state of $[Fe_4S_4]$ core. In particular, the latter approach is also employed in biological $[Fe_4S_4]$ core transformations as mentioned in 1.2.3.

Scheme 1.6.

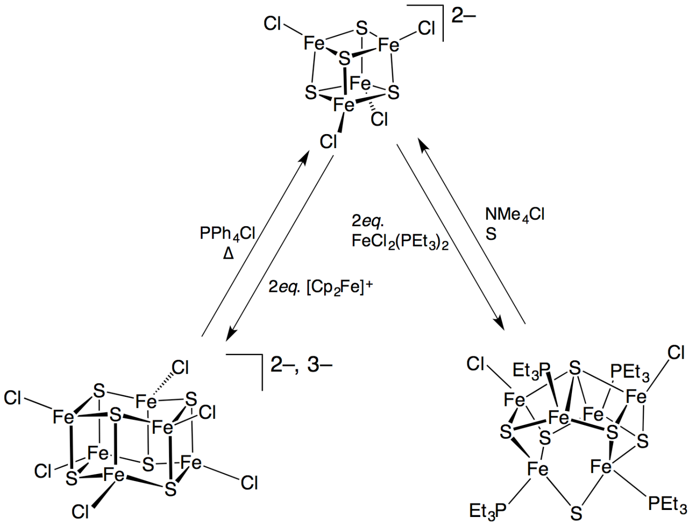

Scheme 1.7.

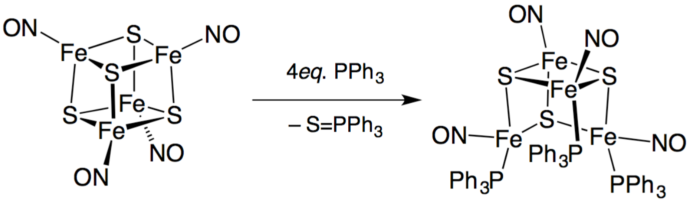

1.3.6. Section Conclusions

The investigation of synthetic [Fe_4S_4] clusters has shed light on their basic physical properties and reactivity, and contributed to give a better understanding on biological clusters.

So far, the model chemistry of [Fe_4S_4] clusters have been developed with a central focus on the clusters having $[Fe_4S_4]^{2+}$ oxidation state because of the stability and the established route to derivatives. However, since the biologically *active* and *reactive* states of [Fe_4S_4] clusters are not the resting $[Fe_4S_4]^{2+}$ state in many cases, more development of model chemistry on these unusual states is clearly required. Additionally, the trithiolate ligands are certainly useful to synthesize a series of {3:1} site-differentiated models, but the isolated clusters are still scarce. In other words, there is room for improvement in synthetic methodology of this type of clusters.

1.4. Outlook of the Thesis

As long as thiolate ligands are introduced in self-assembly reaction, the thermodynamically stable oxidation state of $[Fe_4S_4]$ clusters is, in most cases, $[Fe_4S_4]^{2+}$. On the other hand, the author's group has reported the synthesis of $[Fe_4S_4\{N(SiMe_3)_2\}_4]$ having highly oxidized $[Fe_4S_4]^{4+}$ core.[86] This unusual oxidation state is stabilized by strong electron donation from basic amide ligands. Using this cluster as a precursor, the author describes projects grouped into two parts in the following chapters: (1) replacement of the ligands bound to $[Fe_4S_4]$ core (Chapter 2-4), and (2) transformation reactions of the $[Fe_4S_4]$ core (Chapter 5 and 6).

In Chapter 2, a work on the synthesis of [3:1] site-differentiated $[Fe_4S_4]$ clusters modeling $[Fe_4S_4(Cys)_3(His)]$ in hydrogenases and $[Fe_4S_4]^{3+}$ HiPIP^{ox} model is reported. In this work, we found that thiolate ligands bound to highly oxidized $[Fe_4S_4]$ cluster is oxidized generating disulfide (RS—SR), and this reaction can be applied to the synthesis of [3:1] site-differentiated clusters. Moreover, $[Fe_4S_4\{N(SiMe_3)_2\}_4]^-$ derived from the reduction of $[Fe_4S_4\{N(SiMe_3)_2\}_4]$ was turned out to be a good precursor for the synthesis of the second isolated model of HiPIP^{ox}.

In Chapter 3, we developed the work on the HiPIP^{ox} model to a broader scope. The discovery of easy-to-access synthetic pathway of $[Fe_4S_4]^{3+}$ clusters enabled us to investigate the properties of these clusters in a systematic manner. The experimental and electrochemical results revealed that the more oxidized $[Fe_4S_4]$ core than $[Fe_4S_4]^{2+}$ state can be stabilized by bulky substituents. The relevance between the synthetic clusters and those in HiPIP is also discussed.

Chapter 4 focuses on the application of our new synthetic methodology to link a metal complex with a [Fe_4S_4] cluster. The combination of reductive elimination of thiolate ligand and introduction of a metal thiolate complex led to the formation of the unprecedented [Fe-Fe_4S_4] cluster, which consists of an [Fe_4S_4] cluster bridged by a monodentate thiolate with an Fe complex.

Chapter 5 presents a core transformation of [$Fe_4S_4\{N(SiMe_3)_4\}_4$] with alkyl phosphines, leading to the formation of [Fe_8S_7] cluster relevant to P-cluster in MoFe protein. The key point of this reaction is desulfurization from the highly oxidized [Fe_4S_4] core, which induces a reductive fusion of Fe-S core. This reaction is indicative of the relevance to the process of P-cluster maturation, since this process is also proposed to include the reductive fusion of two [Fe_4S_4]-like clusters.

In Chapter 6, the instability of highly oxidized [Fe_4S_4] core is examined further. Surprisingly, the $[Fe_4S_4]^{4+}$ core can be split into two [Fe_2S_2] cores in the presence of excess pyridine or derivatives. This reaction was turned out to be reversible, and thermodynamic parameters were determined from NMR experiments. The results imply that the unstable $[Fe_4S_4]^{4+}$ state may be produced during the deconstruction of [Fe_4S_4] clusters observed such as in FNR protein.

References and Note

[1] (a) Barras, F.; Loiseau, L.; Py, B. *Adv. Microb. Physiol.* **2005**, *50*, 41–101. (b) Rouault, T. A.; Tong, W. H. *Trends Genet.* **2008**, *24*, 398–407. (c) Xu, X. M.; Møller, S. G. *ChemBioChem* **2008**, *9*, 2355–2362. (d) Sheftel, A.; Stehling, O.; Lill, R. *Trends Endocrinol. Metab.* **2010**, *21*, 302–314. (e) Py, B.; Barras, F. *Nat. Rev. Microbiol.* **2010**, *8*, 436–446. (f) Roche, B.; Aussel, L.; Ezraty, B.; Mandin, P.; Py, B.; Barras, F. *Biochim. Biophys. Acta* **2013**, *1827*, 455–469.

[2] Mortenson, L. E.; Valentine, R. C.; Carnahan, J. E. *Biochem. Biophys. Res. Commun.* **1962**, *7*, 448–452.

[3] Frazzon, J. *Curr. Opin. Chem. Biol.* **2003**, *7*, 166–173.

[4] (a) Holm, R. H.; Kennepohl, P.; Solomon, E. I. *Chem. Rev.* **1996**, 96, 2239–2314. (b) Beinert, H.; Holm, R. H.; Münck, E. *Science* **1997**, 277, 653–659. (c) Beinert, H. *J. Biol. Inorg. Chem.* **2000**, 5, 2–15. (d) Johnson, D. C.; Dean, D. R.; Smith, A. D.; Johnson, M. K. *Annu. Rev. Biochem.* **2005**, 74, 247–281.

[5] White, M. F.; Dillingham, M. S. *Curr. Opin. Struct. Biol.* **2012**, 22, 94–100.

[6] Reports on crystal structures of Fd, see: (a) Sieker, L. C.; Adman, E.; Jensen, L. H. *Nature* **1972**, *235*, 40–42. (b) Fukuyama, K.; Nagahara, Y.; Tsukihara, T.; Katsube, Y.; Hase, T.; Matsubara, H. *J. Mol. Biol.* **1988**, *199*, 183–193. (c) Dauter, Z.; Wilson, K. S.; Sieker, L. C.; Meyer, J.; Moulis, J. M. *Biochemistry* **1997**, *36*, 16065–16073.

[7] Reports on crystal structures of HiPIP, see: (a) Carter, C. W.; Kraut, J.; Freer, S. T.; Alden, R. A.; Sieker, L. C.; Adman, E.; Jensen, L. H. *Proc. Natl. Acad. Sci. U.S.A.* **1972**, *69*, 3526–3529. (b) Rayment, I.; Wesenberg, G.; Meyer, T. E.; Cusanovich, M. A.;

Holden, H. M. *J. Mol. Biol.* **1992**, *228*, 672–686. (c) González, A.; Benini, S.; Ciurli, S. *Acta Crystallogr. D Biol. Crystallogr.* **2003**, *59*, 1582–1588. (d) Stelter, M.; Melo, A. M. P.; Hreggvidsson, G. O.; Hjorleifsdottir, S.; Saraiva, L. M.; Teixeira, M.; Archer, M. *J Biol Inorg Chem* **2009**, *15*, 303–313.

[8] (a) Meyer, T. E.; Przyshecki, C. T.; Watkins, J. A.; Bhattacharyya, A.; Simondsen, R. P.; Cusanovich, M. A.; Tollin, G. *Proc. Natl. Acad. Sci. U.S.A.* **1983**, 80, 6740-6744. (b) Heering, H. A.; Bulsink, Y. B. M.; Hagen, W. R.; Meyer, T. E. *Biochemistry*, **1995**, 34, 14675-14686.

[9] Hochkoeppler, A.; Ciurli, S.; Venturoli, G.; Zannoni, D. *FEBS Lett.* **1995**, *357*, 70–74.

[10] Nogi, T.; Fathir, I.; Kobayashi, M.; Nozawa, T.; Miki, K. *Proc. Natl. Acad. Sci. U.S.A.* **2000**, *97*, 13561–13566.

[11] Fukuyama, K. *Handbook of Metalloproteins*; John Wiley & Sons, Ltd: West Sussex, England, 2001; Vol 1, pp 543-552.

[12] (a) Van Driessche, G.; Vandenberghe, I.; Devreese, B.; Samyn, B.; Meyer, T. E.; Leigh, R.; Cusanovich, M. A.; Bartsch, R. G.; Fischer, U.; Van Beeumen, J. J. *J. Mol. Evol.* **2003**, *57*, 181–199. (b) Stelter, M.; Melo, A. M. P.; Hreggvidsson, G. O.; Hjorleifsdottir, S.; Saraiva, L. M.; Teixeira, M.; Archer, M. *J. Biol. Inorg. Chem.* **2009**, *15*, 303–313.

[13] (a) Agarwal, A.; Li, D.; Cowan, J. A. *Proc. Natl. Acad. Sci. U.S.A.* **1995**, *92*, 9440–9444. (b) Jia, Z.; Liu, Q.; Zhang, X.; Mo, H.; Wang, Y.; Chen, Q.; Liu, Y. *J. Microbiol. Biotechnol.* **2010**, *20*, 294–300.

[14] Li, D.; Agarwal, A.; Cowan, J. A. *Inorg. Chem.* **1996**, *35*, 1121–1125.

[15] Dey, A.; Jenney, F. E.; Adams, M. W. W.; Babini, E.; Takahashi, Y.; Fukuyama, K.; Hodgson, K. O.; Hedman, B.; Solomon, E. I. *Science* **2007**, *318*, 1464–1468.

[16] Reports on crystal structures of [NiFe] hydrogenase, see: (a) Volbeda, A.; Charon, M. H.; Piras, C.; Hatchikian, E. C.; Frey, M.; Fontecilla-Camps, J. C. *Nature* **1995**, *373*, 580-587. (b) Volbeda, A.; Garcin, E.; Piras, C.; L. de Lacey, A.; Fernández, V. M.; Hatchikian, E. C.; Frey, M.; Fontecilla-Camps, J. C. *J. Am. Chem. Soc.* **1996**, *118*, 12989-12996. (c) Higuchi, Y.; Yagi, T.; Yasuoka, N. *Structure* **1997**, *5*, 1671-1680. (d) Rousset, M.; Montet, Y.; Guigliarelli, B.; Forget, N.; Asso, M.; Bertrand, P.; Fontecilla-Camps, J. C.; Hatchikian, E. C. *Proc. Natl. Acad. Sci. U.S.A.* **1998**, *95*, 11625-11630. (e) Higuchi, Y.; Ogata, H.; Miki, K.; Yasuoka, N.; Yagi, T. *Structure* **1999**, *7*, 549-556. (f) Garcin, E.; Vernede, X; Hatchikian, E. C.; Volbeda, A.; Frey, M.; Fontecilla-Camps, J. C. *Structure* **1999**, *7*, 557-566. (g) Matias, M. P.; Soares, C. M.; Saraiva, L. M.; Coelho, R.; Morais, J.; Gall, J. L.; Carrondo, M. A. *J. Biol. Inorg. Chem.* **2001**, *6*, 63-81. (h) Volbeda, A.; Martin, L.; Cavazza, C.; Matho, M.; Faber, B. W.; Roseboom, W.; Albracht, S. P. J.; Garcin, E.; Rousset, M.; Fontecilla-Camps, J. C. *J. Biol. Inorg. Chem.* **2005**, *10*, 239-249. (i) Ogata, H.; Hirota, S.; Nakahara, A.; Komori, H.; Shibata, N.; Kato, T.; Kano, K.; Higuchi, Y. *Structure* **2005**, *13*, 1635-1642.

[17] Reports on crystal structures of [FeFe] hydrogenase from *Clostridium pasteurianum*, see: (a) Peters, J. W.; Lanzilotta, W. N.; Lemon, B. J.; Seefeldt, L. C. *Science* **1998**, *282*, 1853-1858. (b) Lemon, B. J.; Peters, J. W. *Biochemistry* **1999**, *38*, 12969-12973. (c) Pandey, A. S.; Harris, T. V.; Giles, L. J.; Peters, J. W.; Szilagyi, R. K. *J. Am. Chem. Soc.* **2008**, *130*, 4533-4540.

[18] Dementin, S.; Belle, V.; Bertrand, P.; Guigliarelli, B.; Adryanczyk-Perrier, G.; de Lacey, A. L.; Fernandez, V. M.; Rousset, M.; Léger, C. *J. Am. Chem. Soc.* **2006**, *128*, 5209–5218.

[19] (a) Teixeira, M.; Moura, I.; Xavier, A. V.; Moura, J. J.; LeGall, J.; DerVartanian, D. V.; Peck, H. D., Jr; Huynh, B. H. *J. Biol. Chem.* **1989**, *264*, 16435–16450. (b) Rousset, M.; Montet, Y.; Guigliarelli, B.; Forget, N.; Asso, M.; Bertrand, P.; Fontecilla-Camps, J. C.; Hatchikian, E. C. *Proc. Nat. Acad. Sci. U.S.A.* **1998**, *95*, 11625–11630.

[20] Adams, M. W. W. *J. Biol. Chem.* **1987**, *262*, 15054–15061.

[21] (a) Flint, D. H.; Allen, R. M. *Chem. Rev.* **1996**, *96*, 2315–2334. (b) Beinert, H.; Kennedy, M. C.; Stout, C. D. *Chem. Rev.* **1996**, *96*, 2335–2373.

[22] (a) Lauble, H.; Kennedy, M. C.; Beinert, H.; Stout, C. D. *Biochemistry* **1992**, *31*, 2735–2748. (b) Lloyd, S. J.; Lauble, H.; Prasad, G. S.; Stout, C. D. *Protein Science* **1999**, *8*, 2655–2662.

[23] (a) Moulis, J. M.; Davasse, V.; Golinelli, M.-P.; Meyer, J.; Quinkal, I. *J. Biol. Inorg. Chem.* **1996**, *1*, 2–14. (b) Imlay, J. A. *Mol. Microbiol.* **2006**, *59*, 1073–1082.

[24] Beinert, H.; Thomson, A. J. *Arch. Biochem. Biophys.* **1983**, *222*, 333–361.

[25] Robbins, A. H.; Stout, C. D. *Proc. Nat. Acad. Sci. U.S.A.* **1989**, *86*, 3639–3643.

[26] Kennedy, M. C.; Emptage, M. H.; Dreyer, J. L.; Beinert, H. *J. Biol. Chem.* **1983**, *258*, 11098–11105.

[27] (a) Beinert, H.; Kennedy, M. C. *FASEB J.* **1993**, *7*, 1442–1449. (b) Eisenstein, R. S. *Annu. Rev. Microbiol.* **2000**, *20*, 627–662. (c) Tong, W.-H.; Rouault, T. A. *Biometals* **2007**, *20*, 549–564. (d) Matasova, L. V.; Popova, T. N. *Biochemistry Moscow* **2008**, *73*,

957–964.

[28] Henderson, B. R. *BioEssays* **1996**, *18*, 739–746.

[29] Recent reviews on radical SAM reductase superfamily, see: (a) Roach, P. L. *Curr. Opin. Chem. Biol.* **2011**, *15*, 267–275. (b) Vey, J. L.; Drennan, C. L. *Chem. Rev.* **2011**, *111*, 2487–2506. (c) Dowling, D. P.; Vey, J. L.; Croft, A. K.; Drennan, C. L. *Biochim. Biophys. Acta* **2012**, *1824*, 1178–1195. (d) Lanz, N. D.; Booker, S. J. *Biochim. Biophys. Acta* **2012**, *1824*, 1196–1212.

[30] Vey, J. L.; Yang, J.; Li, M.; Broderick, W. E.; Broderick, J. B.; Drennan, C. L. *Proc. Natl. Acad. Sci. U.S.A.* **2008**, *105*, 16137–16141.

[31] (a) Cosper, N. J.; Booker, S. J.; Ruzicka, F.; Frey, P. A.; Scott, R. A. *Biochemistry* **2000**, *39*, 15668–15673. (b) Jarrett, J. T. *Curr. Opin. Chem. Biol.* **2003**, *7*, 174–182.

[32] Wang, S. C.; Frey, P. A. *Biochemistry* **2007**, *46*, 12889–12895.

[33] Review on metalloproteins containing metal sulfur clusters, see: Fontecilla-Camps, J. C.; Amara, P.; Cavazza, C.; Nicolet, Y.; Volbeda, A. *Nature* **2009**, *460*, 814–822.

[34] Crane, B. R.; Siegel, L. M.; Getzoff, E. D. *Science* **1995**, *270*, 59–67.

[35] (a) Crane, B. R.; Siegel, L. M.; Getzoff, E. D. *Science* **1995**, *270*, 59–67. (b) Crane, B. R.; Siegel, L. M.; Getzoff, E. D. *Biochemistry* **1997**, *36*, 12101–12119. (c) Nakayama, M.; Akashi, T.; Hase, T. *J. Inorg. Biochem.* **2000**, *82*, 27–32. (d) Swamy, U.; Wang, M.; Tripathy, J. N.; Kim, S.-K.; Hirasawa, M.; Knaff, D. B.; Allen, J. P. *Biochemistry* **2005**, *44*, 16054–16063. (e) Smith, K. W.; Stroupe, M. E. *Biochemistry* **2012**, *51*, 9857–9868.

[36] Christner, J. A.; Janick, P. A.; Siegel, L. M.; Münck, E. *J. Biol. Chem.* **1983**, *258*, 11157–11164.

[37] Siegel, L. M.; Rueger, D. C.; Barber, M. J.; Krueger, R. J.; Orme-Johnson, N. R.; Orme-Johnson, W. H. *J. Biol. Chem.* **1982**, *257*, 6343–6350.

[38] (a) Ragsdale, S. W. *J. Inorg. Biochem.* **2007**, *101*, 1657–1666. (b) Ragsdale, S. W.; Pierce, E. *Biochim. Biophys. Acta* **2008**, *1784*, 1873–1898.

[39] (a) Doukov, T. I.; Iverson, T. M.; Seravail, J.; Ragsdale, S. W.; Drennan, C. L. *Science* **2002**, *298*, 567–572. (b) Darnault, C.; Volbeda, A.; Kim, E. J.; Legrand, P.; Vernède, X.; Lindahl, P. A.; Fontecilla-Camps, J. C. *Nat. Struct. Biol.* **2003**, *10*, 271–279. (c) Volbeda, A.; Fontecilla-Camps, J. C. *J. Biol. Inorg. Chem.* **2004**, *9*, 525–532.

[40] Recent reviews on [FeFe] hydrogenase, see: (a) Fontecilla-Camps, J. C.; Volbeda, A.; Cavazza, C.; Nicolet, Y. *Chem. Rev.* **2007**, *107*, 4273–4303. (b) Capon, J.-F.; Gloaguen, F.; Pétillon, F. Y.; Schollhammer, P.; Talarmin, J. *Coord. Chem. Rev.* **2009**, *253*, 1476–1494. (c) Mulder, D. W.; Shepard, E. M.; Meuser, J. E.; Joshi, N.; King, P. W.; Posewitz, M. C.; Broderick, J. B.; Peters, J. W. *Structure* **2011**, *19*, 1038–1052. (d) Winkler, M.; Esselborn, J.; Happe, T. *Biochim. Biophys. Acta* **2013**, *1827*, 974–985.

[41] Silakov, A.; Wenk, B.; Reijerse, E.; Lubitz, W. *Phys. Chem. Chem. Phys.* **2009**, *11*, 6592–6599.

[42] Berggren, G.; Adamska, A.; Lambertz, C.; Simmons, T. R.; Esselborn, J.; Atta, M.; Gambarelli, S.; Mouesca, J. M.; Reijerse, E.; Lubitz, W.; Happe, T.; Artero, V.; Fontecave, M. *Nature* **2013**, *499*, 66–69.

[43] (a) Einsle, O.; Tezcan, F. A.; Andrade, S. L. A.; Schmid, B.; Yoshida, M.; Howard, J. B.; Rees, D. C. *Science* **2002**, *297*, 1696–1700. (b) Spatzal, T.; Aksoyoglu, M.; Zhang, L.; Andrade, S. L. A.; Schleicher, E.; Weber, S.; Rees, D. C.; Einsle, O. *Science* **2011**, *334*,

940–940. (c) Lancaster, K. M.; Roemelt, M.; Ettenhuber, P.; Hu, Y.; Ribbe, M. W.; Neese, F.; Bergmann, U.; DeBeer, S. *Science* **2011**, *334*, 974–977.

[44] Hu, Y.; Ribbe, M. W. *J. Biol. Chem.* **2013**, *288*, 13173–13177.

[45] (a) Hu, Y.; Ribbe, M. W. *Microbiol. Mol. Biol. Rev.* **2011**, *75*, 664–677. (b) Hu, Y.; Ribbe, M. W. *Biochim. Biophys. Acta* **2013**, *1827*, 1112–1122.

[46] Ribbe, M. W.; Hu, Y.; Guo, M.; Schmid, B.; Burgess, B. K. *J. Biol. Chem.* **2002**, *277*, 23469–23476.

[47] (a) Corbett, M. C.; Hu, Y.; Naderi, F.; Ribbe, M. W.; Hedman, B.; Hodgson, K. O. *J. Biol. Chem.* **2004**, *279*, 28276–28282. (b) Cotton, M. S.; Rupnik, K.; Broach, R. B.; Hu, Y.; Fay, A. W.; Ribbe, M. W.; Hales, B. J. *J. Am. Chem. Soc.* **2009**, *131*, 4558–4559.

[48] Lee, C. C.; Blank, M. A.; Fay, A. W.; Yoshizawa, J. M.; Hu, Y.; Hodgson, K. O.; Hedman, B.; Ribbe, M. W. *Proc. Nat. Acad. Sci. U.S.A.* **2009**, *106*, 18474–18478.

[49] Reviews on sensor-regulators including Fe-S clusters, see: (a) Kiley, P. J.; Beinert, H. *FEMS Microbiol. Rev.* **1998**, *22*, 341–352. (b) Kiley, P. J.; Beinert, H. *Curr. Opin. Microbiol.* **2003**, *6*, 181–185. (c) Green, J.; Paget, M. S. *Nat. Rev. Microbiol.* **2004**, *2*, 954–966. (d) Fleischhacker, A. S.; Kiley, P. J. *Curr. Opin. Chem. Biol.* **2011**, *15*, 335–341. (e) Crack, J. C.; Green, J.; Thomson, A. J.; Le Brun, N. E. *Curr. Opin. Chem. Biol.* **2012**, *16*, 35–44. (f) Unden, G.; Nilkens, S.; Singenstreu, M. *Dalton Trans.* **2013**, *42*, 3082–3087.

[50] Crack, J. C.; Green, J.; Cheesman, M. R.; Le Brun, N. E.; Thomson, A. J. *Proc. Nat. Acad. Sci. U.S.A.* **2007**, *104*, 2092–2097.

[51] Popescu, C.; Bates, D. M.; Beinert, H.; Münck, E.; Kiley, P. J. *Proc. Nat. Acad. Sci.*

U.S.A. **1998**, *95*, 13431–13435.

[52] (a) Lazazzera, B. A.; Beinert, H.; Khoroshilova, N.; Kennedy, M. C.; Kiley, P. J. *J. Biol. Chem.* **1996**, *271*, 2762–2768. (b) Crack, J.; Green, J.; Thomson, A. J. *J. Biol. Chem.* **2004**, *279*, 9278–9286.

[53] Zhang, B.; Crack, J. C.; Subramanian, S.; Green, J.; Thomson, A. J.; Le Brun, N. E.; Johnson, M. K. *Proc. Nat. Acad. Sci. U.S.A.* **2012**, *109*, 15734–15739.

[54] Crack, J. C.; Gaskell, A. A.; Green, J.; Cheesman, M. R.; Le Brun, N. E.; Thomson, A. J. *J. Am. Chem. Soc.* **2008**, *130*, 1749–1758.

[55] Herskovitz, T.; Averill, B. A.; Holm, R. H.; Ibers, J. A.; Phillips, W. D.; Weiher, J. F. *Proc. Natl. Acad. Sci. U.S.A.* **1972**, *69*, 2437–2441.

[56] (a) Ogino, H.; Inomata, S.; Tobita, H. *Chem. Rev.* **1998**, *98*, 2093–2122. (b) Hidai, M.; Kuwata, S.; Mizobe, Y. *Acc. Chem. Res.* **2000**, *33*, 46–52. (c) Seino, H.; Hidai, M. *Chem. Sci.* **2011**, *2*, 847-857.

[57] Rao, P. V.; Holm, R. H. *Chem. Rev.* **2004**, *104*, 527–560.

[58] DePamphilis, BV; Averill, B. A.; Herskovitz, T.; Que, L., Jr; Holm, R. H. *J. Am. Chem. Soc.* **1974**, *96*, 4159–4167.

[59] (a) Mascharak, P. K.; Hagen, K. S.; Spence, J. T.; Holm, R. H. *Inorg. Chim. Acta* **1983**, *80*, 157–170. (b) Ohno, R.; Ueyama, N.; Nakamura, A. *Chem. Lett.* **1989**, *18*, 399–402. (c) Ohno, R.; Ueyama, N.; Nakamura, A. *Inorg. Chim. Acta* **1990**, *169*, 253–255. (d) Blonk, H. L.; Kievit, O.; Roth, E.; Jordanov, J.; Van der Linden, J.; Steggerda, J. J. *Inorg. Chem.* **1991**, *30*, 3231–3234.

[60] (a) Nakamoto, M.; Tanaka, K.; Tanaka, T. *J. Chem. Soc., Chem. Commun.* **1988**,

1422-1423. (b) Kambayashi, H.; Nakamoto, M.; Peng, S. M.; Nagao, H. *Chem. Lett.* **1992**, *21*, 919–922. (c) Kambayashi, H.; Nagao, H.; Tanaka, K.; Nakamoto, M.; Peng, S.-M. *Inorg. Chim. Acta* **1993**, *209*, 143–149.

[61] O'Sullivan, T.; Millar, M. M. *J. Am. Chem. Soc.* **1985**, *107*, 4096–4097.

[62] Papaefthymiou, V.; Millar, M. M.; Münck, E. *Inorg. Chem.* **1986**, *25*, 3010–3014.

[63] (a) Rius, G.; Lamotte, B. *J. Am. Chem. Soc.* **1989**, *111*, 2464–2469. (b) Mouesca, J.-M.; Rius, G.; Lamotte, B. *J. Am. Chem. Soc.* **1993**, *115*, 4714–4731.

[64] Hagen, K. S.; Reynolds, J. G.; Holm, R. H. *J. Am. Chem. Soc.* **1981**, *103*, 4054–4063.

[65] For example: (a) Que, L., Jr; Bobrik, M. A.; Ibers, J. A.; Holm, R. H. *J. Am. Chem. Soc.* **1974**, *96*, 4168–4178. (b) Ueyama, N.; Yamada, Y.; Okamura, T.-A.; Kimura, S.; Nakamura, A. *Inorg. Chem.* **1996**, *35*, 6473–6484.

[66] (a) Bobrik, M. A.; Hodgson, K. O.; Holm, R. H. *Inorg. Chem.* **1977**, *16*, 1851–1858. (b) Wong, G. B.; Bobrik, M. A.; Holm, R. H. *Inorg. Chem.* **1978**, *17*, 578–584.

[67] (a) Holm, R. H. *Pure Appl. Chem.* **1998**, *70*, 931–938. (b) van der Geer, E. P. L. Ph.D. Thesis, Universiteit Utrecht, March 2008.

[68] (a) Stack, T.; Holm, R. H. *J. Am. Chem. Soc.* **1988**, *110*, 2484–2494. (b) Ciurli, S.; Carrie, M.; Weigel, J. A.; Carney, M. J.; Stack, T.; Papaefthymiou, G. C.; Holm, R. H. *J. Am. Chem. Soc.* **1990**, *112*, 2654–2664. (c) Whitener, M. A.; Peng, G.; Holm, R. H. *Inorg. Chem.* **1991**, *30*, 2411–2417. (d) Weigel, J. A.; Holm, R. H. *J. Am. Chem. Soc.* **1991**, *113*, 4184–4191. (e) Cai, L.; Weigel, J. A.; Holm, R. H. *J. Am. Chem. Soc.* **1993**, *115*, 9289–9290. (f) Zhou, C.; Cai, L.; Holm, R. H. *Inorg. Chem.* **1996**, *35*, 2767–2772. (g) Walsdorff, C.; Saak, W.; Pohl, S. *J. Chem. Soc., Chem. Commun.* **1997**, 1857–1862.

(h) Milward, G. C.; Calderón, M. J.; Littlewood, P. B. *Nature* **2005**, *433*, 607–610. (i) van der Geer, E. P. L.; van Koten, G.; Klein Gebbink, R. J. M.; Hessen, B. *Inorg. Chem.* **2008**, *47*, 2849–2857. (j) van der Geer, E. P. L.; Li, Q.; Koten, G. V.; Klein Gebbink, R. J. M.; Hessen, B. *Inorg. Chim. Acta* **2008**, *361*, 1811–1818.

[69] (a) Stack, T.; Holm, R. H. *J. Am. Chem. Soc.* **1987**, *109*, 2546–2547. (b) Stack, T.; Holm, R. H. *J. Am. Chem. Soc.* **1988**, *110*, 2484–2494. (c) Zhou, C.; Holm, R. H. *Inorg. Chem.* **1997**, *36*, 4066–4077. (d) Walsdorff, C.; Saak, W.; Pohl, S. *J. Chem. Soc., Dalton Trans.* **1997**, 1857–1862. (e) Walsdorff, C.; Saak, W. *Chem. Commun.* **1997**, 1931–1932. (f) Rao, P. V.; Bhaduri, S.; Jiang, J.; Hong, D.; Holm, R. H. *J. Am. Chem. Soc.* **2005**, *127*, 1933–1945. (g) Panda, R.; Berlinguette, C. P.; Zhang, Y.; Holm, R. H. *J. Am. Chem. Soc.* **2005**, *127*, 11092–11101. (h) Sun, J.; Tessier, C.; Holm, R. H. *Inorg. Chem.* **2007**, *46*, 2691–2699. (i) Terada, T.; Wakimoto, T.; Nakamura, T.; Hirabayashi, K.; Tanaka, K.; Li, J.; Matsumoto, T.; Tatsumi, K. *Chem. Asian J.* **2012**, *7*, 920–929. (j) Terada, T.; Hirabayashi, K.; Liu, D.; Nakamura, T.; Wakimoto, T.; Matsumoto, T.; Tatsumi, K. *Inorg. Chem.* **2013**, *52*, 11997–12004.

[70] (a) Laskowski, E. J.; Frankel, R. B.; Gillum, W. O.; Papaefthymiou, G. C.; Renaud, J.; Ibers, J. A.; Holm, R. H. *J. Am. Chem. Soc.* **1978**, *100*, 5322–5337. (b) Stephan, D. W.; Papaefthymiou, G. C.; Frankel, R. B.; Holm, R. H. *Inorg. Chem.* **1983**, *22*, 1550–1557. (c) Hagen, K. S.; Watson, A. D.; Holm, R. H. *Inorg. Chem.* **1984**, *23*, 2984–2990. (d) Carney, M. J.; Papaefthymiou, G. C.; Spartalian, K.; Frankel, R. B.; Holm, R. H. *J. Am. Chem. Soc.* **1988**, *110*, 6084–6095. (e) Carney, M. J.; Papaefthymiou, G. C.; Frankel, R. B.; Holm, R. H. *Inorg. Chem.* **1989**, *28*, 1497–1503.

(f) Segal, B. M.; Hoveyda, H. R.; Holm, R. H. *Inorg. Chem.* **1998**, *37*, 3440–3443.

[71] (a) Shethna, Y. I.; Stombaugh, N. A.; Burris, R. H. *Biochem. Biophys. Res. Commun.* **1971**, *42*, 1108–1116. (b) Zubieta, J. A.; Mason, R.; Postgate, J. R. *Biochem. J.* **1973**, *133*, 851–854. (c) Strombaugh, N. A.; Burris, R. H.; Orme-Johnson, W. H. *J. Biol. Chem.* **1973**, *248*, 7951–7956. (d) Mullinger, R. N.; Cammack, R.; Rao, K. K.; Hall, D. O. *Biochem. J.* **1975**, *151*, 75–83. (e) Cammack, R.; Rao, K. K.; Hall, D. O.; Moura, J.; Xavier, A. V.; Bruschi, M.; Le Gall, J.; Deville, A.; Gayda, J.-P. *Biochim. Biophys. Acta* **1977**, *490*, 311–321.

[72] (a) Watt, G. D.; Reddy, K. *J. Inorg. Biochem.* **1994**, *53*, 281–294. (b) Angove, H. C.; Yoo, S. J.; Münck, E.; Burgess, B. K. *J. Biol. Chem.* **1998**, *273*, 26330–26337.

[73] (a) DePamphilis, BV; Averill, B. A.; Herskovitz, T.; Que, L., Jr; Holm, R. H. *J. Am. Chem. Soc.* **1974**, *96*, 4159–4167. (b) Cambray, J.; Lane, R. W.; Wedd, A. G.; Johnson, R. W.; Holm, R. H. *Inorg. Chem.* **1977**, *16*, 2565–2571. (c) Zhou, C.; Raebiger, J. W.; Segal, B. M.; Holm, R. H. *Inorg. Chim. Acta* **2000**, *300*, 892–902.

[74] (a) Goh, C.; Segal, B. M.; Huang, J.; Long, J. R.; Holm, R. H. *J. Am. Chem. Soc.* **1996**, *118*, 11844–11853. (b) Zhou, H.-C.; Holm, R. H. *Inorg. Chem.* **2003**, *42*, 11–21. (c) Deng, L.; Majumdar, A.; Lo, W.; Holm, R. H. *Inorg. Chem.* **2010**, *49*, 11118–11126.

[75] Scott, T. A.; Berlinguette, C. P.; Holm, R. H.; Zhou, H.-C. *Proc. Nat. Acad. Sci. U.S.A.* **2005**, *102*, 9741–9744.

[76] Deng, L.; Holm, R. H. *J. Am. Chem. Soc.* **2008**, *130*, 9878–9886.

[77] (a) Hu, X.; Castro-Rodriguez, I.; Olsen, K.; Meyer, K. *Organometallics* **2004**, *23*, 755–764. (b) Jacobsen, H.; Correa, A.; Costabile, C.; Cavallo, L. *J. Organomet. Chem.*

2006, *691*, 4350–4358. (c) Khramov, D. M.; Lynch, V. M.; Bielawski, C. W. *Organometallics* **2007**, *26*, 6042–6049. (d) Kausamo, A.; Tuononen, H. M.; Krahulic, K. E.; Roesler, R. *Inorg. Chem.* **2008**, *47*, 1145–1154.

[78] Gall, R. S.; Chu, C. T.-W.; Dahl, L. F. *J. Am. Chem. Soc.* **1974**, *96*, 4019–4023.

[79] Chu, C. T.-W.; Lo, F. Y.-K.; Dahl, L. F. *J. Am. Chem. Soc.* **1982**, *104*, 3409–3422.

[80] (a) Zhou, J.; Holm, R. H. *J. Am. Chem. Soc.* **1995**, *117*, 11353–11354. (b) Zhou, J.; Hu, Z.; Münck, E.; Holm, R. H. *J. Am. Chem. Soc.* **1996**, *118*, 1966–1980.

[81] (a) Zhou, J.; Raebiger, J. W.; Crawford, C. A.; Holm, R. H. *J. Am. Chem. Soc.* **1997**, *119*, 6242–6250. (b) Panda, R.; Zhang, Y.; McLauchlan, C. C.; Venkateswara Rao, P.; Tiago de Oliveira, F. A.; Münck, E.; Holm, R. H. *J. Am. Chem. Soc.* **2004**, *126*, 6448–6459. (c) Panda, R.; Berlinguette, C. P.; Zhang, Y.; Holm, R. H. *J. Am. Chem. Soc.* **2005**, *127*, 11092–11101. (d) Sun, J.; Tessier, C.; Holm, R. H. *Inorg. Chem.* **2007**, *46*, 2691–2699.

[82] Coucouvanis, D.; Kanatzidis, M. G.; Dunham, W. R.; Hagen, W. R. *J. Am. Chem. Soc.* **1984**, *106*, 7998–7999.

[83] Kanatzidis, M. G.; Hagen, W. R.; Dunham, W. R.; Lester, R. K.; Coucouvanis, D. *J. Am. Chem. Soc.* **1985**, *107*, 953–961.

[84] Snyder, B. S.; Holm, R. H. *Inorg. Chem.* **1988**, *27*, 2339–2347.

[85] (a) Scott, M. J.; Holm, R. H. *Angew. Chem. Int. Ed.* **1993**, *32*, 564–566. (b) Goh, C.; Holm, R. H. *Inorg. Chim. Acta* **1998**, *270*, 46–54.

[86] Ohki, Y.; Sunada, Y.; Tatsumi, K. *Chem. Lett.* **2005**, *34*, 172–173.

Chapter 2

Synthetic Analogues of [$Fe_4S_4(Cys)_3(His)$] in Hydrogenases and [$Fe_4S_4(Cys)_4$] in HiPIP Derived from All-Ferric $Fe_4S_4\{N(SiMe_3)_2\}_4$

This chapter is partly reproduced with permission from: Ohki, Y.; Tanifuji, K.; Yamada, N.; Imada, M.; Tajima, T.; Tatsumi, K. *Proc. Nat. Acad. Sci. U.S.A.* **2011**, *108,* 12635–12640.

2.1. Introduction

As reviewed in Chapter 1, biological [Fe_4S_4] clusters are usually bound to four cysteinyl thiolates (Cys) as can be seen in the high-potential iron-sulfur proteins (HiPIP) and widely distributed ferredoxins (Fd). These [Fe_4S_4] clusters are present in three oxidation states, $[Fe_4S_4]^{3+}$ (HiPIP^{ox}), $[Fe_4S_4]^{2+}$ (HiPIP^{red}/Fd^{ox}), and $[Fe_4S_4]^{+}$ (Fd^{red}). The $[Fe_4S_4]^0$ state has been suggested for the super-reduced state of the cluster in the Fe-protein of nitrogenase,[1] while no $[Fe_4S_4]^{4+}$ cluster has been found in proteins.

The influence of the ligands around the [Fe_4S_4] core on the cluster properties is an important issue. For Fd and HiPIP the formation of hydrogen bonds with water has been suggested to account for most of the difference between the redox potentials of HiPIP and Fd,[2] indicating the importance of hydrophobic shielding of the [Fe_4S_4] clusters in the more oxidized form. A different way to modulate the redox potentials is to replace the cysteinyl thiolates, as has been observed for the Rieske proteins featuring His-bound [Fe_2S_2] centers.[3] Some [Fe_4S_4] clusters carrying an N- or O-donor ligand and three Cys ligands are also known, for example the [Fe_4S_4(Cys)$_3$(His)] clusters (His = histidinyl imidazole) in [NiFe] and [FeFe] hydrogenases (Figure 2.1)[4, 5] and the [Fe_4S_4(Cys)$_3$(O-donor)] clusters in aconitase[6] and protochlorophyllide reductase.[7] However, only limited data are available to evaluate the effect of ligands on the redox properties of [Fe_4S_4] clusters.[4d, 8]

Thus synthetic analogues of [Fe_4S_4(Cys)$_3$(His)] clusters, with a (thiolate)$_3$(imidazole) ligand set, are required to elucidate the influence of histidine coordination. Although a number of synthetic [Fe_4S_4] clusters have been reported,

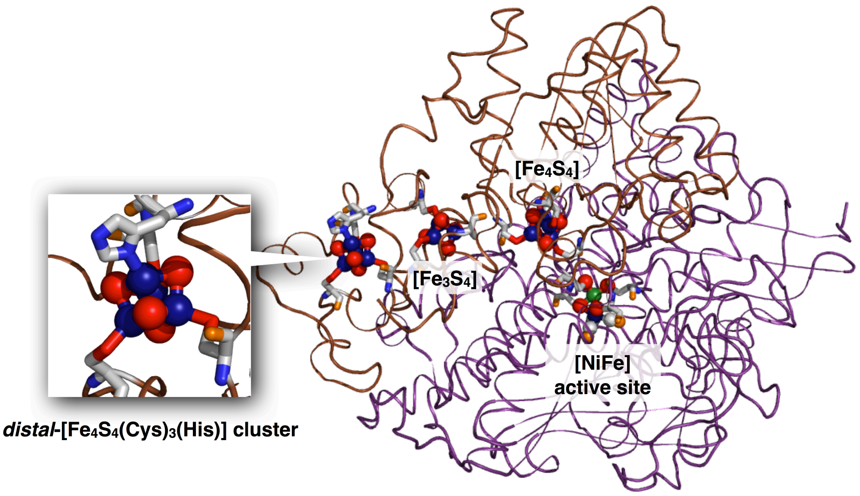

Figure 2.1. The iron-sulfur clusters in [NiFe] hydrogenases. The coordinates have been taken from the crystal data for the protein of *D. v. Miyazaki F* (PDB ID: 1WUL).[4i]

most of these are of the type $[Fe_4S_4(SR)_4]^{2-}$, which is in the $[Fe_4S_4]^{2+}$ ($HiPIP^{red}/Fd^{ox}$) oxidation state,[9] and the synthesis of other types such as analogues of $HiPIP^{ox}$ and $[Fe_4S_4(Cys)_3(His)]$ clusters remains difficult. There is only one isolated compound for the $[Fe_4S_4]^{3+}$ cluster modeling $HiPIP^{ox}$, $[Fe_4S_4(STip)_4]^{-}$ (Tip = 2,4,6-triisopropylphenyl), [10] which was prepared by chemical oxidation of $[Fe_4S_4(STip)_4]^{2-}$. As for $[Fe_4S_4(Cys)_3(His)]$ analogues, generation of $[Fe_4S_4(LS_3)(imidazole)]^{2-}$ [LS_3 = 1,3,5-tris((4,6-dimethyl-3-mercaptophenyl)thio)-2,4,6-tris(*p*-tolylthio)-benzenate] was inferred from the ^1H NMR spectrum of a mixture containing $[Fe_4S_4(LS_3)Cl]^{2-}$, excess imidazoles, and $NaBF_4$, [11] however isolation and detailed characterization of the imidazole-bound $[Fe_4S_4]$ cluster have not been accomplished.

We[12] and Lee *et al.*[13] have reported the synthesis of an all-ferric $[Fe_4S_4]^{4+}$ cluster carrying four amide ligands, $Fe_4S_4\{N(SiMe_3)_2\}_4$ (**1**). The $[Fe_4S_4]^{4+}$ oxidation state is unknown in proteins, as it has two less electrons than the $[Fe_4S_4]^{2+}$ state common for biological (and synthetic) [Fe_4S_4] clusters. The [Fe_4S_4]$^{4+}$ cluster **1** is susceptible to reduction, and the cyclic voltammetry of **1** in THF shows that the first reduction process at $E_{1/2} = 0.10$ V vs. Ag/Ag$^+$. This property opens a unique possibility for the preparation of synthetic analogues of HiPIP^{ox} and [Fe_4S_4(Cys)$_3$(His)] clusters, via reduction. In this chapter, we report the successful synthesis of the second isolated example of [Fe_4S_4]$^{3+}$ cluster [Fe_4S_4(SDmp)$_4$]$^-$ (**3**; Dmp = 2,6-dimesitylphenyl) modeling HiPIP^{ox} and the 3 : 1 site-differentiated [Fe_4S_4] clusters having a tetramethyl-imidazole (Me_4Im) ligand, [Fe_4S_4(SDmp)$_3$(Me_4Im)] (n = 0, **4**; n = 1, [**4**]$^-$), starting from the all-ferric cluster **1** or from its one-electron reduced form [**1**]$^-$. We have also prepared another 3 : 1 site-differentiated [Fe_4S_4] cluster Fe_4S_4(SDmp)$_3$(THF)$_3$ (**2**) containing an octahedral iron atom with three THF ligands, which is structurally relevant to the active site of aconitase. The redox properties of the unique [Fe_4S_4] clusters and the influence of the bulky –SDmp ligand on the redox potential are also discussed.

2.2. Results and Discussion

2.2.1. Synthesis of $[Fe_4S_4\{N(SiMe_3)_2\}_4]^-$ ($[\mathbf{1}]^-$)

Chemical reduction of **1** was attained by treatment of **1** with one equiv of sodium naphthalenide ($NaC_{10}H_8$) in THF at 0 °C (Scheme 2.1, top). Formation of the anionic cluster $[\mathbf{1}]^-$ is manifested in the electro-spray ionization mass spectrum (ESI-MS), showing an anionic signal at m/z = 992.4. After removal of naphthalene by sublimation, $[Na(THF)_2][Fe_4S_4\{N(SiMe_3)_2\}_4]$ was isolated in 71% yield as black crystals. This anionic cluster has been also prepared recently using NaSH or Na_2S as reductants.[13] Two redox couples at $E_{1/2}$ = 0.11 V and −0.98 V vs. Ag/Ag^+ were observed in the cyclic voltammogram (CV) of $[\mathbf{1}]^-$, as in the case of **1**.

The crystal structure of $[Na(THF)_2][Fe_4S_4\{N(SiMe_3)_2\}_4]$ was determined by X-ray analysis, using single crystals obtained from a hexane solution. As the structure of the same cluster has been reported,[13] here we describe only its salient features. An amide nitrogen atom (N1) and a sulfur atom of $[\mathbf{1}]^-$ interact weakly with a $[Na(THF)_2]$ unit, and the Na-N1 and Na-S distances are 2.528(2) Å and 3.1992(11) Å, respectively. The Na-N1 interaction results in a slight pyramidalization at N1, displacing the N atom 0.3721(20) Å from the plane defined by the Fe and Si neighbors, while displacement of the other nitrogen atoms is less than 0.0948(22) Å. The planarity of the amide nitrogen suggests a strong N → Fe π-interaction, which shortens the Fe-N distances and efficiently stabilizes the oxidized $[Fe_4S_4]^{3+}$ core of $[\mathbf{1}]^-$. Indeed the iron-amide (N1) distance of 1.9466(19) Å is notably longer than the other iron-amide distances (Fe-N2, N3, N4, 1.892(2)–1.897(2) Å). Interestingly, the Fe-Fe distances of

Scheme 2.1.

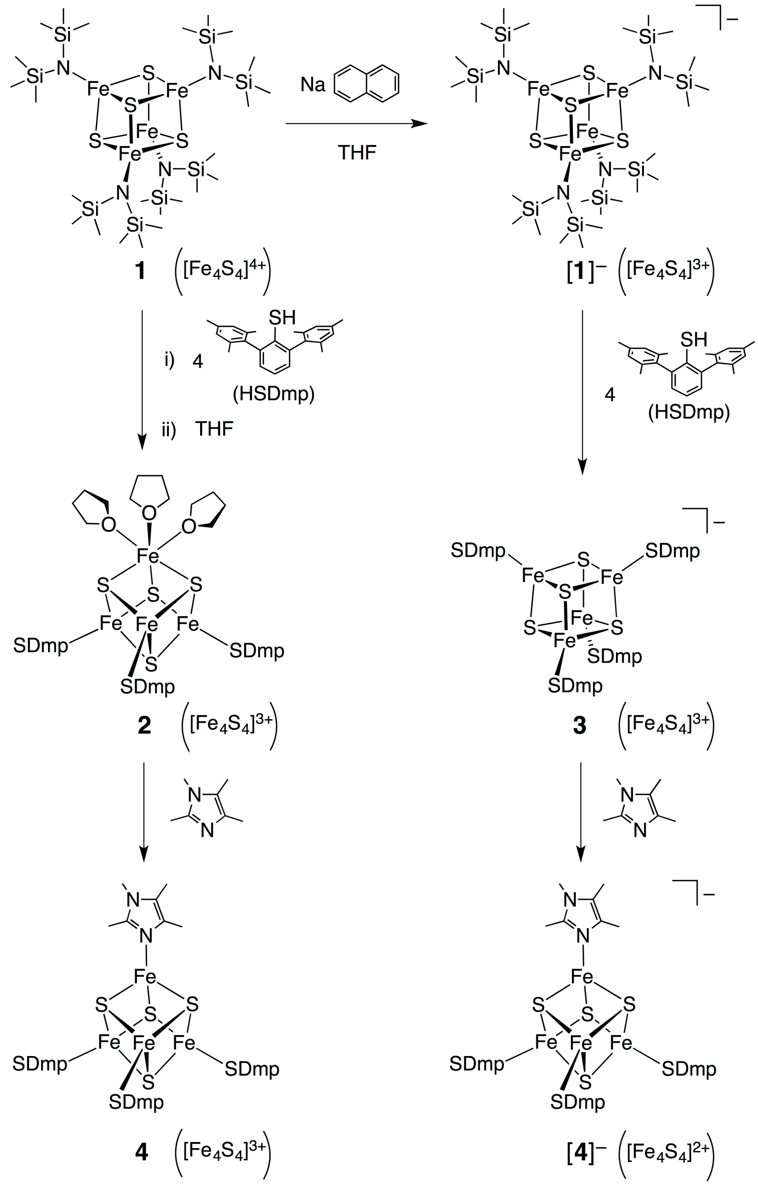

[**1**]$^-$, ranging from 2.8044(4) Å to 2.9151(5) Å, are shorter than those of **1** (2.8667(7)–3.0014(5) Å), while they are longer than those of $[Fe_4S_4(SR)_4]^{2-}$ (2.71–2.82 Å).[9]

2.2.2. Reactions of 1 and [1]$^-$ with HSDmp (Dmp = 2,6-dimesitylphenyl)

The amide nitrogen of $N(SiMe_3)_2$ bound to iron is a Brϕnsted base, and the author's group utilized this property to synthesize various iron complexes[14] and iron-sulfide clusters.[15] Here, we describe the reactions of clusters **1** and [**1**]$^-$ with the bulky thiol HSDmp (Dmp = 2,6-(mesityl)$_2$C$_6$H$_3$).[16]

2.2.2.1. Reactions of 1

Addition of four equiv of HSDmp to a toluene solution of **1** led to a color change from reddish black to purplish black, and the removal of volatile materials afforded a black solid. Although characterization of this black solid has been unsuccessful, treatment with THF resulted in the isolation of $Fe_4S_4(SDmp)_3(THF)_3$ (**2**) in 67% yield as black crystals (Scheme 2.1, second-row (left)). On the other hand, the reaction of **1** with HSDmp in THF did not afford cluster **2**, and the product(s) of this reaction remains uncharacterized. Cluster **2** consists of one ferrous and three ferric iron atoms, and thus the all-ferric $[Fe_4S_4]^{4+}$ core in **1** is reduced by one electron during the reaction with HSDmp. We presume that one of the $^-$SDmp ligands introduced onto the $[Fe_4S_4]$ core has been oxidized generating the disulfide (1/2 DmpS—SDmp), while the resulting vacant coordination site on iron is occupied by three THF molecules.

The generation of one unique iron site in a $[Fe_4S_4]^{3+}$ cubane cluster by reduction of **1** is intriguing, and this reaction offers a new synthetic route to 3 : 1 site-differentiated $[Fe_4S_4]$ clusters without invoking the use of tridentate thiolate auxiliaries.[11, 17] This route complements the recently reported oxidation reactions of the all-ferrous $[Fe_4S_4]^0$ clusters $[Fe_4S_4(P^iPr_3)_3]_2$ or $[Fe_4S_4(P^iPr_3)_2]_4$ with disulfides, diselenides, or I$_2$, yielding 3 : 1 site-differentiated $[Fe_4S_4]^+$ clusters.[18]

Cluster **2** was structurally identified by X-ray crystallographic analysis. The molecule displays threefold crystallographic symmetry, and there are two unique molecules in the asymmetric unit, and one of these is shown in Figure 2.2, along with selected bond distances and angles. The threefold axis lies along the Fe1-S2 vector, and thus three of the four iron atoms (Fe2, Fe2*, Fe2′) are crystallographically equivalent. These iron atoms have a distorted tetrahedral geometry surrounded by four sulfur atoms, three from the [Fe_4S_4] core and fourth from a thiolate ligand. On the other hand, Fe1 is nearly octahedral, bound to three oxygen atoms of THF molecules and three sulfur atoms from the core, with the S1-Fe1-S1* and S1-Fe1-O1 angles being 95.53(4)° and 87.72(11)°, respectively. Due to the octahedral coordination geometry at Fe1, the Fe1-Fe2 distance (2.9600(9) Å) is significantly

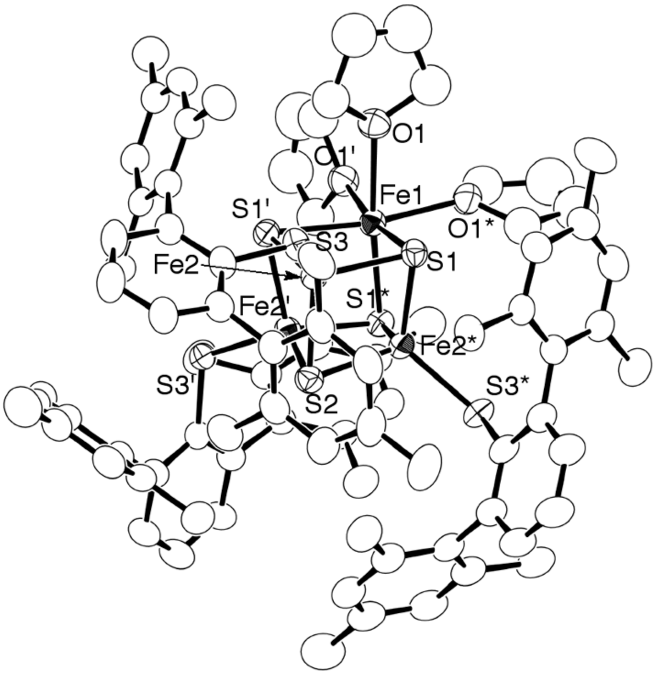

Figure 2.2. Crystal structure of $Fe_4S_4(SDmp)_3(THF)_3$ (**2**) with thermal ellipsoids at the 50% probability level. The THF ligand on Fe1 is disordered over two positions, and one of these is shown for clarity. Selected bond distances (Å) and angles (°): Fe1-Fe2, 2.9600(9); Fe2-Fe2* 2.7328(11); Fe1-S1, 2.3938(12); Fe2-S1, 2.2412(10); Fe2-S2, 2.2732(13); Fe2-S3, 2.2234(14); Fe1-O1, 2.234(3); S1-Fe1-S1*, 95.53(4); S1-Fe1-O1, 87.72(11).

elongated compared with the Fe2-Fe2* distance (2.7328(11) Å), indicating no Fe1-Fe2 bonding interaction. The Fe1-S1 bond (2.3938(12) Å) is also longer than the Fe2-S1 and Fe2-S2 bonds (2.2412(10) and 2.2732(13) Å) by 0.1–0.15 Å. It is noteworthy that the octahedral geometry of Fe1 coordinated by three O-donors and three S-donors resembles that of the active site of aconitase,[6] which catalyzes the reversible isomerization of citrate and isocitrate. In fact, the Fe1-S and Fe1-O distances of **2** (Fe-S; 2.3939(12) Å, Fe-O; 2.234(3) Å) are similar to those for the isocitrate complex of aconitase (Fe-S; 2.33–2.36 Å, Fe-O; 2.20 (water), 2.28 and 2.37 Å (isocitrate)).[6] This similarity opens the possibility that the unique iron atom of molecule **2** may have catalytic properties. The THF ligands bound to Fe1 may be weakly held, so that **2** may serve as a synthetic precursor to 3 : 1 site-differentiated [Fe_4S_4] clusters.

2.2.2.2. Reaction of [1]$^-$

Treatment of [**1**]$^-$ with four equiv of HSDmp in toluene resulted in the isolation of [Fe_4S_4(SDmp)$_4$]$^-$ (**3**) (Scheme 2.1, second-row, right) in 69% yield as crystals. In this reaction, all four amide ligands of [**1**]$^-$ were all replaced by thiolates, without changing the [Fe_4S_4]$^{3+}$ oxidation state. The ESI-MS spectrum of a THF solution of **3** gave an anionic signal at m/z = 1732.4, and the isotope pattern matches that calculated. The oxidation state of **3**, [Fe_4S_4]$^{3+}$, is the same as that of HiPIP^{ox} , for which only one isolated model cluster, [Fe_4S_4(STip)$_4$]$^-$, has been reported.[10] The structure of **3** was determined by X-ray analysis, using single crystals obtained from a toluene-hexamethyldisiloxane (HMDSO) solution (Figure 2.3). The details of this structure and EPR characterization of [Fe_4S_4]$^{3+}$ core are discussed in Chapter 3, combined with those of other [Fe_4S_4]$^{3+}$ clusters.

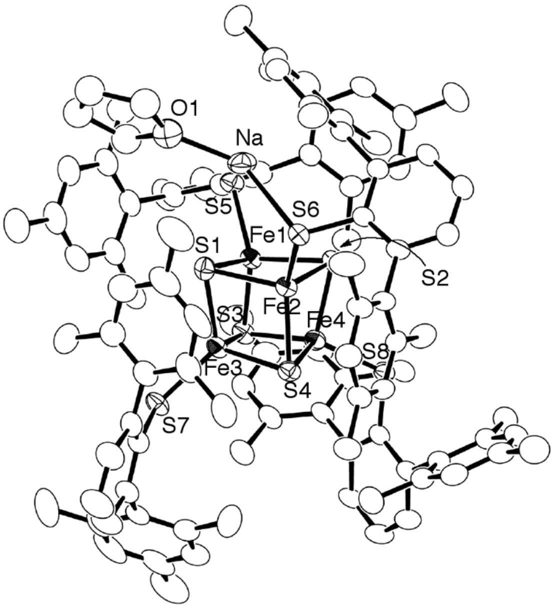

Figure 2.3. Crystal structure of [Na(THF)][Fe_4S_4(SDmp)$_4$] (**3**) with thermal ellipsoids at the 50% probability level. The [Na(THF)[group is disordered over two positions, and one of these is shown for clarity. Selected bond distances (Å): Fe1-Fe2, 2.7282 (8); Fe1-Fe3, 2.8127(10); Fe1-Fe4, 2.7894(8); Fe2-Fe3, 2.7561(6); Fe2-Fe4, 2.7306(6); Fe3-Fe4, 2.7889(7); Fe1-S1, 2.2810(12); Fe1-S2, 2.2885(11); Fe1-S3, 2.2316(11); Fe2-S1, 2.3020(12); Fe2-S2, 2.2625(13); Fe2-S4, 2.2716(13); Fe3-S1, 2.2471(12); Fe3-S3, 2.3057(13); Fe3-S4, 2.2791(13); Fe4-S2, 2.2177(11); Fe4-S3, 2.2716(12); Fe4-S4, 2.2674(14); Fe1-S5, 2.2445(15); Fe2-S6, 2.2615(9); Fe3-S7, 2.2408 (11); Fe4-S8, 2.2128(10); S6-Na1, 2.894(3).

2.2.3. Synthesis and Structures of 3:1 Site-Differentiated [Fe_4S_4] Clusters with a Tetramethyl-Imidazole Ligand

In toluene the THF ligands of **2** were replaced by one tetramethyl-imidazole (Me_4Im), and Fe_4S_4(SDmp)$_3$(Me_4Im) (**4**) was isolated in 46% yield as crystals (Scheme 2.1, bottom (left)). Alternatively, cluster **4** was synthesized directly from **1** in 54% yield, via successive treatment with four equiv of HSDmp and with one equiv of Me_4Im. An analogous [Fe_4S_4]$^{3+}$ cluster with histidine ligation has been generated as the oxidized form of the site-directed Cys → His mutant of the DNA repair enzyme

MutY, and this cluster has been reported to degrade readily into an $[Fe_3S_4]^+$ cluster by release of an iron atom.[19]

The one-electron reduced form of **4**, $[Fe_4S_4(SDmp)_3(Me_4Im)]^-$ [**4**]$^-$, was obtained in 72% yield as black crystals from the reaction of **3** ($[Fe_4S_4(SDmp)_4]^-$) with one equiv of Me_4Im in toluene (Scheme 2.1, bottom (right)), and the ESI-MS spectrum of a THF solution of [**4**]$^-$ exhibits an anionic signal at m/z = 1511.6 (M^-). Interestingly, liberation of a SDmp ligand in **3** induces one-electron reduction of the $[Fe_4S_4]^{3+}$ core to $[Fe_4S_4]^{2+}$ of [**4**]$^-$, presumably via formation of DmpS—SDmp. Thus single-site ligand replacement via reduction is also applicable to the HiPIP^{ox}-type $[Fe_4S_4]^{3+}$ cluster **3**. In a similar manner to the direct synthesis of **4** from **1**, the one-pot reaction of [**1**]$^-$ with four equiv of HSDmp and one equiv of Me_4Im in toluene gave crystals of [**4**]$^-$ in 86% yield. As demonstrated here by the formation of the Me_4Im-adducts **4** and [**4**]$^-$, this ligand exchange reaction accompanied by one-electron reduction is a promising tool for the incorporation of one external biologically relevant ligand onto $[Fe_4S_4(SR)_4]^{n-}$ clusters. We have also examined chemical oxidation/reduction of **4**/[**4**]$^-$. However, oxidation of [**4**]$^-$ with $[CP_2Fe][PF_6]$ and reduction of **4** with $Na[C_{10}H_8]$ yielded uncharacterizable black solids.

The coordination of three thiolates and a tetramethyl-imidazole to the $[Fe_4S_4]$ core of **4** and [**4**]$^-$ models the structure of the $[Fe_4S_4(Cys)_3(His)]$ cluster found in hydrogenases. The overall similarity among the core structures of **4**, [**4**]$^-$, and the $[Fe_4S_4(Cys)_3(His)]$ cluster from *Desulfovibrio gigas* can be seen in Figure 2.4. One feature common to all three clusters is a slight bending of the imidazole coordinaton,as is manifested by the deviation of the S*-Fe1-N angles from 180°,

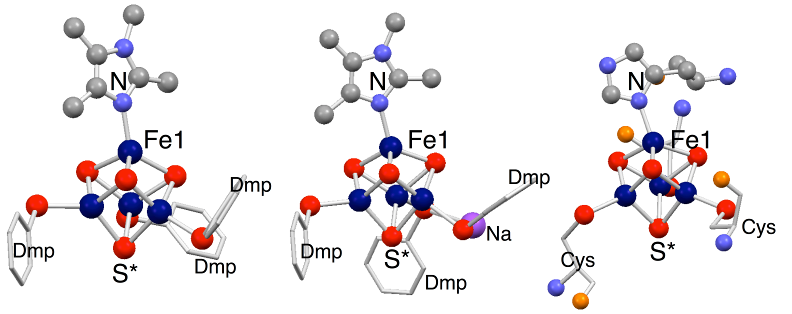

[**4**] [**4**]$^-$ *distal*-[$Fe_4S_4(Cys)_3(His)$] from *D. gigas*

Figure 2.4. The core structures of **4**, [**4**]$^-$, and the [$Fe_4S_4(Cys)_3(His)$] cluster from *D.gigas* (PDB ID: 2FRV).[4b] For clarity, only the central aromatic rings of —SDmp ligands are shown for **4** and [**4**]$^-$.

namely, 167.70(15)° for **4**, 165.67 (8)° for [**4**]$^-$, and 160.9° for *D. gigas*. As a consequence, the tetrahedral geometry at Fe1 is distorted. The distances in *D. gigas*, Fe-Fe (2.70–2.75 Å), Fe-N(imidazole) (1.99 Å), Fe-S(thiolate) (2.25–2.42 Å), and Fe-S(core) (2.23–2.36 Å), are comparable to those listed in Table 2.1 for **4** and [**4**]$^-$, taking the lower accuracy of distances in protein structures into consideration. The oxidation state of the [$Fe_4S_4(Cys)_3(His)$] cluster in the crystal structure of *D. gigas* has not been clarified yet, although the [Fe_4S_4]$^{2+/1+}$ states have been suggested to be involved in the enzymatic process. Successful isolation of **4** and [**4**]$^-$ suggests that the [Fe_4S_4]$^{3+/2+}$ states might be another possibility for the [$Fe_4S_4(Cys)_3(His)$] clusters. It should be also noted that **4** and [**4**]$^-$ are structurally analogous to the His-bound [$Fe_4S_4(Cys)_3(His)$] clusters serving as one of the electron-transfer sites of the membrane-bound nitrate reductase from *Escherichia coli*,[20] and as the active site of 4-hydroxybutyryl-CoA dehydratase.[21]

While the structures of **4** and [**4**]$^-$ shown in Figure 2.5 and A1.2 are very much alike, there are some differences in distances due to the different oxidation states, as

Table 2.1. Selected bond distances (Å) and angle (°) for clusters **4** and [**4**]$^-$

	4	[**4**]$^-$
Oxidation state	$[Fe_4S_4]^{3+}$	$[Fe_4S_4]^{2+}$
Ave. Fe-Fe	2.7450(11)	2.7116(8)
Fe1-Fe	2.7272(11)	2.7102(7)
Other Fe-Fe	2.7628(10)	2.7130(8)
Ave. Fe-S(core)	2.2681(17)	2.2846(12)
Fe1-S(core)	2.2782(17)	2.2796(12)
Other Fe-S(core)	2.2647(16)	2.2862(12)
Ave. Fe-S(thiolate)	2.2179(17)	2.2627(10)
Fe-N(imidazole)	1.992(5)	2.017(2)
S4-Fe1-N	167. 70(15)	165.67(8)

listed in Table 2.1. The higher oxidation state for **4** leads to slightly shorter Fe-N(imidazole), Fe-S(core), and Fe-S(thiolate) distances than those for [**4**]$^-$. The most notable difference among these can be found in the Fe-S(thiolate) distances, 2.2090(17)– 2.2351(15) Å (average (Ave.) 2.218 Å) for **4** and 2.2361(10)–2.2866(10) Å (Ave. 2.263 Å) for [**4**]$^-$, indicating more flexibility for the thiolate ligands than the core sulfur atoms in response to the change of oxidation state. Similarly, the Fe-S (thiolate) distances in the $[Fe_4S_4]^{3+}$ cluster **3**, 2.2128(10)–2.2615 (9) Å (Ave. 2.227 Å), are shorter than those for [**4**]$^-$, although the Na-S(thiolate) interaction elongates one of the Fe-S(thiolate) bonds of **3** to 2.2615(9) Å. In contrast to the Fe-N(imidazole), Fe-S(core), and Fe-S(thiolate) distances, the Fe-Fe distances for **4**, 2.6946(10)–

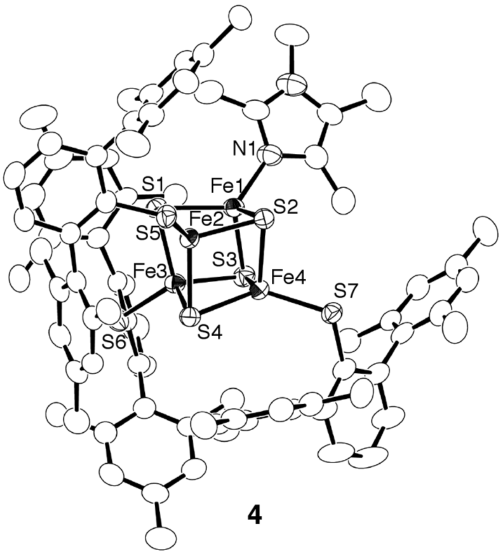

4

Figure 2.5. Crystal structure of $Fe_4S_4(SDmp)_3(Me_4Im)$ (**4**) with thermal ellipsoids at the 50% probability level. The crystal solvent is omitted for clarity.

2.7978(10) Å (Ave. 2.745Å), and **3**, 2.7282(8)– 2.8127(10) Å (Ave. 2.768 Å), are slightly longer than those for [**4**]$^-$, 2.6834(6)–2.7335(7) Å (Ave. 2.712 Å).

2.2.4. Electronic Properties of 3, 4, and [4]$^-$ as Models of HiPIP and $[Fe_4S_4(Cys)_3(His)]$

The CV for the HiPIP model **3** and the $[Fe_4S_4(Cys)_3(His)]$ models **4** and [**4**]$^-$ have been measured and compared to assess the influence of the imidazole ligand on the redox potentials. Figure 2.6 shows the CV data for **3** and [**4**]$^-$ in the range between 0 and −1.2 V, where the potentials are referenced to Ag/Ag^+.

The $[Fe_4S_4]^{3+}/[Fe_4S_4]^{2+}$ redox couple between **4** and [**4**]$^-$ was found to be reversible at $E_{1/2}$ = −380 mV, and the corresponding reversible redox couple for **3** and [**3**]$^-$ appeared at $E_{1/2}$ = −820 mV. Thus the redox potential is shifted by +440 mV, when one of the —SDmp ligands in **3** is replaced by Me_4Im. The positive shift is

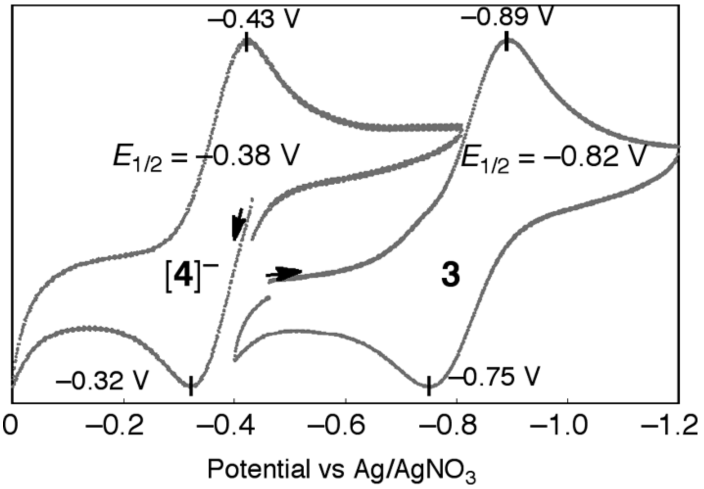

Figure 2.6. Redox couples of **3**/[**3**]$^-$ and **4**/[**4**]$^-$ measured by CV in THF at room temperature.

reasonable, as the electron-donating abilities of anionic thiolate ligands should be greater than those of neutral imidazoles. Similarly, the *in situ* generated [Fe_4S_4] cluster with a 4-methyl-imidazole (4-MeIm) ligand, [Fe_4S_4(LS_3)(4-MeIm)]$^-$, shows a redox couple more positive by 320 mV than the cluster having an ethane-thiolate instead of 4-MeIm, [Fe_4S_4(LS_3)(SEt)]$^{2-}$.[11]

The significantly higher redox potential for **4** relative to **3** implies that facile electron transfer could occur from the [Fe_4S_4(Cys)$_4$] cluster, which is proximal to the Ni-Fe active site of [NiFe] hydrogenases, to the *distal*-[Fe_4S_4(Cys)$_3$(His)] cluster. This direction is the electron flow that promotes the oxidation of H_2 at the active site. On the other hand, hydrogenases also promote the reduction of H^+ that requires the reverse electron transfer from the *distal*- to *proximal*-[Fe_4S_4] clusters. Therefore, there must be a mechanism, which promotes the reverse electron transfer process, by modulating the redox potentials of the [Fe_4S_4] clusters. The unique positioning of the *distal*-[Fe_4S_4(Cys)$_3$(His)] cluster in the protein may give a clue. The *distal* cluster is located at the protein surface with the imidazole N—H group oriented toward outside of the protein (Figure 2.1). We hypothesize here that the imidazole N—H group is exposed to water, and that coordination of the imidazole to iron enhances the N—H acidity facilitating its deprotonation. This deprotonation at imidazole would cause a substantial negative shift of the potential of the $[Fe_4S_4(Cys)_3(His)]$ cluster, due to the addition of an extra negative charge with retention of the oxidation state of the iron atoms. Therefore, protonation/deprotonation at the imidazole may act as a changeover switch reversing the electron transfer between the *distal*- and *proximal*-$[Fe_4S_4]$ clusters.

Interestingly, upon scanning a CV of **3** toward positive potential, a reversible redox couple at $E_{1/2}$ = +80 mV was observed (Figure 2.7), which indicates the generation of an all-ferric $[Fe_4S_4]^{4+}$ cluster, $[Fe_4S_4(SDmp)_4]^0$. Cluster **1** is the sole example of an all-ferric $[Fe_4S_4]^{4+}$ cluster, and a thiolate-bound $[Fe_4S_4]^{4+}$ cluster is unprecedented. Stabilization of the all-ferric state of the $[Fe_4S_4]^{4+}$ core requires a strongly basic, electron donating set of ligands to counter the large positive charge of

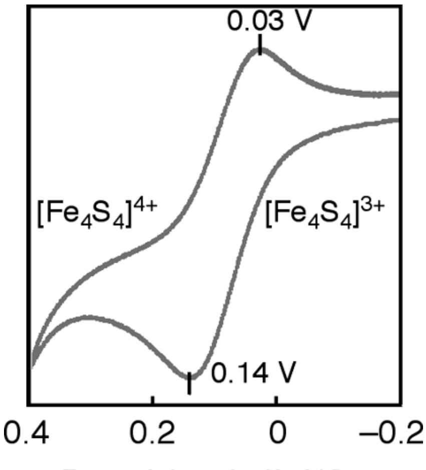

Figure 2.7. CV of **3** in the range between 0.4 and –0.2 V vs. Ag/Ag^+.

the iron atoms. Even the removal of a small amount of negative charge due to the formation of hydrogen bonds appears to destabilize the all-ferric oxidation state. As for the HiPIP^{ox} cluster, the $[Fe_4S_4]^{3+}$ core is buried in a hydrophobic pocket of the protein, while the $[Fe_4S_4]^{2+/1+}$ core of Fd is exposed to hydrogen bonding by water.[2] In this context, the unique ability of higher oxidation states of **3** may arise from the environment provided by the bulky hydrocarbon groups of the —SDmp ligands, which mimics a hydrophobic pocket of the protein.

2.3. Conclusions

The reduction and/or the ligand substitution of highly oxidized [Fe_4S_4] cluster **1** led to the formation of [3:1] site-differentiated clusters **2**, **4**, and [**4**]$^-$, and the HiPIP^{ox} model **3**. Features of each cluster are as follows: (1) for **2**, the unique site-differentiated cluster of which one iron atom has octahedral coordination sphere, (2) for **3**, the second isolated [Fe_4S_4]$^{3+}$ cluster having four thiolate ligands, and (3) for **4** and [**4**]$^-$, the unprecedented structurally characterized models of [Fe_4S_4(Cys)$_3$(His)] in hydrogenase. The successful synthesis of **2**, **4**, and [**4**]$^-$ indicates that single-site ligand replacement shown here should be applicable to the introduction of one biologically relevant ligand upon [Fe_4S_4(SR)$_4$]$^{n-}$ (n = 0 or 1). The point of these reactions is the use of oxidized [Fe_4S_4] core because liberation of thiolate leading to the generation of disulfide triggers the formation of a vacant site on iron atom via reduction of [Fe_4S_4] core. Additionally, synthesis of [Fe_4S_4(SR)$_4$]$^-$ from [**1**]$^-$ can also be applied to a broader scope.

The electrochemical measurements of **3** and [**4**]$^-$ revealed that the redox potential of [Fe_4S_4]$^{3+}$/[Fe_4S_4]$^{2+}$ couple is positively shifted by the replacement of thiolate to imidazole. The higher redox potential for **4** compared with **3** indicate electrons can be transferred from the *proximal*-[Fe_4S_4(Cys)$_4$] to the *distal*-[Fe_4S_4(Cys)$_3$(His)] in [NiFe] hydrogenase, corresponding to the electron flow which facilitates H_2 oxidation at the active site. Based on this insight, we propose the existence of some mechanisms, such as deprotonation of His residue, causing a negative shift of the potential of [Fe_4S_4(Cys)$_3$(His)], since [NiFe] hydrogenase also catalyzes H_2 production.

The electrochemical properties of **3** also suggests an influence of steric shielding on the redox potentials of [Fe_4S_4] clusters which is relevant to that how HiPIP stabilizes its [Fe_4S_4]$^{3+}$ core. This theme is discussed more in Chapter 3.

2.4. Experimental Section

General Procedures. All reactions were carried out using standard Schlenk techniques and a glove box with a nitrogen atmosphere. Toluene, THF, hexane, and hexamethyldisiloxane (HMDSO) were purified by the method of Grubbs,[22] where the solvents were passed over columns of activated alumina and a supported copper catalyst supplied by Hansen & Co. Ltd. ESI-TOF-MS spectra were recorded on a Micromass LCT TOF-MS at room temperature. UV-vis spectra were measured on a JASCO V560 spectrometer at room temperature. The EPR spectrum of **3** was recorded on a Bruker EMX-plus spectrometer at X-band frequencies. Cyclic voltammograms (CV) were recorded in THF at room temperature using glassy carbon as the working electrode with 0.2 M $[N^nBu_4][PF_6]$ as the supporting electrolyte. The potentials are referenced to Ag/Ag^+. Elemental analyses were performed on a LECO-CHNS-932 elemental analyzer where the crystalline samples were sealed in silver capsules under nitrogen. 1,2,4,5-tetramethylimidazole (Me_4Im) was purchased from TCI co., Ltd. and used as received. $Fe_4S_4\{N(SiMe_3)_2\}_4$ (**1**)[12, 13] and HSDmp[16] were prepared according to literature procedures.

Synthesis of $[Fe_4S_4\{N(SiMe_3)_2\}_4]^-$ [1]⁻. A THF solution (0.16 M) of sodium naphthalenide was prepared from the reaction of naphthalene (0.423 g, 3.30 mmol) with excess sodium (0.155g, 6.74 mmol) in THF (20 mL) at 0 °C, followed by stirring overnight at room temperature and filtration to remove excess Na. A portion of this solution (18.9 mL, 3.03 mmol) was added dropwise to a THF (15 mL) solution of $Fe_4S_4\{N(SiMe_3)_2\}_4$ (**1**) (3.01 g, 3.03 mmol) at 0 °C. The reaction mixture was allowed to warm to room temperature and was stirred for 15 hr. The resulting yellowish black solution was evaporated under reduced pressure, and then naphthalene was removed by sublimation under low pressure (< 10^{-1} Pa). The residue was extracted with hexane (130 mL), and the solution was centrifuged to remove a small amount of insoluble solid. The extract was evaporated until dryness, and the residue was again dissolved into hexane (2 mL). This solution was stored at –30 °C to give black crystals of $[Na(THF)_2][Fe_4S_4\{N(SiMe_3)_2\}_4]$ ($[Na(THF)_2][\mathbf{1}]$) (2.49 g, 2.15 mmol, 71 %). UV-vis (hexane): λ_{max} = 434 nm (ε 4.0×10^4). UV-vis (toluene): λ_{max} = 433 nm (ε 5.3×10^3). UV-vis (THF): λ_{max} = 400 nm (ε 2.4×10^4). Cyclic voltammetry (THF, room temperature): $E_{1/2}$ = 0.11 V ($\mathbf{1}/[\mathbf{1}]^-$), $E_{1/2}$ = –0.98 V ($[\mathbf{1}]^-/[\mathbf{1}]^{2-}$). ESI-TOF-MS (THF): *m*/*z* = 992.4 (M^-). Anal. Calcd for $C_{32}H_{88}Fe_4N_4NaO_2S_4Si_8$: C, 33.12; H, 7.64; N, 4.83; S, 11.05. Found: C, 32.77; H, 7.41; N, 4.80; S, 11.01.

Synthesis of $Fe_4S_4(SDmp)_3(THF)_3$ (2). A toluene solution (40 mL) of HSDmp (1.18 g, 3.41 mmol) was added dropwise to a toluene (10 mL) solution of **1** (845 mg, 0.851 mmol) at room temperature. After stirring for 18 hr, the solution was evaporated until dryness under reduced pressure. The black residue was extracted with THF (60 mL), and the solution was centrifuged to remove a small amount of insoluble solid. The extract was concentrated to *ca.* 15 mL, and then HMDSO (55 mL) was layered. Slow diffusion at room temperature led to the formation of $Fe_4S_4(SDmp)_3(THF)_3$ (**2**) (913 mg, 0.569 mmol, 67%) as black crystals, which were separated from the solution and were washed with HMDSO (2 mL×2). UV-vis (toluene): λ_{max} = 495 nm (ε 6.6×10^3). UV-vis (THF): λ_{max} = 498 nm (ε 4.0×10^4). Anal. Calcd for $C_{84}H_{99}Fe_4O_3S_7$: C, 62.88; H, 6.22; S, 13.99. Found: C, 63.03; H, 6.32; S, 14.00. The CV of **2** measured in THF using $[N^nBu_4][PF_6]$ as the electrolyte gave the identical redox couple to that of cluster **3**, while the peak current was low. Cluster **2** possibly degrades in the presence of excess electrolyte in THF to give a complex mixture containing **3**.

Synthesis of $[Fe_4S_4(SDmp)_4]^-$ (3). A toluene solution (70 mL) of HSDmp (2.01 g, 5.80 mmol) was added dropwise to a toluene (10 mL) solution of $[\mathbf{1}]^-$ (1.65 g, 1.42 mmol) at room temperature. After stirring overnight, the solution was evaporated until dryness under reduced pressure. The black residue was extracted with a mixture of THF (1 mL) and toluene (30 mL), and the solution was centrifuged to remove a small amount of insoluble solid. The extract was concentrated to *ca.* 10 mL, and then HMDSO (60 mL) was layered. Slow diffusion at room temperature led to the formation of $[Na(THF)][Fe_4S_4(SDmp)_4]\cdot C_7H_8$, $\mathbf{3}\cdot C_7H_8$ (1.89 g, 0.983 mmol, 69%) as black crystals. UV-vis (THF): λ_{max} = 348 (ε 1.7 × 10^4), 446 nm (ε 1.4 × 10^4). Cyclic voltammetry (THF, room temperature): $E_{1/2}$ = 0.082 V ($[\mathbf{3}]^+/\mathbf{3}$), $E_{1/2}$ = –0.82 V ($\mathbf{3}/[\mathbf{3}]^-$). EPR (X-band, microwave 1.0 mW, room temperature): g = 2.076, 2.035, 2.018. ESI-TOF-MS (THF): m/z = 1732.4 (M^-). Anal. Calcd for $C_{100}H_{108}Fe_4NaOS_8\cdot C_7H_8$: C, 66.90; H, 6.09; S, 13.35. Found: C, 66.81; H, 6.33; S, 13.05.

Synthesis of $Fe_4S_4(SDmp)_3(Me_4Im)$ (4). Method A, from **2**: A toluene solution (10 mL) of Me_4Im (15.4 mg, 0.124 mmol) was added to a toluene (40 mL) solution of **2** (200 mg, 0.124 mmol) at room temperature. After stirring overnight, the solution was evaporated until dryness under reduced pressure. The black residue was extracted with toluene (6 mL), and the solution was centrifuged to remove a small amount of insoluble solid. Hexane (50 mL) was layered onto this solution, and slow diffusion at room temperature led to the formation of $[Fe_4S_4(SDmp)_3(Me_4Im)]\cdot C_7H_8$,

4·C_7H_8 (92 mg, 0.057 mmol, 46%) as black crystals. Method B, from **1**: A toluene solution (22 mL) of HSDmp (419 mg, 1.21 mmol) was slowly added to a toluene (5 mL) solution of **1** (300 mg, 0.302 mmol) at room temperature, and the mixture was stirred for 24 hr. A toluene (6 mL) solution of Me_4Im (37 mg, 0.30 mmol) was then added to the reaction mixture. After stirring for 45 min, the solution was evaporated until dryness. The resultant black solid was washed with hexane (3 mL). The residue was extracted with toluene (10 mL), and the solution was centrifuged to remove a small amount of insoluble solid. The extract was concentrated to *ca.* 5 mL, and then HMDSO (20 mL) was layered. Slow diffusion at room temperature led to the formation of **4**·C_7H_8 as black crystals (260 mg, 0.162 mmol, 54%). UV-vis (THF): λ_{max} = 463 nm (ε 1.5 × 10^4). Cyclic voltammetry (THF, room temperature): $E_{1/2}$ = –0.35 V (**4**/[**4**]$^-$). Anal. Calcd for $C_{79}H_{87}Fe_4N_2S_7 \cdot C_7H_8$: C, 65.13; H, 6.05; N, 1.70; S, 13.60. Found: C, 65.11; H, 6.46; N, 1.89; S, 13.55.

Synthesis of [Fe_4S_4(SDmp)$_3$(Me_4Im)]$^-$ [4]$^-$. Method A, from **3**: A toluene solution (10 mL) of Me_4Im (39 mg, 0.314 mmol) was added dropwise to a toluene (5 mL) solution of **3** (625 mg, 0.356 mmol) at room temperature. After stirring for 1hr, the solution was evaporated until dryness under reduced pressure. The resultant black solid was washed with hexane (10 mL). The residue was extracted with toluene (15 mL), and the solution was centrifuged to remove a small amount of insoluble solid. The extract was concentrated to *ca.* 3 mL, and then hexane was layered. Slow diffusion at room temperature led to the formation of [Na][Fe_4S_4(SDmp)$_3$(Me_4Im)]·C_7H_8·1/2(C_6H_{14}), [**4**]$^-$·C_7H_8·1/2(C_6H_{14}) (430 mg, 0.257 mmol, 72%) as black crystals. Method B, from [**1**]$^-$: A toluene solution (25 mL) of

HSDmp (1.19 g, 3.44 mmol) was slowly added to a toluene (10 mL) solution of [**1**]$^-$ (1.01 g, 0.870 mmol) at room temperature, and the mixture was stirred for 17 hr. At –40 °C, a toluene (13 mL) solution of Me_4Im (107 mg, 0.862 mmol) was then added to the reaction mixture. The solution was allowed to warm to room temperature, and was stirred for 18 hr. The solution was evaporated until dryness, and the resultant black solid was washed with hexane (5 mL). The residue was extracted with toluene (17 mL), and the solution was centrifuged to remove a small amount of insoluble solid. The extract was concentrated to *ca.* 6 mL, and then HMDSO (15 mL) was layered. Slow diffusion at room temperature led to the formation of [**4**]$^-$ as black crystals (1.14 g, 0.745 mmol, 86%). UV-vis (THF): λ = 434 nm (shoulder). Cyclic voltammetry (THF, room temperature): $E_{1/2}$ = –0.38 V (**4**/[**4**]$^-$). ESI-TOF-MS (THF): m/z = 1511.6 (M^-). Anal. Calcd for $C_{79}H_{87}Fe_4N_2NaS_7$: C, 61.80; H, 5.71; N, 1.82; S, 14.62. Found: C, 61.31; H, 5.58; N, 1.85; S, 14.16.

X-ray Crystal Structure Determination. Crystal data and refinement parameters for [**1**]$^-$-[**4**]$^-$ are summarized in Table A1.1. Single crystals were coated with oil (Immersion Oil, type B: Code 1248, Cargille Laboratories, Inc.) and mounted on loops. Diffraction data were collected at –100 ˚C under a cold nitrogen stream on a Rigaku AFC8 equipped with a Mercury CCD detector, or on a Rigaku RA-Micro7 equipped with a Saturn70 CCD detector, using graphite-monochromated Mo Kα radiation (λ = 0.710690 Å). Six preliminary data frames were measured at 0.5˚ increments of ω, to assess the crystal quality and preliminary unit cell parameters. The intensity images were also measured at 0.5˚ intervals of ω. The frame data were integrated using the CrystalClear program package, and the data sets were corrected for absorption using a REQAB program. The calculations were performed with the CrystalStructure program package. All structures were solved by direct methods, and refined by full-matrix least squares. Anisotropic refinement was applied to all non-hydrogen atoms except for disordered atoms, and all hydrogen atoms were put at calculated positions. The THF ligands in **2** are disordered over two positions in a 1:1 ratio. The Na(THF) group in **3**·C_7H_8 is disordered over two positions, with 75:25 occupancy factors, and the B_{eq} factors for THF were fixed using a rigid model. The toluene molecules in **3**·C_7H_8 are disordered over two positions in a 1:1 ratio. Isotropic refinement was applied to the toluene molecule in **4**·C_7H_8. The toluene molecule in [**4**]$^-$·C_7H_8·1/2(C_6H_{14}) was not well refined, and some carbon atoms were put at the residual peaks and they were isotropically refined. The hexane molecule in [**4**]$^-$·C_7H_8·1/2(C_6H_{14}) is disordered over two positions in a 1:1 ratio.

References and Notes

[1] (a) Watt, G. D.; Reddy, K. *J. Inorg. Biochem.* **1994**, *53*, 281–294. (b) Angove, H. C.; Yoo, S. J.; Münck, E.; Burgess, B. K. *J. Biol. Chem* **1998**, *273*, 26330–26337.

[2] Dey, A.; Jenny, F. E. Jr.; Adams, M. W. W.; Babini, E.; Takahashi, Y.; Fukuyama, K.; Hodgson, K. O.; Hedman, B.; Solomon, E. I. *Science* **2007**, *318*, 1464-1468.

[3] Stephens, P. J.; Jollie, D. R.; Warshel, A. *Chem. Rev.* **1996**, *96*, 2491-2514.

[4] Reports on crystal structures of [NiFe] hydrogenase, see: (a) Volbeda, A.; Charon, M. H.; Piras, C.; Hatchikian, E. C.; Frey, M.; Fontecilla-Camps, J. C. *Nature* **1995**, *373*, 580-587. (b) Volbeda, A.; Garcin, E.; Piras, C.; L. de Lacey, A.; Fernández, V. M.; Hatchikian, E. C.; Frey, M.; Fontecilla-Camps, J. C. *J. Am. Chem. Soc.* **1996**, *118*, 12989-12996. (c) Higuchi, Y.; Yagi, T.; Yasuoka, N. *Structure* **1997**, *5*, 1671-1680. (d) Rousset, M.; Montet, Y.; Guigliarelli, B.; Forget, N.; Asso, M.; Bertrand, P.; Fontecilla-Camps, J. C.; Hatchikian, E. C. *Proc. Natl. Acad. Sci. USA* **1998**, *95*, 11625-11630. (e) Higuchi, Y.; Ogata, H.; Miki, K.; Yasuoka, N.; Yagi, T. *Structure* **1999**, *7*, 549-556. (f) Garcin, E.; Vernede, X; Hatchikian, E. C.; Volbeda, A.; Frey, M.; Fontecilla-Camps, J. C. *Structure* **1999**, *7*, 557-566. (g) Matias, M. P.; Soares, C. M.; Saraiva, L. M.; Coelho, R.; Morais, J.; Gall, J. L.; Carrondo, M. A. *J. Biol. Inorg. Chem.* **2001**, *6*, 63-81. (h) Volbeda, A.; Martin, L.; Cavazza, C.; Matho, M.; Faber, B. W.; Roseboom, W.; Albracht, S. P. J.; Garcin, E.; Rousset, M.; Fontecilla-Camps, J. C. *J. Biol. Inorg. Chem.* **2005**, *10*, 239-249. (i) Ogata, H.; Hirota, S.; Nakahara, A.; Komori, H.; Shibata, N.; Kato, T.; Kano, K.; Higuchi, Y. *Structure* **2005**, *13*, 1635-1642.

[5] Reports on crystal structures of [FeFe] hydrogenase from *Clostridium pasteurianum*, see: (a) Peters, J. W.; Lanzilotta, W. N.; Lemon, B. J.; Seefeldt, L. C. *Science* **1998**, *282*,

1853-1858. (b) Lemon, B. J.; Peters, J. W. *Biochemistry* **1999**, *38*, 12969-12973. (c) Pandey, A. S.; Harris, T. V.; Giles, L. J.; Peters, J. W.; Szilagyi, R. K. *J. Am. Chem. Soc.* **2008**, *130*, 4533-4540.

[6] (a) Lauble, H.; Kennedy, M. C.; Beinert, H.; Stout, C. D. *Biochemistry* **1992**, *31*, 2735-2748. (b) Lloyd, S. J.; Lauble, H.; Prasad, G. S.; Stout, C. D. *Protein Sci.* **1999**, *8*, 2655-2662. (c) Dupuy, J.; Volbeda, A.; Carpentier, P.; Darnault, C.; Moulis, J. –M.; Fontecilla-Camps, J. C. *Structure* **2006**, *14*, 129-139.

[7] Muraki, N.; Nomata, J.; Ebata, K.; Mizoguchi, T.; Shiba, T.; Tamiaki, H.; Kurisu, G.; Fujita, Y. *Nature* **2010**, *465*, 110-114.

[8] Teixeira, M.; Moura, I.; Xavier, A. V.; Moura, J. J. G.; LeGall, J.; DerVartanian, D. V.; Peck, H. D. Jr.; Huynh, B. –H. *J. Biol. Chem.* **1989**, *264*, 16435-16450.

[9] Rao, P. V.; Holm, R. H. *Chem. Rev.* **2004**, *104*, 527-559, and references cited therein.

[10] (a) O'Sullivan, T.; Millar, M. M. *J. Am. Chem. Soc.* **1985**, *107*, 4096-4097. (b) Papaefthymiou, V.; Millar, M. M.; Münck, E. *Inorg. Chem.* **1986**, *25*, 3010-3014.

[11] Zhou, C.; Holm, R. H. *Inorg. Chem.* **1997**, *36*, 4066-4077.

[12] Ohki, Y.; Sunada, Y.; Tatsumi, K. *Chem. Lett.* **2005**, *34*, 172-173.

[13] Sharp, C. R.; Duncan, J. S.; Lee, S. C. *Inorg. Chem.* **2010**, *49*, 6697-6705.

[14] (a) Ohki, Y.; Takikawa, Y.; Hatanaka, T.; Tatsumi, K. *Organometallics* **2006**, *25*, 3111-3113. (b) Ohta, S.; Ohki, Y.; Ikagawa, Y.; Suizu, R.; Tatsumi, K. *J. Organomet. Chem.* **2007**, *692*, 4792-4799. (c) Ohki, Y.; Hatanaka, T.; Tatsumi, K. *J. Am. Chem. Soc.* **2008**, *130*, 17174-17186.

[15] (a) Ohki, Y.; Sunada, Y.; Honda, M.; Katada, M.; Tatsumi, K. *J. Am. Chem. Soc.* **2003**,

125, 4052-4053. (b) Ohki, Y.; Ikagawa, Y.; Tatsumi, K. *J. Am. Chem. Soc.* **2007**, *129*, 10457-10465. (c) Ohki, Y.; Murata, A.; Imada, M.; Tatsumi, K. *Inorg. Chem.* **2009**, *48*, 2358-2360. (d) Ohki, Y.; Imada, M.; Sunada, Y.; Murata, A.; Ohta, S.; Honda, M.; Sasamori, T.; Tokitoh, N.; Katada, M.; Tatsumi, K. *J. Am. Chem. Soc.* **2009**, *131*, 13168-13178.

[16] Ellison, J. J.; Ruhlandt-Senge, K.; Power, P. P. *Angew. Chem. Int. Ed.* **1994**, *33*, 1178-1180.

[17] For example: (a) Stack, T. D. P.; Holm, R. H. *J. Am. Chem. Soc.* **1988**, *110*, 2484-2494. (b) Walsdorff, C.; Saak, W.; Pohl, S. *J. Chem. Soc., Dalton Trans.* **1997**, 10857-1861.

[18] Deng, L.; Majumdar, A.; Lo, W.; Holm, R. H. *Inorg. Chem.* **2010**, *49*, 11118-11126.

[19] (a) Messick, T. E.; Chmiel, N. H.; Golinelli, M. –P.; Langer, M. R.; Joshua-Tor, L.; David, S. S. *Biochemistry* **2002**, *41*, 3931-3942. (b) Boon, E. M.; Livingston, A. L.; Chmiel, N. H.; David, S. S.; Barton, J. K. *Proc. Natl. Acad. Sci. U.S.A.* **2003**, *100*, 12543-12547.

[20] Bertero, M. G.; Rothery, R. A.; Palak, M.; Hou, C.; Lim, D.; Blasco, F.; Weiner, J. H.; Strynadka, N. C. J. *Nat. Struct. Biol.* **2003**, *10*, 681-687.

[21] Martins, B. M.; Dobbek, H.; Cinkaya, I.; Buckel, W.; Messerschmidt, A. *Proc. Natl. Acad. Sci. USA.* **2004**, *101*, 15645-15649.

[22] Pangborn, A. B.; Giardello, M. A.; Grubbs, R. H.; Rosen, R. K.; Timmers, F. J. *Organometallics* **1996**, *15*, 1518-1520.

Appendix 1

Supporting Information for Chapter 2

Table A1.1. Crystal Data for [Na(THF)$_2$][Fe$_4$S$_4${N(SiMe$_3$)$_2$}$_4$] ([**1**]$^-$), Fe$_4$S$_4$(SDmp)$_3$(THF)$_3$ (**2**), [Na(THF)][Fe$_4$S$_4$(SDmp)$_4$]·C$_7$H$_8$ **3**·C$_7$H$_8$, [Fe$_4$S$_4$(SDmp)$_3$(Me$_4$Im)]·C$_7$H$_8$ 4·C$_7$H$_8$, and [Na][Fe$_4$S$_4$(SDmp)$_3$(Me$_4$Im)]·C$_7$H$_8$·1/2(C$_6$H$_{14}$) [4]$^-$·C$_7$H$_8$·1/2(C$_6$H$_{14}$).

	[**1**]$^-$	**2**	**3**·C$_7$H$_8$
formula	$C_{32}H_{88}Fe_4N_4NaO_2S_4Si_8$	$C_{168}H_{198}Fe_8O_6S_{14}$	$C_{107}H_{116}Fe_4NaOS_8$
Formula wt (g mol^{-1})	1160.37	3209.02	2192.22
Crystal system	Monoclinic	Trigonal	Triclinic
Space group	$P2_1/c$ (No. 14)	R3c(h) (#161)	P-1 (#2)
a (Å)	12.322(2)	22.1344(5)	14.4755(19)
b (Å)	21.680(4)	22.1344(5)	15.3293(18)
c (Å)	22.708(4)	57.5967(17)	25.520(4)
α (°)	90	90	82.580(7)
β (°)	96.403(2)	90	87.684(7)
γ (°)	90	120	61.671(4)
V (Å^3)	6028.1(18)	24437.9(11)	4941.4(12)
Z	4	6	2
D_{calcd} (g/cm^3)	1.278	1.308	1.291
$Max\ 2\theta$ (°)	55.0	55.0	55.0
No. of Reflections Measured	13618	12430	20690
No. of Data Used (I >2.00 s(I))	11832	12009	16067
No. of Parameters Refined	497	578	1037
$R_1{}^a$	0.0448	0.0553	0.0727
$wR_2{}^b$	0.1280	0.1738	0.2142
GOF^c	1.034	1.022	1.069

[a] $I > 2\sigma(I)$, $R1=\Sigma||F_o|-|F_c||/\Sigma|F_o|$. [b] refined with all data, $wR2=[\{\Sigma w(F_o{}^2-F_c{}^2)^2\}/\Sigma w(F_o{}^2)^2]^{1/2}$. [c] GOF$=[\{\Sigma w(F_o{}^2-F_c{}^2)^2\}/(N_o-N_p)]^{1/2}$, where N_o and N_p denote the numbers of reflection data and parameters.

(Continued)

	4·C_7H_8	**[4]**$^-$·C_7H_8·1/2(C_6H_{14})
formula	$C_{86}H_{95}Fe_4N_2S_7$	$C_{88.5}H_{105}Fe_4N_2NaS_7$
Formula wt (g mol^{-1})	1604.52	1667.61
Crystal system	Monoclinic	Monoclinic
Space group	$P2_1/c$ (No. 14)	$P2_1/c$ (No. 14)
a (Å)	16.435(5)	14.928(5)
b (Å)	15.275(5)	24.680(8)
c (Å)	32.157(9)	24.281(8)
α (°)	90	90
β (°)	92.576(4)	104.824(4)
γ (°)	90	90
V (Å^3)	8065(4)	8648(5)
Z	4	4
D_{calcd} (g/cm^3)	1.321	1.281
$Max\ 2\theta$ (°)	55.0	55.0
No. of Reflections Measured	18455	19772
No. of Data Used (I >2.00 s(I))	11290	15038
No. of Parameters Refined	843	911
$R_1{}^a$	0.0808	0.0708
$wR_2{}^b$	0.2442	0.2340
GOF^c	1.040	1.090

[a] $I > 2\sigma(I)$, $R1=\Sigma||F_o|-|F_c||/\Sigma|F_o|$. [b] refined with all data, $wR2=[\{\Sigma w(F_o{}^2-F_c{}^2)^2\}/\Sigma w(F_o{}^2)^2]^{1/2}$. [c] $GOF=[\{\Sigma w(F_o{}^2-F_c{}^2)^2\}/(N_o-N_p)]^{1/2}$, where N_o and N_p denote the numbers of reflection data and parameters.

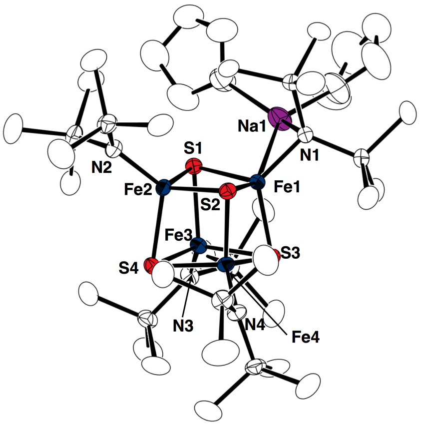

Figure A1.1. Crystal structure of [Na(THF)]$_2$][Fe$_4$S$_4${N(SiMe$_3$)$_2$}$_4$] ([Na(THF)$_2$][**1**]) with thermal ellipsoids at 50% probability level. All hydrogen atoms are omitted for clarity. Selected bond distances (Å): Fe1-Fe2, 2.8044(4); Fe1-Fe3, 2.8716(5); Fe1-Fe4, 2.8356(4); Fe2-Fe3, 2.9151(5); Fe2-Fe4, 2.8970(4); Fe3-Fe4, 2.8613(4); Fe1-S1, 2.3041(7); Fe1-S2, 2.2675(7); Fe1-S3, 2.2742(7); Fe2-S1, 2.3199(7); Fe2-S2, 2.2917(7); Fe2-S4, 2.3161(7); Fe3-S1, 2.2873(7); Fe3-S3, 2.3033(7); Fe3-S4, 2.2884(7); Fe4-S2, 2.2620(7); Fe4-S3, 2.2840(7); Fe4-S4, 2.3140(7); Fe1-N1, 1.9466(19); Fe2-N2, 1.897(2); Fe3-N3, 1.892(2); Fe4-N4, 1.8945(19); Na1-N1, 2.528(2).

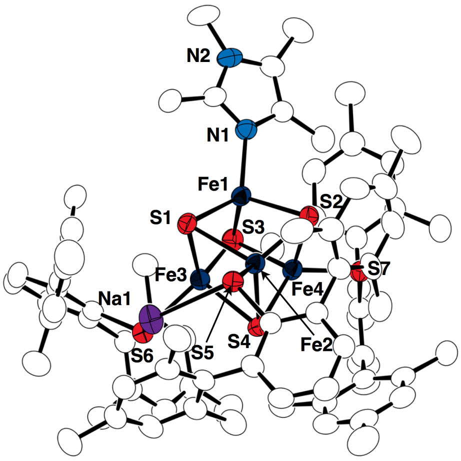

Figure A 1.2. Crystal structure of [Fe$_4$S$_4$(SDmp)$_3$- (Me$_4$Im)]$^-$ ([**4**]$^-$) with thermal ellipsoids at the 50% probability level. All hydrogen atoms and the crystal solvents are omitted for clarity. Selected bond distances (Å): Fe1-Fe2, 2.7335(7); Fe1-Fe3, 2.7138(6); Fe1-Fe4, 2.6834(6); Fe2-Fe3, 2.6903(8); Fe2-Fe4, 2.7250(7); Fe3-Fe4, 2.7238(6); Fe1-S1, 2.2297(9); Fe1-S2, 2.3042(12); Fe1-S3, 2.3048(12); Fe2-S1, 2.3415(11); Fe2-S2, 2.2298(9); Fe2-S4, 2.2833(11); Fe3-S1, 2.3255(11); Fe3-S3, 2.2169(10); Fe3-S4, 2.3106(11); Fe4-S2, 2.2322(12); Fe4-S3, 2.3139(12); Fe4-S4, 2.2322(9); Fe1-N1, 2.017(2); Fe2-S5, 2.2866(10); Fe3-S6, 2.2655(10); Fe4-S7, 2.2361(10); Na1-S5, 2.939(2); Na1-S6, 2.952(2).

Chapter 3

A Convenient Route to Synthetic Analogues of the Oxidized Form of High-Potential Iron-Sulfur Proteins

This chapter is partly reproduced with permission from: Tanifuji, K.; Yamada, N.; Tajima, T.; Sasamori, T.; Tokitoh, N.; Matsuo, T.; Tamao, K.; Ohki, Y.; Tatsumi, K. *submitted for publication*. Unpublished work copyright 2014 American Chemical Society.

3.1. Introduction

As mentioned in Chapters 1 and 2, high-potential iron-sulfur protein (HiPIP) and ferredoin (Fd) are known as electron-transfer proteins having [Fe_4S_4] cluster(s). While their electron carriers are commonly described as [$Fe_4S_4(Cys)_4$] (Cys = cysteinyl thiolate), the redox processes in operation are different between the ferredoxin (Fd) family and the high-potential iron-suflur protein (HiPIP) family. This difference has been attributed to the environment around the [Fe_4S_4] cluster. The smaller number of hydrogen bonds between water and the [Fe_4S_4] cluster of HiPIP has been proposed to account for the stability of the $[Fe_4S_4]^{3+}$ state,[1] and the crystal structures of HiPIP have revealed hydrophobic binding pockets for the [Fe_4S_4] cluster.[2] However, a wide range of $[Fe_4S_4]^{3+}/[Fe_4S_4]^{2+}$ redox potentials has been observed for HiPIPs, from +50 mV to +500 mV vs NHE,[3] and the factors contributing to the variety of redox potentials remain in discussion.[2f]

Synthetic analogues of [Fe_4S_4] clusters have provided insights into the structures and the properties of the clusters in proteins. Thus far, more than 70 examples of $[Fe_4S_4]^{2+}$ clusters $[Fe_4S_4(SR)_4]^{2-}$ (SR = thiolates) and around 10 examples of $[Fe_4S_4]^{+}$ clusters $[Fe_4S_4(SR)_4]^{3-}$ have been reported,[4] and comparisons of their properties have been useful to evaluate the correlation of hydrogen bonding,[5] the net charge of the clusters,[6] solvents,[7] and bulkiness of ligands[8] to the redox potentials and the accessible oxidation states of these clusters. On the other hand, $[Fe_4S_4(STip)_4]^{-}$ (Tip = 2,4,6-triisopropylphenyl) has been the only isolated $[Fe_4S_4]^{3+}$ cluster modeling the oxidized form of HiPIP until recently.[9]

Chapter 2 described the successful synthesis of the second isolated model of the oxidized form of HiPIP, $[Fe_4S_4(SDmp)_4]^-$ (renamed as **3a** in this chapter), from the reaction of the amide-ligated $[Fe_4S_4]^{3+}$ cluster $[Fe_4S_4\{N(SiMe_3)_2\}_4]^-$ ([**1**]$^-$)[10, 11] with 4 equiv of HSDmp (Dmp = 2,6-di(mesityl)phenyl). This result prompted us to expand the scope of the reaction, to synthesize various clusters modeling the oxidized form of HiPIP. In this chapter, we report the synthesis and properties of a series of $[Fe_4S_4]^{3+}$ clusters $[Fe_4S_4(SR)_4]^-$ (R = Tbt (**3b**), R = Eind (**3c**), R = Dxp (**3d**), R = Dpp (**3e**); Tbt = 2,4,6-tris[bis(trimethylsilyl)methyl]- phenyl, Eind = 1,1,3,3,5,5,7,7-octaethyl-*s*-hydrindacen-4-yl, Dxp = 2,6-di(*m*-xylyl)phenyl, Dpp = 2,6-di(phenyl)phenyl), combined with **3a**.

3.2. Results and Discussion

3.2.1. Synthesis of $[Fe_4S_4]^{3+}$ Clusters

Treatment of $[Na(THF)_2][Fe_4S_4\{N(SiMe_3)_2\}_4]$ ($[Na(THF)_2]$[**1**]) with 4 equiv of bulky thiols (HSR) in toluene led to the formation of the $[Fe_4S_4]^{3+}$ clusters $[Fe_4S_4(SR)_4]^-$ (**3a**-**e**) (Scheme 3.1). Subsequent cation exchange from $[Na]^+$ to $[N^nBu_4]^+$ was carried out for **3a** and **3c**-**e**, by treatment with $[N^nBu_4][PF_6]$ in THF. The crystal yields of **3a**-**e**, either with Na or N^nBu_4 cations, range from 26% to 72% depending on their readiness to crystallize, while the dominant formation of $[Fe_4S_4(SR)_4]^-$ was observed in the electro-spray ionization mass spectrum (ESI-MS) of the reaction mixtures where the anionic signals appeared at *m*/*z* = 1732.4 (**3a**), 2006.1 (**3c**), 1620.4 (**3d**), and 1396.4 (**3e**), respectively, as shown in Figure 3.1 for the mixture of **1** and **4** equiv of HSDmp. An exception was the reaction mixture of **1** and HSTbt, from which no significant ESI-MS signal for the iron-sulfur cluster was detected in the range of *m*/*z* = 500-3000. The absence of the signal of **3b** in the ESI-MS may be due to efficient

Scheme 3.1

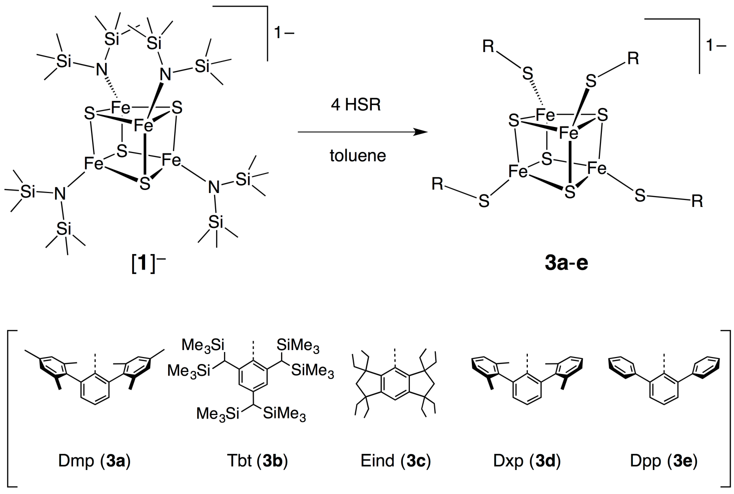

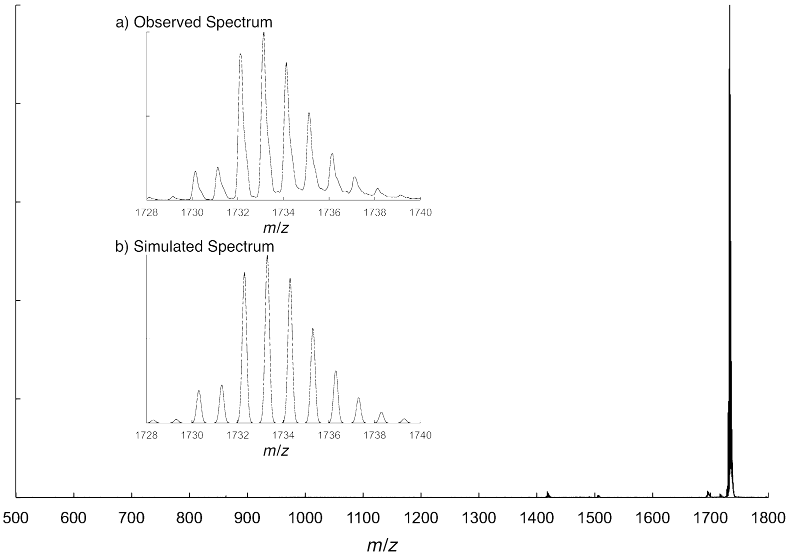

Figure 3.1. ESI-MS spectrum of **3a**.

capture of the Na cation by the STbt group and the [Fe_4S_4] core, hindering the separation of the Na cation from the cluster anion. The reaction depicted in Scheme 3.1 demonstrates a convenient and a clean synthetic route to less common $[Fe_4S_4]^{3+}$ clusters, which are now readily accessible by changing the thiols to be added to **1**.

Less polar organic solvents, such as toluene and THF, appeared to be crucial for this reaction. Although the reactions performed in CH_3CN gave $[Fe_4S_4(SR)_4]^-$ as the initial product, the ESI-MS of the CH_3CN solution gradually exhibited the signals of thiolates (^-SR), $[Fe_4S_4(SR)_4]^{2-}$, and other unidentified anions as time passed. Dimethylformamide (DMF) and methanol, which are often used as solvents in the synthesis of [Fe_4S_4] clusters, reacted rapidly with [**1**]$^-$ to give unidentified products. Furthermore, clusters **3a**-**e** appeared to be unstable when dissolved in DMF or methanol. A similar observation was reported by Millar *et al.*, who found that the stability of $[Fe_4S_4(STip)_4]^-$ is in the following order, $CH_2Cl_2 > CH_3CN >> DMF$.[9] This trend is consistent with the ascending order of the donor number (Lewis basicity) of these solvents, and hence degradation of $[Fe_4S_4(SR)_4]^-$ may be triggered by the coordination of polar organic solvents to iron.

The use of bulky thiols appeared to be important for the successful synthesis of $[Fe_4S_4(SR)_4]^-$ (**3a**-**e**), partly because the bulky thiolate ligands would hinder the access of solvents to the iron center. Another advantage of introducing bulky thiolates is the high solubility of $[Fe_4S_4(SR)_4]^-$ into less polar organic solvents. Bulky alkyl-thiolates $–S^tBu$ and $–SC(SiMe_3)_3$ are applicable for the synthesis of $[Fe_4S_4(SR)_4]^-$ (R = ^{t}Bu, $C(SiMe_3)_3$) from [**1**]$^-$ and HSR in THF. The ESI-MS signals of $[Fe_4S_4(SR)_4]^-$ appeared at *m*/*z* = 707.8 (R = ^{t}Bu) and 1406.1 (R = $C(SiMe_3)_3$), while crystallization of these clusters has been unsuccessful. On the other hand, the reaction mixtures of [**1**]$^-$ and less bulky thiols, such as HSPh, $HS(C_6H_4\text{-}4\text{-}^tBu)$, HS^iPr, and HSEt, did not show the ESI-MS signals of $[Fe_4S_4(SR)_4]^-$. The subsequent workup gave ill-defined products.

3.2.2. Absorption Spectra and EPR Spectra of $[Fe_4S_4]^{3+}$ Clusters

The absorption spectra of clusters **3a**, **3c**, and **3d** exhibited two bands in the ranges of 342-348 nm and 446-502 nm, while a single absorption maximum was observed for **3b** and **3e** at 459-465 nm (Table 3.1). These absorptions are assignable to the ligand-to-metal charge transfer (LMCT) bands.[12] The absorption maxima of **3a**, **3c**, and **3d** (λ_{max} = 342-348 nm, 446-502 nm) are slightly lower in energy as compared with those for the $[Fe_4S_4]^{3+}$ cluster $[Fe_4S_4(SAd)_4]^-$ (λ_{max} = 326, 430 nm, Ad = adamantyl), which was generated in-situ via electrochemical oxidation of $[Fe_4S_4(SAd)_4]^{2-}$ (λ_{max} = 318, 418 nm).8 Comparison of the absorptions for $[Fe_4S_4(SAd)_4]^{-/2-}$ indicates the red-shift of absorption maxima upon oxidation, and

Table 3.1. Absorption maxima and EPR data of $[Fe_4S_4]^{3+}$ clusters **3a-e**.

	λ_{max}/ nm (ε/ M^{-1} cm^{-1})[a]		g values	g_{av}
[Na(THF)]**3a**	348 ($1.7 \cdot 10^4$)	446($1.4 \cdot 10^4$)	2.076, 2.035, 2.018 [b]	2.043
$[N^nBu_4]$**3a**	343 ($2.1 \cdot 10^4$)	469 ($2.3 \cdot 10^4$)	2.100, 2.051, 2.021 [b]	2.057
[Na(THF)]**3b**		459 ($2.0 \cdot 10^4$)	2.100, 2.041 [b]	2.071
$[N^nBu_4]$**3c**	342 ($1.4 \cdot 10^4$)	502 ($3.1 \cdot 10^4$)	2.136, 2.043, 2.025 [c]	2.068
$[N^nBu_4]$**3d**	344 ($2.2 \cdot 10^4$)	466 ($2.6 \cdot 10^4$)	2.109, 2.051 [c]	2.070
$[N^nBu_4]$**3e**		465 ($2.1 \cdot 10^4$)	2.071, 2.028 [c]	2.042

[a] Measured in THF. [b] Measured at 8 K. [c] Measured at 16 K.

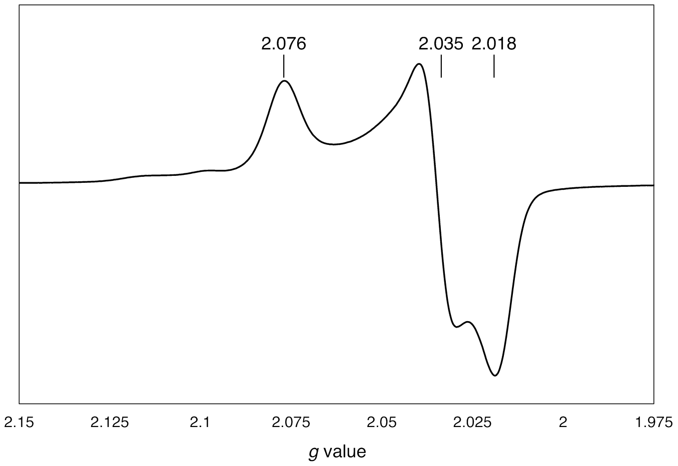

Figure 3.2. EPR spectrum (X band, microwave 1.0 mW) of [Na(THF)]**3a** measured in frozen toluene at 8 K.

this is also the case for $[Fe_4S_4\{N(SiMe_3)_2\}_4]^{n-}$ (n = 0, 1, 2)[11] and the $[Fe_4S_4]$ cluster of *Rhodothermus marinus* HiPIP.[2f]

Clusters **3a-e** indicated the $S = 1/2$ ground state in the EPR spectrum, as shown in Figure 3.2 for [Na(THF)]**3a** (g = 2.076, 2.035, 2.018). As summarized in Table 3.1, the EPR signals of other clusters appeared as rhombic for $[N^nBu_4]$**3a** (g = 2.100, 2.051, 2.021) and $[N^nBu_4]$**3c** (g = 2.136, 2.043, 2.025), and axial for [Na(THF)]**3b** (g = 2.100, 2.041), [N^{n}Bu$_4$]**3d** (g = 2.109, 2.051), and [N^{n}Bu$_4$]**3e** (g = 2.071, 2.028). The averaged g values, g_{av} = 2.043 ([Na(THF)]**3a**), 2.057([N^{n}Bu$_4$]**3a**), 2.071 ([Na(THF)]**3b**), 2.068 ([N^{n}Bu$_4$]**3c**), 2.070 ([N^{n}Bu$_4$]**3d**), and 2.042 ([N^{n}Bu$_4$]**3e**), are comparable to that of $[Fe_4S_4(STip)_4]^-$ (g_{av} = 2.06, g = 2.10, 2.05, 2.03),[13] and are higher than those of $[Fe_4S_4(SR)_4]^{3-}$, g_{av} = 1.97 (R = CH_2Ph), 1.97 (R = Ph).[14] These results are consistent with the EPR observation on *Rhodophia globiformis* HiPIP, where the g_{av} value is higher for the $[Fe_4S_4]^{3+}$ state (g_{av} = 2.08, g = 2.12, 2.03) than that for the $[Fe_4S_4]^+$ state (g_{av} = 1.98, g = 2.04,1.92).[15] The g_{av} values for the $[Fe_4S_4]^{3+}$ state of other HiPIPs are 2.056 (*Rhodopseudomonas gelatinosa*),[16] 2.065 (*Thiobacillus ferrooxidans*),[17] and 2.069 (*Ectothiorhodospiza halophila*),[18] which are also comparable to those of clusters **3a**-**e**.

3.2.3. Structures of $[Fe_4S_4]^{3+}$ Clusters

Single crystals of clusters **3a**-**e** suitable for X-ray crystallography were obtained with Na (**3a**, **3b**) or N^{n}Bu$_4$ (**3a**, **3c**, **3d**, **3e**) counter-cations. The representative structures of [Na(THF)]**3a**, [Na(THF)]**3b**, and [N^{n}Bu$_4$]**3c** are shown in Figure 3.3-3.5.[19]

The Na(THF) groups of [Na(THF)]**3a** (R = Dmp) and [Na(THF)]**3b** (R = Tbt) are disordered over two and four positions, respectively, and only one of each type of group is shown for clarity. The coordination geometry of Na varies depending on the thiolate substituent, as the *m*-terphenyl groups (R = Dmp, Dxp, Dpp) offer a possible interaction between Na and one of the aryl moieties attached to the 2,6-positions of the central ring. For example, the Na cation of [Na(THF)]**3a** is in a distorted tetrahedral geometry, interacting with an oxygen atom of THF, two sulfur atoms of SDmp and the $[Fe_4S_4]$ core, in addition to one of the mesityl rings of

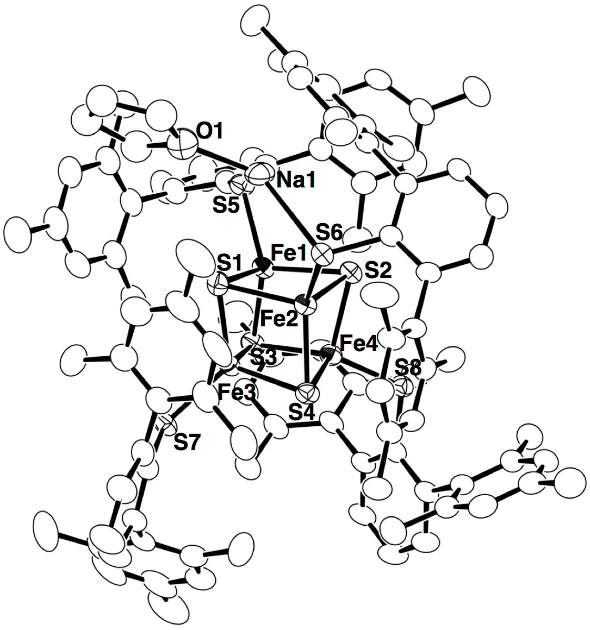

Figure 3.3. Molecular structure of [Na(THF)]**3a** with thermal ellipsoids at the 50% probability level. All hydrogen atoms and the disordered Na(THF) group are omitted for clarity.

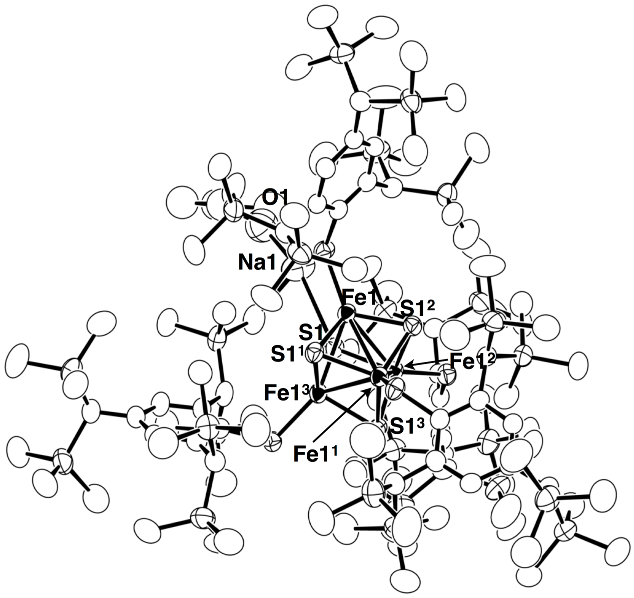

Figure 3.4. Molecular structure of [Na(THF)]**3b** with thermal ellipsoids at the 50% probability level. All hydrogen atoms and the disordered [Na(THF)] group are omitted for clarity.

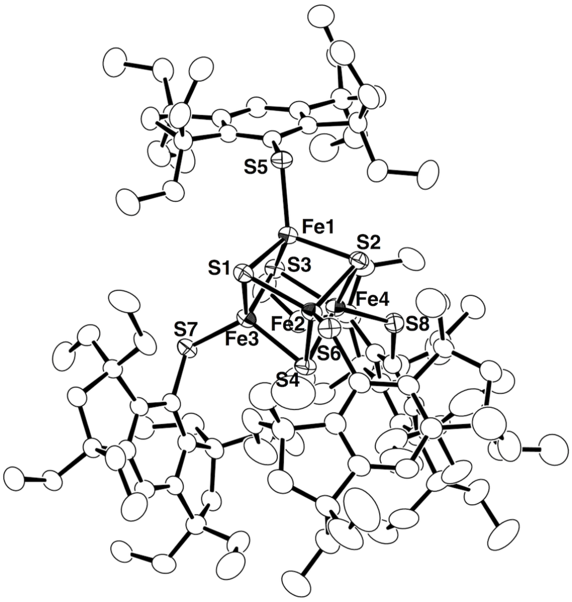

Figure 3.5. Molecular structure of $[\mathrm{N}^n\mathrm{Bu}_4]$**3c** with thermal ellipsoids at the 50% probability level. All hydrogen atoms, the disordered atoms, $\mathrm{N}^n\mathrm{Bu}_4$ cation and the crystal solvent are omitted for clarity.

the Dmp group. The Na-C(mesityl) distances (2.885(4)–2.979(5) Å) are in the range of the Na-C(Tip) distances determined for $\mathrm{NaS(2,6\text{-}Tip_2C_6H_3)}$ (2.839(5)–3.249(5) Å).[20] On the other hand, the Na cation in [Na(THF)]**3b** is in a distorted T-shape geometry, with the S(core)-Na-O, S(core)-Na-S(thiolate), and S(thiolate)-Na-O angles being 156.2(4)°, 77.0(3)°, and 126.3(5)°, respectively. An additional C-H---Na interaction may be present, if the shortest C---Na distance of 2.7661(4) Å is taken into account. In the cases of $[\mathrm{N}^n\mathrm{Bu}_4]$**3a**, $[\mathrm{N}^n\mathrm{Bu}_4]$**3c** (R = Eind), $[\mathrm{N}^n\mathrm{Bu}_4]$**3d** (R = Dxp), and $[\mathrm{N}^n\mathrm{Bu}_4]$**3e** (R = Dpp), weak C-H---S hydrogen bonds may be present between the $\mathrm{N}^n\mathrm{Bu}_4$ cation and sulfur atoms of thiolates or the $[\mathrm{Fe_4S_4}]$ core, with the shortest C---S distances of 3.512(2)-3.733(4) Å, while some of these distances are longer than the structurally identified C-H---S hydrogen bond (C---S, 3.649(3) Å) found for 2,3-diphenyl-4-morpholinomethyl-5-ehynyl-2-thio-2-phosphabicyclo[4.4.0]decan-

5-ol.[21]

The iron atoms of clusters **3a**-**e** are in a distorted tetrahedral geometry, coordinated by three sulfur atoms of the [Fe_4S_4] core and one thiolate sulfur. The mean Fe-Fe and Fe-S(core) distances, ranging from 2.7324(4) to 2.7985(10) Å and from 2.2618(5) to 2.2819(11) Å, respectively, are shorter than those of cluster **1** (Fe-Fe : 2.8044(4)-2.9203(7) Å, Fe-S : 2.2620(7)-2.3199(7) Å).[10, 11] Whereas the mean Fe-S(core) and Fe-S(thiolate) distances are similar between [Na(THF)]**3a** and [N^nBu_4]**3a**, the S6-Na interaction (2.894(3) Å) in [Na(THF)]**3a** leads to the longer Fe2-S6 distance (2.2615(9) Å) relative to the other Fe-S(thiolate) distances (2.2128(10)-2.2445(15) Å).

The averaged Fe-Fe, Fe-S, and S-C distances of clusters **3a**-**e**, $[Fe_4S_4(STip)_4]^-$,[9] $[Fe_4S_4(SDpp)_4]^{2-}$,[22] $[Fe_4S_4(SMes)_4]^{2-}$ (Mes = mesityl),[23] $[Fe_4S_4(SPh)_4]^{2-}$,[24] and $[Fe_4S_4(SPh)_4]^{3-}$,[14] are listed in Table 3.2. Comparison of the mean Fe-Fe distances between $[Fe_4S_4(SDpp)_4]^-$ (**3e**, 2.7324(4) Å) and $[Fe_4S_4(SDpp)_4]^{2-}$ (2.759(2) Å) indicates that the higher oxidation state leads to slightly shorter Fe-Fe distances. A similar comparison can be made with the known $[Fe_4S_4]^{2+/+}$ clusters, $[Fe_4S_4(SPh)_4]^{2-}$ (2.736(3) Å) and $[Fe_4S_4(SPh)_4]^{3-}$ (2.744(17) Å), although their difference is within the standard deviations. The variety of thiolate substituents has greater effect on the mean Fe-Fe distances than the difference of the oxidation states, and the range of 2.7324(4)-2.7985(10) Å found for **3a**-**e** is larger than the differences caused by the change in oxidation states. A small influence of the oxidation states on Fe-Fe distances can be also seen in the volume of the Fe_4 tetrahedron. The values of clusters **2a**-**e** (2.40-2.58 $Å^3$) are slightly large but not much different from the averaged values for $[Fe_4S_4(SAr)_4]^{2-}$ (Ar = aryl, 2.41 $Å^3$) and $[Fe_4S_4(SAr)_4]^{3-}$ (2.42 $Å^3$).[25]

Table 3.2. Averaged bond distances (Å) for clusters **3a-e**, $[Fe_4S_4(STip)_4]^{-}$, $[Fe_4S_4(SDpp)_4]^{2-}$, $[Fe_4S_4(SMes)_4]^{2-}$, $[Fe_4S_4(SPh)_4]^{2-}$, and $[Fe_4S_4(SPh)_4]^{3-}$.

	[Na(THF)]**3a**	[N^{n}Bu$_4$]**3a**	**3b**	**3c**
oxidation state	$[Fe_4S_4]^{3+}$			
av. Fe-Fe	2.7677(10)	2.7846(9)	2.7854(7)	2.7685(8)
av. Fe-S(core)	2.2688(14)	2.2691(15)	2.2819(11)	2.2661(11)
av. Fe-S(thiolate)	2.2268(11)	2.2439(13)	2.2423(11)	2.2308(11)
av. S(thiolate)-C	1.784(6)	1.785(5)	1.786(3)	1.792(4)

	3d	**3e**	$[Fe_4S_4(STip)_4]^{-}$[a]	$[Fe_4S_4(SDpp)_4]^{2-}$[b]
oxidation state	$[Fe_4S_4]^{3+}$	$[Fe_4S_4]^{3+}$	$[Fe_4S_4]^{3+}$	$[Fe_4S_4]^{2+}$
av. Fe-Fe	2.7985(10)	2.7324(4)	2.74(1)	2.759(2)
av. Fe-S(core)	2.2719(13)	2.2618(5)	2.262(8)	2.287(3)
av. Fe-S(thiolate)	2.2431(14)	2.2239(6)	2.206(7)	2.287(3)
av. S(thiolate)-C	1.784(5)	1.7786(19)	1.90(3)	1.772(10)

	$[Fe_4S_4(SMes)_4]^{2-}$[c]	$[Fe_4S_4(SPh)_4]^{2-}$[d]	$[Fe_4S_4(SPh)_4]^{3-}$[e]
oxidation state	$[Fe_4S_4]^{2+}$		$[Fe_4S_4]^{1+}$
av. Fe-Fe	2.760(5)	2.736(3)	2.744(17)
av. Fe-S(core)	2.286(5)	2.286(5)	2.309(6)
av. Fe-S(thiolate)	2.274(6)	2.263(3)	2.294(10)
av. S(thiolate)-C	1.778(14)	1.771(2)	1.751(26)

[a] Reference 9. [b] Reference 22. [c] Reference 23. [d] Reference 24. [e] Reference 14.

Much like the Fe-Fe distances, the Fe-S(core) distances become slightly shorter upon oxidation, *i.e.* $[Fe_4S_4(SDpp)_4]^{-}$ (**3e**, 2.2618(5) Å) vs $[Fe_4S_4(SDpp)_4]^{2-}$ (2.287(3) Å), and $[Fe_4S_4(SPh)_4]^{2-}$ (2.286(5) Å) vs $[Fe_4S_4(SPh)_4]^{3-}$ (2.309(6) Å). The slight shortening of Fe-Fe and Fe-S(core) distances is consistent with the reduction of the ionic radius of iron atoms upon oxidation, and is also in agreement with the theoretical analysis on the qualitative energy level scheme of $[Fe_4S_4(SR)_4]^{-/2-/3-}$ clusters, which suggested that the redox events occur in the Fe-Fe nonbonding and the Fe-S(core) antibonding orbitals.[26] The difference in Fe-S(thoiolate) distances between two oxidation states, **3e** (2.2239(6) Å) and $[Fe_4S_4(SDpp)_4]^{2-}$ (2.287(3) Å), is larger than the those found in the Fe-Fe and Fe-S(core) distances, and is also larger than the difference in Fe-S(thoiolate) distances caused by changing the thiolate substituents in the same $[Fe_4S_4]^{3+}$ oxidation state, 2.206(7)-2.2439(13) Å for clusters **3a**-**e** and $[Fe_4S_4(STip)_4]^{-}$. Similarly, the difference in the Fe-N(SiMe$_3$)$_2$ distances among the three oxidation states of $[Fe_4S_4\{N(SiMe_3)_2\}_4]^{0/1-/2-}$ is larger than those found for the Fe-Fe and Fe-S(core) distances.[10, 11] This indicates that the Fe-S(thiolate) and Fe-N(amide) distances are more flexible than the Fe-Fe and Fe-S(core) distances in the robust and structurally less flexible $[Fe_4S_4]$ core.

3.2.4. Cyclic Voltammograms of $[Fe_4S_4]^{3+}$ Clusters and the influence of bulky substituents.

An important function of HiPIP is the $[Fe_4S_4]^{3+}/[Fe_4S_4]^{2+}$ redox process. Thus the cyclic voltammograms (CVs) of $[Fe_4S_4]^{3+}$ clusters **3a**-**e**, $[Fe_4S_4(STip)_4]^{-}$, and $[Fe_4S_4(SPh)_4]^{2-}$ were measured to evaluate the influence of thiolates on redox potentials. The results are summarized in Table 3.3, and Figure 3.6 shows the CV diagram of **3c**. The origin of the weak feature around –0.4 V in Figure 3.6 is probably a decomposed compound formed by the $[Fe_4S_4]^{4+}/[Fe_4S_4]^{3+}$ process of **3c**, because this feature was not observed in the CV measurement between –0.2 V and

Table 3.3. Redox potentials (vs Ag/$AgNO_3$) of clusters **3a-e**, $[Fe_4S_4(STip)_4]^-$, and $[Fe_4S_4(SPh)_4]^{2-}$.

redox couple	$[Fe_4S_4]^{4+}/[Fe_4S_4]^{3+}$	$[Fe_4S_4]^{3+}/[Fe_4S_4]^{2+}$	$[Fe_4S_4]^{2+}/[Fe_4S_4]^{+}$	solvent
3a	0.08	–0.82	-	THF
3b	-	–0.86	-	THF
3c	0.08	–0.84	-	THF
3d	-	–0.74	-	THF
3e	-	–0.63	–1.77	THF
$[Fe_4S_4(STip)_4]^-$	-	–0.53	–1.71	THF
$[Fe_4S_4(SPh)_4]^{2-}$	-	–0.21	–1.30	THF

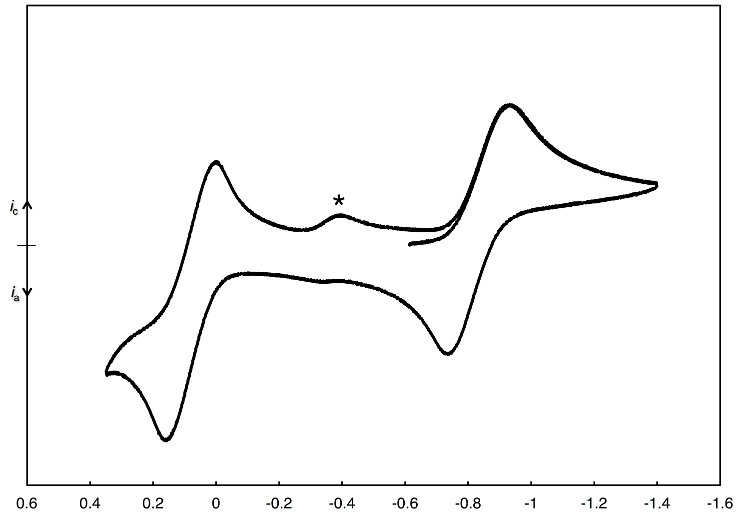

Figure 3.6. Cyclic voltammogram of [N^nBu_4]**3c**. Conditions: sample concentration, 3 mM in THF; supporting electrolyte, 0.3 M [N^nBu_4][PF_6]; working electrode, glassy carbon; counter electrode, Pt. The potential sweep was started at –0.614 V in the negative-going direction. The weak feature at –0.4 V (*) appears only after the scanning at $E_{1/2}$ = 0.08 V.

–1.4 V. All measurements were carried out in THF in the presence of [N^nBu_4][PF_6] as the supporting electrolyte, and the potentials were referenced to Ag/$AgNO_3$.

The Ag/Ag$^+$ reference was used instead of Fc/Fc$^+$ (Fc = $(C_5H_5)_2Fe$) because the $[Fe_4S_4]^{4+}/[Fe_4S_4]^{3+}$ process was obscured by the Fc/Fc$^+$ redox couple. Since a large excess of N^{n}Bu$_4$ cation was present in the CV measurements, we speculate that the cation exchange from Na to N^{n}Bu$_4$ occurs for [Na(THF)]**3a** and [Na(THF)]**3b**.

The $[Fe_4S_4]^{3+}/[Fe_4S_4]^{2+}$ redox couple in THF was observed at $E_{1/2}$ = –0.82 V (**3a**; R = Dmp), –0.86 V (**3b**; R = Tbt), –0.84 V (**3c**; R = Eind), –0.74 V (**3d**; R = Dxp), –0.63 V (**3e**; R = Dpp), and –0.53 V ($[Fe_4S_4(STip)_4]^-$). These $E_{1/2}$ values are significantly more negative than that with smaller benezenethiolates $[Fe_4S_4(SPh)_4]^{2-}$ ($E_{1/2}$ = –0.21 V). These comparisons suggest that the thiolate substituents have a major impact on the redox potentials. An interesting comparison can be made among clusters **3a** (R = Dmp), **3d** (R = Dxp), and **3e** (R = Dpp), as a wide range of redox potentials from –0.63 V (**3e**) to –0.82 V (**3a**) is achieved simply by changing the number of methyl groups incorporated to the 2,6-aryl moieties attached to the central phenyl ring. In contrast to this observation, the potentials for the oxidation of thiolate anions (E = –0.34 V for $^-$SDpp, –0.34 V for $^-$SDxp, and –0.36 V for $^-$SDmp) fall within a narrower range. Since these potentials indicate that the electronic effect of methyl groups on the 2,6-aryl moieties is indirect and small, we assume that the difference in potentials is more attributable to the steric effect of thiolate ligands.

Steric shielding of the $[Fe_4S_4]$ core by the bulky thiolates would be a key to understanding the varied and negatively shifted potentials of the $[Fe_4S_4]^{3+}/[Fe_4S_4]^{2+}$ redox couple observed for clusters **3a-e** and $[Fe_4S_4(STip)_4]^-$ compared to $[Fe_4S_4(SPh)_4]^{2-}$ and the substituent-dependent variation among these clusters. Figure 3.7 summarizes the redox potentials of clusters **3a-e**, $[Fe_4S_4(STip)_4]^-$, and $[Fe_4S_4(SPh)_4]^{2-}$ in

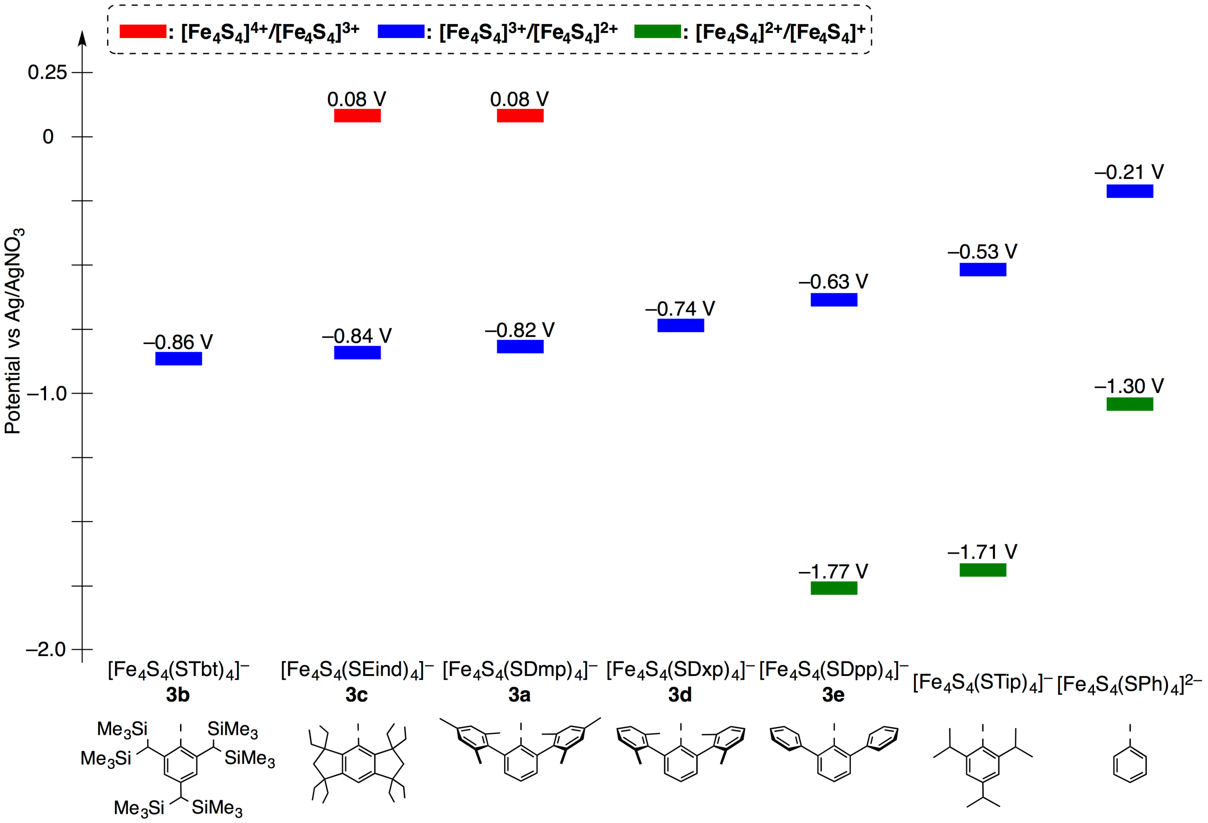

Figure 3.7. Redox potentials of clusters **3a-e**, $[Fe_4S_4(STip)_4]^-$, and $[Fe_4S_4(SPh)_4]^{2-}$.

descending order of the $[Fe_4S_4]^{3+}/[Fe_4S_4]^{2+}$ couple. Using $[Fe_4S_4(SPh)_4]^{2-}$ as a standard, the series of clusters can be categorized into two groups. One group includes clusters having super-bulky substituents, **3b** (R = Tbt), **3c** (R = Eind), and **3a** (R = Dmp). The other consists of clusters bearing moderately-bulky substituents, **3d** (R = Dxp), **3e** (R = Dpp) and $[Fe_4S_4(STip)_4]^-$. As can be seen from the space-filling models of clusters **3a-e** (Figure 3.8), the bulky substituents nearly encapsulate the cluster anion, indicating that the latter group (R = Dxp, Dpp, Tip) has more space among substituents compared with the former group (R = Tbt, Eind, Dmp). We speculate that the degree of encapsulation is a major factor of the substituent-dependent redox properties found in the comparison of clusters **3a-e** and

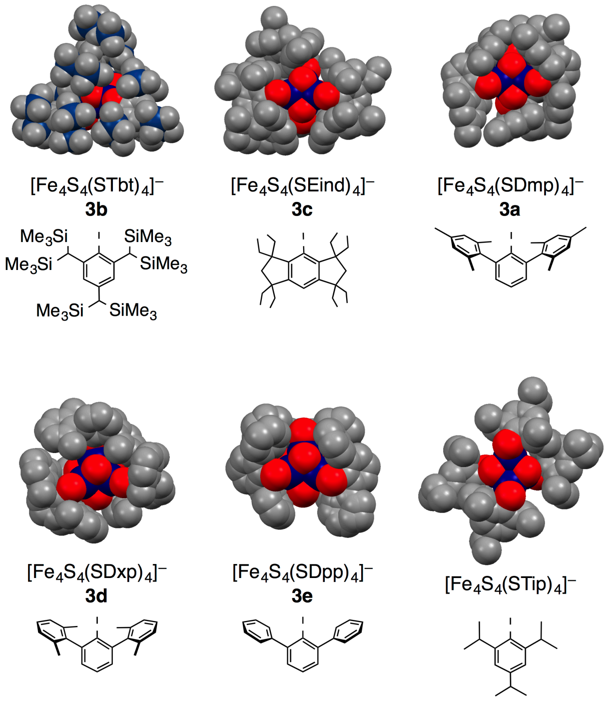

$[Fe_4S_4(STbt)_4]^-$ **3b**
$[Fe_4S_4(SEind)_4]^-$ **3c**
$[Fe_4S_4(SDmp)_4]^-$ **3a**
$[Fe_4S_4(SDxp)_4]^-$ **3d**
$[Fe_4S_4(SDpp)_4]^-$ **3e**
$[Fe_4S_4(STip)_4]^-$

Figure 3.8. Space-filling descriptions of molecular structures of cluster **3a**-**e** and $[Fe_4S_4(STip)_4]^{-9}$. Fe = blue, S = red, Si = light blue, carbon = dark gray.

$[Fe_4S_4(STip)_4]^-$. Encapsulation of the $[Fe_4S_4]$ anion hinders its contact with solvent or the counter-cation, and hence leads to a less efficient solvation and a decrease in charge neutralization by the interaction of the ion-pair. The electrochemical reduction of $[Fe_4S_4(SR)_4]^-$ gives the dianionic form $[Fe_4S_4(SR)_4]^{2-}$, which would require more efficient charge neutralization and solvation. Thus for clusters **3a**-**e** and $[Fe_4S_4(STip)_4]^-$, steric shielding would destabilize the dianionic clusters $[Fe_4S_4(SR)_4]^{2-}$, and it also leads to the more negative potentials for the reduction of $[Fe_4S_4]^{3+}$ clusters $[Fe_4S_4(SR)_4]^-$. The negative shift of potentials by steric shielding is further supported by the potentials of the $[Fe_4S_4]^{2+}/[Fe_4S_4]^+$ redox couple observed for $[Fe_4S_4(SPh)_4]^{2-}$ ($E_{1/2}$ = –1.30 V), $[Fe_4S_4(STip)_4]^-$ ($E_{1/2}$ = –1.71 V), and **3e** (R = Dpp, $E_{1/2}$ = –1.77 V). Clusters **3a**-**d** only exhibit irreversible reduction waves from the $[Fe_4S_4]^{2+}$ state within the potential window of THF. Although it is difficult to quantify the coverage of the [Fe_4S_4] core by substituents, these results suggest that the bulkiness of substituents controls not only the redox potentials but also the stable oxidation states of [Fe_4S_4] clusters.

The steric effect of bulky thiolates in **3a**-**e** and [$Fe_4S_4(STip)_4$]$^-$ may be relevant to the hydrophobic environment around the [Fe_4S_4] cluster of HiPIP. The [Fe_4S_4] cluster in HiPIP is buried in a hydrophobic cavity consisting of alkyl and aromatic residues of amino acids, whereas the cluster in Fd is located around the protein surface and exposed to water. Therefore, the stable oxidation states of [Fe_4S_4] clusters would be modulated by the adjustment of solvent accessibility to the clusters. This function of the hydrophobic cavity corresponds to the effect of steric shielding discussed above; that is, encapsulation of the [Fe_4S_4] core stabilizes the [Fe_4S_4]$^{3+}$ oxidation state because bulky substituents would hinder the interaction between the cluster anion and the counter-cation or solvent molecules. Further, the substituent-dependent large shifts of the redox potentials observed in **3a**-**e** and [$Fe_4S_4(STip)_4$]$^-$ imply that a wide range of redox potentials for HiPIP is generated by even a small structural modulation of the hydrophobic cavity.

In contrast to the known [Fe_4S_4] clusters which usually exhibit the [Fe_4S_4]$^{2+}$/[Fe_4S_4]$^+$ redox couple, clusters **3a**-**d** only exhibit irreversible reduction waves from the [Fe_4S_4]$^{2+}$ state within the potential window of THF. Instead, the [Fe_4S_4]$^{4+}$/[Fe_4S_4]$^{3+}$ redox couple was observed for **3a** and **3c** at $E_{1/2}$ = +0.08 V, although the [Fe_4S_4]$^{4+}$ state has been unprecedented for synthetic and biological [Fe_4S_4] clusters. This result is probably due to the large negative shift of redox potentials caused by the bulky thiolate ligands. The large negative shift would also result in the stabilization of the more oxidized $[Fe_4S_4]^{4+}$ state within the timescale of CV measurements, whereas synthesis of [**3a**]$^+$ or [**3c**]$^+$ via chemical oxidation has been unsuccessful thus far. The observation of the $[Fe_4S_4]^{4+}/[Fe_4S_4]^{3+}$ redox couple again shows the significant impact of the bulky thiolate ligands on the redox potentials.

3.3. Conclusions

A series of $[Fe_4S_4]^{3+}$ clusters $[Fe_4S_4(SR)_4]^-$ (**3a**-**e**) modeling the oxidized form of HiPIP were synthesized from the ligand exchange reactions of $[Fe_4S_4\{N(SiMe_3)_2\}_4]^-$ ($[\mathbf{1}]^-$) with 4 equiv of thiols (HSR), while bulky thiols were needed for stabilization of the products. This work offers a simple and convenient synthetic route to the $[Fe_4S_4]^{3+}$ clusters, and notably the precursor $[\mathbf{1}]^-$ is available from the one-pot reaction of $FeCl_3$, $NaN(SiMe_3)_2$, and NaSH, according to the synthetic procedure reported by Lee *et al.*[11] The structures of clusters **3a**-**e** were determined by X-ray crystallography, and they revealed that the Fe-S(thiolate) distances are more susceptible to redox than the Fe-Fe and Fe-S(core) distances of the $[Fe_4S_4]$ core. The CV measurements of clusters **3a**-**e** exhibited the $[Fe_4S_4]^{3+}/[Fe_4S_4]^{2+}$ redox couples, whose $E_{1/2}$ values were significantly more negative than that of $[Fe_4S_4(SPh)_4]^{2-}$. The large negative shift of the $[Fe_4S_4]^{3+}/[Fe_4S_4]^{2+}$ redox couples also enabled us to observe the uncommon $[Fe_4S_4]^{4+}/[Fe_4S_4]^{3+}$ redox couple for clusters **3a** and **3c**. We speculate that the steric effect of the bulky thiolate ligands is important for modulation of the redox potentials, as the bulky groups would efficiently hinder the electrostatic interaction between the cluster anion and the counter-cation, resulting in the destabilization of more negatively charged $[Fe_4S_4(SR)_4]^{2-}$ and $[Fe_4S_4(SR)_4]^{3-}$ clusters in the relatively reduced $[Fe_4S_4]^{2+}$ and $[Fe_4S_4]^{+}$ oxidation states.

3.4. Experimental Section

General Procedures. All reactions were manipulated using Schlenk techniques and a glove box under a nitrogen atmosphere. Hexane, toluene, diethylether, dichloromethane, THF, and hexamethyldisiloxane (HMDSO) were purified by the method of Grubbs,[27] where the solvents were passed over columns of activated alumina and a supported copper catalyst supplied by Hansen & Co. Ltd. The electro-spray ionization mass spectra (ESI-MS) were recorded on a Bruker Micromass LCT TOF-MS or MicroTOF II at room temperature. UV-vis spectra were measured on a JASCO V560 spectrometer at room temperature. The EPR spectra of **3a**-**e** were recorded on a Bruker EMX-plus spectrometer at X-band frequencies. Cyclic voltammograms (CV) were recorded in THF at room temperature using glassy carbon as the working electrode with 0.3 M (for cluster **2a**-**e**, $[Fe_4S_4(STip)_4]^-$, and $[Fe_4S_4(SPh)_4]^{2-}$) or 0.2 M (for $^-$SDmp, $^-$SDxp, and $^-$SDpp) $[N^nBu_4][PF_6]$ as the supporting electrolyte. The potentials were measured against an Ag/AgNO$_3$ (0.01 M in CH$_3$CN) reference electrode separated from the working compartment by a Vycor junction. ^{1}H and ^{13}C{^{1}H} NMR spectra were recorded on a JEOL ECA-600 or a JEOL ECA-500, and the data were analyzed by MestReNova software (version 8.1.2). ^{1}H NMR signals were referenced to the residual peaks of solvents. ^{13}C{^{1}H} NMR signals were referenced to signals of CD$_3$CN. ^{1}H NMR characterization of $[Na(THF)][Fe_4S_4(SDmp)_4]$ ([Na(THF)]**2a**) and $[Na(THF)][Fe_4S_4(STbt)_4]$ ([Na(THF)]**2b**) were unsuccessful because the number of signals was more than expected. For example, ^{1}H NMR ([Na(THF)]**2a** in CD$_2$Cl$_2$): δ 9.79 (br), 8.12 (br), 7.04 (br), 6.80 (br), 6.58 (br), 4.88 (br), 3.69 (br), 2.65 (br), 2.61 (br), 2.46 (br), 2.29 (br). This may be because of a non-equivalence of thiolate ligands in solution; however, the integrated values were not helpful for the assignment. Elemental analyses were performed on a LECO-CHNS-932 elemental analyzer where the crystalline samples were sealed in tin capsules under nitrogen. [N^{n}Bu$_4$][PF$_6$] was purchased from TCI co., Ltd. and used after recrystallization from THF. [Na(THF)$_2$][Fe$_4$S$_4${N(SiMe$_3$)$_2$}$_4$] ([Na(THF)$_2$][**1**]),[10, 11] HSDmp,[28] HSTbt,[29] HSEind,[30] HSDxp,[31] and HSDpp[32] were prepared according to literature procedures.

Synthesis of [Na(THF)][Fe$_4$S$_4$(SDmp)$_4$] ([Na(THF)]3a). A toluene (70 mL) solution of HSDmp (2.01 g, 5.80 mmol) was added to a toluene (10 mL) solution of [Na(THF)$_2$][Fe$_4$S$_4${N(SiMe$_3$)$_2$}$_4$] ([Na(THF)$_2$][**1**], 1.65 g, 1.42 mmol) at room temperature. The solution was stirred overnight before being evaporated to dryness. The black residue was extracted with a mixture of THF (1 mL) and toluene (30 mL), and the solution was centrifuged to remove a small amount of insoluble solid. The extract was concentrated to *ca.* 10 mL, and HMDSO (60 mL) was carefully layered. After slow diffusion at room temperature, black crystals of [Na(THF)][Fe$_4$S$_4$(SDmp)$_4$]·C$_7$H$_8$ ([Na(THF)]**3a**·C$_7$H$_8$, 1.89 g, 0.983 mmol, 69%) were obtained. UV-vis (THF): λ_{max} = 348 (ε 1.7 × 10^4), 446 nm (ε 1.4 × 10^4). Cyclic voltammetry (THF, room temperature): $E_{1/2}$ = 0.08 V ([**3a**]$^+$/[**3a**]), $E_{1/2}$ = –0.82 V ([**3a**]/[**3a**]$^-$). EPR (X-band, microwave 1.0 mW, 8 K): g = 2.076, 2.035, 2.018. ESI-TOF-MS (THF): m/z = 1732.4 (M$^-$). Anal. Calcd for C$_{100}$Fe$_4$H$_{108}$NaOS$_8$·C$_7$H$_8$: C, 66.90; H, 6.09; S, 13.35. Found: C, 66.81; H, 6.33; S, 13.05.

Synthesis of [Na(THF)][Fe$_4$S$_4$(STbt)$_4$] ([Na(THF)]3b). A pentane (20 mL) solution of HSTbt (605 mg, 1.03 mmol) was added to a pentane (10 mL) solution of

$[Na(THF)_2][Fe_4S_4\{N(SiMe_3)_2\}_4]$ ($[Na(THF)_2][\mathbf{1}]$, 300 mg, 0.258 mmol) at room temperature, and the solution was stirred overnight. After concentrating to 10 mL, a small amount of black insoluble solid was filtered off. The solution was cooled at –30°C to give $[Na(THF)][Fe_4S_4(STbt)_4]$ ($[Na(THF)]$**3b**, 190 mg, 0.0682 mmol, 26%) as black crystals. UV-vis (THF): λ_{max} = 459 nm (ε 2.0×10^4). Cyclic voltammetry (THF, room temperature): $E_{1/2}$ = –0.86 V ([**3b**] /[**3b**]$^-$). EPR (X-band, microwave 5.0×10^2 mW, 16 K): g = 2.100, 2.041. Anal. Calcd for $C_{112}Fe_4H_{244}NaOS_8Si_{24}$: C, 48.32; H, 8.83; S, 9.21. Found: C, 48.29; H, 8.52; S, 8.83.

Synthesis of $[N^nBu_4][Fe_4S_4(SDmp)_4]$ ($[N^nBu_4]$3a). A toluene (12.5 mL) solution of HSDmp (358 mg,1.03 mmol) was added to a toluene (6 mL) solution of $[Na(THF)_2][Fe_4S_4\{N(SiMe_3)_2\}_4]$ ($[Na(THF)_2][\mathbf{1}]$, 300 mg, 0.259 mmol) at room temperature. The solution was stirred overnight before being evaporated to dryness. The residue was extracted with THF (7.5 mL), and the black solution was mixed with a THF (12.5 mL) solution of $[N^nBu_4][PF_6]$ (100 mg, 0.258 mmol). The mixture was stirred overnight at room temperature. After evaporating to dryness under reduced pressure, the black residue was extracted with a mixture of toluene (15 mL) and dichloromethane (1.5 mL). The extract was centrifuged to remove an insoluble solid, and the solution was concentrated to *ca*. 3 mL. Black crystals of $[N^nBu_4][Fe_4S_4(SDmp)_4]\cdot(C_7H_8)_{1.5}$ ($[N^nBu_4]\mathbf{3a}\cdot(C_7H_8)_{1.5}$, 373 mg, 0.176 mmol, 68%) grew at –30 °C. UV-vis (THF): λ_{max} = 343 nm (ε 2.1×10^4), 469 nm (ε 2.3×10^4). Cyclic voltammetry (THF, room temperature): $E_{1/2}$ = 0.09 V ([**3a**]$^+$/[**3a**]), $E_{1/2}$ = –0.83 V ([**3a**]/[**3a**]$^-$). EPR (X-band, microwave 1.0 mW, 8K): g = 2.100, 2.051, 2.021. ESI-TOF-MS (THF): m/z = 1733.5 (M$^-$). ^{1}H NMR (CD_2Cl_2): δ 10.15 (br, 8H, *m-H*), 6.75

(br, 16H, *m′-H*), 4.21 (br, 4H, *p-H*), 3.04 (br, 8H, $NCH_2CH_2CH_2CH_3$), 2.55 (br, 24H, *p′*-CH_3), 2.38 (br, 48H, *o′*-CH_3), 1.66 (br, 8H, $NCH_2CH_2CH_2CH_3$), 1.43 (br, 8H, $NCH_2CH_2CH_2CH_3$), 1.03 (br, 12H, $NCH_2CH_2CH_2CH_3$). Anal. Calcd for $C_{112}Fe_4H_{136}NS_8{\cdot}(C_7H_8)_{1.5}$: C, 69.58; H, 7.06; N, 0.66; S, 12.13. Found: C, 69.59; H, 7.00; N, 0.74; S, 11.87.

Synthesis of [N^{n}Bu$_4$][Fe$_4$S$_4$(SEind)$_4$] ([N^{n}Bu$_4$]3c). The procedure for the synthesis of [N^{n}Bu$_4$]**3a** is analogous to that of [N^{n}Bu$_4$]**3a**, using [Na(THF)$_2$][**1**] (500 mg, 0.431 mmmol), HSEind (715 mg, 1.72 mmol), and [N^{n}Bu$_4$][PF$_6$] (167 mg, 0.431 mmol). The residue derived from the reaction mixture was extracted with a mixture of pentane (15 mL) and toluene (15 mL), and was concentrated to *ca*. 5 mL. This solution was layered with hexane (20 mL) and was kept standing at room temperature. [N^{n}Bu$_4$][Fe$_4$S$_4$(SEind)$_4$]·C_6H_{14} ([N^{n}Bu$_4$]**3c**, 722 mg, 0.309 mmol, 72%) was obtained as black crystals. UV-vis (THF): λ_{max} = 342 nm (ε 1.4 × 10^4), 502 nm (ε 3.1 × 10^4). Cyclic voltammetry (THF, room temperature): $E_{1/2}$ = 0.08 V ([**3c**]$^+$/[**3c**]), $E_{1/2}$ = –0.84 V ([**3c**]/[**3c**]$^-$). EPR (X-band, microwave 1.0 × 10^{-1} mW, 16 K): *g* = 2.136, 2.043, 2.025. ESI-TOF-MS (THF): *m*/*z* = 2006.1 (M$^-$). ^{1}H NMR (CD_2Cl_2): δ 6.37 (br, 4H, *p-H*), 5.55 (br, 16H, CH_2CH_3), 3.84 (br, 16H, CH_2CH_3), 3.07 (br, 8H, $NCH_2CH_2CH_2CH_3$), 1.90 (br, 16H, CCH_2C), 1.65 (br, 16H, CH_2CH_3), 1.52 (br, 16H, CH_2CH_3), 1.44 (br, 48H, CH_2CH_3), 1.06 (br, 12H, $NCH_2CH_2CH_2CH_3$) 0.77 (br, 48H, CH_2CH_3). Anal. Calcd for $C_{128}Fe_4H_{216}NS_8{\cdot}C_6H_{14}$: C, 68.92; H, 9.93; N, 0.60; S, 10.99. Found: C, 68.51; H, 9.64; N, 0.56; S, 10.81.

Synthesis of [N^{n}Bu$_4$][Fe$_4$S$_4$(SDxp)$_4$] ([N^{n}Bu$_4$]3d). The reaction of [Na(THF)$_2$][**1**] (500 mg, 0.431 mmmol) with HSDxp (549 mg, 1.72 mmol) and [N^{n}Bu$_4$][PF$_6$] (167 mg, 0.431

mmol) gave a black solution, which was evaporated to dryness. The black residue was washed with hexane (15 mL), and was extracted with a mixture of toluene (25 mL) and dichloromethane (2 mL). After being concentrated to *ca*. 5 mL, the solution was stored at –30°C. [N^{n}Bu$_4$][Fe$_4$S$_4$(SDxp)$_4$] ([N^{n}Bu$_4$]**3d),** 368 mg, 0.197 mmol, 46%) was obtained as black crystals. UV-vis (THF): λ_{max} = 344 nm (ε 2.2 × 10^4), 466 nm (ε 2.6 × 10^4). Cyclic voltammetry (THF, room temperature): $E_{1/2}$ = –0.74 V ([**3d**]/[**3d**]$^-$). EPR (X-band, microwave 1.0 mW, 16 K): g = 2.109, 2.051. ESI-TOF-MS (THF): *m*/*z* = 1620.4 (M$^-$). ^{1}H NMR (CD_2Cl_2): δ 10.19 (br, 8H, *m-H*), 7.02 (br, 16H, *m'-H*), 6.58 (br, 8H, *p'-H*), 4.01 (br, 4H, *p-H*), 2.90 (br, 8H, $NCH_2CH_2CH_2CH_3$), 2.45 (br, 48H, *o'*-C*H*$_3$), 1.56 (br, 8H, $NCH_2CH_2CH_2CH_3$), 1.45 (br, 8H, $NCH_2CH_2CH_2CH_3$), 1.05 (br, 12H, $NCH_2CH_2CH_2CH_3$). Anal. Calcd for $C_{104}Fe_4H_{120}NS_8$: C, 67.01; H, 6.49; N, 0.75; S, 13.76. Found: 66.64; H, 6.89; N 0.70; S, 13.34.

Synthesis of [N^{n}Bu$_4$][Fe$_4$S$_4$(SDpp)$_4$] ([N^{n}Bu$_4$]3e). The reaction of [Na(THF)$_2$][**1**] (500 mg, 0.431 mmmol) with HSDpp (452 mg, 1.72 mmol) and [N^{n}Bu$_4$][PF$_6$] (167 mg, 0.431 mmol) gave a black solution, which was evaporated to dryness. The black residue was washed with hexane (30 mL), and was extracted with a mixture of toluene (50 mL) and dichloromethane (5 mL). After being concentrated to *ca*. 15 mL, the solution was kept standing at room temperature to give black crystals of [N^{n}Bu$_4$][Fe$_4$S$_4$(SEind)$_4$] ([N^{n}Bu$_4$]**3e**, 368 mg, 0.224 mmol, 52%). UV-vis (THF): λ_{max} = 465 nm (ε 2.1 × 10^4). Cyclic voltammetry (THF, room temperature): $E_{1/2}$ = –0.63 V ([**3e**]/[**3e**]$^-$), $E_{1/2}$ = –1.77 V ([**3e**]$^-$/[**3e**]$^{2-}$). EPR (X-band, microwave 1.0 mW, 16 K): g = 2.071, 2.028. ESI-TOF-MS (THF): *m*/*z* = 1396.4 (M$^-$). ^{1}H NMR (CD_2Cl_2): δ 10.03 (br, 8H, *m-H*), 8.07 (br, 16H, *m'-H*), 7.05 (br, 8H, *p'-H*), 7.00 (br, 16H, *o'-H*), 5.49 (br, 4H, *p-H*), 2.88 (br, 8H, $NCH_2CH_2CH_2CH_3$), 1.49 (br, 8H, $NCH_2CH_2CH_2CH_3$), 1.29 (br, 8H, $NCH_2CH_2CH_2CH_3$), 0.96 (br, 12H, $NCH_2CH_2CH_2CH_3$). Anal. Calcd for $C_{88}Fe_4H_{88}NS_8$: C, 64.47; H, 5.41; N, 0.85; S, 15.65. Found: C, 64.31; H, 5.33; N, 0.86; S, 15.37.

[Na][Fe_4S_4(STip)$_4$]. Synthesis and spectroscopic data of [N^nBu_4][Fe_4S_4(STip)$_4$] were reported by Millar et al.[9] The reaction of [Na(THF)$_2$]**1** (200 mg, 0.172 mmol) with HSTip (166 mg, 0.702 mmol) gave a black solution, which was evaporated to dryness. The black residue was washed with hexane (2 mL), and was extracted with Et_2O (10 mL). After being evaporated to dryness, [Na][Fe_4S_4(STip)$_4$] (30 mg, 13%) was obtained as a black solid. ESI-TOF-MS (THF): *m/z* = 1291.9 (M^-). Cyclic voltammetry (THF, room temperature): $E_{1/2}$ = –0.53 V ([Fe_4S_4(STip)$_4$]$^-$/[Fe_4S_4(STip)$_4$]$^{2-}$), –1.71 V ([Fe_4S_4(STip)$_4$]$^{2-}$/[Fe_4S_4(STip)$_4$]$^{3-}$).

[N^nBu_4][Fe_4S_4(SPh)$_4$]. This compound was prepared according to the procedure described in the literature.[33] ESI-TOF-MS (CH_3CN): *m/z* = 393.85 (M^{2-}). Cyclic Voltammetry (THF, room temperature; Figure A2.4): $E_{1/2}$ = –0.21 V ([Fe_4S_4(SPh)$_4$]$^-$ /[Fe_4S_4(SPh)$_4$]$^{2-}$), –1.30 V ([Fe_4S_4(SPh)$_4$]$^{2-}$/[Fe_4S_4(SPh)$_4$]$^{3-}$).

NaSDmp. To a THF (10 mL) solution of HSDmp (301 mg, 0.869 mmol) was added Na (63 mg, 2.74 mmol). The suspension was stirred overnight at room temperature before filtration. The colorless solution was evaporated to dryness. The residue was washed with hexane (8 mL) to give NaSDmp (197 mg, 0.535 mmol, 62% yield) as white powder. ESI-TOF-MS (THF): *m/z* = 345.2 ($^-$SDmp). ^{1}H NMR (CD_3CN): δ 6.82 (br, 4H, *m′-H*), 6.63 (dd, J_{HH} = 7.9, 6.6 Hz, 1H, *p-H*), 6.55 (dd, J_{HH} = 7.3, 0.4 Hz, 2H, *m-H*), 2.27 (s, 6H, *m′*-CH_3), 2.00 (s, 12H, *o′*-CH_3). $^{13}C\{H\}$ NMR (CD_3CN): δ 156.2, 144.9, 144.3, 136.7, 128.1, 126.9, 117.8, 21.1, 20.7. Cyclic voltammetry (THF, room temperature; Figure A2.5): $E = -0.36$ V (irreversible oxidation).

NaSDxp. The procedure for the synthesis of NaSDxp is analogous to that of NaSDmp, using HSDxp (301 mg, 0.945 mmmol), Na (74 mg, 3.22 mmol). NaSDxp (259 mg, 0.761 mmol, 81% yield) was obtained as white powder. ESI-TOF-MS (THF): $m/z = 317.2$ ($^{-}$SDxp). ^{1}H NMR (CD_3CN): δ 6.98 (br, 6H, *m′-H*, *p′-H*), 6.66 (dd, $J_{HH} = 7.3, 6.6$, 1H, *p-H*), 6.57 (dd, $J_{HH} = 7.3, 0.5$, 2H, *m-H*), 2.05 (s, 12H, *o′*-CH_3). ^{13}C{H} NMR (CD_3CN): δ 156.6, 148.0, 144.6, 137.0, 127.2, 126.6, 125.7, 117.5, 20.8. Cyclic voltammetry (THF, room temperature): $E = -0.34$ V (irreversible oxidation).

NaSDpp. To a THF (10 mL) solution of HSDpp (202 mg, 0.770 mmol) was added NaH (46 mg, 1.92 mmol). The suspension was stirred 4 hours at room temperature before filtration. The afforded light yellow solution was evaporated to dryness. The residue was washed with hexane (4 mL) to give NaSDpp (181 mg, 0.639 mmol, 83% yield) as white powder. ESI-TOF-MS (THF): $m/z = 261.1$ ($^{-}$SDpp). ^{1}H NMR: δ 7.58 (m, 4H, *o′*- or *m′-H*), 7.26 (m, 4H, *o′*- or *m′-H*), 7.14 (m, 2H, *p′-H*), 6.83 (d, $J_{HH} = 7.4$ Hz, 2H, *m-H*), 6.63 (dd, $J_{HH} = 7.6, 7.1$, 1H, *p*-H). ^{13}C{H} NMR (CD_3CN): δ 157.2, 148.3, 145.4, 131.1, 128.6, 127.5, 125.7, 117.4. Cyclic voltammetry (THF, room temperature): $E = -0.34$ V (irreversible oxidation).

X-ray Crystal Structure Determination. Crystal data and refinement parameters for [Na(THF)]**3a**·C_7H_8, [Na(THF)]**3b**·$(C_7H_8)_2$, [N^{n}Bu$_4$]**3a**, [N^{n}Bu$_4$]**3c**·C_6H_{14}, [N^{n}Bu$_4$]**3d**·$(C_7H_8)_3$, and [N^{n}Bu$_4$]**3e** are summarized in Table A2.1. Single crystals were coated with oil (Immersion Oil, type B: Code 1248, Cargille Laboratories, Inc.) and mounted on loops (CryoLoop). Diffraction data were collected at –100°C under a cold nitrogen stream on a Rigaku AFC8 equipped with a Mercury CCD detector, or on a Rigaku RA-Micro7 equipped with a Saturn70 CCD detector, using graphite-monochromated Mo Kα radiation (λ = 0.710690 Å). Six preliminary data frames were measured at 0.5° increments of ω, to assess the crystal quality and preliminary unit cell parameters. The intensity images were also measured at 0.5° intervals of ω. The frame data were integrated using the CrystalClear program package, and the data sets were corrected for absorption using the REQAB program. The calculations were performed with the CrystalStructure program package. All structures were solved by direct methods and refined by full–matrix least squares. Anisotropic refinement was applied to all non-hydrogen atoms except for the disordered atoms, and all hydrogen atoms were put at calculated positions.

References and Notes

[1] (a) Adman, E.; Warenpaugh, K. D.; Jensen, L. H. *Proc. Natl. Acad. Sci. U.S.A.* **1975**, *72*, 4854-4858. (b) Dey, A.; Jenney Jr., F. E.; Adam, M. W. W.; Babini, E.; Takahashi, Y.; Fukuyama, K.; Hodgson, K. O.; Hedman, B.; Solomon, E. I. *Science*, **2007**, *318*, 1464-1468.

[2] (a) Rayment, I.; Wesenberg, G.; Cusanovich, M. A.; Holden, H. M. *J. Mol. Biol.* **1992**, *228*, 672-686. (b) Dauter, Z. D.; Wilson, K. S.; Sieker, L. C.; Meyer, J.; Moulis, J-M. *Biochemistry*, **1997**, *36*, 16065-16073. (c) Liu, L.; Nogi, T.; Kobayashi, M.; Nozawa, T.; Miki, K. *Acta Cryst.* **2002**, *D58*, 1085-1091. (d) Mansy, S. S.; Xiong, Y.; Hemann, C.; Hille, R.; Sundaralingam, M.; Cowan, J. A. *Biochemistry* **2002**, *41*, 1195-1201. (e) González, A.; Brenini, S.; Ciurli, S. *Acta Cryst.* **2003**, *D59*, 1582-1588. (f) Stelter, M.; Melo, A. M. P.; Hreggvidsson, G. O.; Hjorleifsdottir, S.; Saraiva, L. M.; Teixeira, M.; Archer, M. *J. Biol. Inorg. Chem.* **2010**, *15*, 303-313.

[3] (a) Meyer, T. E.; Przyshecki, C. T.; Watkins, J. A.; Bhattacharyya, A.; Simondsen, R. P.; Cusanovich, M. A.; Tollin, G. *Proc. Natl. Acad. Sci. U.S.A.* **1983**, *80*, 6740-6744. (b) Heering, H. A.; Bulsink, Y. B. M.; Hagen, W. R.; Meyer, T. E. *Biochemistry*, **1995**, *34*, 14675-14686.

[4] Rao, P. V.; Holm, R. H. *Chem. Rev.* **2004**, *104*, 527-559. and references cited therein.

[5] (a) Ohno, R.; Ueyama, N.; Nakamura, A. *Inorg. Chem.* **1990**, *30*, 4887-4891. (b) Ueyama, N.; Yamada, Y.; Okamura, T.-A.; Kimura, S.; Nakamura, A. *Inorg. Chem.* **1996**, *35*, 6473–6484.

[6] Zhou, C.; Raebiger, J. W.; Segal, B. M.; Holm, R. H. *Inorg. Chim. Acta* **2000**, *300*,

892-902.

[7] Blonk, H. L.; Kievit, O.; Roth, E. K. -H.; Jordanov, J.; van der Linden, J. G. M.; Steggerda, J. J. *Inorg. Chem.* **1991**, *30*, 3231-3234.

[8] Kambayashi, H.; Nagao, H.; Tanaka, K. *Inorg. Chim. Acta* **1993**, *209*, 143-149.

[9] O'Sullivan, T.; Millar M. M. *J. Am. Chem. Soc.* **1985**, *107*, 4096-4097.

[10] Ohki, Y.; Tanifuji, K.; Yamada, N.; Imada, M.; Tajima, T.; Tatsumi, K. *Proc. Natl. Acad. Sci. U.S.A.* **2011**, *108*, 12635-12640.

[11] Sharp, C. R.; Duncan, J. S.; Lee, S. C. *Inorg. Chem.* **2010**, *49*, 6697-6705.

[12] Aizman, A.; Case, D. A. *J. Am. Chem. Soc.* **1982**, *104*, 3269-3279.

[13] Papaefthymiou, V.; Millar, M. M.; Münck, E. *Inorg. Chem.* **1986**, *25*, 3010-3014.

[14] Laskowski, E. J.; Frankel, R. B.; Gillum, W. O.; Papaefthymiou, G.C.; Renaud, J.; Ibers, J. A.; Holm, R. H. *J. Am. Chem. Soc.* **1978**, *100*, 5322-5337.

[15] Heering, H. A.; Bulsink, Y. B. M.; Hagen, W. R.; Meyer, T. E. *Eur. J. Biochem.* **1995**, *232*, 811-817.

[16] Beinert, H.; Thomson, A. J. *Arch. Biochem. Biophys.* **1983**, *222*, 333-361.

[17] Cavazza, C.; Guigirarelli, B.; Bertrand, P.; Bruschi, M. *FEMS Microbiol. Lett.* **1995**, *130*, 193-200.

[18] Bertini, I.; Campos, A. P.; Luchinat, C.; Teixeira, M. *J. Inorg. Biochem.* **1993**, *52*, 227-234.

[19] Other structures are shown in Figures A2.1-A2.3 (Supporting Information).

[20] Niemeyer, M.; Power, P. P. *Inorg. Chem.* **1996**, *35*, 7264-7272.

[21] (a) Shalmov, A. E.; Agashkin, O. V.; Yanovskii, A. I.; Struchkov, Y. T.; Logunov, A.

P.; Revenko, G. P.; Bosyakov, Y. G. *J. Struct. Chem.* **1990**, *31*, 512-515. (b) Desiraju, G. R.; Steiner, T. *The Weak Hydrogen Bond in Structural Chemistry and Biology*; Oxford University Press: New York, 2001; pp 226-231.

[22] Lawson Daku, L. M.; Pcaut, J.; Lenormand-Foucaut, A.; Vieux-Melchior, B.; Iveson, P.; Jordanov, J. *Inorg. Chem*. **2003**, *42*, 6824-6850.

[23] Ueyama, N.; Sugawara, T.; Fuji, M.; Nakamura, A.; Yasuoka, N. *Chem. Lett*. **1985**, *14*, 175-178

[24] Que, Jr., L.; Bobrik, M.A.; Ibers, J. A.; Holm, R. H. *J. Am. Chem. Soc.* **1974**, *96*, 4168-4178.

[25] Tan, L. L.; Holm, R. H.; Lee, S. C. *Polyhedron* **2013**, *58*, 206–217.

[26] Harris, S. *Polyhedron* **1989**, *8*, 2843-2882.

[27] Pangborn, A. B.; Giardello, M. A.; Grubbs, R. H.; Rosen, R. K.; Timmers, F. J. *Organometallics* **1996**, *15*, 1518-1520.

[28] (a) Ellison, J. J.; Ruhlandt-Senge, K.; Power, P. P. *Angew. Chem. Int. Ed.* **1994**, *33*, 1178-1180. (b) Ohki, Y.; Ohta, S.; Tatsumi, K. *Inorg. Synth.* **2010**, *35*, 137-143.

[29] Takeda, N.; Shimizu, D.; Tokitoh, N. *Inorg. Chem.* **2005**, *44*, 8561-8568

[30] (a) Matsuo, T.; Suzuki, K.; Fukawa, T.; Li, B.; Ito, M.; Shoji, Y.; Otani, T.; Li, L.; Kobayashi, M.; Hachiya, M.; Tahara, Y.; Hashizume, D.; Fukunaga, T.; Fukazawa, A.; Li, Y.; Tsuji, H.; Tamao, K. *Bull. Chem. Soc. Jpn.* **2011**, *84*, 1178–1191. (b) Nishigaki, J.; Tsunoyama, R.; Tsunoyama, H.; Ichikuni, N.; Yamazoe, S.; Negishi, Y.; Ito, M.; Matsuo, T.; Tamao, K.; Tsukuda, T. *J. Am. Chem. Soc.* **2012**, *134*, 14295-14297.

[31] Luening, U.; Baumgartner, H. *Synlett* **1993**, *8*, 571–572.

[32] Bishop, P. T.; Dilworth, J. R.; Nicholson, T.; Zubieta, J. *J. Chem. Soc., Dalton Trans.*

1991, 385-392.

[33] Christou, G.; Garner, C. D. *J. Chem. Soc., Dalton Trans.* **1979**, 1093-1094.

Appendix 2

Supporting Information for Chapter 3

Table A2.1. Crystal Data for $[Na(THF)][Fe_4S_4(SDmp)_4]\cdot C_7H_8$ ([Na(THF)]**3a**·C_7H_8), $[N^nBu_4][Fe_4S_4(SDmp)_4]\cdot (C_7H_8)_2$ ([N^nBu_4]**3a**·$(C_7H_8)_2$), $[Na(THF)][Fe_4S_4(STbt)_4]$ ([Na(THF)]**3b**), $[N^nBu_4][Fe_4S_4(SEind)_4]\cdot C_6H_{14}$ ([N^nBu_4]**3c**·C_6H_{14}), $[N^nBu_4][Fe_4S_4(SDxp)_4]\cdot (C_7H_8)_3$ ([N^nBu_4]**3d**·$(C_7H_8)_3$), and $[N^nBu_4][Fe_4S_4(SDpp)_4]$ ([N^nBu_4]**3e**).

	[Na(THF)]**3a**·C_7H_8	[N*n*Bu$_4$]**3a**·$(C_7H_8)_2$	[Na(THF)]**3b**
formula	$C_{107}H_{116}Fe_4NaOS_8$	$C_{123}H_{136}Fe_4NS_8$	$C_{112}H_{244}Fe_4S_8Si_{24}NaO$
Formula wt (g mol^{-1})	2192.22	2108.30	2784.07
Crystal system	Triclinic	Triclinic	Ttragonal
Space group	P-1 (#2)	P-1 (#2)	$I4_1/a$ (#88)
a (Å)	14.4755(19)	15.765(2)	32.2442(9)
b (Å)	15.3293(18)	16.021(2)	
c (Å)	25.520(4)	25.024(3)	17.7890(7)
α (°)	82.580(7)	83.258(5)	
β (°)	87.684(7)	83.814(5)	
γ (°)	61.671(4)	64.542(4)	
V (Å^3)	4941.4(12)	5665.6(11)	18495.0(11)
Z	2	2	4
D_{calcd} (g/cm^3)	1.291	1.238	1.000
Max 2θ (°)	55.0	55.0	55.0
No. of Reflections Measured	20690	46230	92270
No. of Data Used (I >2.00 s(I))	16067	25523	10571
No. of Parameters Refined	1037	1209	339
R_1^{a}	0.0727	0.0553	0.0947
wR_2^{b}	0.2142	0.1743	0.2454
GOF^c	1.069	1.034	1.097

^{a} $I > 2\sigma(I)$, $R1=\Sigma||F_o|-|F_c||/\Sigma|F_o|$. ^{b} refined with all data, $wR2=[\{\Sigma w(F_o^2-F_c^2)^2\}/\Sigma w(F_o^2)^2]^{1/2}$.

^{c} $GOF=[\{\Sigma w(F_o^2-F_c^2)^2\}/(N_o-N_p)]^{1/2}$, where N_o and N_p denote the numbers of reflection data and parameters.

(Continued)

	$[\mathrm{N}n\mathrm{Bu}_4]$**3c**$\cdot\mathrm{C_6H_{14}}$	$[\mathrm{N}n\mathrm{Bu}_4]$**3d**$\cdot(\mathrm{C_7H_8})_3$	$[\mathrm{N}n\mathrm{Bu}_4]$**3e**
formula	$\mathrm{C_{134}H_{206}Fe_4NS_8}$	$\mathrm{C_{125}H_{134}Fe_4NS_8}$	$\mathrm{C_{88}H_{78}Fe_4NS_8}$
Formula wt (g mol^{-1})	2310.98	2130.31	1629.46
Crystal system	Monoclinic	Triclinic	Triclinic
Space group	$P2_1/c$ (#14)	P-1 (#2)	$P2_1/n$ (#14)
a (Å)	17.359(2)	14.982(2)	20.1852(12)
b (Å)	24.540(3)	16.228(2)	18.3077(11)
c (Å)	31.797(4)	23.468(3)	22.3279(13)
α (°)		94.710(3)	
β (°)	92.8329(13)	92.628(2)	94.5234(9)
γ (°)		100.580(3)	
V (Å^3)	13529(3)	5579.0(13)	8225.5(8)
Z	4	2	4
D_{calcd} (g/cm^3)	1.135	1.268	1.316
Max 2θ (°)	55.0	55.0	55.0
No. of Reflections Measured	137618	69030	98601
No. of Data Used (I >2.00 s(I))	30990	25391	18804
No. of Parameters Refined	1312	1193	934
$R_1{}^a$	0.0606	0.0687	0.0373
$wR_2{}^b$	0.1920	0.2499	0.0976
GOF^c	1.098	1.097	1.216

[a] $I > 2\sigma(I)$, $R1=\Sigma||F_o|-|F_c||/\Sigma|F_o|$. [b] refined with all data, $wR2=[\{\Sigma w(F_o{}^2-F_c{}^2)^2\}/\Sigma w(F_o{}^2)^2]^{1/2}$.

[c] GOF$=[\{\Sigma w(F_o{}^2-F_c{}^2)^2\}/(N_o-N_p)]^{1/2}$, where N_o and N_p denote the numbers of reflection data and parameters.

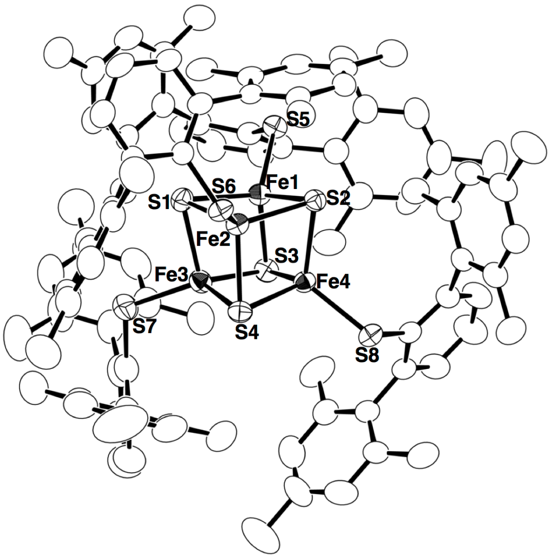

Figure A2.1. Molecular structure of $[N^nBu_4][Fe_4S_4(SDmp)_4]\cdot(C_7H_8)_2$ ($[N^nBu_4]$**3a**$\cdot(C_7H_8)_2$) with thermal ellipsoids at the 50% probability level. All hydrogen atoms, N^nBu_4 cation, and crystal solvents are omitted for clarity.

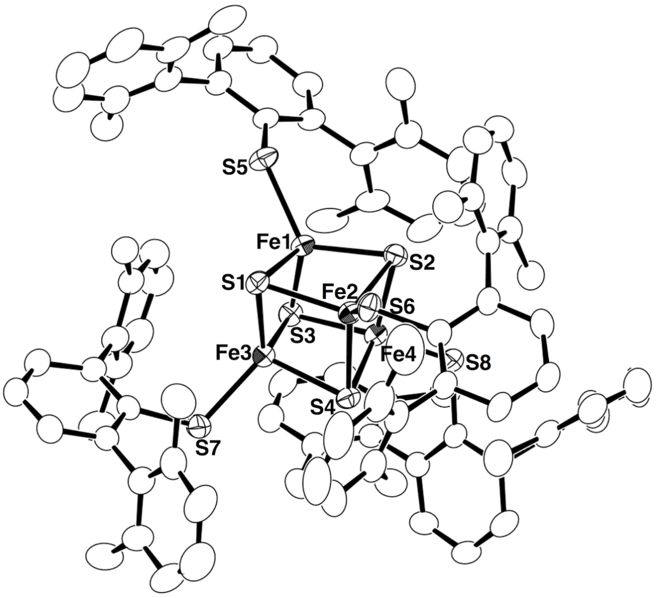

Figure A2.2. Molecular structure of $[N^nBu_4][Fe_4S_4(SDxp)_4]\cdot(C_7H_8)_3$ ($[N^nBu_4]$**3d**$\cdot(C_7H_8)_3$) with thermal ellipsoids at the 50% probability level. All hydrogen atoms, N^nBu_4 cation, and crystal solvents are omitted for clarity.

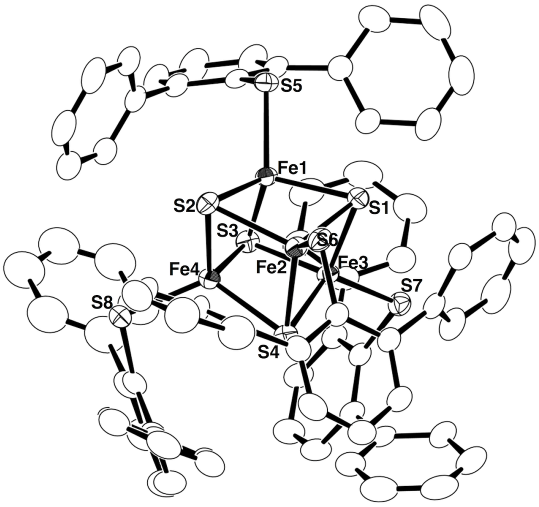

Figure A2.3. Molecular structure of [N^{n}Bu$_4$][Fe$_4$S$_4$(SDpp)$_4$] ([N^{n}Bu$_4$]**3e**) with thermal ellipsoids at the 50%probability level. All hydrogen atoms and N^{n}Bu$_4$ cation are omitted for clarity.

Table A 2.2 Selected Bond Distances (Å) of [Na(THF)]**3a**, [N^{n}Bu$_4$]**3a**, [Na(THF)]**3b**, [N^{n}Bu$_4$]**3c**, [N^{n}Bu$_4$]**3d**, and [N^{n}Bu$_4$]**3e**.

	[Na(THF)]**3a**	[N^{n}Bu$_4$]**3a**	[Na(THF)]**3b**
Fe1-Fe2	2.7282(8)	2.7498(8)	2.7996(8)[a]
Fe1-Fe3	2.8127(10)	2.7963(7)	2.7572(8)[b]
Fe1-Fe4	2.7894(8)	2.7542(8)	2.7996(8)[c]
Fe2-Fe3	2.7561(6)	2.7885(9)	-
Fe2-Fe4	2.7306(6)	2.8417(7)	-
Fe3-Fe4	2.7889(7)	2.7777(8)	-
Fe1-S1	2.2810(12)	2.2835(9)	2.2830(11)
Fe1-S2	2.2885(11)	2.2506(13)	2.3007(12)[d]
Fe1-S3	2.2316(11)	2.2725(12)	2.2619(11)[e]
Fe2-S1	2.3020(12)	2.2105(13)	-
Fe2-S2	2.2625(13)	2.2792(9)	-
Fe2-S4	2.2716(13)	2.2911(11)	-
Fe3-S1	2.2471(12)	2.2854(11)	-
Fe3-S3	2.3057(13)	2.2900(9)	-
Fe3-S4	2.2791(13)	2.2628(14)	-
Fe4-S2	2.2177(11)	2.2871(10)	-
Fe4-S3	2.2716(12)	2.2247(13)	-
Fe4-S4	2.2674(14)	2.2918(9)	-
Fe1-S5	2.2445(15)	2.2495(11)	2.2424(12)[f]
Fe2-S6	2.2615(9)	2.2392(12)	-
Fe3-S7	2.2408(11)	2.2523(13)	-
Fe4-S8	2.2128(10)	2.2444(12)	-

[a] Fe1-Fe1^1. [b] Fe1-Fe1^2. [c] Fe1-Fe1^3. [d] Fe1-S1^1. [e] Fe1-S1^2. [f] Fe1-S2.

(Continued)

	[N^{n}Bu$_4$]**3c**	[N^{n}Bu$_4$]**3d**	[N^{n}Bu$_4$]**3e**
Fe1-Fe2	2.2868(8)	2.8650(7)	2.7243(4)
Fe1-Fe3	2.7758(8)	2.7773(8)	2.6815(4)
Fe1-Fe4	2.7575(8)	2.7463(9)	2.6965(4)
Fe2-Fe3	2.7577(7)	2.8151(8)	2.7280(4)
Fe2-Fe4	2.7606(8)	2.7516(8)	2.7412(4)
Fe3-Fe4	2.7536(7)	2.8360(8)	2.8286(4)
Fe1-S1	2.2876(10)	2.3198(10)	2.2719(5)
Fe1-S2	2.2757(9)	2.2724(11)	2.2697(5)
Fe1-S3	2.1949(10)	2.2343(12)	2.2240(5)
Fe2-S1	2.2867(11)	2.2922(12)	2.2714(5)
Fe2-S2	2.2923(9)	2.2761(10)	2.2825(6)
Fe2-S4	2.2032(10)	2.2523(13)	2.2459(5)
Fe3-S1	2.2892(10)	2.2393(13)	2.2107(5)
Fe3-S3	2.2849(10)	2.2831(10)	2.2822(6)
Fe3-S4	2.2700(11)	2.3018(13)	2.2947(5)
Fe4-S2	2.2536(9)	2.2352(12)	2.2146(5)
Fe4-S3	2.2863(11)	2.2896(12)	2.2814(5)
Fe4-S4	2.2691(11)	2.2665(12)	2.2913(6)
Fe1-S5	2.2343(11)	2.2401(14)	2.2162(5)
Fe2-S6	2.2280(10)	2.2472(11)	2.2365(5)
Fe3-S7	2.2407(9)	2.2540(13)	2.2198(5)
Fe4-S8	2.2199(10)	2.2303(12)	2.2238(6)

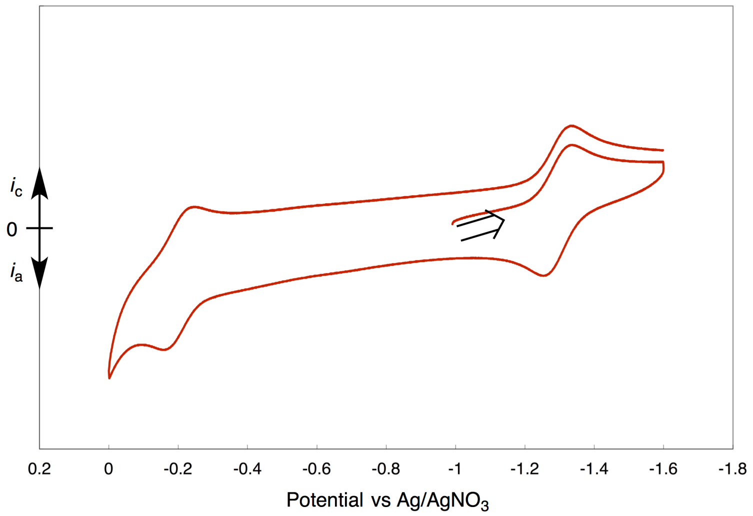

Figure A2.4. Cyclic voltammogram of $[Fe_4S_4(SPh)_4]^{2-}$. Conditions: sample concentration, 2 mM in THF; supporting electrolyte, 0.3 M $[N^nBu_4][PF_6]$; working electrode, glassy carbon; counter electrode, Pt; sweep speed, 0.1 V s^{-1}.

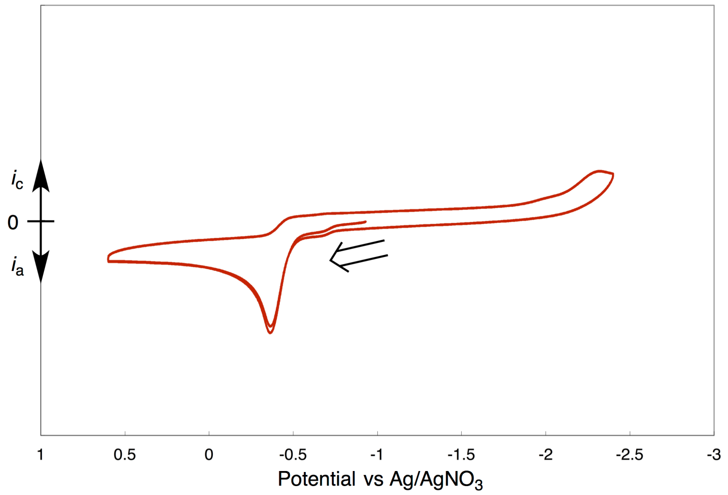

Figure A2.5. Cyclic voltammogram of $^{-}$SDmp. Conditions: sample concentration, 2 mM in THF; supporting electrolyte, 0.2 M $[N^nBu_4][PF_6]$; working electrode, glassy carbon; counter electrode, Pt; sweep speed, 0.1 V s^{-1}.

Chapter 4

Synthesis and Properties of a Thiolate-Bridged [Fe_4S_4]-[Fe] Cluster Relevant to the Active Site of Sulfite Reductase

4.1. Introduction

In anaerobic enzymes, cuboidal [Fe_4S_4] clusters are found as the prevalent electron carriers. They constitute a part of the enzyme active sites in some cases, while the reactions occur at the metals connected to the [Fe_4S_4] units. One of such enzymes is the sulfite reductase (Figure 4.1, the protein structure is shown in Figure 1.4),[1] in which the [Fe_4S_4] unit is linked to a siroheme through a Cys-thiolate. The Cys-thiolate bridges between [Fe_4S_4] units and metals are also found in the Acetyl CoA Synthase (Figure 1.5) and the [FeFe] hydrogenase (Figure 1.6), the active sites of which consist of [Fe_4S_4] clusters and the Ni-Ni or the Fe-Fe moieties, respectively. The direct linkage in these enzymes probably leads to efficient electron transfer to and from the metals in charge of the reactions.

Efforts have been paid to the synthesis of [Fe_4S_4] clusters having a sulfur linkage to metal moieties, to elucidate the possible electronic coupling between the [Fe_4S_4] cluster and metals. Sulfido-bridged [Fe_4S_4]-S-Fe(porphyrine) clusters modeling the active site of sulfite reductase were synthesized from the reactions of Fe-porphyrine

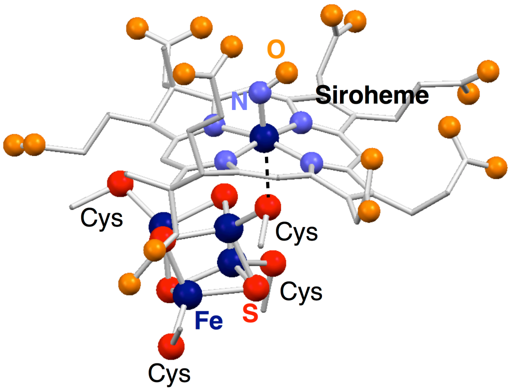

Figure 4.1. Ball and stick description of the active site of sulfite reductase extracted from the protein structure (PDB ID: 6GEP).[1b]

complexes with $[Fe_4S_4]$ clusters having a tridentate thiolate and ^{-}SH, $^{-}SSiEt_3$, or $^{-}S–S^{-}$ ligands.[2] For the linkage between $[Fe_4S_4]$ clusters and nickel complexes to prepare models of the active site of Acetyl CoA Synthase, Pohl *et al*. used the sulfur atoms of square-planar nickel complexes having tetradentate dithiolate ligands, $Ni(EtN_2S_2)$ (EtN_2S_2 = *N,N'*-diethyl-3,7-diazanonane-1,9-dithiolate) and Ni(*'S₄'*) (*'S₄'* = 3,7-dithianonane-1,9- dithiolate). These nickel complexes were found to replace the iodides in $[Fe_4S_4I_4]^{2-}$ or $[Fe_4S_4I_2(STip)_2]^{2-}$ (Tip = 2,4,6-triisopropyl-phenyl) to give $[\{Ni(L)\}_2Fe_4S_4I_2]$ (L = EtN_2S_2, *'S₄'*) and $[\{Ni(L)\}_2Fe_4S_4(STip)_2]$.[3] Picket and co-workers found that an –SEt ligand of $[Fe_4S_4]$ clusters can migrate to an acetyl moiety of thioether ($RSCOCH_3$) hanging in an Fe-Fe complex, resulting in the formation of $EtSCOCH_3$ and $[Fe_4S_4]$ clusters having a thiolate bridge to an Fe-Fe moiety.[4] The resultant $[Fe_4S_4]$-(Fe-Fe) clusters are good structural models for the active site of [FeFe] hydrogenase, and these clusters showed electrocatalytic response in the presence of a proton source (4,6-dimethyl pyridinium cation).

In this chapter, we tried to apply the single-site substitution of the $[Fe_4S_4]$ cluster described in Chapter 2 to develop a new method to link a $[Fe_4S_4]$ cluster with a metal complex. Our attempts led to a serendipitous discovery of a new $[Fe_4S_4]$-[Fe] cluster, which is a rare example of $[Fe_4S_4]$ cluster with a monodentate thiolate bridge to a metal.

4.2. Results and Discussion

As described in Chapter 2, treatment of $Fe_4S_4\{N(SiMe_3)_2\}_4$ (**1**)[5] with thiols leads to the opening of one of the iron sites for accommodating THF or tetramethyl-imidazole. An extension of this method is to use iron-thiolate complexes as ligands for the vacant iron site, to link the $[Fe_4S_4]$ unit to an iron complex through a thiolate ligand. Therefore we prepared an iron precursor stabilized by a bidentate ligand, $Fe\{N(SiMe_3)_2\}_2$(TMS-bpzm) (**5**) (TMS-bpzm = 5-trimetylsilyl-1-[(5-trimethylsilyl-1H-pyrazol-1-yl)methyl]-1H-pyrazole), by addition of TMS-bpzm to $Fe\{N(SiMe_3)_2\}_2$. The amide ligands in **5** are expected to be replaced by thiolates upon treatment with thiols, and the same is true for the amide ligands in cluster **1**.

The new $[Fe_4S_4]$-[Fe] cluster $[Fe_4S_4(STip)_3(\mu_2\text{-}STip)Fe(TMS\text{-}bpzm)_2(NCMe)]$ (**6**, Tip = 2,4,6-triisopropylphenyl) was unexpectedly obtained in a small amount when a mixture of cluster **1** and complex **5** in toluene was treated with 6 equiv of HSTip and was kept standing in CH_3CN. The crystal yields went up to 20%, when the reaction was carried out at –40°C in the presence of TMS-bpzm. The molar ratio of the reactants was **1**:**5**:(HSTip):(TMS-bpzm) = 1:1:6:1 (Scheme 4.1).

Scheme 4.1.

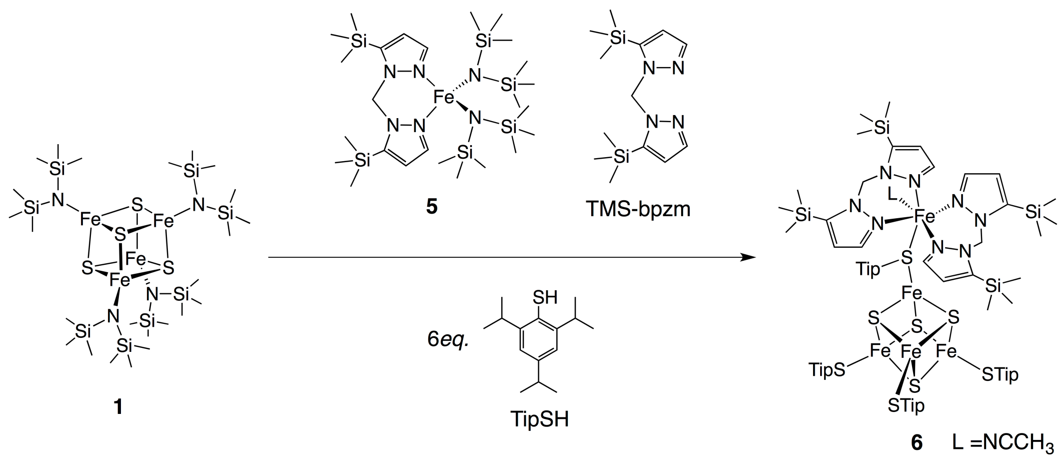

The molecular structure of cluster **6** was determined by X-ray crystallography (Figure 4.2). The [Fe_4S_4] core is supported by four STip ligands, and one of these bridges to an external Fe moiety. The Fe moiety is six-coordinate, with two TMS-bpzm and one each CH_3CN and STip. Notably, the [Fe_4S_4] cluster having a monodentate thiolate bridge to an external metal is rare, and interestingly, cluster **6** consisting of an N_4-coordinated Fe complex and the [Fe_4S_4] unit is relevant to the active site of sulfite reductase.

Selected structural parameters of **6** are listed in Table 4.1. The averaged Fe-S(core) bond distance is slightly shorter with the unique iron (Fe1) bearing the bridging thiolate (2.2790(17) Å) than with other Fe atoms (2.2900(17) Å), while the S(core)-Fe-S(core) angles around Fe1 (103.68(6)-106.68(6)°) are almost in the same range as with other Fe atoms (102.59(5)-106.68(5)°). Thus, the binding of an external

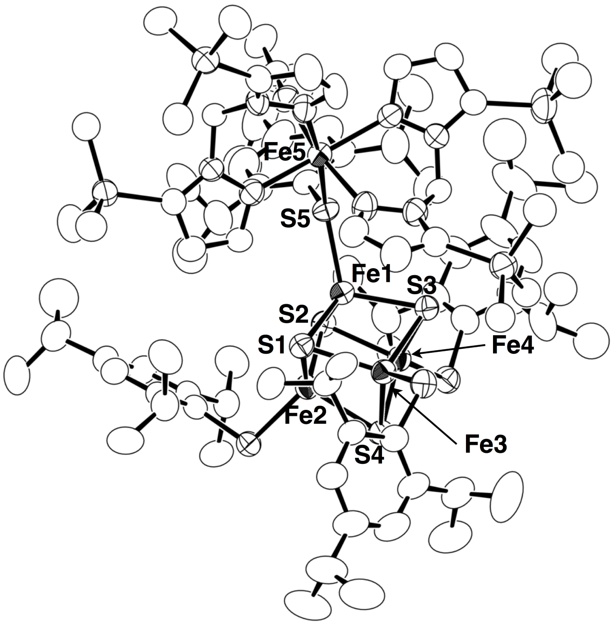

Figure 4.2. Molecular structure of **6** with thermal ellipsoids at the 50% probability level. All hydrogen and disordered atoms are omitted for clarity.

Table 4.1. Selected bond distances (Å) and angles (°) of **6**.

av. Fe(1)-S(core)	2.2790(17)	Fe5-S5	2.4872(16)
av. Fe*-S(core)	2.2900(17)	Fe1-S5-C1	107.26(8)
Fe1-S5	2.3056(17)	Fe*-S(thiolate)-C	102.6(2)-104.6(2)
av. Fe*-S(thiolate)	2.2629(17)	Fe1-S5-Fe5	136.23(7)

Fe* = Fe2, Fe3, Fe4

Fe unit to one of the thiolates (S5) seems to have a limited influence on the $[Fe_4S_4]$ core structure, while a decrease in electron donation from S5 to Fe1 is expected. In the [1:3] site-differentiated $[Fe_4S_4]$ clusters, the structural parameters for the *unique* iron having a monodentate ligand ($^-$Cl, $^-$OCOR, $^-$OR, or imidazole derivative)[6] are different from those of other iron atoms. The volumes of the Fe_4 and S_4 tetrahedrons (Fe_4: 2.39 Å^3; S_4: 5.56 Å^3) of **6** are within the range for $[Fe_4S_4]^{2+}$ clusters bearing $^-$SAr (Ar = aryl) ligands (Fe_4: 2.38-2.47 Å^3; S_4: 5.44-5.61 Å^3).[7] Thus, the oxidation state of Fe atoms in **6** could be assigned to EPR-silent $[Fe_4S_4]^{2+}$ and Fe^{2+}. Additionally, this assignment may explain the fact that the EPR spectra of **6** showed no signals even at cryogenic temperature (8 or 16 K).

In contrast to the structure of the $[Fe_4S_4]$ core, we could find clear influences of the thiolate bridge in the structure around S5 atom. Fe1-S5 bond distance (2.3056(17) Å) is longer than the averaged value of the other Fe-S(thiolate) distances (2.2629(17) Å) and the corresponding distances (2.274(6) Å) of $[Fe_4S_4(STip)_4]^{2-}$ [8] due to the μ_2 coordination of the thiolate. Additionally, although the Fe moiety has a normal octahedral coordination sphere, Fe5-S5 bond length (2.4872(16) Å) has a larger value relative to those of the non-distorted octahedral complexes of Fe (2.209(1)-2.427(1 or 4) Å).[9] The Fe1-S5-C1 angle (107.26(18)°) is also different from the other Fe-S(thiolate)-C angles (102.6(2)-104.6(2)°). This would be because of the planarity of S5 with Fe1, Fe5, and C1, supported by the sum of the angles around S5 (359.56°), whereas the S atoms bridging Fe and Ni in $[\{Ni(EtN_2S_2)\}_2Fe_4S_4X_2]$ (X = $^{-}$I or $^{-}$STip) and $[\{Ni(S_4)\}_2Fe_4S_4(STip)_2]$ are in a more folded geometry.[3] We speculate that the relatively large Fe1-S5-Fe5 angle (136.23(7)°) caused by a steric hindrance between $[Fe_4S_4]$ and Fe moieties induces a preference for the planar geometry of the bridging S atom.

To assess the redox property of **6**, the cyclic voltammetry (CV) measurement was carried out in THF. The CV diagrams of **6** are shown in Figure 4.3, where the potential was referenced to Ag/Ag^{+}. The redox couples of $[Fe_4S_4]^{3+}/[Fe_4S_4]^{2+}$ and $[Fe_4S_4]^{2+}/[Fe_4S_4]^{+}$ in THF were observed at –0.47 V and –1.75 V, respectively, while the

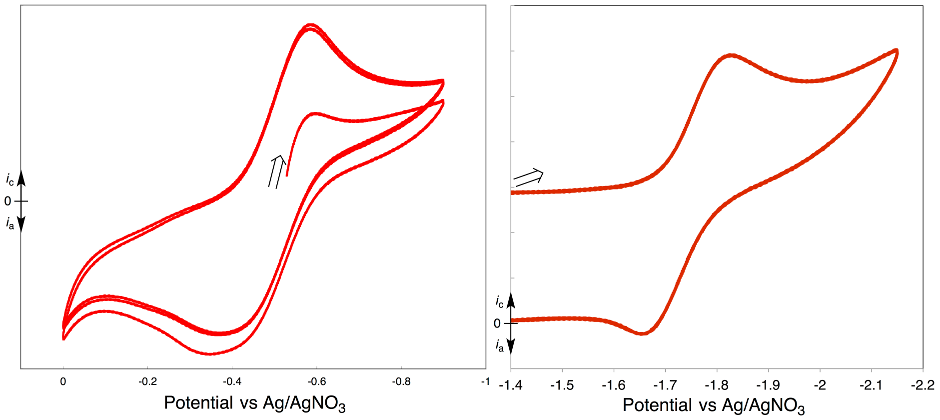

Figure 4.3. Cyclic voltammograms of **6** swept in the rage from 0 V to –0.9 V (left) and from –1.4 V to –2.2 V (right). Conditions: solvent, THF; reference electrode, Ag/AgNO$_3$ (0.01 M in CH_3CN); working electrode, glassy carbon; counter electrode, Pt; sample concentration, 3 mM; supporting electrolyte, $[N^nBu_4][PF_6]$ (0.3 M); sweep speed, 0.1 V s^{-1}.

corresponding redox potentials of $[Fe_4S_4(STip)_4]^-$ are –0.53 V and –1.71 V.[10] The positive shift of the $[Fe_4S_4]^{3+}/[Fe_4S_4]^{2+}$ couple in cluster **6** would be because of the less efficient donation from the bridging thiolate compared with the "non-bridged" $[Fe_4S_4]$ cluster, as can be seen in the potential shift of the $[Fe_4S_4]^{3+}/[Fe_4S_4]^{2+}$ couple from –0.40 V vs $[Cp_2Fe]^+/[Cp_2Fe]$ for $[Fe_4S_4(S\text{-}p\text{-}MePh)_4]^{2-}$ to –0.33 V vs $[Cp_2Fe]^+/[Cp_2Fe]$ for $[Fe_4S_4(SPh)_4]^{2-}$.[11] The reason of the negative shift for the $[Fe_4S_4]^{2+}/[Fe_4S_4]^+$ couple is unclear. However, the equilibrium dissociation of the bridged Fe complex of cluster **6** may lead the broadening of the corresponding redox wave, which was concurrently observed, and as a result, the apparent potential shift.

Since cluster **6** was synthesized by the multi-component reaction, how the formation of **6** occurs remains ambiguous. We have attempted to isolate potential intermediate(s) by the reaction among fewer components. The reaction of **1** with 1 equiv of **5** gave black crystals by the recrystallization from pentane at –35°C. The crystal structure was determined by X-ray analysis and is described as $[Fe\{N(SiMe_3)_2\}_2(TMS\text{-}bpzm)][Fe_4S_4\{N(SiMe_3)_2\}_4]$ (**A**, Figure 4.4). Selected bond

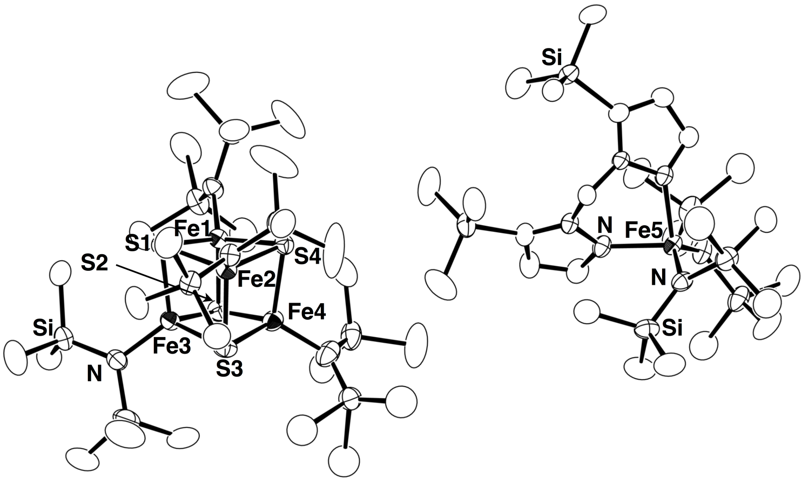

Figure 4.4. Molecular structure of **A** with thermal ellipsoids at 50% probability level. All hydrogens atoms are omitted for clarity.

Table 4.2. Selected bond distances (Å) and angles (°) of **A**, **1**, $[Fe_4S_4\{N(SiMe_3)_2\}_4]^-$, $[Fe_4S_4\{N(SiMe_3)_2\}_4]^{2-}$, and **5**.

	A ($[Fe_4S_4]$ cluster)	**1** ($[Fe_4S_4\{N(SiMe_3)_2\}_4]$)[c]	$[Fe_4S_4\{N(SiMe_3)_2\}_4]^-$[d]	$[Fe_4S_4\{N(SiMe_3)_2\}_4]^{2-}$[e]
Oxidation State		$[Fe_4S_4]^{4+}$	$[Fe_4S_4]^{3+}$	$[Fe_4S_4]^{2+}$
av. Fe-Fe	2.8991(9)	2.9081(7)	2.8642(5)	2.86(4)
av. Fe-S(core)	2.2985(13)	2.2955(8)	2.2927(7)	2.31(2)
av. Fe-N(L_1)[a]	1.916(3)	1.864(5)	1.908(2)	1.95(3)

	A (Fe complex)	**5**
Oxidation State		Fe^{2+}
Fe-N(L_1)[a]	1.897(3), 1.888(3)	1.973(4), 2.002(4)
Fe-N(L_2)[b]	2.094(3), 2.069(3)	2.149(4), 2.175(4)
N(L_1)-Fe-N(L_1)[a]	127.99(12)	139.33(17)
N(L_2)-Fe-N(L_2)[b]	87.44(11)	82.23(15)

[a] L_1 = $^-N(SiMe_3)_2$. L_1 is described as "amide" in the manuscript. [b] L_2 = TMS-bpzm. [c] Reference 5. [d] Reference 6b. [e] Reference 12.

distances and angles of **A**, **1** ($[Fe_4S_4\{N(SiMe_3)_2\}_4]$),[5] $[Fe_4S_4\{N(SiMe_3)_2\}_4]^-$,[6b] $[Fe_4S_4\{N(SiMe_3)_2\}_4]^{2-}$,[12] and complex **5**[13] are summarized in Table 4.2. The averaged Fe-N(amide) bond distance of the $[Fe_4S_4]$ cluster in **A** has a proximal value to that of $[Fe_4S_4\{N(SiMe_3)_2\}_4]^-$ rather than cluster **1** and $[Fe_4S_4\{N(SiMe_3)_2\}_4]^{2-}$. Additionally, the Fe-N(amide) distances (1.897(3), 1.888(3) Å) of the Fe complex part in **A** are ~0.07 Å shorter than those of **5** (1.973(4), 2.002(4) Å), which suggests that the Fe atom has the more oxidized state relative to Fe^{2+} in **5**. We conclude, therefore, that compound **A** is the ion-pair comprising the $[Fe_4S_4]$-cluster anion ($[Fe_4S_4\{N(SiMe_3)_2\}_4]^-$) and the Fe-complex cation ($[Fe\{N(SiMe_3)_2\}_2(\text{TMS-bpzm})]^+$), formed as a result of the redox reaction between cluster **1** and complex **5** (Scheme 4.2).

In contrast to the insight from the crystal structure of **A**, this ion-pair showed different behavior in solution. The λ_{max} (445 nm), observed in the UV-vis spectrum of **A** in toluene, varies from the reported value of $[Fe_4S_4\{N(SiMe_3)_2\}_4]^-$ (433 nm) in the

Scheme 4.2.

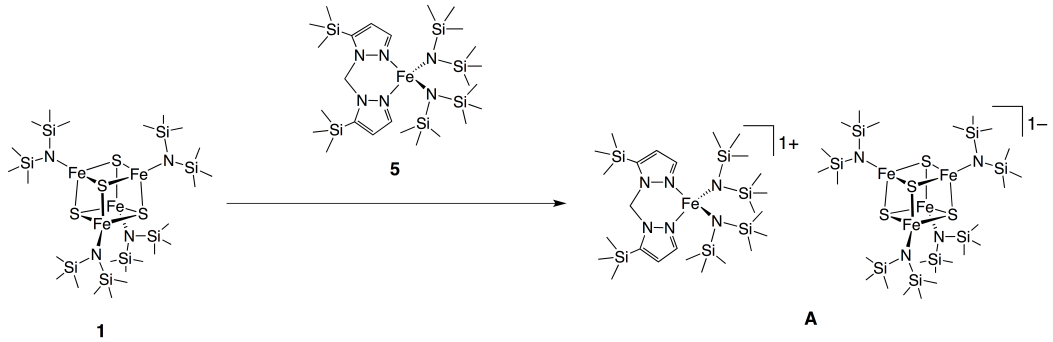

same solvent.[6b] Further, the ^{1}H NMR spectrum of **A** in toluene-d^8 gave two broad singlets at 10.52 and 1.96 ppm corresponding to the $SiMe_3$ groups of complex **5**, and a broad singlet at 2.39 ppm assigned to the $SiMe_3$ groups of cluster **1**. These spectroscopic data indicate that ion-pair **A** goes back to the original state, the mixture of **1** and **5**, at least in the toluene solution at room temperature.

The variable-temperature ^{1}H NMR study of **A** provided a clue to explain the directly opposite insights in the crystal state and the solution state. As shown in Figure 4.5, the signals assigned to the $SiMe_3$ groups of complex **5** is shifted to lower field with temperature decrease, whereas the signal of cluster **1** moved to higher field. These results imply the temperature dependence of the redox equilibrium between **1** plus **5** and **A** (eq. 4.1).

$$\begin{aligned}&\mathrm{Fe_4S_4\{N(SiMe_3)_2\}_4 + Fe\{N(SiMe_3)_2\}_2(TMS\text{-}bpzm)}\\ &\qquad \rightleftharpoons \mathrm{[Fe_4S_4\{N(SiMe_3)_2\}_4]^- + [Fe\{N(SiMe_3)_2\}_2(TMS\text{-}bpzm)]^+} \qquad \textbf{(4.1)}\end{aligned}$$

Thus, at low temperature, the mixture of **1** and **5** should partly be converted into $[Fe_4S_4\{N(SiMe_3)_2\}_4]^-$ and $[Fe\{N(SiMe_3)_2\}_2(TMS\text{-}bpzm)]^+$, and hence **A** was afforded as an ion pair.

Based on the results shown here, we can not conclude whether ion-pair **A** can be an intermediate during the formation of cluster **6**. Nonetheless, when HSTip is

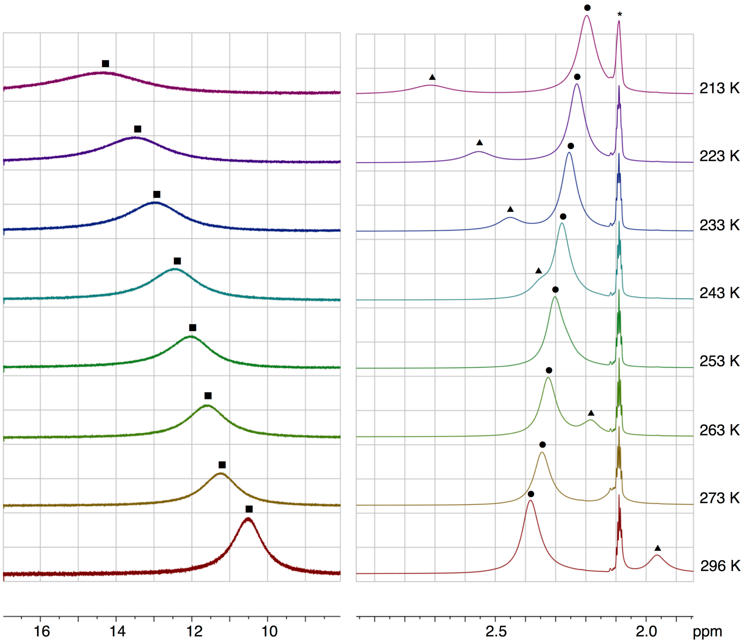

Figure 4.5. Variable-temperature ^{1}H NMR spectra of **A** in the range from (left) 8.0 to 17.0 ppm (right) 1.95 to 2.95 ppm. Legends: ■, $SiMe_3$ group (amide) of $[Fe\{N(SiMe_3)_2\}_2(TMS\text{-}bpzm)]$; ▲, $SiMe_3$ group (TMS-bpzm) of $[Fe\{N(SiMe_3)_2\}_2(TMS\text{-}bpzm)]$; •, $SiMe_3$ group of $[Fe_4S_4\{N(SiMe_3)_2\}_4]$; *, solvent.

added to the reaction mixture, one of $^-$STip ligands in ideally-formed $[Fe(STip)_2(TMS\text{-}bpzm)]$ would be eliminated from the Fe center. Assuming that this process occurs as the reductive formation of TipS-STip because the reaction was carried out in the non-polar solvent, the oxidation of Fe complex to give Fe^{3+} state by the electron transfer to the highly oxidized $[Fe_4S_4]$ cluster may be included in the course of the formation of cluster **6**.

4.3. Conclusions

In this work, we synthesized [Fe_4S_4]-[Fe] cluster **6** as a rare example of the [Fe_4S_4] cluster linked with a metal complex through a monodentate thiolate bridge. Cluster **6** was structurally characterized, and the effect of the thiolate bridge on its electrochemical property was investigated by the CV measurement. We could not afford a clear insight on the reaction mechanism for the formation of cluster **6**; however, the reaction of cluster **1** with complex **5** showed that the electron transfer between these complexes occurs at low temperature. Further, the use of the single-site substitution of the highly oxidized [Fe_4S_4] cluster to link a metal complex could be applied to a broader scope.

4.4. Experimental Section

General Procedures. All reactions were manipulated under a nitrogen atmosphere using Schlenk techniques and a glove box. CH_3CN, hexane, pentane, toluene, and THF were purified by the method of Grubbs,[14] where the solvents were passed over columns of activated alumina and a supported copper catalyst supplied by Hansen & Co. Ltd. UV-vis spectra were measured on a JASCO V560 spectrometer at room temperature. ^1H NMR spectra were recorded on a JEOL ECA-600 or ECA-500, and the data were analyzed by MestReNova (version 8.1.2). ^1H NMR signals were referenced to the residual peaks of the solvents (C_6D_6: δ 7.16; THF-d^8: δ 1.73; toluene-d^8: δ 2.09). The variable-temperature ^1H NMR measurement of **A** was carried out in the range between room temperature and –60°C. Cyclic voltammograms were measured in THF at room temperature. The measurement conditions were as follows: reference electrode, Ag/$AgNO_3$ (0.01 M in CH_3CN); working electrode, glassy carbon; counter electrode, Pt; sample concentration, 3 mM; supporting electrolyte, $[N^nBu_4][PF_6]$ (0.3 M). The reference electrode was freed from the working compartment by a Vycor junction. Elemental analyses were performed on an Elementar Analytical vario MICRO cube elemental analyzer where the crystalline samples were sealed in tin capsules under nitrogen. $[Fe_4S_4\{N(SiMe_3)_2\}_4]$ (**1**), $Fe\{N(SiMe_3)_2\}_2$,[15] TMS-bpzm,[16] HSTip[17] and were prepared according to the procedures described in the publications. The supporting electrolyte $[N^nBu_4][PF_6]$ was recrystallized from THF before use. All other chemicals were used as purchased.

$Fe\{N(SiMe_3)_2\}_2$(TMS-bpzm) (5). To a toluene (5 mL) solution of $Fe\{N(SiMe_3)_2\}_2$ (3.00 g, 7.96 mmol) was added a toluene (20 mL) solution of TMS-bpzm (2.33 g, 7.96 mmol). The solution was stirred overnight at room temperature followed by evaporation in *vacuo*. The afforded light yellow solid was extracted with pentane (30 mL), and then the upper solution was crystalized at –35°C to give Fe{N(SiMe$_3$)$_2$}$_2$(TMS-bpzm) (**5**, 3.68 g, 5.52 mmol, 69% yield) as light greenish yellow crystals. This complex was also structurally characterized (Figure A3.1). UV-vis (toluene): λ_{max} = 378 nm (ε 6.7 × 10^2). Cyclic Voltammetry (THF, room temperature; Figure A3.2): $E_{1/2}$ = 0.01 V (Fe^{3+}/Fe^{2+}), E = 0.28 V (irreversible oxidation). ^{1}H NMR (C$_6$D$_6$): δ 43.25 (br), 10.55 (br, 36H, N{Si(CH_3)$_3$}$_2$), 1.95 (br, 18H, CSi(CH_3)$_3$). *Anal. Calcd* for $C_{25}FeH_{60}Si_6N_6$: C, 44.87; H, 9.038; N, 12.56. Found: C, 44.54; H, 8.97; N, 12.47.

[Fe$_4$S$_4$(STip)$_3$(μ_2-STip)Fe(TMS-bpzm)$_2$(NCMe)] (6). To a toluene (10 mL) solution of [Fe$_4$S$_4${N(SiMe$_3$)$_2$}$_4$] (**1**, 500 mg, 0.503 mmol), **5** (337 mg, 0.503 mmol), and TMS-bpzm (147 mg, 0.501 mmol) was added a toluene (25 mL) solution of HSTip (714 mg, 3.02 mmol) at –40°C, and the solution was allowed to warm up to room temperature with stirring overnight. The afforded black suspension was evaporated to dryness. The black residue was washed with hexane (15 mL), toluene (15 mL), and THF (15 mL) followed by the extraction with CH$_3$CN (20 mL). After centrifugation to remove insoluble solid, the black supernatant was concentrated to *ca* 10 mL and cooled at –35°C to give Fe$_4$S$_4$(STip)$_3$(μ_2-STip)Fe(TMS-bpzm)$_2$(NCMe) (**5**, 199 mg, 20% yield) as black crystals. UV-vis (THF): λ_{max} = 456 nm (ε 2.1 × 10^4), λ = 342 nm (shoulder). Cyclic Voltammetry (THF, room temperature): $E_{1/2}$ = –0.47 V ([Fe$_4$S$_4$]$^{3+}$/[Fe$_4$S$_4$]$^{2+}$), $E_{1/2}$ = –1.77 V ([Fe$_4$S$_4$]$^{2+}$/[Fe$_4$S$_4$]$^{+}$). ^{1}H NMR (THF-d^8): δ 10.08, 7.39, 7.00, 6.39, 5.78, 4.29, 2.18, 2.03, 1.96, 1.22, 0.47, 0.39. EPR (X-band, microwave

1.0 mW, 8 K and 16K): silent. *Anal. Calcd* for $C_{88}Fe_5S_8H_{143}N_9Si_4$: C, 53.51; H, 7.30; N, 6.38; S, 12.99. Found: C, 53.86; H, 7.50; N, 6.58; S, 12.51.

[Fe{N(SiMe$_3$)$_2$(TMS-bpzm)}[Fe$_4$S$_4${N(SiMe$_3$)$_2$}$_4$] (A). To a toluene solution (10 mL) of **1** (400 mg, 0.403 mmol) was added a toluene (5 mL) solution of **5** (269 mg, -.402 mmol). The solution was stirred 5 hours at room temperature and evaporated to dryness. The black residue was extracted with pentane followed by centrifugation to remove the insoluble solid. After a few drops of hexane was added to the black supernatant, the solution was cooled at –35°C to give [Fe{N(SiMe$_3$)$_2$}$_2$(TMS-bpzm)]-[Fe$_4$S$_4${N(SiMe$_3$)$_2$}$_4$] (**A**, 445 mg, 0.268 mmol, 56% yield) as black crystals. UV-vis (toluene): $\lambda_{max} = 445$ nm (ε 1.5×10^4). *Anal. Calcd* for $C_{49}Fe_5S_4H_{139}Si_{14}N_{10}$: C, 35.40; H, 8.00; N, 8.43; S, 7.72. Found: C, 35.49; H, 7.50; N, 8.01; S, 7.53.

X-ray Crystal Structure Determination. Crystal data and refinement parameters for **5**, **6**$\cdot$(CH$_3$CN)$_{1.4}$, and **A**$\cdot$(C$_6$H$_{14}$) are summarized in Table A3.1. Single crystals were coated with oil (Immersion Oil, type B: Code 1248, Cargille Laboratories, Inc.) and mounted on loops (CryoLoop). Diffraction data were collected at –100 °C under a cold nitrogen stream on a Rigaku AFC8 equipped with a Mercury CCD detector, or on a Rigaku RA-Micro7 equipped with a Saturn70 CCD detector, using graphite-monochromated Mo Kα radiation (λ = 0.710690 Å). Eighteen preliminary data frames were measured at 0.5° increments of ω, to assess the crystal quality and preliminary unit cell parameters. The intensity images were also measured at 0.5° intervals of ω. The frame data were integrated using the CrystalClear program package, and the data sets were corrected for absorption using the REQAB program. The calculations were performed with the CrystalStructure program package. All structures were solved by direct methods and refined by full–matrix least squares. Anisotropic refinement was applied to all non-hydrogen atoms except for the disordered atoms and crystal solvents, and all hydrogen atoms were put at calculated positions. The four ^{i}Pr groups in **6**·$(CH_3CN)_{1.4}$ are disordered over two positions in a 65:35, a 90:10, a 70:30, and a 50:50 ratio. The two trimethylsilyl groups in **6**·$(CH_3CN)_{1.4}$ are disordered over two positions with 75:25 and 80:20 occupancy factors. Isotropic refinement was applied to one of the acetonitrile molecules in **6**·$(CH_3CN)_{1.4}$, and this crystal solvent was solved with the fixed occupancy factor (0.4) because of the low intensity of the residual peaks. One of the trimethylsilyl group in **A**·(C_6H_{14}) is disordered over two positions in a 1:1 ratio. The hexane molecule of **A**·(C_6H_{14}) was isotropically refined.

References and Notes

[1] (a) Crane, B. R.; Siegel, L. M.; Getzoff, E. D. *Science* **1995**, *270*, 59–67. (b) Crane, B. R.; Siegel, L. M.; Getzoff, E. D. *Biochemistry* **1997**, *36*, 12101–12119. (c) Nakayama, M.; Akashi, T.; Hase, T. *J. Inorg. Biochem.* **2000**, *82*, 27–32. (d) Swamy, U.; Wang, M.; Tripathy, J. N.; Kim, S.-K.; Hirasawa, M.; Knaff, D. B.; Allen, J. P. *Biochemistry* **2005**, *44*, 16054–16063. (e) Smith, K. W.; Stroupe, M. E. *Biochemistry* **2012**, *51*, 9857–9868.

[2] (a) Cai, L.; Weigel, J. A.; Holm, R. H. *J. Am. Chem. Soc.* **1993**, *115*, 9289–9290. (b) Cai, L.; Holm, R. H. *J. Am. Chem. Soc.* **1994**, *116*, 7177–7188. (c) Zhou, C.; Cai, L.; Holm, R. H. *Inorg. Chem.* **1996**, *35*, 2767–2772.

[3] Osterloh, F.; Saak, W.; Pohl, S. *J. Am. Chem. Soc.* **1997**, *119*, 5648–5656.

[4] Pickett, C. J.; Tard, C.; Liu, X.; Ibrahim, S. K.; Bruschi, M.; De Gioia, L.; Davies, S. C.; Yang, X.; Wang, L.-S.; Sawers, G. *Nature* **2005**, *433*, 610–613.

[5] Ohki, Y.; Sunada, Y.; Tatsumi, K. *Chem. Lett.* **2005**, *34*, 172–173.

[6] (a) Stack, T.; Holm, R. H. *J. Am. Chem. Soc.* **1988**, *110*, 2484–2494. (b) Ohki, Y.; Tanifuji, K.; Yamada, N.; Imada, M.; Tajima, T.; Tatsumi, K. *Proc. Nat. Acad. Sci. U.S.A.* **2011**, *108*, 12635–12640. (c) Terada, T.; Hirabayashi, K.; Liu, D.; Nakamura, T.; Wakimoto, T.; Matsumoto, T.; Tatsumi, K. *Inorg. Chem.* **2013**, *52*, 11997–12004.

[7] Lee, S. C.; Tan, L. L.; Holm, R. H. *Polyhedron* **2013**, *58*, 206–217.

[8] Ueyama, N.; Sugawara, T.; Fuji, M.; Nakamura, A.; Yasuoka, N. *Chem. Lett.* **1985**, 175–178.

[9] We have searched the Cambridge Crystallographic Data Center for finding the crystal structures of the complexes having $[Fe(L)_5(SR)]$ (L = ligands) chemical

formula. From the afforded structures, the bond distances between Fe and a non-bridged thiolate ligand were picked up. The longest bond distances were reported in the following publications: (a) Sellmann, D.; Hofmann, T.; Knoch, F. *Inorg. Chim. Acta* **1994**, *224*, 61–71. (b) Sellmann, D.; Utz, J.; Heinemann, F. W. *Inorg. Chem.* **1999**, *38*, 459–466. The shortest bond distance was reported in the following publication: Uraev, A. I.; Nivorozhkin, A. L.; Kurbatov, V. P.; Divaeva, L. N.; Korobov, M. S.; Lyssenko, K. A.; Antipin, M. Y.; Pavlenko, D. A.; Garnovskii, A. D. *Russ. Chem. Bull., Int. Ed.* **2003**, *52*, 2523–2526. Since the octahedral coordination spheres of [Fe(L′)$_3$] (L′ = pyrimidine-2-thiolate, pyridine-2-thiolate) are highly distorted, in this survey, we excluded the structures reported in the following publications: (a) Latham, I. A.; Leigh, G. J.; Pickett, C. J.; Huttner, G.; Jibrill, I.; Zubieta, J. *J. Chem. Soc., Dalton Trans.* **1986**, 1181. (b) Rosenfield, S. G.; Swedberg, S. A.; Arora, S. K.; Mascharak, P. K. *Inorg. Chem.* **1986**, *25*, 2109–2114. (c) Rosenfield, S. G.; Mascharak, P. K.; Arora, S. K. *Inorg. Chim. Acta* **1987**, *129*, 39–46.

[10] In Chapter 3, we have reported the potentials of $[Fe_4S_4(STip)_4]^-$ under the same condition used in this work.

[11] Blonk, H. L.; Kievit, O.; Roth, E.; Jordanov, J.; Van der Linden, J.; Steggerda, J. J. *Inorg. Chem.* **1991**, *30*, 3231–3234.

[12] Sharp, C. R.; Duncan, J. S.; Lee, S. C. *Inorg. Chem.* **2010**, *49*, 6697–6705.

[13] The molecular structure of **4** is shown in Figure A3.1.

[14] Pangborn, A. B.; Giardello, M. A.; Grubbs, R. H.; Rosen, R. K.; Timmers, F. *J. Organometallics* **1996**, *15*, 1518-1520.

[15] Andersen, R. A.; Faegri, K., Jr; Green, J. C.; Arne, H.; Lappert, M. F.; Leung, W.-P.; Rypdal, K. *Inorg. Chem.* **1988**, *27*, 1782–1786.

[16] Hill, M. S.; Mahon, M. F.; McGinley, J. M.; Molloy, K. C. *Polyhedron* **2001**, *20*, 1995–2002.

[17] Blower, P. J.; Dilworth, J. R.; Hutchinson, J. P.; Zubieta, J. A. *J. Chem. Soc., Dalton Trans.* **1985**, 1533–1541.

Appendix 3

Supporting Information for Chapter 4

Table A3.1. Crystal data for Fe{N(SiMe$_3$)$_2$}$_2$(TMS-bpzm) (**5**), [Fe$_4$S$_4$(STip)$_3$(μ_2-STip)-Fe(TMS-bpzm)$_2$(NCMe)] ·(CH$_3$CN)$_{1.4}$ (**6**·(CH$_3$CN)$_{1.4}$), and [Fe{N(SiMe$_3$)$_2$}$_2$-(TMS-bpzm)][Fe$_4$S$_4${N(SiMe$_3$)$_2$}$_4$] ·(C$_6$H$_{14}$) (**A**·(C$_6$H$_{14}$)).

	5	**6**·(CH$_3$CN)$_{1.4}$	**A**·(C$_6$H$_{14}$)
formula	$C_{25}H_{60}N_6FeSi_6$	$C_{90.8}H_{100}Fe_5N_{10.4}S_8Si_4$	$C_{52}H_{123}Fe_5N_{10}S_4Si_{14}$
Formula wt (g mol^{-1})	669.15	1985.12	1689.28
Crystal system	Monoclinic	Monoclinic	Triclinic
Space group	*Cc* (#9)	*P*2$_1$/*c* (#14)	*P*-1 (#2)
a (Å)	16.463(9)	27.679(3)	12.113(3)
b (Å)	19.858(19)	16.8894(19)	18.441(5)
c (Å)	12.262(4)	24.321(3)	21.397(6)
α (°)			91.275(4)
β (°)	100.32(3)	97.112(3)	90.820(4)
γ (°)			101.654(4)
V (Å^3)	3944(4)	11282(2)	4679(2)
Z	4	4	2
D_{calcd} (g/cm^3)	1.127	1.169	1.199
Max 2θ (°)	55.0	55.0	55.0
No. of Reflections Measured	15773	76372	45921
No. of Data Used (I >2.00 s(I))	7065	25759	20944
No. of Parameters Refined	403	1053	747
R_1^{a}	0.0573	0.0845	0.0542
wR_2^{b}	0.1557	0.2788	0.1575
GOF^c	1.013	1.026	1.063

[a] $I > 2\sigma(I)$, $R1=\Sigma||F_o|-|F_c||/\Sigma|F_o|$. [b] refined with all data, $wR2=[\{\Sigma w(F_o^2-F_c^2)^2\}/\Sigma w(F_o^2)^2]^{1/2}$.

[c] $\mathrm{GOF}=[\{\Sigma w(F_o^2-F_c^2)^2\}/(N_o-N_p)]^{1/2}$, where N_o and N_p denote the numbers of reflection data and parameters.

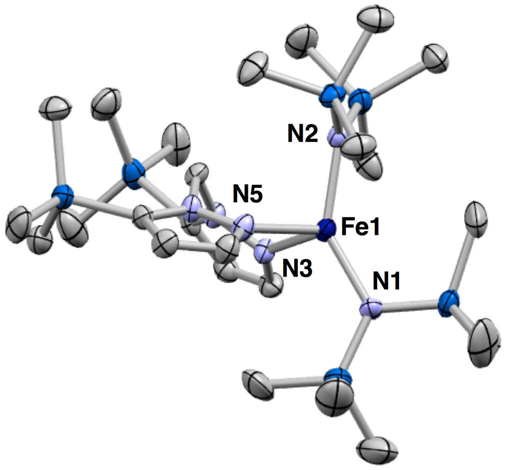

Figure A3.1. Molecular structure of Fe{N($SiMe_3$)$_2$}$_2$(TMS-bpzm) (**5**) with thermal ellipsoids at the 50% probability level. All hydrogen atoms are omitted for clarity. Selected bond distances (Å) and angles(°): Fe1-N1, 1.973(4); Fe1-N2, 2.002(4); Fe1-N3, 2.149(4), Fe1-N5, 2.175(4); N1-Fe1-N2, 139.33(17); N1-Fe1-N3, 106.74(16); N1-Fe1-N5, 111.00(18); N2-Fe1-N3, 104.27(17); N2-Fe1-N5, 98.62(17); N3-Fe1-N5, 82.23(15).

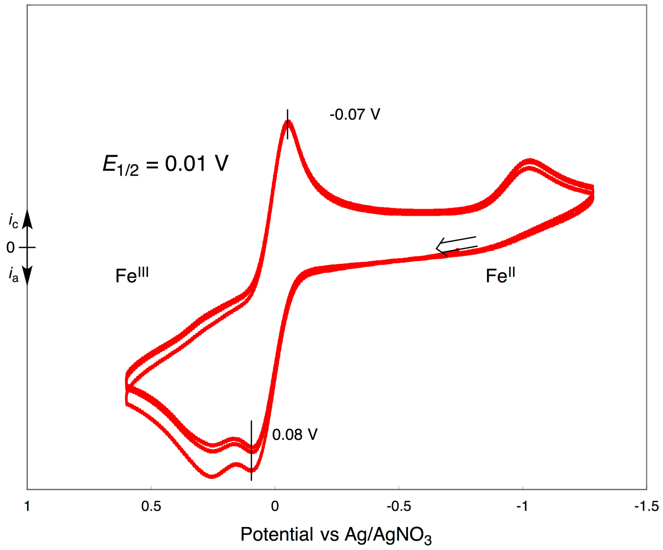

Figure A3.2. Cyclic voltammogram of complex **5**. Conditions: sample concentration, 3 mM in THF; supporting electrolyte, 0.3 M [N^{n}Bu$_4$][PF$_6$]; working electrode, glassy carbon; counter electrode, Pt; sweep speed, 0.1 V s^{-1}.

Chapter 5

Formation of a Nitrogenase P-cluster [Fe_8S_7] Core via Reductive Fusion of Two All-Ferric [Fe_4S_4] Clusters

This chapter is partly partly reproduced with permission from: Ohki, Y.; Tanifuji, K.; Yamada, N.; Cramer, R. E.; Tatsumi, K. *Chem. Asian J.* **2012**, *7*, 2222–2224. Copyright 2012 WILEY-VCH verlag GmbH & Co.

5.1. Introduction

As described in Chapter 1, the cuboidal [Fe_4S_4] core is thermodynamically robust and exhibits multiple oxidation states with only minor geometry change. On the other hand, the [Fe_4S_4] core transformation has been suggested to occur in some biological processes.[1] A representative example is the inter-conversion between [Fe_4S_4] and [Fe_3S_4] clusters in Aconitase. Another interesting example would be the biosynthesis of the [Fe_8S_7] core of nitrogenase P-cluster (Figure 5.1),[2] which plays an important role in the electron-transfer sequence for the reduction of atmospheric dinitrogen to ammonia. Based on mutagenesis studies, the assembly of the [Fe_8S_7] core has been suggested to occur via the fusion of two [Fe_4S_4] clusters.[3] Since the [Fe_8S_7] core of P-cluster has one less sulfur atoms than two [Fe_4S_4] clusters, the biosynthetic pathway probably involves desulfurization from one of the [Fe_4S_4] cores. We have previously synthesized the [Fe_8S_7] core of P-cluster by a self-assembly reaction using Fe{N($SiMe_3$)$_2$}$_2$ as the precursor,[4] and therefore the postulated biosynthetic pathway has drawn our interest. As the cuboidal [Fe_4S_4] core is robust, a key to initiate the fusion process is the removal of a sulfur atom from the [Fe_4S_4]

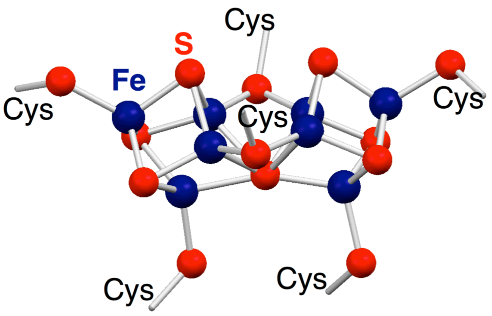

Figure 5.1. Expanded structure of Nitrogenase P-cluster (PDB ID: 3U7Q). Cys denotes cysteine.[5]

core.[6, 7, 8] An example for such desulfurization is the reaction of the NO-bound cluster $Fe_4S_4(NO)_4$ with PEt_3, which results in the formation of $Fe_4S_3(NO)_4(PEt_3)_3$ and $SPEt_3$.[8] The all-ferric $[Fe_4S_4]^{4+}$ cluster $Fe_4S_4\{N(SiMe_3)_2\}_4$ (**1**),[9, 10] with an oxidation state two units higher than the $[Fe_4S_4]^{2+}$ oxidation state of the more common $[Fe_4S_4X_4]^{2-}$ (X = thiolate, halide) clusters, would be better suited for the desulfurization process, which converts a sulfide ion into an SPR_3 sulfur atom leaving $2e^-$ behind. It is known that the all-ferric $[Fe_4S_4]$ core of **1** can be readily reduced by one or two electrons upon treatment with appropriate reductants.[10, 11] In this chapter, we report the desulfurization of the $[Fe_4S_4]^{4+}$ core of **1** by PR_3 (R=Me, Et), leading to the formation of the $[Fe_8S_7]$ clusters $[Fe_4S_3\{N(SiMe_3)_2\}(SPR_3)]_2(\mu_6\text{-}S)\{\mu\text{-}N(SiMe_3)_2\}_2$ (**7a**, R = Et; **7b**, R = Me).

5.2. Results and Discussions

The reaction of **1** with PEt$_3$ in toluene at room temperature gave a black solution, from which the [Fe$_8$S$_7$] cluster [Fe$_4$S$_3${N(SiMe$_3$)$_2$}(SPEt$_3$)]$_2$(μ$_6$-S){μ-N(SiMe$_3$)$_2$}$_2$ (**7a**) was isolated as black crystals in 29% yield (**Scheme 5.1**). An analogous reaction of **1** with PMe$_3$ also gave rise to black crystals of a similar [Fe$_8$S$_7$] cluster, **7b**, in 16% yield. The yield of **2a** was improved to 36%, when **1** was treated with a mixture of HSTip (Tip = 2,4,6-^{i}Pr$_3$C$_6$H$_2$)[12] and PEt$_3$ at –40 °C followed by stirring at room temperature. Whereas the one-electron reduced form of **1**, [Na(THF)$_2$][Fe$_4$S$_4${N(SiMe$_3$)$_2$}$_4$],[10, 11] reacted with PEt$_3$, no [Fe$_8$S$_7$] cluster has been obtained from this reaction. The molecular structure of **7a** was determined by X-ray crystallography (Figure 5.2). While the structure of **7b** was also identified, the quality of the X-ray diffraction data was not sufficient to discuss detailed structural features. The structures of **7a** and

Scheme 5.1.

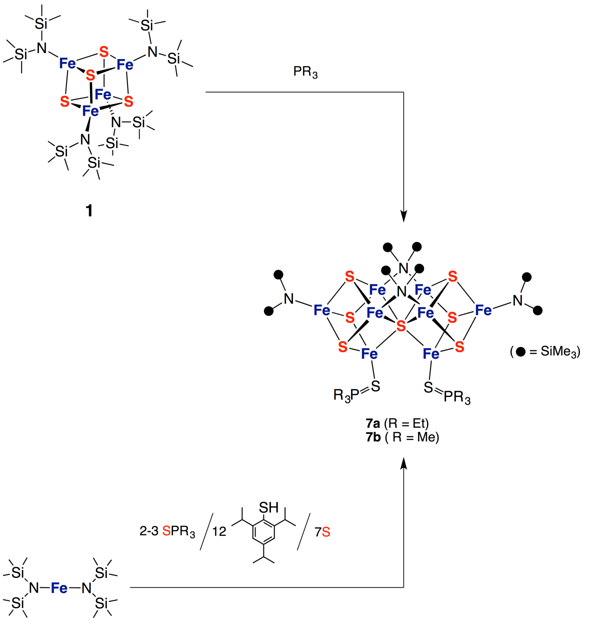

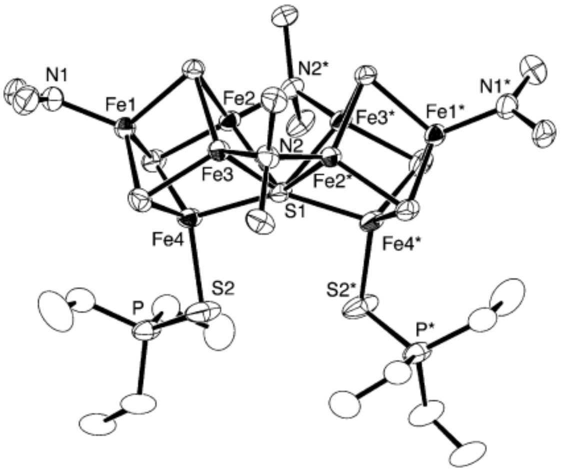

Figure 5.2. Molecular structure of **7a**. Methyl groups of the amide ligands are omitted for clarity. Selected bond distances (Å): Fe1–Fe2 2.8081(5), Fe1–Fe3 2.8007(6), Fe1–Fe4 2.7569(5), Fe2–Fe3 2.7184(6), Fe2–Fe4 2.6527(5), Fe3–Fe4 2.6608(5), Fe2–Fe3* 2.7521(5), Fe2–S1 2.3870(7), Fe3–S1 2.4011(7), Fe4–S1 2.3509(4), Fe4–S2 2.3444(9), S2–P 1.9980(12), Fe1–N1 1.915(2), Fe2–N2 2.058(2), Fe3–N2 2.055(2).

7b are quite similar to that of P-cluster model, $[Fe_4S_3\{N(SiMe_3)_2\}\{SC(NMe_2)_2\}]_2$-$(\mu_6\text{-}S)\{\mu\text{-}N(SiMe_3)_2\}_2$ (**A**),[13] which we have synthesized by a self-assembly reaction of $Fe\{N(SiMe_3)_2\}_2$, $SC(NMe_2)_2$, S_8, and HSTip (Tip = 2,4,6-triisopropylphenyl). Based on the X-ray derived structures, the oxidation state of the iron atoms in **7a**, **b** is $[Fe_8S_7]^{4+}$, which is the same as that of **A**, since SPR_3 (R = Et or Me) and $SC(NMe_3)_2$ are neutral ligands. The mean Fe-Fe and Fe-S distances within the $[Fe_8S_7]$ core of **7a** (Ave. Fe-Fe, 2.7357(6) Å; Ave. F-S, 2.3063(10) Å) are almost identical to those of **A** (Ave. Fe-Fe, 2.7376(7) Å; Ave. Fe-S 2.3072(11) Å). A notable difference can be seen in the coordination geometry of $SPEt_3$ and $SC(NMe_2)_2$. The Fe-$SPEt_3$ bond in **7a** (2.3444(9) Å) is longer than the corresponding Fe-$SC(NMe_2)_2$ distance in **A** (2.3151(10) Å), and the Fe-S-P angle of **7a** opens to 103.06(4)° compared with the Fe-S-C angle of 95.34(12)° in **A**. These findings are indicative of weaker binding of $SPEt_3$ than

$SC(NMe_2)_2$. The reduction potentials of **7a** in THF, $E_{1/2}$ = –1.26 and –1.77V versus Ag/Ag, are also similar to that of A, $E_{1/2}$ = –1.29 and –1.69 V.

The structural analogy between **7a**, **b** and **A** prompted us to examine an alternative route to **7a**–**b**, which is similar to the self-assembly reaction used for the synthesis of **A**.[13] Thus the reaction of $Fe\{N(SiMe_3)_2\}_2$ with $SPEt_3$, HSTip, and S_8, in the ratio of (Fe):($SPEt_3$):(HSTip):(S) = 8:2.4:12:7 was carried out in toluene (Scheme 5.1). From this reaction, **7a** was isolated in 70% yield as crystals. Likewise, cluster **7b** was obtained as crystals in 30% yield using $SPMe_3$ instead of $SPEt_3$. In relation to these reactions, we have recently synthesized an oxygen-incorporated $[Fe_8S_6O]$ cluster $[(DmpS)Fe_4S_3O][(DmpS)Fe_4S_3](\mu\text{-}OCPh_3)$ (Dmp = 2,6-dimesitylphenyl) from the reaction of $Fe\{N(SiMe_3)_2\}_2$ with HSDmp and $HOCPh_3$ followed by treatment with elemental sulfur and water.[14]

It is likely that a phosphine PR_3 abstracts a sulfur atom from a $[Fe_4S_4]$ core as the first step of the reductive fusion of two $[Fe_4S_4]$ clusters. This desulfurization process would generate a transient $[Fe_4S_3]$ cluster and a corresponding phosphine sulfide SPR_3 (Figure 5.3). The void of the transient $[Fe_4S_3]$ cluster could be filled with one of the sulfur atoms of a $[Fe_4S_4]$ cluster, thus generating the central μ_6-sulfur atom of the resulting $[Fe_8S_7]$ core of **7a**, **b**. This coupling scheme of the $[Fe_4S_3]$ intermediate with a $[Fe_4S_4]$ cluster appears to be straightforward as far as the stoichiometry of iron and sulfur atoms is concerned. However, the $[Fe_8S_7]^{4+}$, which is formally described as $2Fe^{3+}6Fe^{2+}$, oxidation state for **7a** or **7b** is reduced by six electrons as compared to the $[Fe_4S_4]^{4+}$ ($4Fe^{3+}$) state for two molecules of **1**, while the desulfurization of a $[Fe_4S_4]$ cluster is a two-electron reducing process. Thus, the desulfurization is not the sole

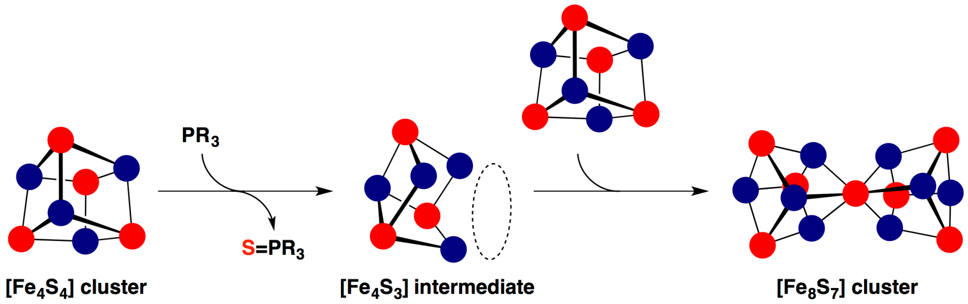

Figure 5.3. Schematic description of formation of the [Fe_8S_7] core from two [Fe_4S_4] clusters.

process accounting for the reduction of iron atoms of **7a**, **b**. The fusion of two $Fe_4S_4\{N(SiMe_3)_2\}_4$ clusters to give $[Fe_4S_3\{N(SiMe_3)_2\}(SPR_3)]_2(\mu_6\text{-}S)\{\mu\text{-}N(SiMe_3)_2\}_2$ (**7a**, **7b**) causes the loss of four amide ligands, and the fate of the dissociated amide ligands remains unclear. It is notable that the presence of HSTip in the reaction mixture led to the better yield of **2a**. The addition of HSTip results in the ligand exchange from $^{-}N(SiMe_3)_2$ to $^{-}$STip by releasing amine $HN(SiMe_3)_2$, and the $^{-}$STip ligands on iron possibly facilitate the reduction of iron atoms by eliminating disulfide TipS-STip. The formation of **2a**-**b** from **1** and PR_3 is concerned with the biosynthesis of P-cluster because the [Fe_8S_7] core is formed from two [Fe_4S_4] clusters through a reduction process. The maturation process of P-cluster has been suggested to require reductase (Fe-protein of nitrogenase), MgATP, and reductant.[3] Therefore, for both the core transformation shown here and P-cluster maturation, unusual oxidation states is supposed to be a key point to convert robust [Fe_4S_4] clusters.

5.3. Conclusion

We have demonstrated that the nitrogenase P-cluster [Fe_8S_7] core can be formed from the reductive fusion of all-ferric [Fe_4S_4] clusters via phosphine desulfurization. This reaction is relevant to the maturation process of the P-cluster, which has been proposed to include reduction of [Fe_4S_4] clusters. Thus reductive desulfurization from an [Fe_4S_4] precursor can occur during the physiological assembly of the [Fe_8S_7] core of the P-cluster, although the desulfurization agent(s) for P-cluster biosynthesis remains an open question.

5.4. Experimental Section

General Procedures. All reactions and manipulations were performed under a nitrogen atmosphere using a glove box or standard Schlenk techniques. Toluene, hexane, and HMDSO (hexamethyldisiloxane) were purified by the method of Grubbs,[15] where the solvents were passed over columns of activated alumina and supported copper catalyst supplied by Hansen & Co. Ltd. Cyclic voltammogram (CV) of **7a** was recorded in THF using Au as the working electrode with 0.5 M $[N^nBu_4][PF_6]$ as supporting electrolyte. The potentials are referenced to Ag/Ag^+. UV-vis spectra were measured on a JASCO V560 spectrometer. Elemental analyses were performed on a LECO-CHNS-932 elemental analyzer where the crystalline samples were sealed in silver capsules under nitrogen. The EPR spectrum was recorded on a Bruker EMX-plus spectrometer at X-band frequencies. The magnetic susceptibility was measured using a Quantum Design MPMS-XL SQUID-type magnetometer, and the crystalline samples were sealed in quartz tubes. X-ray diffraction data were collected on a Rigaku AFC8 or a Rigaku AFC10 equipped with a CCD area detector by using graphite-monochromated MoKα radiation. $Fe_4S_4\{N(SiMe_3)_2\}_4$ (**1**),[9] $Fe\{N(SiMe_3)_2\}_2$,[16] and HSTip[17] (Tip = 2,4,6-triisopropylphenyl) were prepared according to the literature procedures.

Synthesis of $[\{N(SiMe_3)_2\}(SPEt_3)Fe_4S_3]_2(\mu_6\text{-}S)\{\mu\text{-}N(SiMe_3)_2\}_2$ (7a). Method A, from **1** and PEt_3: A toluene solution of PEt_3 (0.18 mL, 1.69 M, 0.304 mmol) was slowly added to a toluene (25 mL) solution of cluster **1** (307 mg, 0.309 mmol) at room temperature. After stirring for 17 hrs, the solution was evaporated under reduced pressure. The resultant black residue was extracted with hexane (12 mL), and the extract was centrifuged to remove a small amount of insoluble solid. The extract was concentrated to *ca.* 6 mL under reduced pressure. After addition of a drop of toluene, the solution was stored at –30 ˚C for a few days. Black crystals of **7a**·C_7H_8 (76 mg, 4.4×10^{-2} mmol, 29%) were obtained. UV-vis (toluene): λ_{max} = 383 (ε 1.7 × 10^4) nm. EPR (microwave power 1.0 mW; microwave frequency 9.517386 GHz; modulation width 1 mT; 4 mM in Toluene): Silent in the range of 8-100 K. Magnetic susceptibility (B.M.): μ_{eff}/Fe = 0.050 (2 K), 0.615 (300 K). Anal. Calcd for $C_{36}H_{102}Fe_8N_4P_2S_9Si_8 \cdot C_7H_8$: C, 30.28; H, 6.50; N, 3.29; S, 16.92. Found: C, 30.12; H, 6.48; N, 3.63; S, 17.07.

Method B, from **1**, HSTip, and PEt_3: A toluene (10 mL) solution containing HSTip (0.095 g, 0.40 mmol) and PEt_3 (0.12 mL of 1.69 M toluene solution, 0.203 mmol) was slowly added to a toluene (5 mL) solution of cluster **1** (201 mg, 0.200 mmol) at –40 ˚C. The solution was gradually warmed to room temperature with stirring, and the stirring was continued for 16 hrs. The solution was evaporated under reduced pressure, and the residue was extracted with hexane (10 mL). After being centrifuged, the extract was concentrated to *ca.* 2.5 mL under reduced pressure. A drop of toluene was added, and the solution was kept at –30 ˚C. Black crystals of **7a**·C_7H_8 were isolated (61 mg, 3.6 ×10^{-2} mmol, 36%).

Method C, from $Fe\{N(SiMe_3)_2\}_2$, $SPEt_3$, HSTip, and elemental sulfur: Toluene (2 mL) was added to a Schlenk tube containing $Fe\{N(SiMe_3)_2\}_2$ (5.00 g, 13.3 mmol), and then a toluene (7 mL) solution of $SPEt_3$ (0.598 g, 3.98 mmol) and HSTip (4.71 g, 19.9 mmol) was added. Subsequently, a toluene (20 mL) solution of S_8 (0.373 g, 1.45 mmol) was added to afford a black solution. After stirring this mixture for 12 hrs at 30 °C (warmed with a water-bath), the solution was evaporated under reduced pressure. The black residue was extracted with a mixture of hexane (40 mL) and toluene (10 mL), and the extract was centrifuged to remove a small amount of insoluble solid. The solution was kept standing at room temperature for several days to afford black crystals of **7a**·C_7H_8 (1.98 g, 1.16 mmol, 70%).

Synthesis of [{N(SiMe$_3$)$_2$}(SPMe$_3$)Fe$_4$S$_3$]$_2$(μ$_6$-S){μ-N(SiMe$_3$)$_2$}$_2$ (7b). Method A, from **1** and PMe_3: The synthetic procedure is analogous to that using PEt_3. A toluene (25 mL) solution containing PMe_3 (0.20 mL of 1.0 M toluene solution, 0.200 mmol) was added to a toluene (5 mL) solution of **1** (207 mg, 0.209 mmol), and then the mixture was stirred for 17 hrs. After evaporation, the residue was extracted with toluene (2 mL). HMDSO (20 mL) was layered over the extract, and slow diffusion at room temperature led to the formation of black crystals of **7b** (25 mg, 0.16 mmol, 16%). UV-vis (toluene): λ_{max} = 385 (ε 2.2 × 10^4) nm. EPR (microwave power 1.0 mW; microwave frequency 9.517386 GHz; modulation width 1 mT; 4 mM in Toluene): Silent in the range of 8-100 K. Magnetic susceptibility (B.M.): μ_{eff}/Fe = 0.066 (2 K), 0.578 (300 K). Anal. Calcd for $C_{30}H_{90}Fe_8N_4P_2S_9Si_8 \cdot C_7H_8$: C, 27.41; H, 6.09; N, 3.46; S, 17.80. Found: C, 27.62; H, 5.77; N, 3.49; S, 17.49. Crystals for elemental analysis were obtained from Method B described below.

Method B, from Fe{N(SiMe$_3$)$_2$}$_2$, $SPMe_3$, HSTip, and elemental sulfur: A toluene (7 mL) solution of $SPMe_3$ (0.431 g, 3.99 mmol) and HSTip (4.71 g, 19.9 mmol) and a toluene (20 mL) solution of S_8 (0.373 g, 1.45 mmol) were successively added to a toluene (2 mL) solution of Fe{N(SiMe$_3$)$_2$}$_2$ (5.00 g, 13.3 mmol). Black crystals of **7b**·C_7H_8 (0.805 g, 0.497 mmol, 30%) were obtained from its toluene/hexane solution (*ca.* 40 mL), which was prepared by concentrating the extract (60 mL, 1:2 v/v toluene/hexane) of the residue.

X-ray Structural Determination. Crystal data and refinement parameters of complexes are summarized in Table A3.1. Single crystals were coated with oil (Immersion Oil, type B: Code 1248, Cargill Laboratories, Inc.) and mounted on loops. Diffraction data were collected at -100 ºC under a cold nitrogen stream on a Rigaku AFC8 or a Rigaku AFC10 with Saturn CCD detector, equipped with a graphite monochromatized MoKα source (λ = 0.71070 Å). Six preliminary data frames were measured at 0.5° increments of ω, to assess the crystal quality and preliminary unit cell parameters. The intensity images were also measured at 0.5° intervals of ω. The frame data were integrated using Rigaku/MSC CrystalClear program package, and the data sets were corrected for absorption using REQAB program. The calculations were performed with Rigaku/MSC CrystalStructure program package. Structures were solved by a direct method, and refined by full-matrix least square procedures on F^2. All non-hydrogen atoms except for disordered $SiMe_3$ and $SPMe_3$ groups in **7b** (refined isotropically) were refined anisotropically. All hydrogen atoms were put at calculated positions. One of the $SPMe_3$ groups in **7b** is disordered over two positions in a 1:1 ratio. Six $SiMe_3$ groups in **7b** are disordered over two positions in a 1:1 ratio. The iron (with Fe4) and two sulfides (with S3 and S4) in **7b**·C_7H_8 are disordered over two positions in a 1:1 ratio. The $SPMe_3$ and all of the $SiMe_3$ groups in **7b**·C_7H_8 are disordered over two positions in a 1:1 ratio. The Me group of toluene in **7b**·C_7H_8 is disordered over two positions in a 1:1 ratio.

References and Notes

[1] (a) Beinert, H.; Kennedy, M. C.; Stout, C. D. *Chem. Rev.* **1996**. (b) Khoroshilova, N.; Popescu, C.; Münck, E.; Beinert, H.; Kiley, P. J. *Proc. Nat. Acad. Sci.U.S.A.* **1997**, *94*, 6087–6092. (c) Bauer, C. E.; Elsen, S.; Bird, T. H. *Annu. Rev. Microbiol.* **1999**, *53*, 495–523.

[2] (a) Peters, J. W.; Stowell, M. H.; Soltis, M.; Finnegan, M. G.; Johnson, M. K.; Rees, D. C. *Biochemistry* **1993**, *36*, 1181–1187. (b) Mayer, S. M.; Lawson, D. M.; Gormal, C. A.; Roe, S. M.; Smith, B. E. *J. Mol. Biol.* **1999**, *292*, 871–891.

[3] Maturation of P-cluster, see: (a) Corbett, M. C.; Hu, Y.; Naderi, F.; Ribbe, M. W.; Hedman, B.; Hodgson, K. O. *J. Biol. Chem.* **2004**, *279*, 28276–28282. (b) Hu, Y.; Fay, A. W.; Lee, C. C.; Ribbe, M. W. *Proc. Nat. Acad. Sci. U.S.A.* **2007**, *104*, 10424–10429. (c) Hu, Y.; Fay, A. W.; Lee, C. C.; Yoshizawa, J.; Ribbe, M. W. *Biochemistry* **2008**, *47*, 3973–3981. (d) Cotton, M. S.; Rupnik, K.; Broach, R. B.; Hu, Y.; Fay, A. W.; Ribbe, M. W.; Hales, B. J. *J. Am. Chem. Soc.* **2009**, *131*, 4558–4559. (e) Lee, C. C.; Blank, M. A.; Fay, A. W.; Yoshizawa, J. M.; Hu, Y.; Hodgson, K. O.; Hedman, B.; Ribbe, M. W. *Proc. Nat. Acad. Sci. U.S.A.* **2009**, *106*, 18474–18478. (f) Hu, Y.; Ribbe, M. W. *Biochim. Biophys. Acta* **2013**, *1827*, 1112–1122.

[4] (a) Ohki, Y.; Sunada, Y.; Honda, M.; Katada, M.; Tatsumi, K. *J. Am. Chem. Soc.* **2003**, *125*, 4052–4053. (b) Ohki, Y.; Imada, M.; Murata, A.; Sunada, Y.; Ohta, S.; Honda, M.; Sasamori, T.; Tokitoh, N.; Katada, M.; Tatsumi, K. *J. Am. Chem. Soc.* **2009**, *131*, 13168–13178.

[5] patzal, T.; Rees, D. C.; Aksoyoglu, M.; Zhang, L.; Andrade, S. L. A.; Schleicher, E.;

Weber, S.; Einsle, O. *Science* **2011**, *334*, 940–940.

[6] Removal of an Fe atom from [Fe_4S_4] clusters, see: (a) Zhou, J.; Holm, R. H. *J. Am. Chem. Soc.* **1995**, *117*, 11353–11354. (b) Zhou, J.; Hu, Z.; Münck, E.; Holm, R. H. *J. Am. Chem. Soc.* **1996**, *118*, 1966–1980.

[7] The reactions of [Fe_4S_4] clusters with phosphines often result in the reduction of the [Fe_4S_4] core, see: (a) Tyson, M. A.; Demadis, K. D.; Coucouvanis, D. *Inorg. Chem.* **1995**, *34*, 4519–4520. (b) Goh, C.; Segal, B. M.; Huang, J.; Long, J. R.; Holm, R. H. *J. Am. Chem. Soc.* **1996**, *118*, 11844–11853.

[8] (a) Scott, M. J.; Holm, R. H. *Angew. Chem. Int. Ed.* **1993**, *32*, 564–566. (b) Goh, C.; Holm, R. H. *Inorg. Chim. Acta* **1998**, *270*, 46–54.

[9] Ohki, Y.; Sunada, Y.; Tatsumi, K. *Chem. Lett.* **2005**, *34*, 172–173.

[10] Sharp, C. R.; duncan, J. S.; Lee, S. C. *Inorg. Chem.* **2010**, *49*, 6697–6705.

[11] Ohki, Y.; Tanifuji, K.; Yamada, N.; Imada, M.; Tajima, T.; Tatsumi, K. *Proc. Nat. Acad. Sci. U.S.A.* **2011**, *108*, 12635–12640.

[12] Blower, P. J.; Dilworth, J. R.; Hutchinson, J. P.; Zubieta, J. A. *J. Chem. Soc., Dalton Trans.* **1985**, 1533-1541.

[13] (a) Ohki, Y.; Sunada, Y.; Honda, M.; Katada, M.; Tatsumi, K. *J. Am. Chem. Soc.* **2003**, *125*, 4052–4053. (b) Ohki, Y.; Imada, M.; Murata, A.; Sunada, Y.; Ohta, S.; Honda, M.; Sasamori, T.; Tokitoh, N.; Katada, M.; Tatsumi, K. *J. Am. Chem. Soc.* **2009**, *131*, 13168–13178.

[14] Ohta, S.; Ohki, Y.; Hashimoto, T.; Cramer, R. E. *Inorg. Chem.* **2012**, *51*, 11217–11219.

[15] Pangborn, A. B.; Giardello, M. A.; Grubbs, R. H.; Rosen, R. K.; Timmers, F. J.

Organometallics **1996**, *15*, 1518–1520.

[16] Andersen, R. A.; Faegri, K., Jr; Green, J. C.; Arne, H.; Lappert, M. F.; Leung, W.-P.; Rypdal, K. *Inorg. Chem.* **1988**, *27*, 1782–1786.

[17] Blower, P. J.; Dilworth, J. R.; Hutchinson, J. P.; Zubieta, J. A. *J. Chem. Soc., Dalton Trans.* **1985**, 1533–1541.

Appendix 4

Supporting Information for Chapter 5

Table A4.1. Crystal Data for **7a**·C_7H_8, **7b**, and **7b**·C_7H_8.

	7a · C_7H_8	**7b**	**7b**·C_7H_8
formula	$C_{43}H_{110}Fe_8N_4P_2S_9Si_8$	$C_{60}H_{180}N_8Fe_{16}S_{18}P_4Si_{16}$	$C_{37}H_{98}N_4Fe_8S_9P_2Si_8$
Formula wt (g mol^{-1})	1705.32	3058.03	1621.16
Crystal system	monoclinic	monoclinic	monoclinic
Space group	$P2/c$ (#13)	$P2_1/n$ (#14)	$C2/c$ (#15)
a (Å)	14.744(5)	27.810(3)	34.781(6)
b (Å)	12.198(4)	19.7617(17)	11.300(2)
c (Å)	22.559(7)	27.788(3)	22.935(4)
α (°)			
β (°)	99.739(4)	115.466(3)	122.924(2)
γ (°)			
V (Å^3)	3999(2)	13788(2)	7566(3)
Z	2	4	4
D_{calcd} (g/cm^3)	1.416	1.473	1.423
Max 2θ (°)	55.0	55.1	55.0
No. of Reflections Measured	31506	127108	30282
No. of Data Used (I >2.00 s(I))	9147 (0.029)	31353 (0.094)	8642 (0.0926)
No. of Parameters Refined	337	1071	507
R_1[a]	0.0451	0.1579	0.0906
wR_2[b]	0.1293	0.3253	0.3262
GOF[c]	1.069	1.064	1.073

[a] $I > 2\sigma(I)$, $R1=\Sigma||F_o|-|F_c||/\Sigma|F_o|$. [b] refined with all data, $wR2=[\{\Sigma w(F_o^2-F_c^2)^2\}/\Sigma w(F_o^2)^2]^{1/2}$. [c] $GOF=[\{\Sigma w(F_o^2-F_c^2)^2\}/(N_o-N_p)]^{1/2}$, where N_o and N_p denote the numbers of reflection data and parameters.

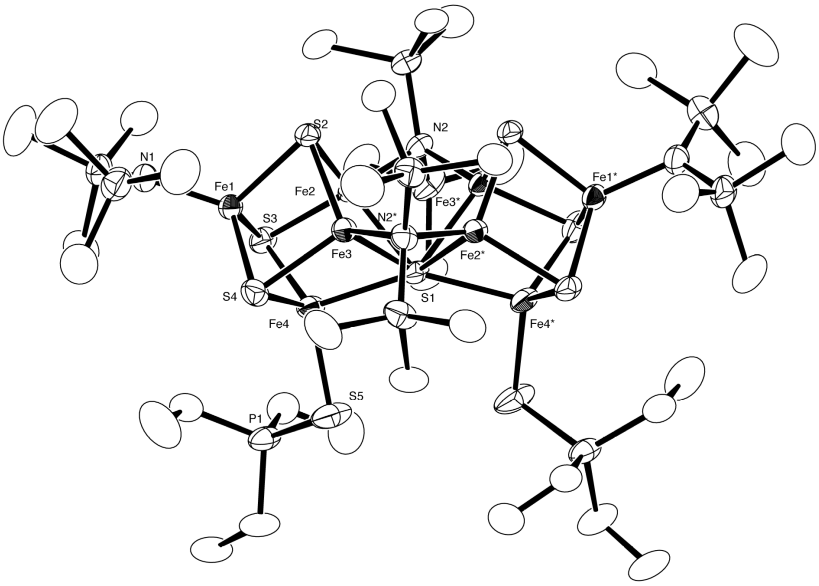

Figure A4.1. Crystal structure of **7a** with thermal ellipsoids at the 50% probability level.

Table A4.2. Selected bond distances (Å) and angles (°) for **7a**.

Fe1-Fe2	2.8081(5)	Fe3-S2	2.2885(8)
Fe1-Fe3	2.8007(6)	Fe3-S4	2.2886(8)
Fe1-Fe4	2.7569(5)	Fe4-S1	2.3509(4)
Fe2-Fe3	2.7184(6)	Fe4-S3	2.2778(9)
Fe2-Fe4	2.6527(5)	Fe4-S4	2.2582(10)
Fe3-Fe4	2.6608(5)	Fe1-N1	1.915(2)
Fe2-Fe3*	2.7521(5)	Fe2-N2	2.058(2)
Fe1-S2	2.2750(8)	Fe3-N2*	2.055(2)
Fe1-S3	2.3041(9)	Fe4-S5	2.3444(9)
Fe1-S4	2.2770(9)	Fe2-S1-Fe3*	70.17(2)
Fe2-S1	2.3870(7)	Fe4-S1-Fe4*	145.44(4)
Fe2-S2	2.2758(9)	Fe4-S5-P1	103.06(4)
Fe2-S3	2.2912(8)	Fe2-N2-Fe3*	83.99(10)
Fe3-S1	2.4011(7)		

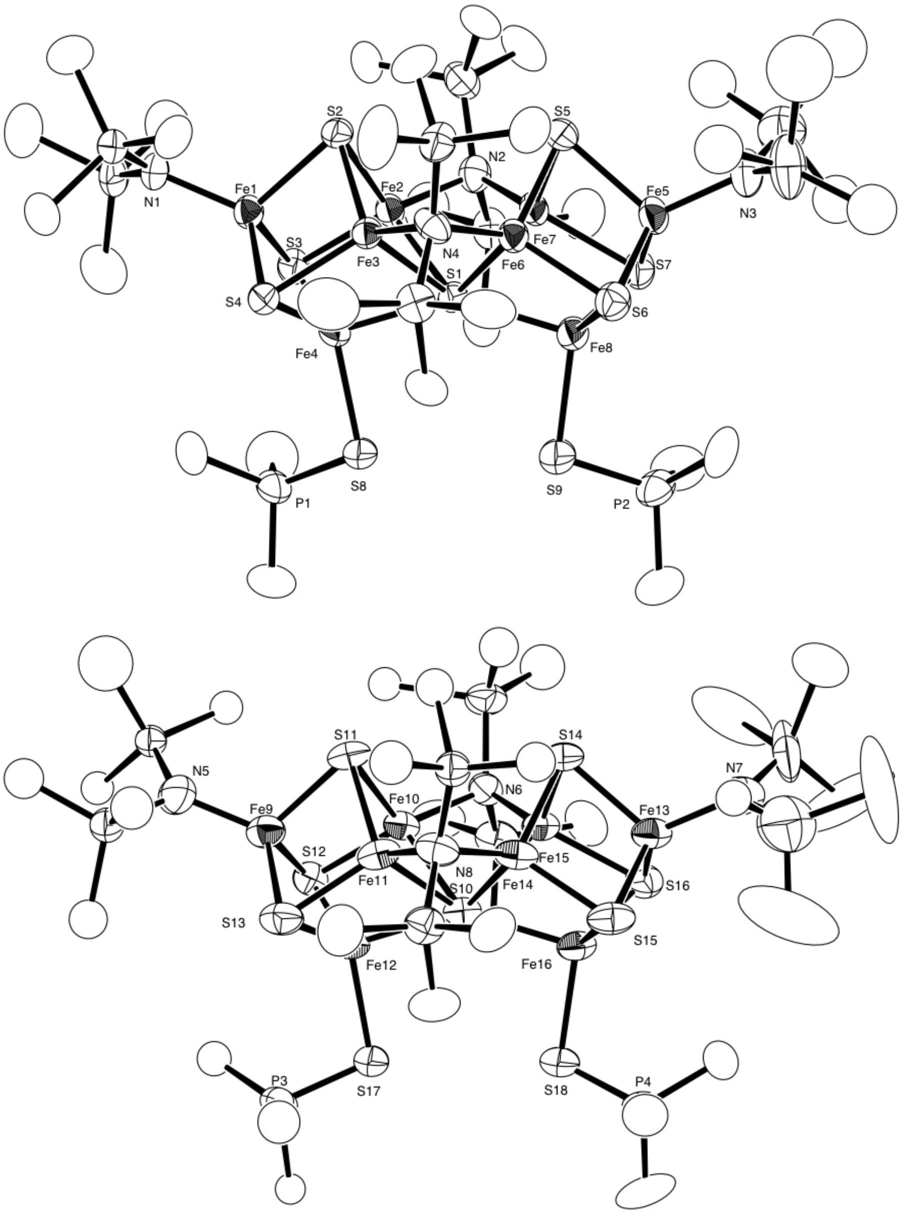

Figure A4.2. Crystal structure of **7b** with thermal ellipsoids at the 50% probability level. The crystal of **7b** (without crystal solvent) was used for this structural analysis. Two independent molecules are present in the asymmetric unit.

Table A4.3. Selected bond distances (Å) and angles (°) for **7b**.

Fe1-Fe2	2.813(2)	Fe9-Fe10	2.829(3)	Fe1-N1	1.919(12)
Fe1-Fe3	2.826(2)	Fe9-Fe11	2.821(3)	Fe2-N2	2.070(10)
Fe1-Fe4	2.753(3)	Fe9-Fe12	2.759(4)	Fe3-N4	2.131(12)
Fe2-Fe3	2.732(2)	Fe10-Fe11	2.715(2)	Fe5-N3	1.926(14)
Fe2-Fe4	2.627(3)	Fe10-Fe12	2.630(3)	Fe6-N4	2.008(11)
Fe3-Fe4	2.658(3)	Fe11-Fe12	2.654(3)	Fe7-N2	2.047(10)
Fe5-Fe6	2.806(2)	Fe13-Fe14	2.820(3)	Fe4-S8	2.344(6)
Fe5-Fe7	2.830(2)	Fe13-Fe15	2.806(3)	Fe8-S9	2.339(7)
Fe5-Fe8	2.740(3)	Fe13-Fe16	2.733(4)	Fe2-S1-Fe7	69.55(11)
Fe6-Fe7	2.712(2)	Fe14-Fe15	2.721(2)	Fe3-S1-Fe6	70.66(12)
Fe6-Fe8	2.620(3)	Fe14-Fe16	2.650(3)	Fe4-S1-Fe8	146.8(2)
Fe7-Fe8	2.675(3)	Fe15-Fe16	2.645(3)	Fe4-S8-P1	102.2(2)
Fe2-Fe7	2.739(2)	Fe10-Fe15	2.775(3)	Fe8-S9-P2	102.5(2)
Fe3-Fe6	2.774(2)	Fe11-Fe14	2.742(3)		
Fe1-S2	2.274(4)	Fe9-S11	2.283(5)		
Fe1-S3	2.296(4)	Fe9-S12	2.310(4)		
Fe1-S4	2.300(4)	Fe9-S13	2.301(5)	Fe9-N5	1.882(17)
Fe2-S1	2.404(3)	Fe10-S10	2.401(4)	Fe10-N6	2.099(11)
Fe2-S2	2.284(4)	Fe10-S11	2.297(5)	Fe11-N8	2.111(13)
Fe2-S3	2.283(4)	Fe10-S12	2.294(4)	Fe13-N7	1.939(18)
Fe3-S1	2.410(4)	Fe11-S10	2.400(4)	Fe14-N8	2.015(13)
Fe3-S2	2.278(4)	Fe11-S11	2.280(5)	Fe15-N6	2.033(11)
Fe3-S4	2.290(4)	Fe11-S13	2.288(6)	Fe12-S17	2.339(7)
Fe4-S1	2.360(4)	Fe12-S10	2.365(5)	Fe16-S18	2.331(7)
Fe4-S3	2.276(4)	Fe12-S12	2.276(4)	Fe10-S10-Fe15	70.79(14)
Fe4-S4	2.269(4)	Fe12-S13	2.265(4)	Fe11-S10-Fe14	69.71(13)
Fe5-S5	2.287(4)	Fe13-S14	2.280(5)	Fe12-S10-Fe16	146.7(2)
Fe5-S6	2.295(4)	Fe13-S15	2.294(5)	Fe12-S17-P3	102.2(2)
Fe5-S7	2.309(5)	Fe13-S16	2.280(4)	Fe16-S18-P4	103.2(2)
Fe6-S1	2.388(4)	Fe14-S10	2.398(4)		
Fe6-S5	2.276(4)	Fe14-S14	2.278(5)		
Fe6-S6	2.295(4)	Fe14-S15	2.294(6)		
Fe7-S1	2.398(3)	Fe15-S10	2.390(4)		
Fe7-S5	2.284(5)	Fe15-S14	2.277(4)		
Fe7-S7	2.295(4)	Fe15-S16	2.314(5)		
Fe8-S1	2.355(4)	Fe16-S10	2.359(5)		
Fe8-S6	2.280(4)	Fe16-S15	2.273(4)		
Fe8-S7	2.251(4)	Fe16-S16	2.272(4)		

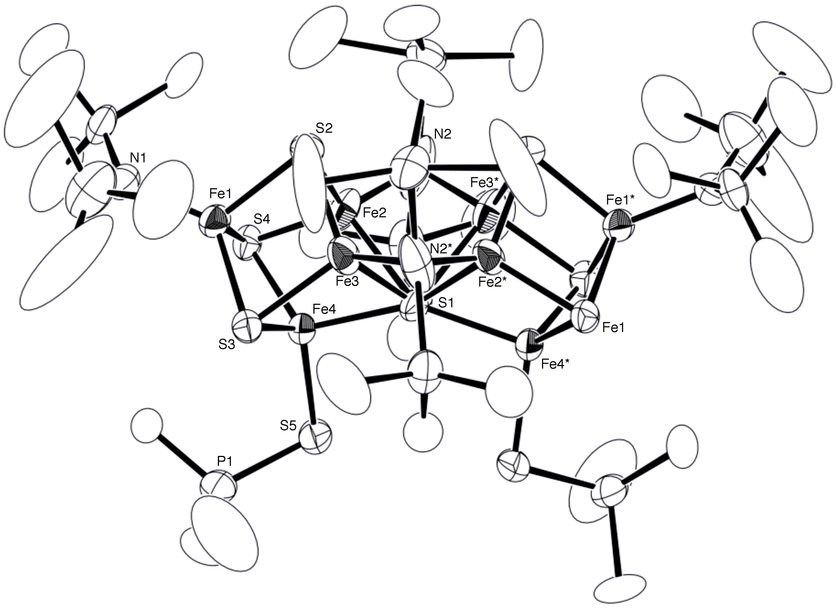

Figure A 4.3. Crystal structure of **7b**·C_7H_8 with thermal ellipsoids at the 30% probability level.

Table A 4.4. Selected bond distances (Å) and angles (°) for **7b**·C_7H_8.

Fe1-Fe2	2.815(2)	Fe3-S2	2.252(2)
Fe1-Fe3	2.8116(14)	Fe3-S4	2.295(6)
Fe1-Fe4	2.848(3)	Fe4-S1	2.289(3)
Fe2-Fe3	2.7088(17)	Fe4-S3	2.280(5)
Fe2-Fe4	2.415(3)	Fe4-S4	2.264(7)
Fe3-Fe4	2.819(3)	Fe1-N1	1.909(8)
Fe2-Fe3*	2.7473(18)	Fe2-N2	2.030(11)
Fe1-S2	2.266(3)	Fe3-N2*	2.036(7)
Fe1-S3	2.429(6)	Fe4-S5	2.334(5)
Fe1-S4	2.274(5)	Fe2-S1-Fe3*	70.02(6)
Fe2-S1	2.3937(17)	Fe4-S1-Fe4*	146.95(14)
Fe2-S2	2.263(3)	Fe4-S5-P1	100.5(4)
Fe2-S3	2.175(5)	Fe2-N2-Fe3*	85.0(3)
Fe3-S1	2.395(2)		

Chapter 6

Inter-Conversion Between [Fe_4S_4] and [Fe_2S_2] Clusters Bearing Amide Ligands

This chapter is partly reproduced with permission from: Tanifuji, K.; Tajima, S.; Ohki, Y.; Tatsumi, K. Inorg. Chem. 2016, 55, 4512-4518.

6.1. Introduction

The major role of iron-sulfur clusters is to serve as electron carriers with retention of the structures.[1] Conversely, reversible conversion of iron-sulfur cores occurs for some proteins in response to stimuli as described in 1.2.3.[2] The FNR (fumarate and nitrate reduction) protein, which controls the expression of various genes by oxygen sensing,[3] undergoes the oxygen-induced disassembly of the [Fe_4S_4] cluster into an [Fe_2S_2] cluster[4] and the recovery of the [Fe_4S_4] cluster upon treatment of the air-oxidized FNR protein with dithiothreitol (DTT) and ferrous ion under an anaerobic condition.[5] The A-type iron-sulfur cluster assembly protein ^{Nif}IscA from *Azotobacter vinelandii* mediates the coupling of two [Fe_2S_2] clusters by DTT-induced 2e-reduction and the oxidative cleavage of an [Fe_4S_4] cluster in the presence of oxygen (Figure 6.1).[6] These examples draw attention to the conversion between [Fe_4S_4] and [Fe_2S_2] clusters with their structural analogues, as a fundamental

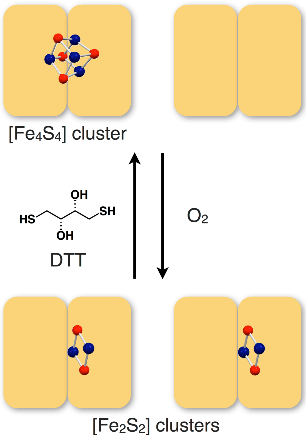

Figure 6.1. Schematic description of proposed mechanism for interconversion between [Fe_2S_2]$^{2+}$ and [Fe_4S_4]$^{2+}$ clusters on ^{Nif}ISCA. Blue = Fe, Red = S.

knowledge for assembly/disassembly and biosynthesis of iron-sulfur clusters.

Although dimerization of [Fe_2S_2] clusters into an [Fe_4S_4] cluster has been demonstrated with model compounds [$Fe_2S_2X_4$]$^{2-}$ (X = Cl, SPh),[7] formation of [Fe_2S_2] clusters from an [Fe_4S_4] cluster has not been published. Transformations of [Fe_4S_4] cores reported thus far include the removal of an iron atom to give the [Fe_3S_4] core[8] and the core rearrangement reactions to give the larger clusters such as the [Fe_6S_6] "prismane" and "basket" clusters.[9] On the other hand, in Chapter 5, we found that the removal of a sulfur atom from the [Fe_4S_4] core occurs for the all-ferric cluster $Fe_4S_4\{N(SiMe_3)_2\}_4$ (**1**)[10, 11] in the presence of phosphines, leading to the formation of [Fe_8S_7] clusters representing the core of nitrogenase P-cluster.[12] This result gave us the idea that highly oxidized [Fe_4S_4] core is not stable like [Fe_4S_4]$^{2+}$ core and can be easily converted into other Fe-S species. In this chapter, we report that cluster **1** splits into two [Fe_2S_2] clusters in the presence of pyridines. The splitting of [Fe_4S_4] core turned out to be reversible, and the removal of pyridines in the presence of $B(C_6F_5)_3$ resulted in the recovery of **1**. Assembly of two [Fe_2S_2] clusters into the reduced [Fe_4S_4] clusters [**1**]$^-$ or [**1**]$^{2-}$ was also found to occur by chemical reductions.

6.2. Results and Discussion

6.2.1. Splitting of an All-Ferric [Fe_4S_4] Cluster into Two [Fe_2S_2] Clusters.

Treatment of a toluene solution of cluster **1** with 8 equiv pyridine led to the immediate formation of a black crystalline powder, which was dissolved and crystallized from THF. This product was identified as an [Fe_2S_2] cluster $Fe_2S_2\{N(SiMe_3)_2\}_2(Py)_2$ (**8a**, Py = pyridine) based on the spectroscopic data and crystallographic analysis (Scheme 6.1). Analogous reactions of **1** with various pyridines also gave rise to $Fe_2S_2\{N(SiMe_3)_2\}_2(L)_2$ (**8b**, L = 4-methoxypyridine; **8c**, L = 4-methylpyridine; **8d**, L = 4-trifluoromethylpyridine; **8e**, L = 3-methylpyridine; **8f**, L = 3-bromopyridine). The isolated yields of [Fe_2S_2] clusters are 88% (**8a**), 75% (**8b**), 73% (**8c**), 64% (**8d**), 75% (**8e**), and 81% (**8f**).

Molecular structures of [Fe_2S_2] clusters **8a-f** were determined by means of X-ray crystallography. A perspective view of **8a** is shown in Figure 6.2. The iron and sulfur atoms in the [Fe_2S_2] core of **8a-f** share the same plane, and the amide and pyridine ligands on tetrahedral iron atoms are mutually *trans* with respect to the

Scheme 6.1

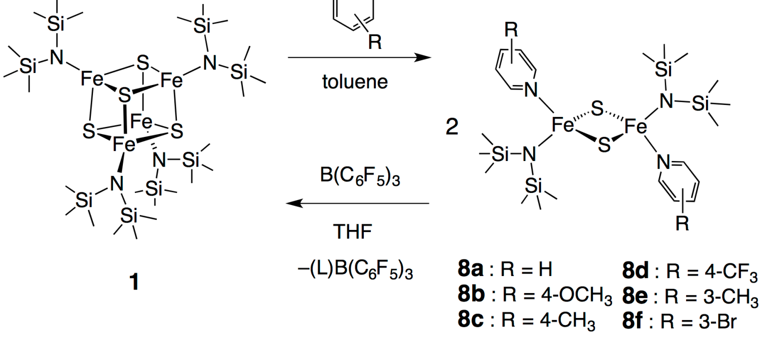

[Fe_2S_2] rhomb. While the Fe-N(L) distances of **8a**, **8b**, **8c**, and **8e** (2.093(2)-2.119(2) Å) are close to those for tetrahedral ferric complexes (2.008(2)-2.108(2) Å), [13] electron-withdrawing groups on pyridine ring lead to the longer Fe-N(L) distances, *i.e.* 2.142(3) Å for **8d** (L = 4-CF_3-pyridine) and 2.152(3) Å for **8f** (L = 3-Br-pyridine). The Fe-S distances of the [Fe_2S_2] cores of **8a-f** are almost constant (2.1987(14)-2.2083(10) Å) and are comparable to those of reported [Fe_2S_2] clusters, $[Fe_2S_2(SPh)_4]^{2-}$, [14] $[Fe_2S_2Cl_4]^{2-}$, [15] and $[Fe_2S_2(NN)_2]^{2-,\ 3-,\ 4-}$ (NN = phenylbis(benzoimidazol-2-yl)methane),[16] listed in Table 6.1. On the other hand, the Fe-Fe distances of **8a-f** (2.7294(11)-2.7602(7) Å) are longer than those of $[Fe_2S_2]^{2+}$ clusters (2.6724(4)-2.7137(5) Å) and are close to those of$[Fe_2S_2]^{+,\ 0}$ clusters $[Fe_4S_4(NN)_2]^{3-,\ 4-}$ (2.7269(12) and 2.7484(6) Å).[16b] The longer Fe-Fe distances in **8a-f** would be due to the strong donating ability of $N(SiMe_3)_2$ ligand which leads the iron centers more electron rich than those bound to thiolates or chloride.

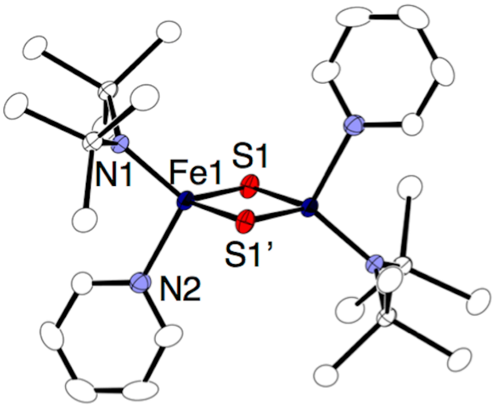

Figure 6.2. Molecular structure of **8a** with thermal ellipsoids at the 50% probability level. All hydrogen atoms are omitted for clarity.

Table 6.1. Selected bond distances (Å) and angles (°) of $Fe_2S_2\{N(SiMe_3)_2\}_2(L)_2$ (**8a**, L = Py; **8b**, L = 4-MeO-Py; **8c**, L = 4-Me-Py; **8d**, L = 4-CF_3-Py; **8e**, L = 3-Me-Py; **8f**, L = 3-Br-Py), $[Fe_4S_4(SPh)_4]^{2-}$, $[Fe_4S_4Cl_4]^{2-}$, $[Fe_2S_2(NN)_2]^{2-}$, $[Fe_2S_2(NN)_2]^{3-}$, and $[Fe_2S_2(NN)_2]^{4-}$ (NN = phenylbis(benzoimidazol-2-yl)methane).

	8a	**8b**	**8c**
Ligand	Py	4-MeO-Py	4-Me-Py
Fe-Fe	2.7444(6)	2.7468(8)	2.7294(11)
Ave Fe-S	2.2056(10)	2.2079(8)	2.1987(14)
Fe-N(amide)	1.9313(15)	1.913(2)	1.921(2)
Fe-N(Py)	2.1126(17)	2.110(2)	2.093(2)
S-Fe-S	103.05(3)	103.07(3)	103.27(4)
	8d	**8e**	**8f**
Ligand	4-CF_3-Py	3-Me-Py	3-Br-Py
Fe-Fe	2.7484(7)[a]	2.7602(7)	2.7460(14)
Ave Fe-S	2.2039(10)	2.2083(10)	2.2056(17)
Fe-N(amide)	1.917(3)[a]	1.9299(19)	1.917(3)
Fe-N(Py)	2.142(3)[a]	2.119(2)	2.152(3)
S-Fe-S	102.85(3)[a]	102.64(3)	103.00(5)
	$[Fe_4S_4(SPh)_4]^{2-}$[b]	$[Fe_2S_2Cl_4]^{2-}$[c]	$[Fe_2S_2(NN)_2]^{2-}$[d]
Fe-Fe	2.6724(4)	2.7137(5)	2.7019(5)
Ave Fe-S	2.1969(6)	2.1993(6)	2.2010(5)
S-Fe-S	105.08(2)	103.81	104.273(16)
	$[Fe_2S_2(NN)_2]^{3-}$[e]	$[Fe_2S_2(NN)_2]^{4-}$[e]	
Fe-Fe	2.7269(12)	2.7484(6)	
Ave Fe-S	2.2355(12)	2.2625(9)	
S-Fe-S	104.83(5)	105.20(4)	

[a] Averaged Values. [b] Reference 14. [c] Reference 15. [d] Reference 16a. [e] Reference 16b.

6.2.2. Equilibrium between [Fe_2S_2] and [Fe_4S_4] Clusters

Assembly of two [Fe_2S_2] clusters **8a** into an [Fe_4S_4] cluster **1** was found to occur upon removal of pyridine, and black crystals of [Fe_4S_4] cluster **1** were isolated in 53% yield from the reaction of **8a** with 2 equiv $B(C_6F_5)_3$ in THF (Scheme 6.1). The amide ligands in clusters **1** and **8a** remain intact in the presence of $B(C_6F_5)_3$, owing to the steric hindrance caused by bulky substituents on boron and amide nitrogen atoms. Whereas the crystal yield of **1** is moderate because of the high solubility, the quantitative formation of **1** in solution was verified by the ^1H NMR spectrum of the reaction mixture in C_6D_6 (Figure A5.15, supporting information). The ^1H NMR spectrum also confirmed the formation of a Lewis complex $C_5H_5N\text{-}B(C_6F_5)_3$,[17] the proton signals of which appeared at δ 7.96, 6.61, and 6.27. $C_5H_5N\text{-}B(C_6F_5)_3$ was further identified by an X-ray diffraction study (Figure A5.28).

The equilibrium between **1**+Py and **8a** illustrated in Scheme 6.1 was supported by the ^1H NMR spectrum of crystalline **8a** in C_6D_5Cl, where a small signal of **1** was observed at d 2.36 in addition to the signals of **8a** at δ 16.20, 12.29, 6.02, and 1.22 (Figure 6.3a top). Similarly, the signal of **1** appeared in the ^1H NMR spectra of **8b**-**f** in C_6D_5Cl, while the ratios between [Fe_2S_2] and [Fe_4S_4] clusters vary by the substituent on the pyridine ring. As shown in Figure 6.3b and A5.1-A5.12, variable-temperature (VT) NMR studies of **8a**-**f** were performed to evaluate the thermodynamic parameters of the equilibrium reactions. The chemical equation and equilibrium constant (*K*) are defined as eq. 6.1 and 6.2, where L denotes pyridines.

$$2\mathrm{Fe_2S_2\{N(SiMe_3)_2\}_2(L)_2} \rightleftharpoons \mathrm{Fe_4S_4\{N(SiMe_3)_2\}_4} + 4\mathrm{L} \qquad \textbf{(6.1)}$$

$$K = \frac{[\mathrm{Fe_4S_4\{N(SiMe_3)_2\}_4}][\mathrm{L}]^4}{[\mathrm{Fe_2S_2\{N(SiMe_3)_2\}_2(L)_2}]^2} \qquad \textbf{(6.2)}$$

The enthalpy change (ΔH°) and entropy change (ΔS°) calculated from $-R\ln K$ vs $1/T$ plot and $-RT\ln K$ vs T plot, respectively, are summarized in Table 6.2.

The positive ΔS° values are in accordance with eq. 6.1 where the more compounds are formed for the right as a result of ligand dissociation. The positive ΔH° values indicate that the $[\mathrm{Fe_2S_2}]$ clusters are thermodynamically more stable than the $[\mathrm{Fe_4S_4}]$

Figure 6.3. (a) ^{1}H NMR spectra of $[\mathrm{Fe_2S_2}]$ clusters **8a-f** in $\mathrm{C_6D_5Cl}$, and (b) variable-temperature ^{1}H NMR spectra of **8a** in the range from 296 to 373 K. Signals of $[\mathrm{Fe_4S_4}]$ cluster **1** and **8a-f** are highlighted in red and blue, respectively. Legend: ● = methyl groups of pyridine ligands.

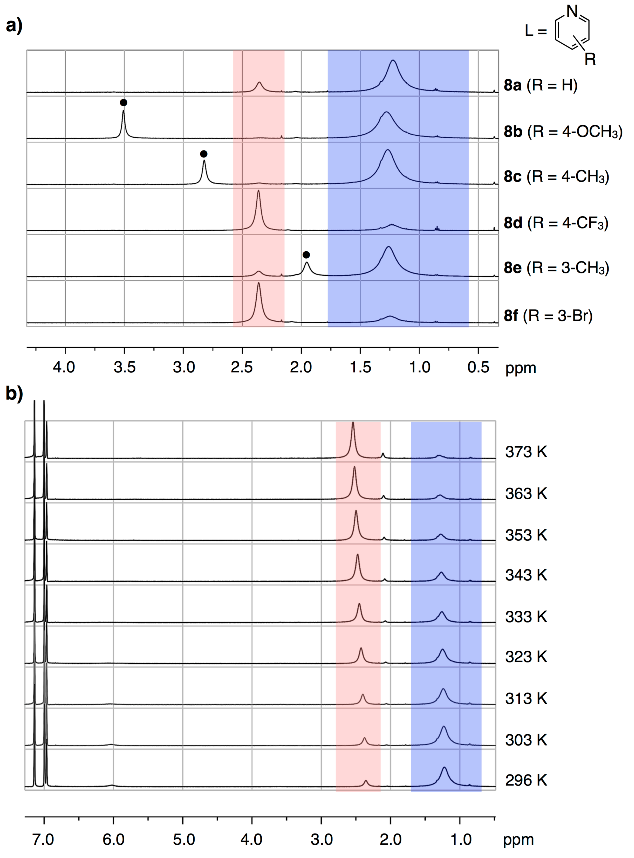

Table 6.2. Thermodynamic parameters for the equilibrium between [Fe_2S_2] clusters **8a**-**f** and [Fe_4S_4] cluster **1** plus pyridines.

[Fe_2S_2] cluster	ΔH^{o}/ kcal mol^{-1}	ΔS^{o}/ cal mol^{-1} K^{-1}
8a	40.1(9)	92(3)
8b	63(2)	145(5)
8c	47(1)	101(4)
8d	27(1)	70(3)
8e	37(1)	79(4)
8f	26(2)	68(5)

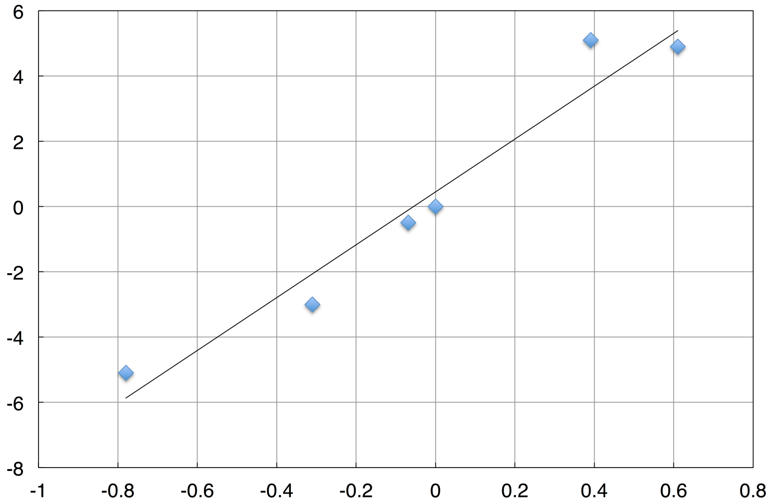

Figure 6.4. Hammett plot of log(K_X/K_H) vs Hammett sigma plus (σ^+) constants for the equilibriums between **8a**-**f** and **1**+L. The value of **8a** was used as reference (K_H).

cluster **1**. Comparison of thermodynamic data of **8a**-**f** reveals the dependence of the stability of [Fe_2S_2] clusters on the donation properties of pyridine ligands, and electron-donating groups on the pyridine ring (*i.e.* 4-OMe group (**8b**) and 4-Me group (**8c**)) enhance the stability of [Fe_2S_2] clusters. The plot between log(K_X/K_H) (K_X

= equilibrium constants for **8a-f** at 298K; K_H = equilibrium constant for **8a** at 298 K) and Hammett sigma plus constants (σ^+) displayed a linear correlation (Figure 6.4), but conversely, the plot vs Hammet sigma constants (σ) showed non-linear correlation (Figure A5.13). This result and the relatively high reaction constant (ϱ = 8.1±0.9) indicate strong electron donation from pyridines to irons of [Fe_2S_2] clusters. As shown in Figure A5.14, compensatory enthalpy-entropy relationship was observed for the equilibrium between **8a-f** and **1**+L, as was found for, for example, the equilibrium reactions of cyclodextrins in molecular recognition systems.[18]

6.2.3. Redox-Induced Assembly/Disassembly between [Fe_2S_2] and [Fe_4S_4] Clusters

The equilibrium reaction between **1**+Py and **8a** occurs with retention of the oxidation state, owing to the stability of the all-ferric [Fe_4S_4]$^{4+}$ and [Fe_2S_2]$^{2+}$ states. On the other hand, the conversions of iron-sulfur cores in proteins are accompanied by redox reactions, and the assembly of [Fe_2S_2] clusters takes place under reducing conditions while the disassembly of [Fe_4S_4] cluster is induced by oxidation with O_2. Instability of the reduced [Fe_2S_2]$^+$ form [**8a**]$^-$ was indicated by the cyclic voltammogram of **8a** in THF, where an irreversible reduction wave appeared at –1.19 V vs Ag^+/Ag (Figure A5.19). Thus chemical reduction of cluster **8a** was examined to find core conversions. Treatment of **8a** with 0.5 and 1.1 equiv sodium naphthalenide (Na[$C_{10}H_8$]) in THF resulted in the dissociation of pyridine and coupling of two [Fe_2S_2] units, producing clusters [**1**]$^-$ and [**1**]$^{2-}$ as crystals in the forms of [Na(THF)$_{0.7}$(Py)$_{1.3}$][**1**] and [Na(THF)(Py)]$_2$[**1**], respectively (Scheme 6.2). Their crystal structures were determined by X-ray crystallography (Figures A5.26 and A5.27),

Scheme 6.2

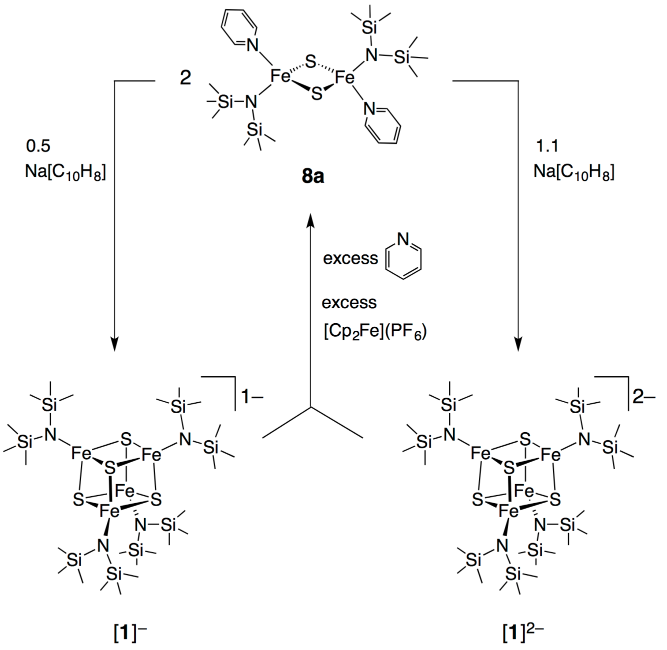

while clusters [**1**]$^-$ and [**1**]$^{2-}$ with different counter-cations [Na(THF)$_2$][**1**] and [Na(THF)$_2$]$_2$[**1**] have been reported.[10b,11] The crystal yields of [**1**]$^-$ (17%) and [**1**]$^{2-}$ (13%) remain low, indicating the less selective formation of the [Fe$_4$S$_4$] core and/or degradation of iron-sulfur cores in these reactions. A relevant chemical reduction of [Fe$_2$S$_2$(SArCOO)$_2$]$^{2-}$ ((SArCOO)$^{2-}$ = thiosalicylate, dianionic bidentate ligand) has been reported to give a linear tetra-ferric cluster [Fe$_4$S$_6$(SArCOO)$_2$]$^{4-}$ via disproportionation of the iron-sulfur core and the loss of (SArCOO)$^{2-}$ ligands.[19] Likewise, the reactions between **8a** and Na[C$_{10}$H$_8$] would cause the [Fe$_2$S$_2$] core degradation and the loss of amide ligands. This assumption is supported by the formation of an uncharacterizable black solid, whose solubility is distinct from the pentane-soluble clusters [**1**]$^-$ and [**1**]$^{2-}$.

Oxidation reactions of clusters [**1**]$^-$ and [**1**]$^{2-}$ with excess [Cp$_2$Fe](PF$_6$) (Cp =

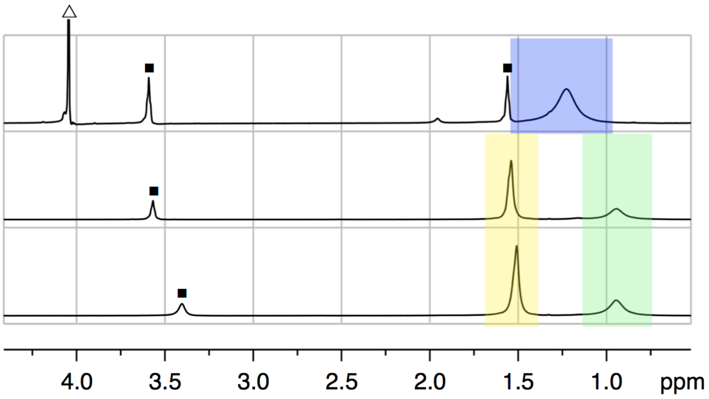

Figure 6.5. ^{1}H NMR spectra of the mixture of [**1**]$^{2-}$ and [**1**]$^-$ (bottom), with excess pyridine (middle), and with excess pyridine and [Cp_2Fe](PF_6) (top) in C_6D_5Cl. Signals of clusters are highlighted in blue (**8a**), green ([**1**]$^{2-}$), and yellow ([**1**]$^-$). Legend: △ = Cp_2Fe, ▪ = THF.

η^5-C_5H_5) in the presence of excess pyridine resulted in the formation of **8a** in 83% yield for both, based on the NMR spectra (Scheme 6.2, Figure 6.5, A5.17 and A5.18). These reactions were triggered by the oxidation with [Cp_2Fe](PF_6), as the ^{1}H NMR signals of [**1**]$^{2-}$ and [**1**]$^-$ remained intact in the presence of >100 fold excess pyridine. The oxidation of [**1**]$^{2-}$ likely goes through [**1**]$^-$ and to cluster **1**, in which iron atoms further take up pyridine to split into the [Fe_2S_2] cluster **8a**. These results indicate the importance of the generation of all-ferric [Fe_4S_4]$^{4+}$ state prior to the splitting into two [Fe_2S_2] units. An extension of this assumption is that the all-ferric [Fe_4S_4]$^{4+}$ cluster may serve as a key intermediate in the O_2-induced [Fe_4S_4] to [Fe_2S_2] core conversion found for the FNR protein and $^{\mathrm{Nif}}$IscA protein.

6.3. Conclusions

In summary, we have demonstrated the first inter-conversion between [Fe_4S_4] and [Fe_2S_2] clusters. Splitting of the [Fe_4S_4] core of **1** in the presence of pyridines appeared to be reversible, and the thermodynamic parameters were determined based on the equilibrium constants. The coupling of two [Fe_2S_2] clusters was also induced by chemical reductions, and oxidation of the reduced [Fe_4S_4] clusters in the presence of pyridine led to the formation of the pyridine-bound [Fe_2S_2] cluster. In this study, the all-ferric $[Fe_4S_4]^{4+}$ cluster **1** appeared to be the key for the core conversion from [Fe_4S_4] to [Fe_2S_2]. Whereas the $[Fe_4S_4]^{4+}$ state is uncommon for proteins, this unstable state may be generated during the biological disassembly of [Fe_4S_4] clusters.

6.4. Experimental Section

General Procedures. All reactions were manipulated under a nitrogen atmosphere using Schlenk techniques and a glove box. Hexane, pentane, toluene, THF, and hexamethyldisiloxane (HMDSO) were purified by the method of Grubbs,[20] where the solvents were passed over columns of activated alumina and a supported copper catalyst supplied by Hansen & Co. Ltd. Elemental analyses were performed on an Elementar Analytical vario MICRO cube elemental analyzer where the crystalline samples were sealed in tin capsules under nitrogen. $Fe_4S_4\{N(SiMe_3)_2\}_4$ (**1**)[10a, 11] and tris(pentafluorophenyl)borane[21] were prepared according to literature procedures. Pyridine (Py), 4-methoxypyridine (4-MeO-Py), 4-methylpyridine (4-Me-Py), 3-methylpyridine (3-Me-Py), 3-bromopyridine (3-Br-Py), C_6D_5Cl, and C_6D_6 were dried over CaH_2 (for Py, 4-MeO-Py, 4-Me-Py, 3-Me-Py, and 3-Br-Py), P_2O_5 (for C_6D_5Cl), or Na (for C_6D_6) and distilled in vacuo before use. Tetrabutylammonium hexafluorophosphate ($[N^nBu_4][PF_6]$) was recrystallized from THF before use as a supporting electrolyte. All other chemicals were used as purchased.

Synthesis of $Fe_2S_2\{N(SiMe_3)_2\}_2(Py)_2$ (8a). Pyridine (648 μL, 8.04 mmol) was added to a toluene (16 mL) solution of $Fe_4S_4\{N(SiMe_3)_2\}_4$ (**1**, 1.00 g, 1.01 mmol) at room temperature. A dark red crystalline powder was formed soon after the addition. After stirring for three hours, hexane (30 mL) was added to the reaction mixture and the mixture was filtered to collect the dark red powder. The powder was subsequently washed with hexane (10 mL) to give $Fe_2S_2\{N(SiMe_3)_2\}_2(Py)_2$ (**8a**, 1.16 g, 1.77 mmol, 88% yield). Single crystals suitable for X-ray crystallography were grown from THF. ^{1}H NMR (C_6D_5Cl): δ 16.20 (br, Py), 12.29 (br, Py), 6.02 (br, Py), 2.36 (br, $Fe_4S_4[N\{Si(CH_3)_2\}_4]_4$), 1.22 (br, $Si(CH_3)_3$ of **8a**). Anal. Calcd for $C_{22}Fe_2H_{46}N_4S_2Si_4$: C, 40.35; H, 7.08; N, 8.56; S, 9.79. Found: C, 40.46; H, 6.61;N, 8.40; S, 9.60.

Synthesis of $Fe_2S_2\{N(SiMe_3)_2\}_2(4\text{-MeO-Py})_2$ (8b). 4-methoxypyridine (245 μL, 2.41 mmol) was added to a toluene (40 mL) solution of **1** (300 mg, 0.302 mmol) at room temperature. After stirring for three hours, a small amount of black solid was removed by filtration. Concentration of the solution to *ca* 10 mL under reduced pressure resulted in the formation of a suspension with a crystalline powder. This suspension was warmed to give a homogeneous solution, and the solution was stored at –30°C to afford black crystals of $Fe_2S_2\{N(SiMe_3)_2\}_2(4\text{-MeO-Py})_2$ (**8b**, 325 mg, 0.455 mmol, 75% yield). ^{1}H NMR (C_6D_5Cl): δ 16.12 (br, 4-MeO-Py), 11.34 (br, 4-MeO-Py), 3.51 (br, 4-MeO-Py), 2.36 (br, $Fe_4S_4[N\{Si(CH_3)_2\}_4]_4$), 1.28 (br, $Si(CH_3)_3$ of **8b**). Anal. Calcd for $C_{24}Fe_2H_{50}N_4O_2S_2Si_4$: C, 48.32; H, 8.83; S, 9.21. Found: C, 48.29; H, 8.52; S, 8.83.

Synthesis of $Fe_2S_2\{N(SiMe_3)_2\}_2(4\text{-CF}_3\text{-Py})_2$ (8d). 4-trifluoromethylpyridine (187 μL, 1.61mmol) was added to a toluene (10 mL) solution of **1** (203 mg, 0.204 mmol) at room temperature. After stirring for two hours, the solution was filtered to remove a small amount of black solid. The solution was stored at –30°C to afford black crystals of $Fe_2S_2\{N(SiMe_3)_2\}_2(4\text{-CF}_3\text{-Py})_2$ (**8d**, 203 mg, 0.257 mmol, 64% yield). ^{1}H NMR (C_6D_5Cl): δ 12.01 (br, 4-CF_3-Py), 8.55 (br, 4-CF_3-Py), 2.36 (br, $Fe_4S_4[N\{Si(CH_3)_2\}_4]_4$), 1.23 (br, $Si(CH_3)_3$ of **8d**). Anal. Calcd for $C_{24}F_6Fe_2H_{44}N_4S_2Si_4$: C, 36.45; H, 5.61; N, 7.09;

S, 8.11. Found: C, 36.04; H, 5.19; N, 6.96; S, 8.60.

Synthesis of $Fe_2S_2\{N(SiMe_3)_2\}_2(3\text{-}Br\text{-}Py)_2$ (8f). 3-bromopyridine (239 μL, 2.42 mmol) was added to a toluene (15 mL) solution of **1** (300 mg, 0.302 mmol) at room temperature. After stirring for three hours, a dark red crystalline powder was formed. The suspension was warmed to give a homogeneous solution, and the solution was stored at –30°C to afford black crystals of $Fe_2S_2\{N(SiMe_3)_2\}_2(3\text{-}Br\text{-}Py)_2$ (**8f**, 399 mg, 0.491 mmol, 81% yield). ^1H NMR (C_6D_5Cl): δ 8.55 (br, 3-Br-Py), 6.05 (br, 3-Br-Py), 2.36 (br, $Fe_4S_4[N\{Si(CH_3)_2\}_4]_4$), 1.25 (br, $Si(CH_3)_3$ of **8f**). Anal. Calcd for $Br_2C_{22}Fe_2H_{44}N_4S_2Si_4$: C, 32.52; H, 5.46; N, 6.90; S, 7.89. Found: C, 32.63; H, 5.26; N, 6.76; S, 8.13.

Synthesis of $Fe_4S_4\{N(SiMe_3)_2\}_4$ (1) from 8a. Tris(pentafluorophenyl)borane ($B(C_6F_5)_3$, 469 mg, 0.916 mmol) dissolved in THF (12 mL) was added to a THF (15 mL) solution of **8a** (301 mg, 0.460 mmol) at room temperature, and then the solution was kept stirring at 55°C for 2 hours. After evaporation of the solvent, the black residue was extracted with pentane (6 mL). The extract was concentrated to 3 mL, and was stored at –30°C to give colorless crystals of $C_5H_5N\text{-}B(C_6F_5)_3$. The mother liquor was separated from the colorless crystals by filtration and was evaporated. Black crystals of $Fe_4S_4\{N(SiMe_3)_2\}_4$ (**1**, 122 mg, 0.122 mmol, 53%) were obtained by recrystallization from hexamethyldisiloxane (3 mL) at –30°C. ^1H NMR (C_6D_6): δ 2.41 (br, s, 72H, $Si(CH_3)_3$).[11]

Synthesis of $[Fe_4S_4\{N(SiMe_3)_2\}_4]^-$ ($[1]^-$) from 8a. In a similar manner to the synthesis of $[\mathbf{1}]^{2-}$, the reaction of **8a** (400 mg, 0.611 mmol) with a THF solution of $Na[C_{10}H_8]$

(2.50 mL, 0.122 M, 0.305 mmol) afforded black crystals of $[Na(THF)_{0.7}(py)_{1.3}][Fe_4S_4\{N(SiMe_3)_2\}_4]$ ($[Na(THF)_{0.7}(py)_{1.3}]$[**1**], 70 mg, 0.0522 mmol, 17%). ^{1}H NMR (C_6D_6): δ 8.08 (br, Py); 6.81 (br, Py); 6.67 (br, Py); 3.28 (br, THF); 1.32 (br, 72H, $Si(CH_3)_3$), 1.42 (br, THF). Anal. Calcd for $C_{33.3}Fe_4H_{84.1}N_{5.3}NaO_{0.7}S_4Si_8$: C, 34.20; H, 7.25; N, 6.35; S, 10.97. Found: C, 34.26; H, 6.89; N, 6.08; S, 11.06.

^{1}H NMR Experiments. The ^{1}H NMR spectra were recorded on a JEOL ECA-500 or ECA-600, and the data were analyzed by MestReNova software (version 8.1.2). The ^{1}H NMR signals were referenced to the residual peaks of the solvents (C_6D_5H (δ 7.16) or C_6D_4HCl (δ 7.14)). 1,4-bis(trimethylsilyl)- benzene (BTMSB) was used as an internal standard for NMR experiments, and it was purified by following the literature procedure.[22]

Variable-temperature ^{1}H NMR studies for 8a-f. C_6D_5Cl solutions of BTMSB (11.5 mg/ 5 mL, 10.3 mM (for **8a**, **8b**, **8c**, **8d**) or 10.0 mg/ 5 mL, 8.99 mM (for **8e**, **8f**)) were used to dissolve **8a**-**f**. In all cases, the initial concentrations of **8a**-**f** were around 10 mM. The solutions were filtered to remove a small amount of insoluble material. The concentrations of **8a**-**f** and **1** were determined by comparison of the signal integrations with the internal standard.

The equilibrium constant (K) is actually calculated by eq. 6.3, where L denotes pyridines.

$$K = \frac{[Fe_4S_4\{N(SiMe_3)_2\}_4][L]^4}{[Fe_2S_2\{N(SiMe_3)_2\}_2(L)_2]^2} = \frac{256[Fe_4S_4\{N(SiMe_3)_2\}_4]^5}{[Fe_2S_2\{N(SiMe_3)_2\}_2(L)_2]^2} \quad \textbf{(6.3)}$$

The NMR measurements were carried out in the temperature range from room temperature to 373K. Seven or more data points have been used for $R\ln K$ vs $1/T$

and *RT*ln*K* vs *T* plots of **8a-f**, and ΔH° and ΔS° values were obtained from the slopes of regression lines in the plots.

^{1}H NMR monitoring of the conversion of 8a to 1 in the presence of $B(C_6F_5)_3$. A C_6D_6 (0.8 mL) solution of BTMSB (11.1 mg/5 mL, 9.98 mM) was added to **8a** (10 mg, 15 μmol) to form a saturated C_6D_6 solution of **8a**. After removal of a small amount of solid by filtration, the ^{1}H NMR was measured. An excess of $B(C_6F_5)_3$ (20 mg, 39 μmol) was added to the solution, and the mixture was sonicated for 30 minutes before the ^{1}H NMR measurement. The signal integrations in the ^{1}H NMR revealed the quantitative conversion of **8a** to **1** (Figure A5.15).

Transformation of $[\mathbf{1}]^{2-}$ and $[\mathbf{1}]^{-}$ to 8a in the presence of pyridine and $[Cp_2Fe](PF_6)$. $[Na(THF)(Py)]_2[\mathbf{1}]$ (3.2 mg, 2.4 μmol), $[Na(THF)_{0.7}(Py)_{1.3}][\mathbf{1}]$ (4.1 mg,3.5 μmol), pyridine (10 μL, 124 *μ*mol), and BTMSB (2.5 mg, 11 μmol, internal standard) were dissolved into C_6D_5Cl (0.8 mL). Ferrocenium hexafluorophosphate ($[Cp_2Fe](PF_6)$, 8.5 mg, 26 μmol) was added to the solution. After 5 minutes, the reaction mixture was filtrated to remove an insoluble powder. The ^{1}H NMR spectrum was measured, and the The NMR yield of **8a** was 72% based on the integrations of BTMSB and the $Si(CH_3)_3$ signals of $[\mathbf{1}]^{2-}$, $[\mathbf{1}]^{-}$ and **8a** (see Figures 6.5 and A5.16).

Transformation of $[\mathbf{1}]^{2-}$ to 8a in the presence of pyridine and $[Cp_2Fe](PF_6)$. $[Na(THF)(Py)]_2[\mathbf{1}]$ (4.1 mg, 3.1 μmol) was dissolved into a C_6D_5Cl solution of BTMSB (10.0 mg/5 mL, 8.99 mM), and then pyridine (10 μL, 124 μmol) was added. $[Cp_2Fe](PF_6)$ (4.4 mg, 13 μmol) was added to the solution. After 5 minutes, the mixture was filtered to remove an insoluble powder. The NMR yield of **8a** was 83%

based on the integrations of BTMSB and the $Si(CH_3)_3$ signals of $[\mathbf{1}]^{2-}$ and **8a** (Figure A5.17).

Transformation of $[\mathbf{1}]^{-}$ to 8a in the presence of pyridine and $[Cp_2Fe](PF_6)$. $[Na(THF)_{0.7}(Py)_{1.3}][\mathbf{1}]$ (4.1 mg, 3.5 μmol) was dissolved into a C_6D_5Cl solution of BTMSB (10.0 mg/5 mL, 8.99 mM), and then pyridine (10 μL, 124 μmol) was added. $[Cp_2Fe](PF_6)$ (2.4 mg, 7.3 μmol) was added to the solution. After 5 minutes, the mixture was filtered to remove an insoluble powder. The NMR yield of **8a** was 83% based on the integrations of BTMSB and the $Si(CH_3)_3$ signals of $[\mathbf{1}]^{-}$ and **8a** (Figure A5.18).

Cyclic Voltammetry Measurements. Cyclic voltammograms (CV) of **8a** and $[\mathbf{1}]^{-}$ were recorded in THF at room temperature using glassy carbon as the working electrode and Pt as the counter electrode with 0.3 M $[^{n}Bu_4N][PF_6]$ as the supporting electrolyte (Figures A5.19 and A5.20). The potentials were referenced to Ag/Ag^{+}. The sweep speed was 0.1 V/sec. $[Na(THF)_2][\mathbf{1}]$ was prepared according to the literature procedure.[10b, 11]

X-ray Crystal Structure Determination. Crystal data and refinement parameters for **8a-f**, $[Na(THF)(py)]_2[\mathbf{1}]$, $[Na(THF)_{0.7}(py)_{1.3}][\mathbf{1}]$, and $(Py)B(C_6F_5)_3$ are summarized in Table A5.1. Single crystals were coated with oil (Immersion Oil, type B: Code 1248, Cargille Laboratories, Inc.) and mounted on loops. Diffraction data were collected at –100 °C under a cold nitrogen stream on a Rigaku RA-Micro7 equipped with a Saturn70 CCD detector, using graphite-monochromated MoKα radiation (λ = 0.710690 Å). Eighteen preliminary data frames were measured at 0.5° increments of ω, to assess the crystal quality and preliminary unit cell parameters. The intensity images were also measured at 0.5° intervals of ω. The frame data were integrated using the CrystalClear program package, and the data sets were corrected for absorption using a REQAB program. The calculations were performed with the *CrystalStructure* program package. All structures were solved by direct methods, and refined by full-matrix least squares. Anisotropic refinement was applied to all non-hydrogen atoms except for disordered atoms (refined isotropically), and hydrogen atoms were included in the refinement as a riding model. One of the trimethylsilyl groups and a pair of THF and pyridine in $[Na(THF)(Py)]_2$[**1**] are disordered over two positions in a 1:1 ratio. The THF molecule bound to sodium in $[Na(THF)_{0.7}(Py)_{1.3}]$[**1**] is disordered with Py in a 0.7:0.3 ratio. Two half molecules are found in an asymmetric unit of **8d**.

References and Notes

[1] For example: (a) Beinert, H.; Holm, R. H.; Münck, E. *Science* **1997**, *277*, 653-659. (b) Stephens, P. J.; Jollie, D. R.; Warshel, A. *Chem. Rev.* **1996**, *96*, 2491-2514. (c) Imsande, J. *Plant Physiol. Biochem.* **1999**, *37*, 87-97. (d) Beinert, H. *J. Biol. Inorg. Chem.* **2000**, *5*, 2. (e) Bentrop, D.; Capozzi, F.; Luchinat, C. Iron-sulfur Proteins. In *Handbook on Metalloproteins*; Bertini, I., Sigel, A., Sigel, H., Eds.; Marcel Dekker, Inc.: New York, 2001; pp 357-447.

[2] Recent reviews on sensing regulator having iron-sulfur clusters: (a) Fleischhacker, A. S.; Kiley, P. J. *Curr. Opin. Chem. Biol.* **2011**, *15*, 335–341. (b) Crack, J. C.; Green, J.; Thomson, A. J.; Le Brun, N. E. *Curr. Opin. Chem. Biol.* **2012**, *16*, 35–44. (c) Unden, G.; Nilkens, S.; Singenstreu, M. *Dalton Trans.* **2013**, *42*, 3082–3087.

[3] Kiley, P. J.; Beinert, H. *FEMS Microbiol. Rev.* **1998**, *22*, 341–352.

[4] (a) Khoroshilova, N.; Popescu, C.; Münck, E.; Beinert, H.; Kiley, P. J. *Proc. Natl. Acad. Sci. U.S.A.* **1997**, *94*, 6087–6092. (b) Crack, J. C.; Green, J.; Cheesman, M. R.; Le Brun, N. E.; Thomson, A. J. *Proc. Natl. Acad. Sci. U.S.A.* **2007**, *104*, 2092–2097.

[5] Zhang, B.; Crack, J. C.; Subramanian, S.; Green, J.; Thomson, A. J.; Le Brun, N. E.; Johnson, M. K. *Proc. Natl. Acad. Sci. U.S.A.* **2012**, *109*, 15734–15739.

[6] Mapolelo, D. T.; Zhang, B.; Naik, S. G.; Huynh, B. H.; Johnson, M. K. *Biochemistry* **2012**, *51*, 8071–8084.

[7] (a) Wong, G. B.; Bobrik, M. A.; Holm, R. H. *Inorg. Chem.* **1978**, *17*, 578–584. (b) Hagen, K. S.; Reynolds, J. G.; Holm, R. H. *J. Am. Chem. Soc.* **1981**, *103*, 4054–4063.

[8] Zhou, J.; Hu, Z.; Münck, E.; Holm, R. H. *J. Am. Chem. Soc.* **1996**, *118*, 1966–1980.

[9] (a) Coucouvanis, D.; Kanatzidis, M. G.; Dunham, W. R.; Hagen, W. R. *J. Am. Chem. Soc.* **1984**, *106*, 7998–7999. (b) Kanatzidis, M. G.; Hagen, W. R.; Dunham, W. R.; Lester, R. K.; Coucouvanis, D. K. *J. Am. Chem. Soc.* **1985**, *107*, 953–961. (c) Snyder, B. S.; Holm, R. H. *Inorg. Chem.* **1988**, *27*, 2339–2347.

[10] (a) Ohki, Y.; Sunada, Y.; Tatsumi, K. *Chem. Lett.* **2005**, *34*, 172–173. (b) Ohki, Y.; Tanifuji, K.; Yamada, N.; Imada, M.; Tajima, T.; Tatsumi, K. *Proc. Natl. Acad. Sci. U.S.A.* **2011**, *108*, 12635–12640.

[11] Sharp, C. R.; duncan, J. S.; Lee, S. C. *Inorg. Chem.* **2010**, *49*, 6697–6705.

[12] Ohki, Y.; Tanifuji, K.; Yamada, N.; Cramer, R. E.; Tatsumi, K. *Chem. Asian J.* **2012**, *7*, 2222–2224.

[13] (a) Stokes, S. L.; Davis, W. M.; Odom, A. L.; Cummins, C. C. *Organometallics* **1996**, *15*, 4521–4530. (b) Weintrob, E. C.; Tofan, D.; Bercaw, J. E. *Inorg. Chem.* **2009**, *48*, 3808–3813.

[14] Tsai, F.-T.; Chiou, S.-J.; Tsai, M.-C.; Tsai, M.-L.; Huang, H.-W.; Chiang, M.-H.; Liaw, W.-F. *Inorg. Chem.* **2005**, *44*, 5872–5881.

[15] Bobrik, M. A.; Hodgson, K. O.; Holm, R. H. *Inorg. Chem.* **1977**, *16*, 1851–1858.

[16] (a) Albers, A.; Demeshko, S.; Dechert, S.; Bill, E.; Bothe, E.; Meyer, F. *Angew. Chem. Int. Ed.* **2011**, *50*, 9191–9194. (b) Albers, A.; Demeshko, S.; Pröpper, K.; Dechert, S.; Bill, E.; Meyer, F. *J. Am. Chem. Soc.* **2013**, *135*, 1704–1707.

[17] Massey, A. G.; Park, A. J. *J. Organomet. Chem.* **1966**, *5*, 218–225.

[18] (a) Leffler, J. E. *J. Org. Chem.* **1955**, *20*, 1202–1231. (b) Rekharsky, M. V.; Inoue, Y. *Chem. Rev.* **1998**, *98*, 1875–1918. (c) Grunwald, E.; Steel, C. *J. Am. Chem. Soc.* **1995**,

117, 5687–5692.

[19] Saouma, C. T.; Kaminsky, W.; Mayer, J. M. *Polyhedron* **2013**, *58*, 60–64.

[20] Pangborn, A. B.; Giardello, M. A.; Grubbs, R. H.; Rosen, R. K.; Timmers, F. *J. Organometallics* **1996**, *15*, 1518-1520.

[21] Lambert, J. B.; Zhang, S.; Ciro, S. M. *Organometallics* **1994**, *13*, 2430–2443.

[22] Pinciroli, V.; Biancardi, R.; Colombo, N.; Colombo, M.; Rizzo, V. *J. Comb. Chem.* **2001**, *3*, 434–440.

Appendix 5

Supporting Information for Chapter 6

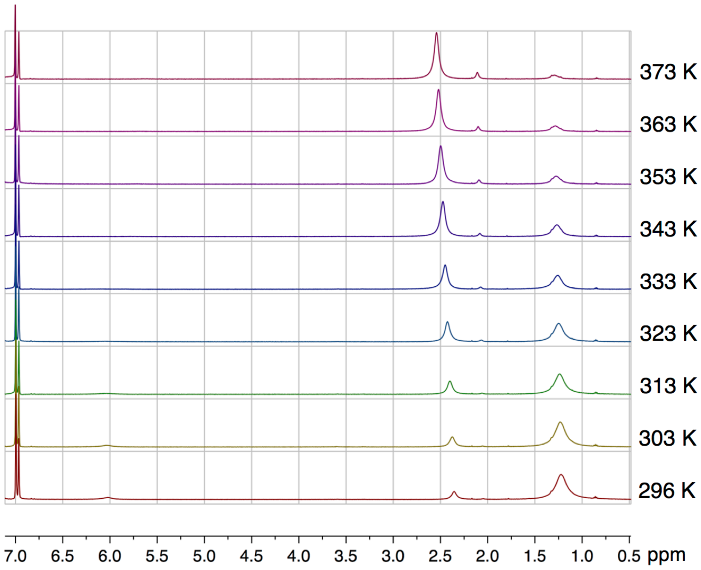

Figure A5.1. Variable-temperature ^{1}H NMR spectra of **8a** in C_6D_5Cl.

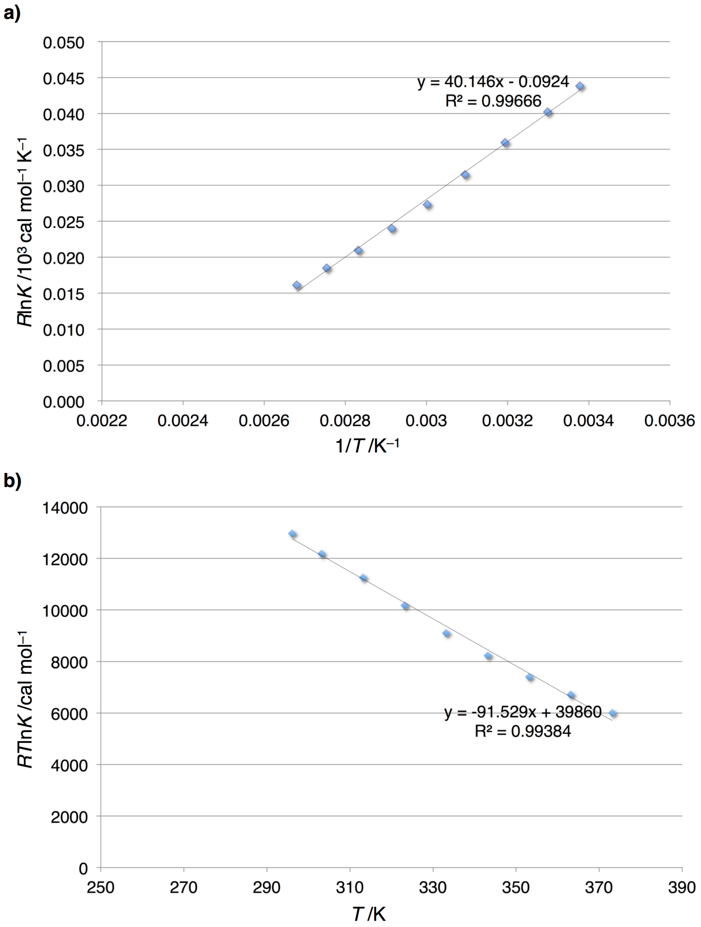

Figure A5.2. (a) *R*ln*K* vs 1/*T* and (b) *RT*ln*K* vs *T* plots of the equilibrium between **8a** and **1**+Py.

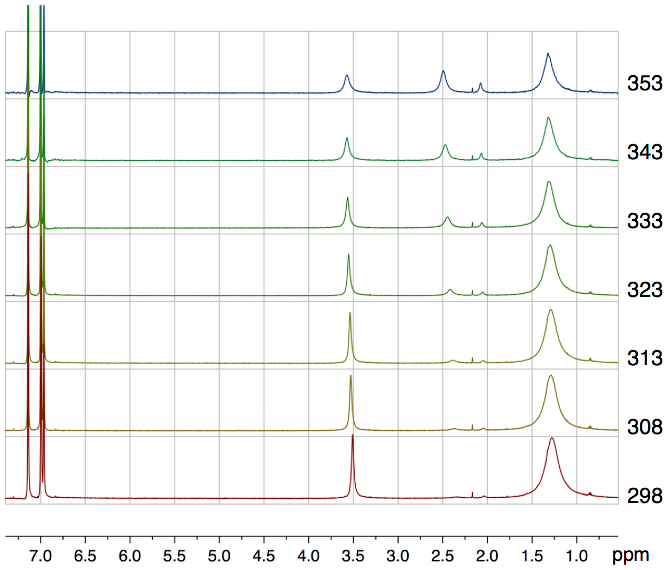

Figure A5.3. Variable-temperature ^{1}H NMR spectra of **8b** in C_6D_5Cl.

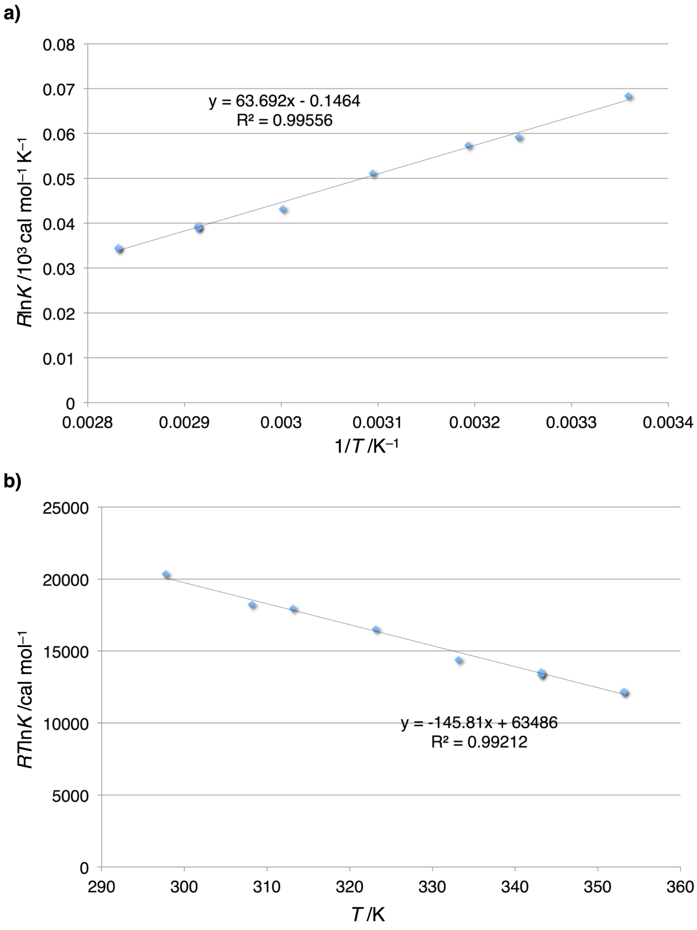

Figure A5.4. (a) R ln*K* vs 1/*T* and (b) *RT*ln*K* vs *T* plots of the equilibrium between **8b** and **1**+4-MeO-Py.

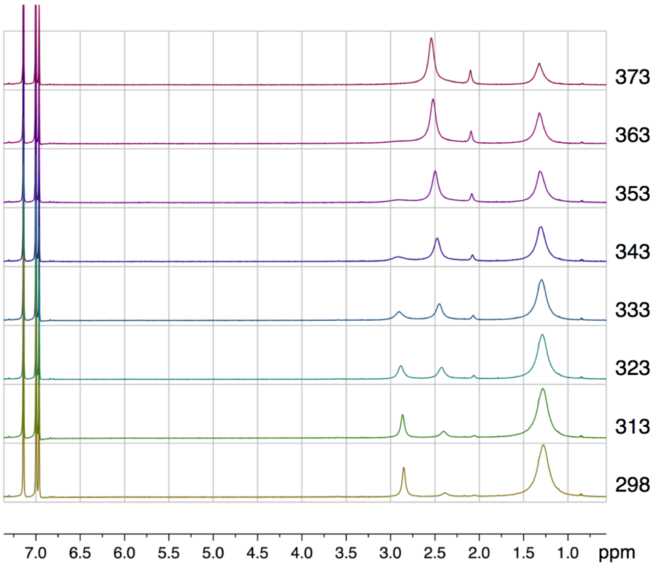

Figure A5.5. Variable-temperature ^{1}H NMR spectra of **8c** in C_6D_5Cl.

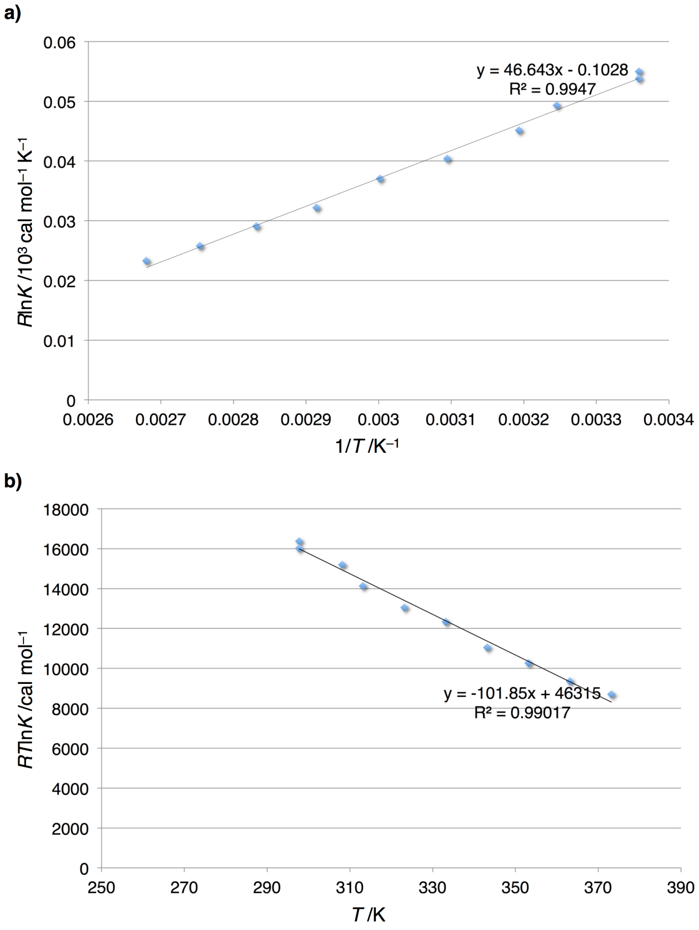

Figure A5.6. (a) $R\ln K$ vs $1/T$ and (b) $RT\ln K$ vs T plots of the equilibrium between **8c** and **1**+4-Me-Py.

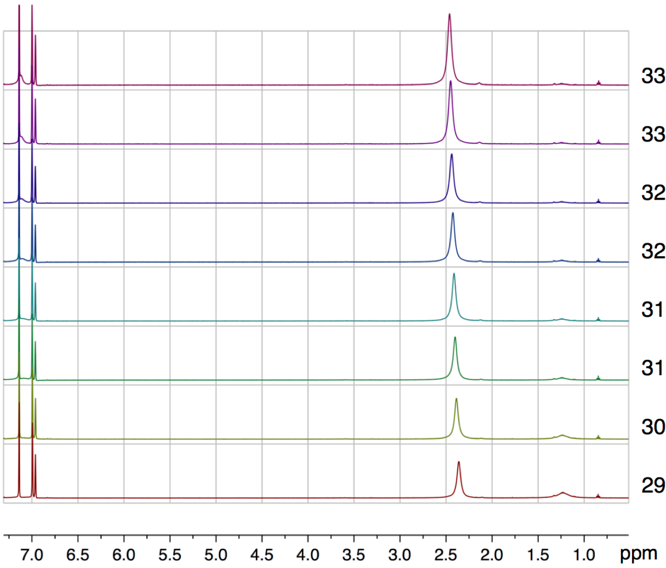

Figure A5.7. Variable-temperature ^{1}H NMR spectra of **8d** in C_6D_5Cl.

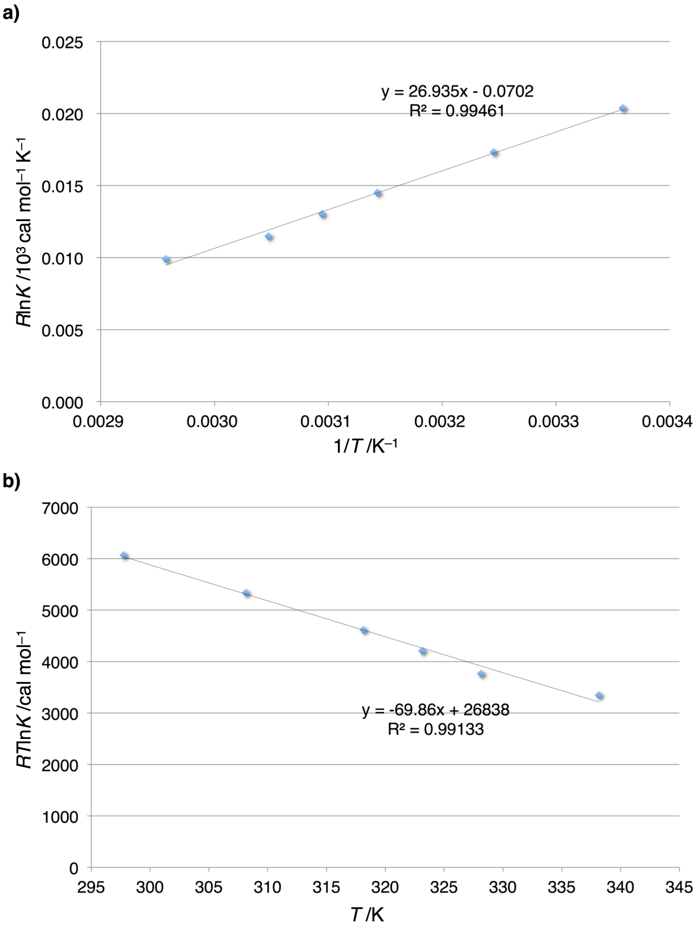

Figure A5.8. (a) $R\ln K$ vs $1/T$ and (b) $RT\ln K$ vs T plots of the equilibrium between **8d** and **1**+4-CF_3-Py.

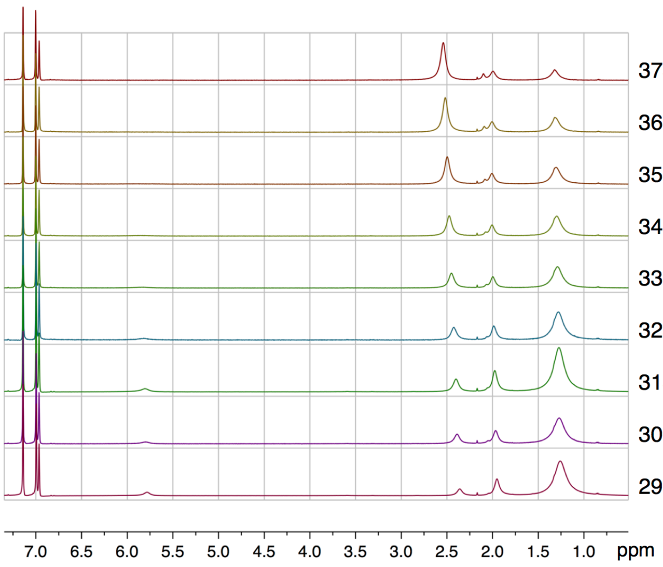

Figure A5.9. Variable-temperature ^{1}H NMR spectra of **8e** in C_6D_5Cl.

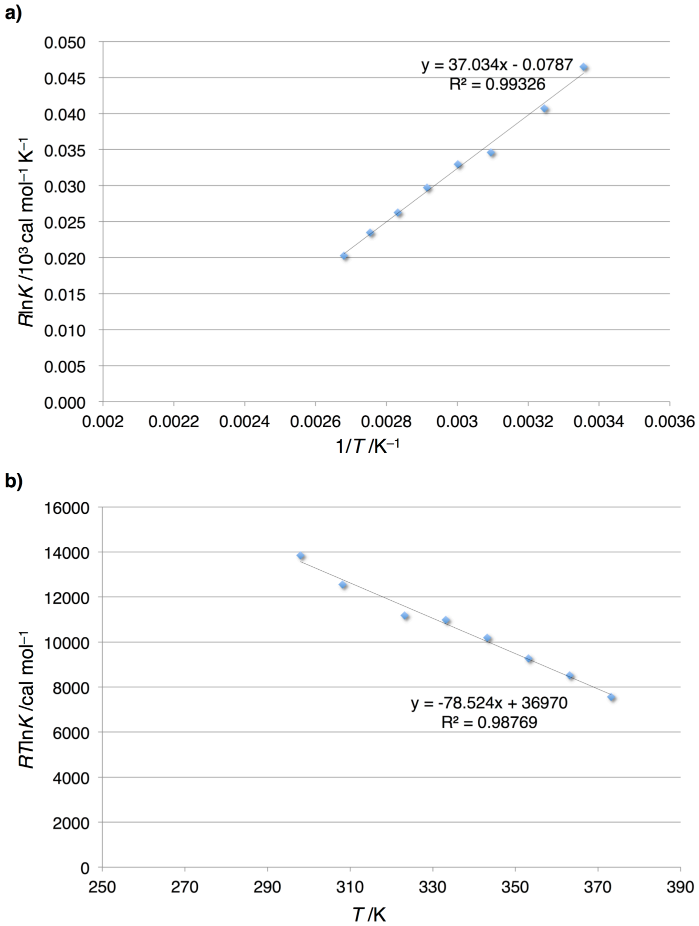

Figure A5.10. (a) *R*ln*K* vs 1/*T* and (b) *RT*ln*K* vs *T* plots of the equilibrium between **8e** and **1**+3-Me-Py.

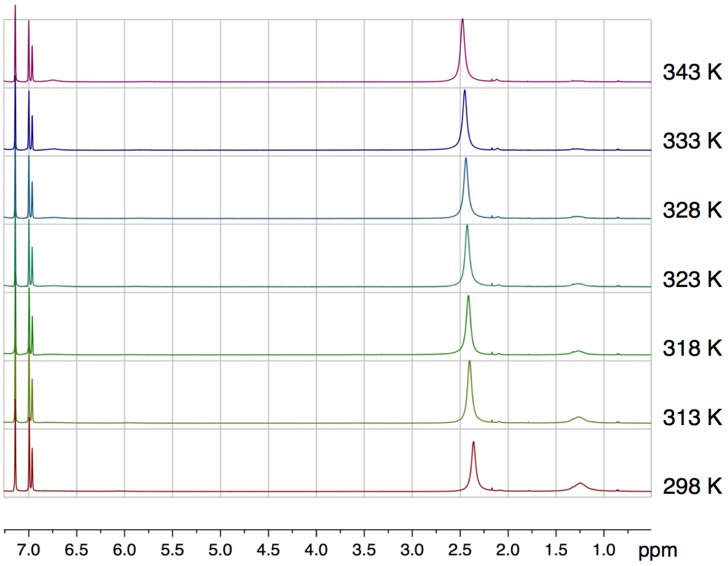

Figure A5.11. Variable-temperature ^{1}H NMR spectra of **8f** in C_6D_5Cl.

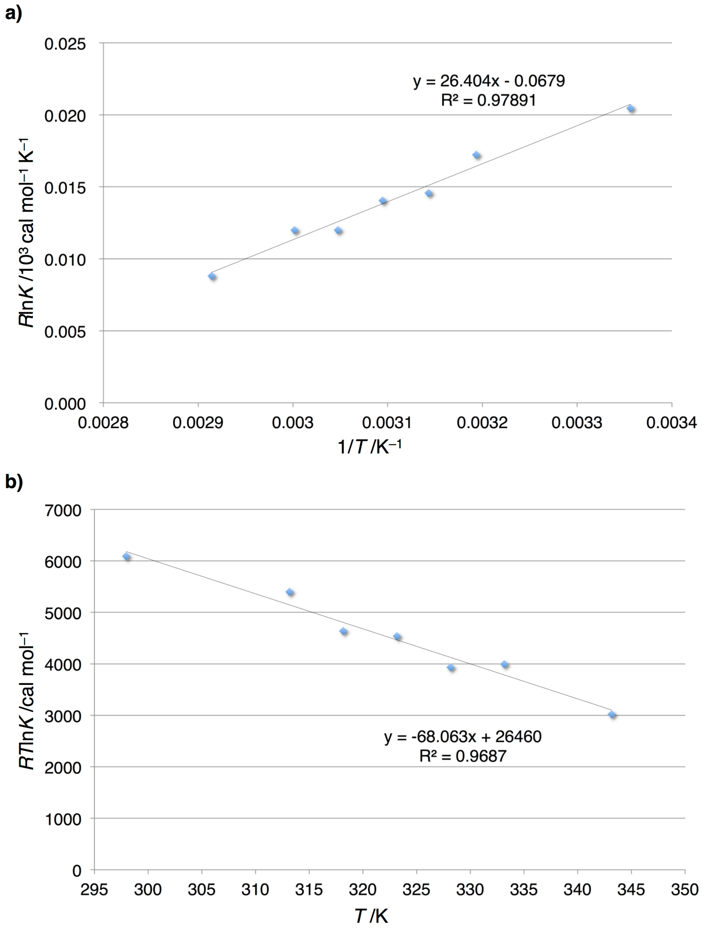

Figure A5.12. (a) $R\ln K$ vs $1/T$ and (b) $RT\ln K$ vs T plots of the equilibrium between **8f** and **1**+3-Br-Py.

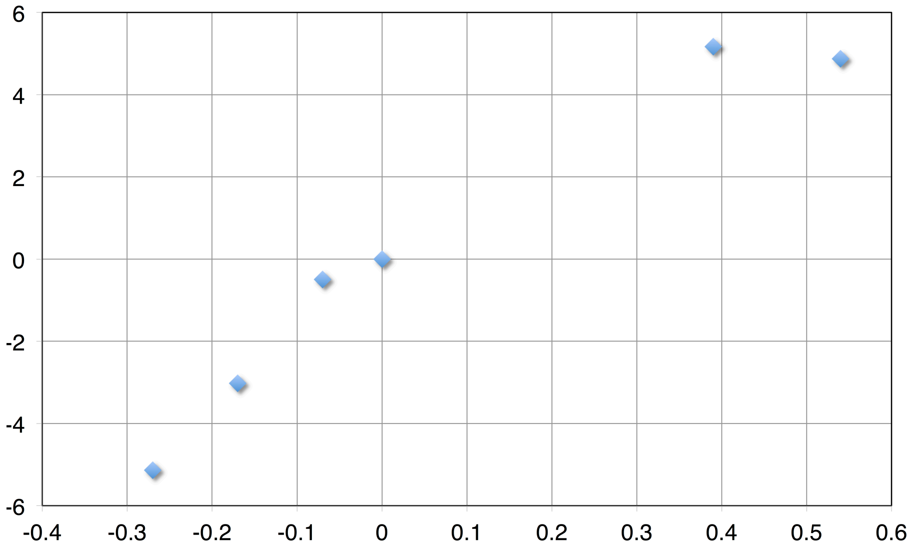

Figure A5.13. Hammett plot of log(K_X/K_H) vs Hammett sigma constants for the equilibriums between **8a**-**f** and **1**+L. The value of **8a** was used as reference (K_H).

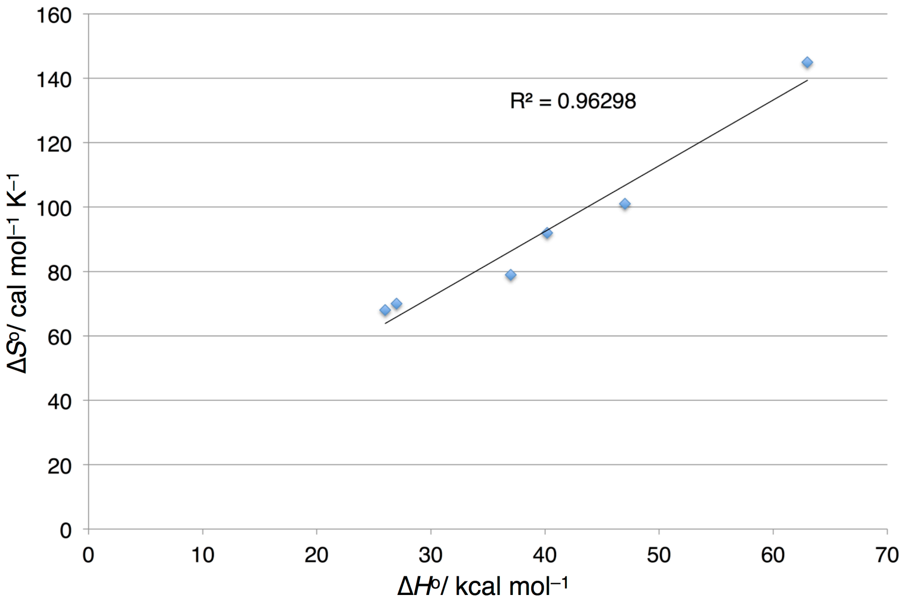

Figure A5.14. ΔS^o vs ΔH^o plot for the equilibrium between **8a**-**f** and **1**+L.

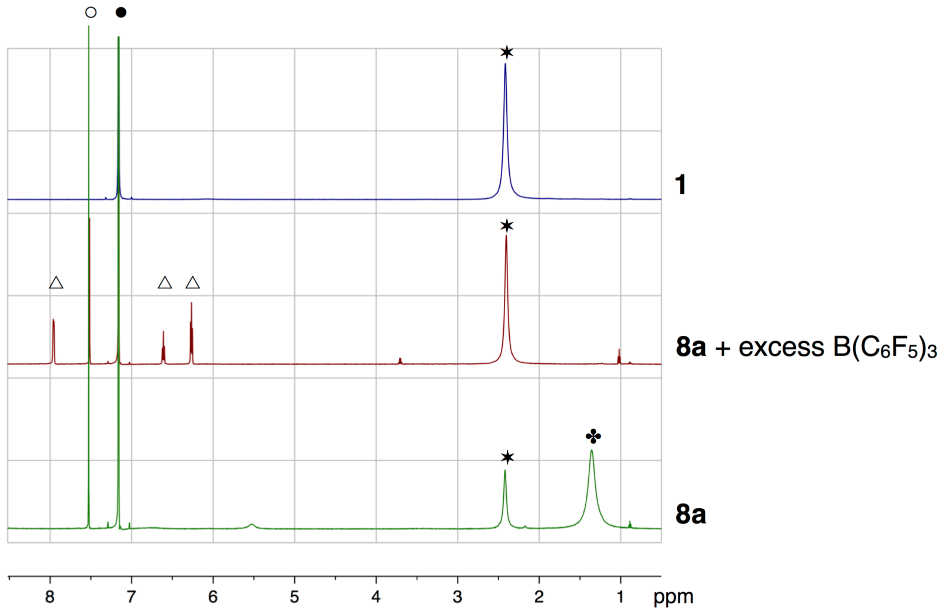

Figure A5.15. ^{1}H NMR spectra of **8a** (bottom), **8a** with excess B(C_6F_5)$_3$ (middle), and **1** (top) in C_6D_6. Legend: △ = (Py)-B(C_6F_5)$_3$, ○ = internal standard, ● = solvent.

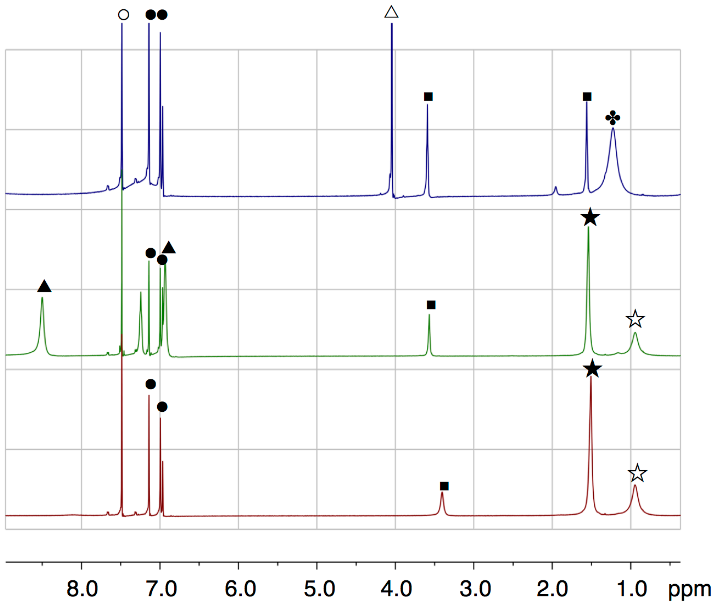

Figure A5.16. ^{1}H NMR spectra of [**1**]$^{2-}$ and [**1**]$^-$ (bottom), with excess pyridine (middle), and with excess pyridine and [Cp_2Fe](PF_6) (top) in C_6D_5Cl. Legend: ☆ = [**1**]$^{2-}$, ★ = [**1**]$^-$, ✤ = **8a**, △ = Cp_2Fe, ▲ = Py, ▪ = THF, ○ = internal standard, ● = solvent.

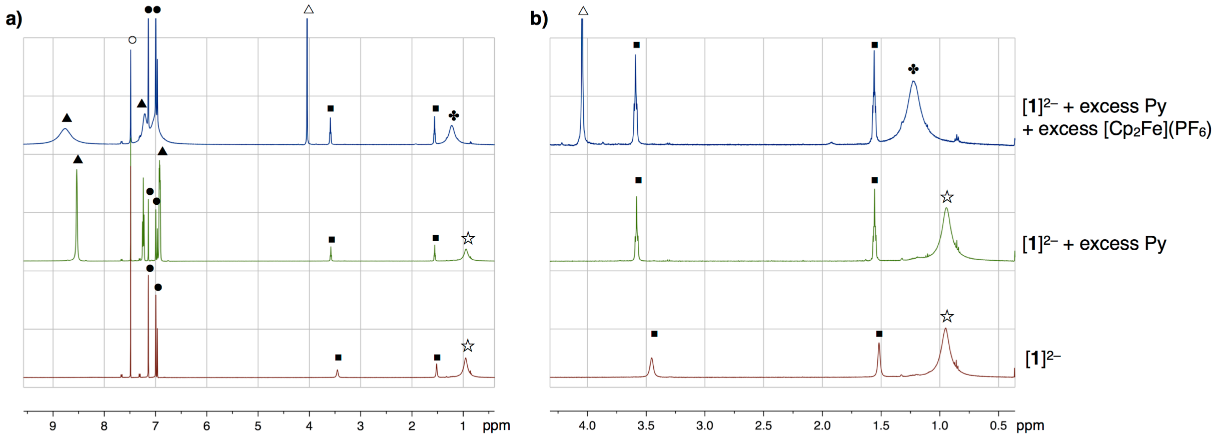

Figure A5.17. ^{1}H NMR spectra of $[\mathbf{1}]^{2-}$ (bottom), with excess pyridine (middle), and with excess pyridine and $[Cp_2Fe](PF_6)$ (top) in C_6D_5Cl. The spectra are shown in the ranges from (a) 9.6 to 0.39 ppm and (b) 4.32 to 0.36 ppm. Legend: ☆ = $[\mathbf{1}]^{2-}$, ✤ = **8a**, △ = Cp_2Fe, ▲ = Py, ▪ = THF, ○ = internal standard, ● = solvent.

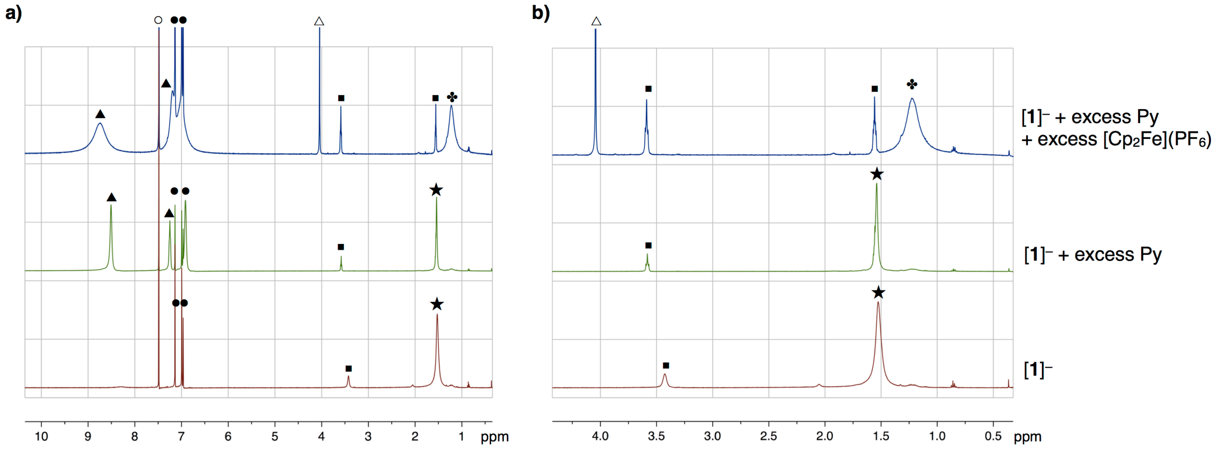

Figure A5.18. ^{1}H NMR spectra of $[\mathbf{1}]^{-}$ (bottom), with excess pyridine (middle), and with excess pyridine and $[Cp_2Fe](PF_6)$ (top) in C_6D_5Cl. The spectra are shown in the ranges from (a) 10.3 to 0.36 ppm and (b) 4.4 to 0.34 ppm. Legend: ★ = $[\mathbf{1}]^{-}$, ✤ = **8a**, △ = Cp_2Fe, ▲ = Py, ▪ = THF, ○ = internal standard, ● = solvent.

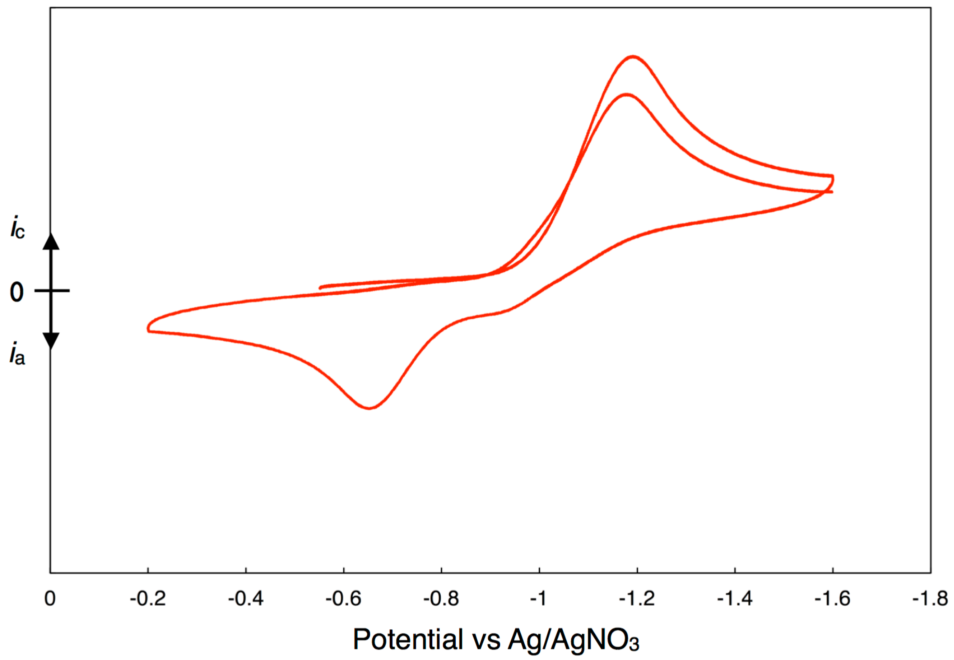

Figure A5.19. Cyclic voltammogram (CV) of **8a** (3 mM) in THF.

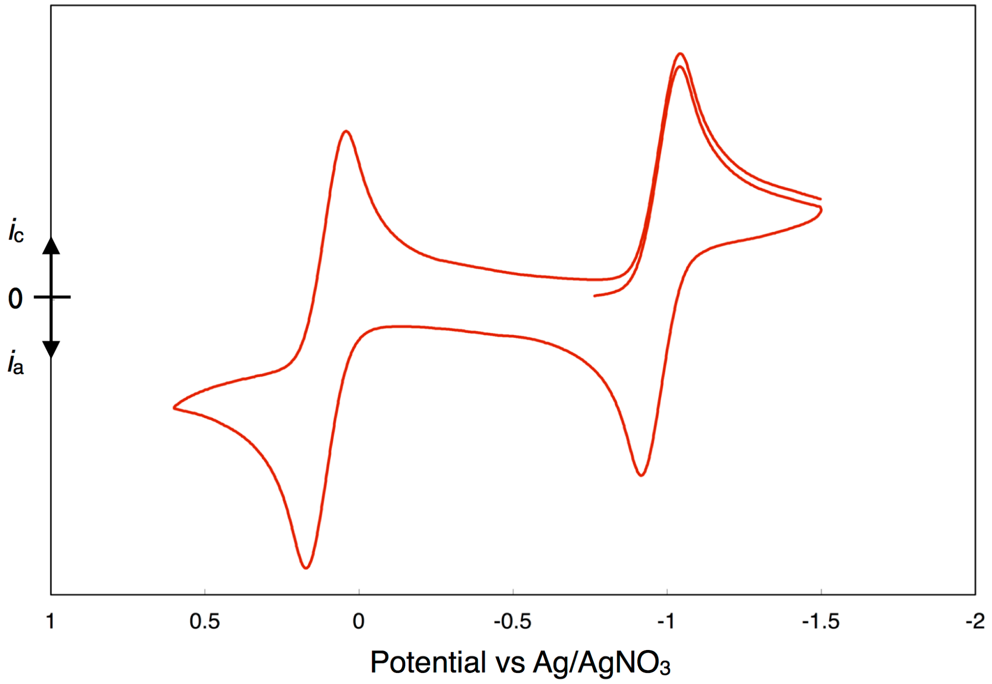

Figure A5.20. CV of [Na(THF)$_2$][**1**] (3 mM) in THF.

Table A 5.1. Crystal Data for $Fe_2S_2\{N(SiMe_3)_2\}_2(L)_2$ (**8a**, L = Py; **8b**, L = 4-MeO-Py; **8c**, L = 4-Me-Py; **8d**, L = 4-CF_3-Py; **8e**, L = 3-Me-Py; **8f**, L = 3-Br-Py), $[Na(THF)(Py)]_2[Fe_4S_4\{N(SiMe_3)_2\}_4]$ ($[Na(THF)(Py)]_2$[**1**]), $[Na(THF)_{0.3}(Py)_{1.3}][Fe_4S_4\{N(SiMe_3)_2\}_4]$ ($[Na(THF)_{0.3}(Py)_{1.3}]$[**1**]), and $C_5H_5N\text{-}B(C_6F_5)_3$.

	8a	**8b**	**8c**	**8d**
formula	$C_{22}H_{46}Fe_2N_4S_2Si_4$	$C_{24}H_{50}Fe_2N_4O_2S_2Si_4$	$C_{24}H_{50}Fe_2N_4S_2Si_4$	$C_{24}H_{44}F_6Fe_2N_4S_2Si_4$
Formula wt (g mol^{-1})	654.79	714.84	682.84	790.78
Crystal system	Triclinic	Monoclinic	Triclinic	Monoclinic
Space group	P-1 (#2)	$C2/c$ (#15)	P-1 (#2)	$P2_1/c$ (#14)
a (Å)	9.045(3)	22.876(7)	9.016(5)	22.728(5)
b (Å)	9.259(3)	11.048(3)	9.904(6)	12.711(3)
c (Å)	11.537(3)	14.488(4)	12.038(7)	13.008(3)
α (°)	105.222(3)		108.444(4)	
β (°)	96.810(3)	92.495(4)	99.449(3)	91.283(4)
γ (°)	114.704(2)		109.722(7)	
V (Å^3)	817.7(5)	3658.1(18)	914.6(9)	3757.0(15)
Z	1	4	1	4
D_{calcd} (g/cm^3)	1.330	1.298	1.240	1.398
Max 2θ (°)	55.0	55.0	55.0	55.0
No. of Reflections Measured	8558	21457	11157	30128
No. of Data Used (I >2.00 s(I))	3709	4131	4132	8556
No. of Parameters Refined	154	172	170	391
$R_1{}^a$	0.0269	0.0408	0.0402	0.0488
$wR_2{}^b$	0.0723	0.1075	0.1148	0.1504
GOF^c	1.056	1.119	1.027	1.009

[a] $I > 2\sigma(I)$, $R1=\Sigma||F_o|-|F_c||/\Sigma|F_o|$. [b] refined with all data, $wR2=[\{\Sigma w(F_o^2-F_c^2)^2\}/\Sigma w(F_o^2)^2]^{1/2}$.

[c] $GOF=[\{\Sigma w(F_o^2-F_c^2)^2\}/(N_o-N_p)]^{1/2}$, where N_o and N_p denote the numbers of reflection data and parameters.

(Continued)

	8e	**8f**	[Na(THF)(Py)]$_2$[**1**]
formula	$C_{24}H_{50}Fe_2N_4S_2Si_4$	$C_{22}H_{44}Br_2Fe_2N_4s_2Si_4$	$C_{33.3}H_{77}Fe_4N_{5.3}NaO_{0.7}S_4Si_8$
Formula wt (g mol^{-1})	682.84	812.58	1162.31
Crystal system	Triclinic	Triclinic	Orthorhombic
Space group	P-1 (#2)	P-1 (#2)	$P2_12_12_1$ (#19)
a (Å)	8.918(3)	8.713(6)	14.492(2)
b (Å)	9.868(4)	8.790(7)	17.789(3)
c (Å)	12.062(5)	12.777(8)	23.398(4)
a (°)	108.9844(18)	103.212(10)	
β (°)	94.950(4)	93.832(9)	
γ (°)	115.360(3)	110.486(7)	
V (Å^3)	874.8(6)	880.8(11)	6032(2)
Z	1	1	4
D_{calcd} (g/cm^3)	1.296	1.532	1.280
$Max\ 2\theta$ (°)	55.0	55.0	55.0
No. of Reflections Measured	10576	10556	49138
No. of Data Used (I >2.00 s(I))	3938	3964	13695
No. of Parameters Refined	163	163	500
$R1^a$	0.0408	0.0388	0.0645
$wR2^b$	0.0936	0.1039	0.1860
GOF^c	1.065	1.023	0.989

[a] $I > 2\sigma(I)$, $R1=\Sigma||F_o|-|F_c||/\Sigma|F_o|$. [b] refined with all data, $wR2=[\{\Sigma w(F_o^2-F_c^2)^2\}/\Sigma w(F_o^2)^2]^{1/2}$.

[c] $\mathrm{GOF}=[\{\Sigma w(F_o^2-F_c^2)^2\}/(N_o-N_p)]^{1/2}$, where N_o and N_p denote the numbers of reflection data and parameters.

(Continued)

	[Na(THF)$_{0.7}$(Py)$_{1.3}$][**1**]	C_5H_5N-$B(C_6F_5)_3$
formula	$C_{42}H_{76}Fe_4N_6Na_2O_2S_4Si_8$	$C_{23}H_5BF_{15}N$
Formula wt (g mol^{-1})	1319.39	591.09
Crystal system	Monoclinic	Monoclinic
Space group	$P2_1/c$ (#14)	$P2_1/n$ (#14)
a (Å)	12.371(3)	10.224(2)
b (Å)	24.482(5)	13.229(3)
c (Å)	23.672(4)	16.189(4)
a (°)		
β (°)	104.827(3)	103.301(3)
γ (°)		
V (Å^3)	6931(2)	2130.9(8)
Z	4	4
D_{calcd} (g/cm^3)	1.264	1.842
$Max\ 2\theta$ (°)	55.0	55.0
No. of Reflections Measured	55944	16432
No. of Data Used (I >2.00 s(I))	15556	4754
No. of Parameters Refined	573	381
$R1^a$	0.0660	0.0414
$wR2^b$	0.2005	0.1229
GOF^c	1.069	0.890

[a] $I > 2\sigma(I)$, $R1 = \Sigma||F_o|-|F_c||/\Sigma|F_o|$. [b] refined with all data, $wR2 = [\{\Sigma w(F_o^2-F_c^2)^2\}/\Sigma w(F_o^2)^2]^{1/2}$. [c] GOF$=[\{\Sigma w(F_o^2-F_c^2)^2\}/(N_o-N_p)]^{1/2}$, where N_o and N_p denote the numbers of reflection data and parameters.

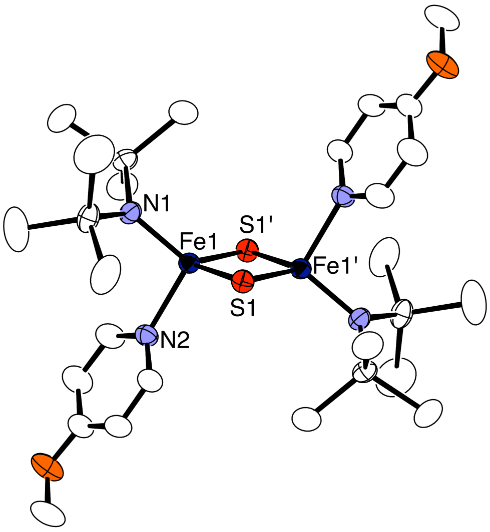

Figure A5.21. Molecular structure of $Fe_2S_2\{N(SiMe_3)_2\}_2(4\text{-MeO-Py})_2$ (**8b**) with thermal ellipsoids at the 50% probability level. Selected distances (Å) and angles (°): Fe1-Fe1′ 2.7468(8), Fe1-S1 2.2116(8), Fe1-S1′ 2.2041(8), Fe1-N1 1.913(2), Fe1-N2 2.110(2), S1-Fe1-S1′ 103.07(3), Na-Fe1-N2 100.76(9).

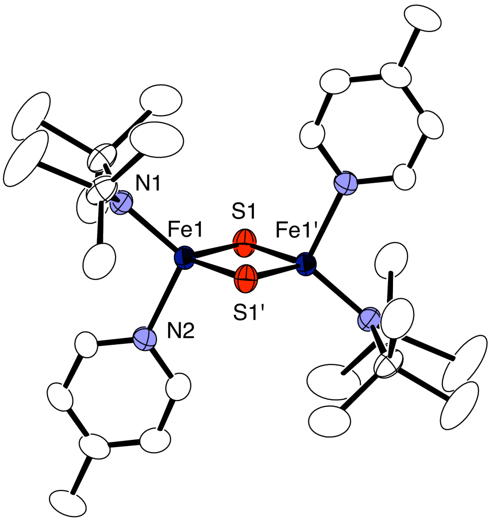

Figure A5.22. Molecular structure of $Fe_2S_2\{N(SiMe_3)_2\}(4\text{-Me-Py})_2$ (**8c**) with thermal ellipsoids at the 50% probability level. Selected bond distances (Å) and angles (°): Fe1-Fe1′, 2.7294(11); Fe1-S1, 2.2004(14); Fe1-S1′, 2.1969(11); Fe1-N1, 1.921(2); Fe1-N2, 2.093(2); S1-Fe1-S1′, 103.27(4); N1-Fe1-N2, 106.36(7).

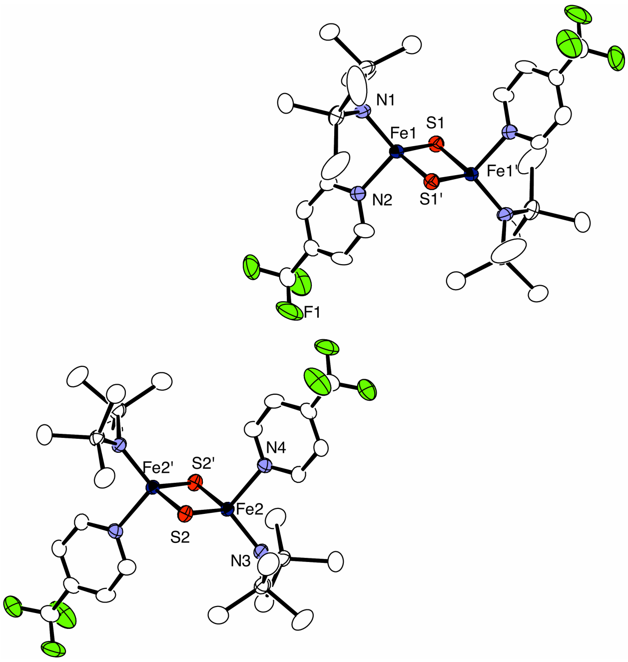

Figure A5.23. Molecular structure of $Fe_2S_2\{N(SiMe_3)_2\}(4\text{-}CF_3\text{-}Py)_2$ (**8d**) with thermal ellipsoids at the 50% probability level. Selected bond distances (Å) and angles (°): Fe1-Fe1′, 2.7553(7); Fe2-Fe2′, 2.7414(7); Fe1-S1, 2.2060(10); Fe1-S1′, 2.2102(10); Fe2-S2, 2.2010(10); Fe2-S2′, 2.1984(10); Fe1-N1, 1.917(3); Fe1-N2, 2.141(3); Fe2-N3, 1.916(2); Fe2-N4, 2.142(3); S1-Fe1-S1′, 102.79(3); S2-Fe2-S2′, 102.91(3); N1-Fe1-N2, 101.34(11); N3-Fe2-N4, 102.42(10).

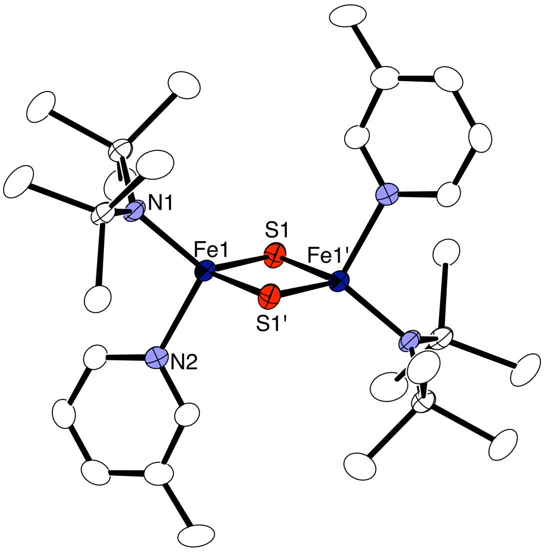

Figure A5.24. Molecular structure of $Fe_2S_2\{N(SiMe_3)_2\}(3\text{-}Me\text{-}Py)_2$ (**8e**) with thermal ellipsoids at the 50% probability level. Selected bond distances (Å) and angles (°): Fe1-Fe1′, 2.7602(8); Fe1-S1, 2.1994(8); Fe1-S1′, 2.2172(10); Fe1-N1, 1.9299(19); Fe1-N2, 2.119(2); S1-Fe1-S1′, 102.64(3); N1-Fe1-N2, 102.74(7).

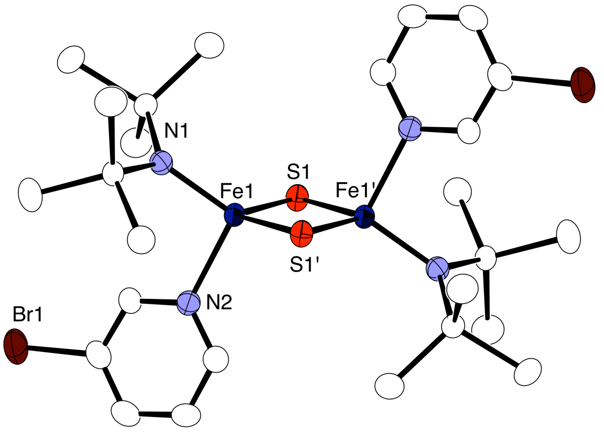

Figure A5.25. Molecular structure of $Fe_2S_2\{N(SiMe_3)_2\}(3\text{-}Br\text{-}Py)_2$ (**8f**) with thermal ellipsoids at the 50% probability level. Selected bond distances (Å) and angles (°): Fe1-Fe1′, 2.7460(14); Fe1-S1, 2.2038(15); Fe1-S1′, 2.2074(17); Fe1-N1, 1.917(3); Fe1-N2, 2.152(3); S1-Fe1-S1′, 103.00(5); N1-Fe1-N2, 99.21(11).

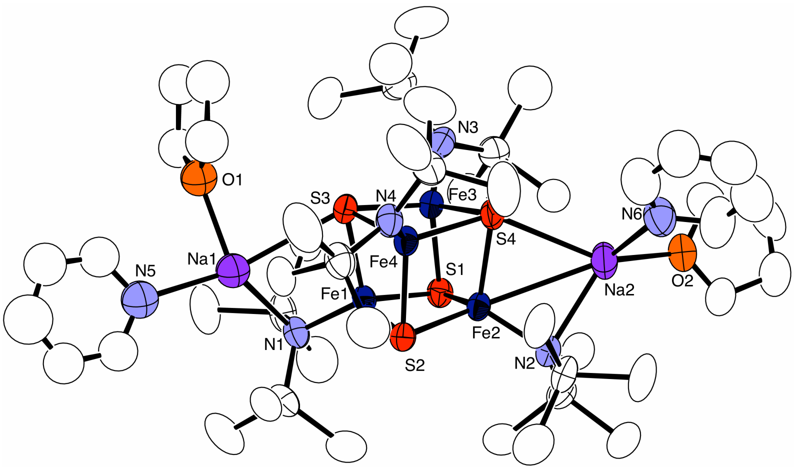

Figure A5.26. Molecular structure of $[Na(THF)(Py)]_2[Fe_4S_4\{N(SiMe_3)_2\}_4]$ ($[Na(THF)(Py)]_2$[**1**]) with thermal ellipsoids at the 50% probability level. Hydrogen atoms, the disordered trimethylsilyl groups, and the disordered THF and pyridine bound to Na1 are omitted for clarity.

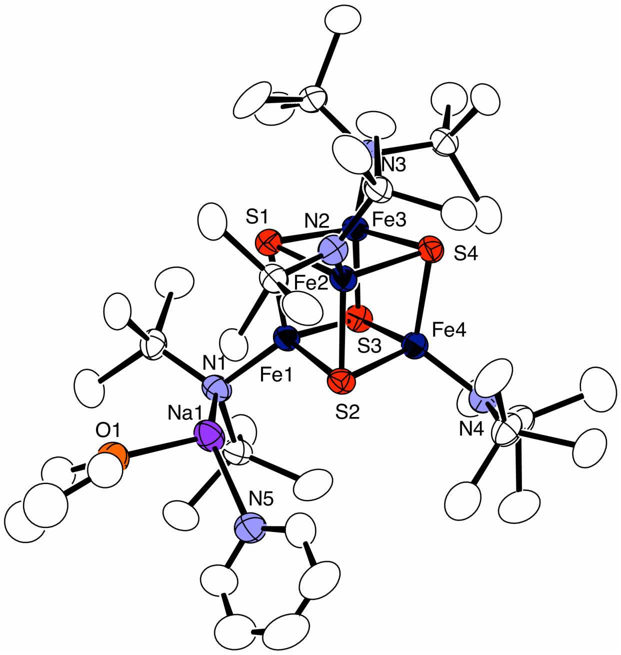

Figure A5.27. Molecular structure of [Na(THF)$_{0.7}$(Py)$_{1.3}$][Fe$_4$S$_4${N(SiMe$_3$)$_2$}$_4$] ([Na(THF)$_{0.7}$(Py)$_{1.3}$][**1**]) with thermal ellipsoids at the 50% probability level. Hydrogen atoms and the disordered pyridine overlapped with THF are omitted for clarity.

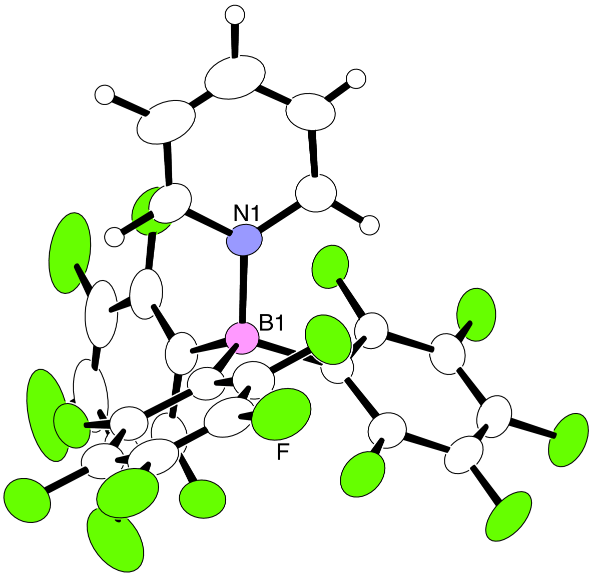

Figure A5.28. Molecular structure of $C_5H_5N\text{-}B(C_6F_5)_3$ with thermal ellipsoids at the 50% probability level. B1-N1, 1.6140(19) Å.

Table A 5.2. Selected bond distances (Å) and angles (°) of [Na(THF)(Py)]$_2$[**1**] and [Na(THF)$_{0.7}$(Py)$_{1.3}$][**1**].

	[Na(THF)(Py)]$_2$[**1**]	[Na(THF)$_{0.7}$(Py)$_{1.3}$][**1**]		[Na(THF)(Py)]$_2$[**1**]	[Na(THF)$_{0.7}$(Py)$_{1.3}$][**1**]
Fe1-Fe2	2.8226(10)	2.8723(13)	Fe3-N3	1.936(5)	1.892(6)
Fe1-Fe3	2.8172(11)	2.8484(13)	Fe4-N4	1.949(5)	1.895(6)
Fe1-Fe4	2.8653(11)	2.8129(14)	Na1-O1	2.387(9)	2.356(11)
Fe2-Fe3	2.8799(10)	2.8445(14)	Na1-N5	2.453(6)	2.423(7)
Fe2-Fe4	2.8620(11)	2.9097(14)	Na1-S3	3.080(2)	-
Fe3-Fe4	2.8787(12)	2.9340(14)	Na1-S2	-	3.121(3)
Fe1-S1	2.2952(15)	2.2876(18)	Na1-N1	2.511(4)	2.550(6)
Fe1-S2	2.2630(14)	2.3033(18)	Na2-O2	2.360(5)	-
Fe1-S3	2.3267(15)	2.2650(19)	Na2-N6	2.400(6)	-
Fe2-S1	2.2524(14)	2.2823(18)	Na2-S4	3.000(2)	-
Fe2-S2	2.3103(15)	2.3020(18)	Na2-N2	2.552(5)	-
Fe2-S4	2.3413(14)	2.2752(18)	S1-Fe1-S2	101.67(5)	100.61(6)
Fe3-S1	2.3446(15)	2.2655(18)	S1-Fe1-S3	105.50(5)	101.68(7)
Fe3-S3	2.3336(14)	2.3081(18)	S2-Fe1-S3	101.47(5)	103.99(7)
Fe3-S4	2.2958(14)	2.3089(18)	N1-Fe1-S1	115.03(13)	119.09(17)
Fe4-S2	2.3353(15)	2.3040(18)	N1-Fe1-S2	121.56(13)	112.26(7)
Fe4-S3	2.2851(14)	2.2948(18)	N1-Fe1-S3	109.76(12)	116.94(17)
Fe4-S4	2.3477(14)	2.3173(18)			
Fe1-N1	1.984(4)	1.958(6)			
Fe2-N2	1.986(4)	1.901(6)			

Acknowledgements

This thesis is the collection of the works carried out under the supervision of Prof. Kazuyuki Tatsumi at Inorganic Chemistry Group in Department of Chemistry, Graduate School of Science, Nagoya University.

First and foremost I would like to mention my gratefulness to Prof. Kazuyuki Tatsumi. His way of logical and critical thinking for chemical science has always stimulated me to think deeply about the results in my hands. Thanks to his scientific and educational support, the course of my graduate years was a fruitful experience. I also wish to acknowledge my second supervisor, Prof. Yasuhiro Ohki for his helpful suggestions and patient instructions. I have learned a great deal from his professional attitude. I would also like to thank Prof. Tsuyoshi Matsumoto for his valuable discussions. To make problems clearer, the discussions with him were extremely helpful for me.

I wish to express my thanks to my committee members: Prof. Yoshihito Watanabe, Prof. Mizuki Tada, and Prof. Hiroshi Nakajima. My deep appreciation goes to the collaborators: Prof. Roger E. Cramer (University of Hawaii) for kind instruction for X-ray crystallography, Prof. Markus W. Ribbe and Prof. Yilin Hu (University of California, Irvine) for acceptance of me as a short-term scholar, Prof. Kohei Tamao (RIKEN) and Prof. Tsukasa Matsuo (Kinki University) for gift of EindBr as the precursor of HSEind, Prof. Norihiro Tokitoh and Prof. Takahiro Sasamori (Kyoto University) for instruction for the synthesis of TbtBr as the precursor of HSTbt, Prof. Yuichi Fujita (Graduate School of Bioagricultural Sciences, Nagoya University) for instruction of bio-chemical techniques and fruitful discussion, and Prof. Yasuyuki Yamada (a faculty member) for his advice about VT NMR measurement.

Many thanks go to the former and current members of Tatsumi group. From the senior members, Mr. Shunsuke Senda, Dr. Tsubasa Hatanaka, Dr. Shun Ohta, Mr. Norihiro Yamada and Dr. Tamaki Terada, I have learned many experimental techniques and much knowledge about chemistry. Dr. Takayoshi Hashimoto often brought me to laughter by giving serious jokes. The *peer* members, Mr. Nobuhiro Taniyama, Mr. Kiyohisa Hirabayashi and Ms. Miku Miki, have stimulated me in many situations. I am deeply grateful for the personal interaction especially with Mr. Kohsuke Miyazaki, Ms. Ryoko Hoshino, Mr. Atsumu Nagahara, Mr. Kanyo Shin, and Ms. Yuka Ozawa. The hard work for laboratory management of the master students together at the "isolated" laboratory in Sougou Kenkyu Jikkentou, Ms. Kaho

Tanaka, Ms. Ayaka Nagasaki, and Mr. Tetsuya Makino, must be appreciated. I also would like to thank Dr. Golam Moura and Dr. Bose Moumita for their proofreading of this thesis. My appreciation goes to Ms. Hiromi Satoh for organizing Tatsumi group's business.

After I joined Tatsumi group, I had many chances to communicate with good-hearted German students from Münster and Berlin. In particular, I would like to thank Dr. Christoph Grohmann and Mr. David Königs for their sharing long time with me, such as eating a *strawberry spaghetti* or a *miso-katsu*. I had a great time with you.

I am truly grateful for the financial support during the course of the works from the following organizations:

- Japan Student Studies Services Organization, Independent Administrative Institution
- Nagoya University Global Center of Excellence program "Establishment of COE for Elucidation and Design of Materials and Molecular Functions"
- Shoshisha Foundation in Takeda Pharmaceutical Company Limited
- Nagoya University Program for Leading Graduate Schools "Integrative Graduate Education and Research Program in Green Natural Sciences" and
- Japan Society for the Promotion of Science for a Young Scientist Research Fellowship.

Finally, my deepest gratitude must go to my parents, Kohshin and Kasumi Tanifuji, my brother, Yuki, and my sister, Saki, for their unconditional support and encouragement. I was able to come this far thanks to you.

Kazuki Tanifuji
February 2014

Publication List

(1) "Synthetic Analogues of [$Fe_4S_4(Cys)_3(His)$] in Hydrogenases and [$Fe_4S_4(Cys)_4$] in HiPIP Derived from All-Ferric [$Fe_4S_4\{N(SiMe_3)_2\}_4$]"
Ohki, Y.; Tanifuji, K.; Yamada, N.; Imada, M.; Tajima, T.; Tatsumi, K. *Proc. Nat. Acad. Sci. U.S.A.* **2011**, *108*, 12635–12640.

(2) "Formation of a Nitrogenase P-cluster [Fe_8S_7] Core via Reductive Fusion of Two All-Ferric [Fe_4S_4] Clusters"
Ohki, Y.; Tanifuji, K.; Yamada, N.; Cramer, R. E.; Tatsumi, K. *Chem. Asian J.* **2012**, *7*, 2222–2224.

(3) "A Convenient Route to Synthetic Analogues of the Oxidized Form of High-Potential Iron-Sulfur Proteins"
Tanifuji, K.; Yamada, N.; Tajima, T.; Sasamori, T.; Tokitoh, N.; Matsuo, T.; Tamao, K.; Ohki, Y.; Tatsumi K. *Inorg. Chem. Under Revision.*

(4) "Non-Centrosymmetric Coordination Polymer with a Highly Hindered Octahedral Copper Center Bridged by Mandelate"
Moriya, M.; Tominaga, S.; Hashimoto, T.; Tanifuji, K.; Matsumoto, T.; Ohki, Y.; Tatsumi, K.; Kaneshiro, J.; Uesu, Y.; Sakamoto, W.; Yogo, T. *Inorg. Chem.* **2012**, *51*, 4689–4693.

(5) "かさ高いチオラート配位子を有する高酸化型[4Fe-4S]クラスターおよび[Fe-4Fe-4S]クラスターの合成"
谷藤一樹 *Bull. Jpn. Soc. Coord. Chem.* **2012**, *59*, 19-21.